Molecular mechanisms of Tea1 cortical anchoring in *Schizosaccharomyces pombe*

Cláudia do Céu Afonso Bicho

Doctor of Philosophy

University of Edinburgh

August 2010

Acknowledgments

First, I would like to thank my supervisor Ken Sawin for accepting my as a PhD student even under the exceptional conditions that were involved. Moreover, I would like to thank Ken for his guidance, patience and permanent enthusiasm with all aspects related with science. Ken really help me to improve my skills as a researcher and will always be to me a role model of what science should be about.

I am very gratefully to the Fundação para a Ciência e Tecnologia/ Portuguese Ministry of Science and Higher Education (SFRH/BD/21633/2005) for funding my PhD.

I am also especially grateful to the people with whom I collaborated with during my PhD, Andrew Goryachev and Juri Rappsilber. Without their generosity and collaboration it would have not been possible to achieve some of the results presented in this thesis. Moreover, working with both Andrew and Juri was very rewarding because it gave me the opportunity to learn about subjects so diverse as mass spectroscopy and mathematical modeling.

I would like to thank all the present and past members in the Sawin lab: Hilary Snaith, Andreas Anders, Itaru Samejima, Lynda Groocok, Vicky Miller, Eric Lynch and Weronika Borek, for making work so interesting and fun. I would like to specially thank Hilary for her generosity and patience in teaching me, for performing some of the experiments shown here and for so much great advice given.

I also need to thank to David Kelly for providing technical support with the microscopy, especially during the set up of the FRAP experiments. Moreover, I need to thank David for never forgetting to check if was “alive and happy” while spending long hours inside the microscope room.

All the mass spectroscopy results shown are of the responsibility of the very talented MS technician, Flávia Alves. Muito obrigada Flávia, não só pelo teu talento e ajuda com as “nossas” amostras, mas também por teres sido sempre uma boa amiga.

I would like to thank you my friends in Edinburgh, especially to the “Portuguese Crowd”, Ana, Ricardo, Vanessa and Susana. Your support, permanent friendship and example of persistence were always very important for me.

To my friends in Portugal, Patrícia, Mónica, Joana and Gelly. Its was always inspiriting to see that despite all the obstacles you manage to keep going and find your own way.

To my “old” friend Irina. It is very rewarding to keep our friendship for so many years and at the same time have our scientific paths running side by side!

A very very special thank you to my dear and very talented friend Susana. You are not only a great friend but also a role model of how life should be lived. I guess you know that without you here, Edinburgh would not have been even half of the fun it was! And yes, one day we will say, “When I was in grad school…” and tell some crazy story.

Finally I need to thank my lovely family. Às minhas irmãs, Gisela e Verónica, que sempre foram as minhas amigas e exemplos que eu quis seguir. Aos meus sobrinhos André e Laura, que sempre me deram os abraços mais fortes nos meus regressos. Finalmente aos meus pais, António e Céu, que sempre me deram todas as oportunidades para fazer o que eu gosto e que sempre demonstraram que a nossa familia é o mais importante. Muito obrigada por todo o vosso carinho e apoio com bolos e comida.

FCT Fundação para a Ciência e a Tecnologia
MINISTÉRIO DA CIÊNCIA, TECNOLOGIA E ENSINO SUPERIOR Portugal

Declaration

This thesis is a presentation of my original research work. Where the contributions of others have been referred to, this has been acknowledged in the text.

Cláudia Bicho

Abstract

Establishment and maintenance of a polarized axis is essential for all organisms. Cells can either change their shape in response to extracellular cues or maintain a stable polarity axis via landmarks defined in relation to internal cues. In the fission yeast *Schizosaccharomyces pombe,* microtubules regulate cortical cell polarity together with the landmark protein Tea1. Tea1 is transported to cell tips on microtubule plus-ends and deposited upon microtubule contact with the membrane. Although Tea1 has been shown to interact with several binding-partners, Tea1 anchoring at the cell tip depends mostly on the membrane-associated protein, Mod5. Tea1 and Mod5 accumulate in clusters at the cell tip in a mutually dependent manner.

I used a combination of live-cell imaging, FRAP (Fluorescence Recovery After Photobleaching) and computational modeling to dissect the dynamics of the Tea1-Mod5 interaction. I have shown that although Tea1 is stably associated with the cell tip, Mod5 is mobile within the cell tip. I proposed a model in which Tea1 is stable at the cell tip due to self-polymerization and association in the form of a cluster-network. In the model, the role of Mod5 in the cluster-network is to facilitate the formation of Tea1-Tea1 interactions. Moreover, in the model, Mod5 is restricted to the cell tip due to iterative binding to and release from the Tea1 cluster-network. The properties of the proposed Tea1 cluster-network might contribute to the behavior of Tea1 as a polarity landmark.

I hypothesized that Tea1 transfer from the microtubules to the cell tip was regulated by phosphorylation. Tea1 phosphorylated residues were mapped using mass spectroscopy (MS), and identified to be mostly enriched within a central region of the protein. Using a combination of mutagenic analysis and live-cell imaging I demonstrate that Tea1 phosphorylation might be required for its dissociation from the cluster-network at the cell tip. This suggests that Tea1 interactions within the cluster network are phospho-regulated by one of the several tip-localized kinases.

It has been shown in other organisms and in this thesis that comparison among MS samples requires quantitative MS methodologies. Thus, I developed a robust SILAC (Stable Isotope Labeling in Cell Culture) method to perform quantitative MS in *S. pombe*. As a

proof-of-principle of the method I performed a proteome-wide comparison between the late G2 and the G1/S transition of the cell cycle. The cell cycle proteome-wide analysis not only quantified variation in expression levels of cell cycle regulated proteins but also identified novel cell cycle regulated proteins.

It has been previously shown that Tea1, Tea3 and Mod5 can interact simultaneously, with each pair interacting independently of the third protein. I describe here a Mod5 mutagenic analysis screen designed to separate Tea1 and Tea3 binding site on Mod5. The Mod5-mutants obtained from this analysis indicate that the Tea3-Mod5 interaction may play a role in cell polarity establishment. Moreover, although Tea3 is non-essential for the cluster-network formation, Tea3 might be important for its compaction, which may be particularly important during *de novo* formation of cell polarity.

Table of Contents

List of figures

List of tables

List of abbreviations

aa	amino acid
AEBSF	4-(2-Aminoethyl)benzenesulfonyl fluoride
Arg	arginine
ATP	adenosine-5'-triphosphate
BSA	bovine serum albumin
CAPS	3-(cyclohexlamino)-1-propanesulfonic acid
DTT	dithiothreitol
DMSO	dimethylsulfoxide
dNTP	deoxyribonucleotide triphosphate
EDTA	ethylene diamine tetraacetic acid
bp	base pair
FRAP	fluorescence recovery after photobleaching
FOA	5-Fluoroorotic acid
GDP	guanosine diphosphate
GFP	green fluorescent protein
GFH	GFP-FLAG-6xHis
GTP	guanosine triphosphate
HEPES	4-(2-hydroxyethyl)-1-piperazineethanesulfonic acid
HU	hydroxyurea
IPTG	Isopropyl β-D-1-thiogalactopyranoside
KS	Sawin laboratory yeast strain
Lat B	latranculin B
Lys	lysine
MBC	benzimidazoyl-carbamate
MBP	maltose binding protein
MS	mass spectroscopy
nmt	no message in thiamine
OKS	Sawin laboratory oligonucleotide
O/N	Overnight
PAGE	poly acrylamide gel electrophoresis
PCR	polymerase chain reaction

PEG	polyethylene glycol
pKS	Sawin laboratory plasmid
PMSF	phenylmethylsulfonyl fluoride
RFP	red fluorescent protein
ROI	region of interest
rpm	revolutions per minute
RT	room temperature
SDS	sodium dodecyl sulfate
SILAC	stable Isotope labeling with amino acid in cell culture
TAP	tandem affinity purification
TBS	tris buffered saline pH 8
TCA	trichloroacetic acid
TE	tris-EDTA solution
TEMED	tetramethylethylenediamine
TEV	tobacco etch virus protease
YE	Yeast extract

Chapter I: Introduction

1.1. Cell polarity

Cell polarization is the process by which a cell responds to stimuli by redistributing and maintaining proteins and organelles in a non-uniform layout. The orientation of cellular components along a defined axis is essential for all organisms and will ultimately create the different shapes of multi cellular organisms (Li and Bowerman, 2010).

Cell polarity defines specific cell functions related with cell shape (Figure 1.1). For example, epithelial cells can polarize in two distinct cell domains (apical and basal) that define their barrier functions in the epithelial (Nelson, 2003). Neurons, one of the most extremely polarized cells, have one long axon used to transmit unidirectional long-range information signals and several short dendrites, which receive signals (Witte and Bradke, 2008). The polarity machinery also orients cell motility, by defining the axis of motility between the leading and trailing edges and promoting directionally persistent cell migration (Petrie et al., 2009). Importantly, the localized accumulation of polarity proteins also occurs before asymmetric cell division, and therefore produces two daughter cells with different characteristics. For example, in the one-cell embryo of the nematode *Caenorhabditis elegans* (*C. elegans*) and in the neuroblasts of *Drosophila melonogaster* (*D. melonogaster*) different sets of proteins, mostly conserved among multi-cellular eukaryotes, accumulate asymmetrically at one side of the cell and after cell division are only inherited by one of the daughter cells (Iden and Collard, 2008).

Although different organisms present a wide range of cell shapes, the basic molecular mechanisms of cell polarity establishment are generally conserved among organisms from humans to yeast and can be broken down into a relatively small number of general features (Li and Gundersen, 2008; Nelson, 2003). First, a polarity cue is generated at the cell membrane. Second the signal is successively amplified. Third, as a response to the polarity signal, the inherently polar cytoskeleton filaments (particularly actin and microtubules) re-orients towards the signal and is used as a track to re-localize the necessary response factors to promote cell growth (Li and Gundersen, 2008; Nelson, 2003).

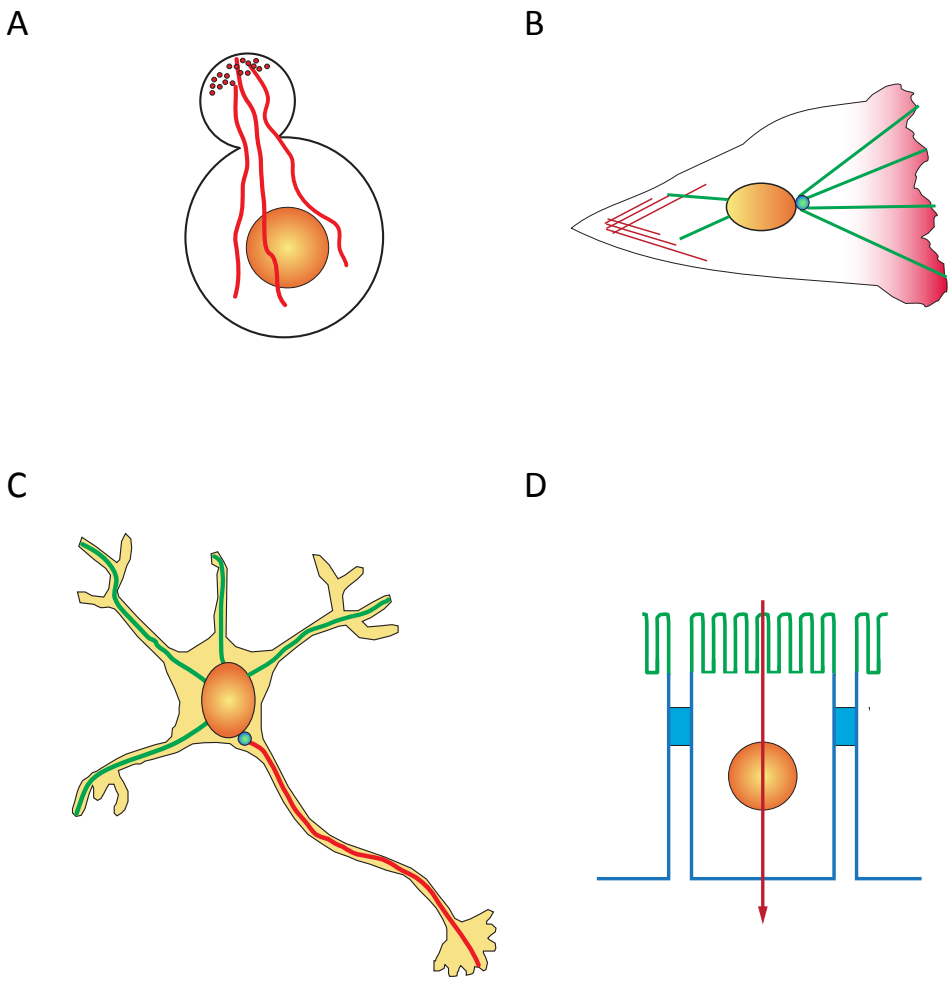

Figure 1.1- Diversity of shapes of polarized cells. A) During cell division *S. cerevisiae* cells form a bud next to the previous site of cytokinesis and polarize the actin cytoskeleton (red) for the transport of vesicles. Adapted from (Park and Bi, 2007). **B)** During cell migration, actin-dependent protrusions form at the leading edge (red) and contractile actin:myosin filaments (red lines) at the rear. Moreover, the centrosome orients towards the leading edge (green and blue dot) and microtubules are stabilized (green lines). Adapted from (Jaffe and Hall, 2005; Li and Gundersen, 2008). **C)** Neurons polarize in a single axon and several dendrites that express different sets of proteins. Moreover, in the dendrites microtubules are dynamic (green) and in the axon they are stable (red). Adapted from (Li and Gundersen, 2008). **D)** Epithelial cells polarize two membrane domains, apical (green) and basal (blue), that allow them to separate two biological compartments and regulate vectorial transport of ions/solutes (red arrow) between those compartments. Adapted from (Nelson, 2003).

1.2. Cell polarity in the fission yeast S. pombe

The fission yeast *Schizosaccharomyces pombe* (*S. pombe*) is an excellent organism in which to study cell polarity. It is a rod-shaped unicellular organism, 3-4 µm wide and 12-15 µm long. These cells are highly polarized and cell growth is restricted to the cell ends. The regular shape of *S. pombe* together with its genetic tractability make it an excellent organism to study cell polarity (Hayles and Nurse, 2001).

Regulation of cell growth and cell cycle are tightly associated in *S. pombe* (Figure 1.2) (Mitchison and Nurse, 1985). Cells grow by extension of the two poles, in a bipolar fashion. Once the cells reach a certain length they undergo mitosis. After chromosome segregation, a contractile cytokinetic actin ring (CAR) assembles and contracts in the cell middle. After cytokinesis, cells septate by medial fission and the two daughter cells separate (Hayles and Nurse, 2001). Immediately after cell separation, growth is resumed from only one of the cell ends, the old end. Later, in G2 phase of the cell cycle, cells reach a certain critical size and NETO occurs (New End Take Off). At this stage cells became bipolar and grow from both ends (Mitchison and Nurse, 1985).

In general cells are symmetric prior to polarization, and create only one new pole. On the contrary, *S. pombe* cells establish a new site of growth in the presence of a strongly polarized old growth site. An important question in cell polarity establishment in *S. pombe* is how cells became bipolar.

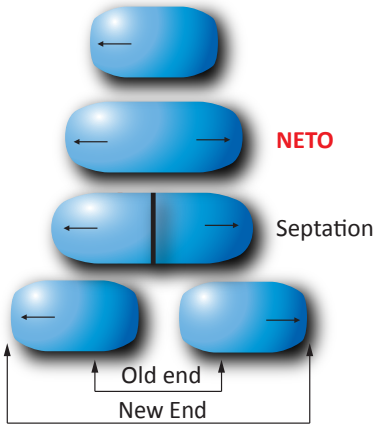

Figure 1.2- New End Take-Off (NETO). After cell division, *S. pombe* cells only grow from their old ends. Once cells reach a certain size, NETO occurs and cells start to grow in a bipolar fashion. Adapted from (Snaith and Sawin, 2005).

S. pombe mutants defective in establishing or maintain cell polarity no longer grow along the long cell axis, and can be visually identified by their cell shape defects, such as branched or round cells. Moreover, some cell polarity mutants fail to activate NETO and only grow from one cell end (Hayles and Nurse, 2001; Snell and Nurse, 1994).

Cell polarity establishment and maintenance in *S. pombe* depends on the accumulation of several polarity factors at the cell tips. The localization of polarity factors is actin- and microtubule-dependent. As in many other eukaryotic organisms, cell polarity in *S. pombe* is

intrinsically linked with the cytoskeleton. In *S. pombe* both microtubules and the actin cytoskeleton are spatially oriented towards the growth sites of the cell (Figure 1.3) (Hayles and Nurse, 2001; Martin, 2009).

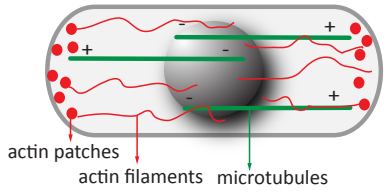

Figure 1.3- Actin and microtubules organization in *S. pombe*. Actin (red) patches accumulate at the sites of cell growth, and actin cables are oriented along the long axis of the cell. Microtubules (green) are oriented along the long axis of the cell. Microtubule minus-ends (-) are bundled in an anti parallel manner in the cell middle and the plus-ends (+) are oriented towards the cell tips.

1.2.1 Actin cytoskeleton

The actin cytoskeleton consists of actin filaments (F-actin), which are polymers of globular actin (G-actin). Actin monomers bind and hydrolyze ATP, and polymerize in a head-to-tail structure (Li and Gundersen, 2008). Actin filaments have a fast growing end called barbed end (or plus-end), and a slow growing end called pointed end (or minus-ends).

In *S. pombe*, F-actin is organized in three distinct structures: patches, cables and CAR. Actin patches are sites where actin nucleation is dependent of the Arp2/3 complex (Pelham and Chang, 2001; Pruyne et al., 2004). During interphase, actin patches are found at the sites of cell growth. After cell separation, actin patches accumulate initially only at the old end (the only site of cell growth) and after NETO, at both ends (Marks et al., 1986; Pelham and Chang, 2001). Although actin patches are extremely mobile, only a subset of patches shows directionality in movement (Pelham and Chang, 2001). Actin patch movement occurs as actin polymerizes and is dependent on actin cables. Actin patches do not seem to be transported to the cell ends. Instead, their “birth” location may be biased near cell growth regions. It has been suggested that in *S. pombe* actin patches might be involved in endocytosis, as in *S. cerevisiae* (Pelham and Chang, 2001).

Actin cables are polar structures and during interphase their barbed-ends face the cell ends (Kamasaki et al., 2005). The formin family of proteins both nucleates and elongates

linear bundled actin filaments (Chesarone et al., 2010). Formin activity is tightly spatially regulated by auto-inhibition that is relieved by GTP-bound Rho GTPases (DeWard and Alberts, 2008). There are three formins in *S. pombe*, each one dedicated to a particular type of actin cable localization. For3 is localized at the cell tip (see section 1.3.2. for details) (Martin and Chang, 2006), Cdc12 localizes at the CAR and nucleates actin cables specifically during cell separation (Chang et al., 1997), and Fus1 only nucleates actin cables during meiosis (Petersen et al., 1995). Actin cables nucleate mainly from the cell ends where For3 is localized (Kamasaki et al., 2005; Martin and Chang, 2006).

During M phase, actin cables and patches re-localize to the cell middle, where the CAR is assembled. The CAR contains both myosins and actin filaments and acts like a band of muscle that bisects the cell as it contracts (Gould and Simanis, 1997).

The role of actin cables as "tracks" for vesicles delivery in *S. pombe* is not as well characterized as for *S. cerevisiae*. However, it is accepted that the two yeasts should share similar molecular mechanisms of vesicle delivery during cell polarization (Fischer et al., 2008). Vesicles are transported by myosins, a large family of actin-binding proteins that contain a motor domain and a cargo-binding domain. Myosins hydrolyze ATP to transform chemical energy into force and motion (Pruyne et al., 2004). The myosin families V and VI are processive motors, meaning that they associate with actin filaments for several cycles of motor activity and thus can move cargo directionally (Nelson, 2003). So far, Myo2/Myo52, a type V myosin, was the only myosin identified in *S. pombe* shown to play a role in vesicle transport towards the cell membrane. Myo2/Myo52 is a non-essential gene and localizes at the cell tips and at the septum, in an actin dependent manner. Myo2/Myo52 mutants show defects in vesicle transport and in cell wall deposition (Motegi et al., 2001; Win et al., 2001).

1.2.2 Microtubules

Microtubules are polymers of heterodimers of α and β tubulin. Within a microtubule, tubulin heterodimers are arranged in head-to-tail fashion and form linear protofilaments. *In vivo*, 13 protofilaments are associated laterally to form 25 nm-wide hollow cylindrical polymers. Within the cylinder, the lateral bonds between monomers of adjacent protofilaments form a 3-start helical path. In this path, there is a three-tubulin monomer shift up after each complete helical turn. The lateral neighboring monomers between

protofilaments are either both α or β tubulin. However, at the seam there is a discontinuity and at each 3-start helical path the lateral interaction changes from α to β or vice-versa (Desai and Mitchison, 1997).

Microtubules are polar structures with two distinct ends, named "plus" (faster) and "minus" (slower) based on polymerization kinetics *in vitro*. Within the α/β dimer, α-tubulin subunits are oriented towards the minus ends, and β -tubulin subunits are oriented towards the plus end. Microtubules grow by GTP-tubulin dimer addition at the ends, which is accompanied by GTP hydrolysis.

Growing plus-ends are open flat sheets extending from the body of the microtubule. It is thought that growth occurs by extension of the sheet, which then folds into a tube just behind the region of growth. By contrast, the protofilaments of shrinking plus ends are peeled back symmetrically around the tube. The growing and the shrinking ends have different conformations and the ends are different from the lattice body of the microtubules (Carvalho et al., 2003; Desai and Mitchison, 1997).

Plus-ends are able to add or lose tubulin dimer subunits and thus grow or shrink (Desai and Mitchison, 1997; Sawin and Tran, 2006). The pattern of microtubule growth is stochastic and is termed dynamic instability (Mitchison and Kirschner, 1984). The transition from growth to shrinkage is called catastrophe and transition from shrinking to growth is called rescue (Carvalho et al., 2003). Dynamic instability enables interphase microtubules to explore the entire volume of the cell efficiently.

In vitro, microtubule nucleation is dependent on tubulin concentration and is a much slower process than *in vivo*. *In vivo*, the minus-ends are anchored in microtubule organizing centers (MTOCs), where the γ-tubulin complex works as a template for microtubule nucleation and capping (Sawin and Tran, 2006).

The dynamics of microtubules are regulated by microtubule-associated proteins (MAPs) that can either promote microtubule stabilization or destabilization (Desai and Mitchison, 1997). MAPs can bind microtubules along the lattice or at the plus-ends. Among proteins that regulate microtubule dynamics are motor proteins and proteins associated with the microtubule plus-ends.

Motor proteins can generate force due to ATP hydrolysis and therefore do mechanical work, either by transporting cargo along the microtubules or by pulling and pushing the microtubules (Hirokawa et al., 2009; Kardon and Vale, 2009). Motor proteins have

directionality, and the kinesin family generally moves towards the plus-end of microtubules and dyneins towards the minus-end. Although dyneins are minus-end directed motors they can associate persistently with microtubule plus-ends (Wu et al., 2006). For instance, in *S. cerevisiae* dynein is loaded at the plus-ends of spindle astral microtubules. Upon microtubule contact with the cortex, dynein is deposited onto the cortex in a Num1-dependent manner and orients the mitotic spindle, ensuring that the mother and the daughter cells have one nucleus each (Sheeman et al., 2003).

Among the MAPs are a specialized group of proteins, often termed "+TIPs" (plus-end tracking proteins), that accumulate at the plus-ends of microtubules. Although there are a few examples of +TIPs associated with depolymerising microtubules, such as the Dam1/DASH complex, XMAP215, or the depolymerising kinesins such as KLP10A, +TIPs bind plus-ends of growing microtubules (Akhmanova and Steinmetz, 2008; Brouhard et al., 2008; Mennella et al., 2005).

Although +TIPs are a group of structurally unrelated proteins, which include motor and non-motor proteins, a few conserved domains, repeated sequences and linear motifs structurally characterize their interactions with other +TIPs and with microtubule plus-ends. It has been shown that +TIPs form a large number of protein-protein interactions at the microtubule plus-ends that can be seen as a network of interactions, with the protein EB1 (End Binding protein 1) in the centre of the hub (Lansbergen and Akhmanova, 2006). EB1 is a small protein with extensive evolutionary conservation. EB1 has an N-terminal CH domain (Calponin Homology), sufficient to bind microtubules, a C-terminal coiled-coil region (see coiled-coil description in section 1.3) involved in relief of auto-inhibition via dimerization (Komarova et al., 2009), an EBH domain (End-binding Homology), and a C-terminal 20-30 amino acid flexible tail, containing the EEY/F motif, with homology with CLIP170 and α-tubulin (Akhmanova and Steinmetz, 2008). There are two main reasons for EB1 is viewed as a master regulator of +TIPS binding to the microtubule plus-ends. Firstly, EB1 was shown *in vitro* to track microtubule plus-ends independently of its binding partners (Bieling et al., 2007; Dixit et al., 2009). Results has suggested that EB1 associates with a structural feature of growing plus-ends of microtubules rather than co-polymerizing together with tubulin dimers (Bieling et al., 2007; Dixit et al., 2009; Dragestein et al., 2008; Sandblad et al., 2006). Secondly, it has been shown both *in vivo* and *in vitro* that the majority of +TIPs bind EB1 in order to become associated with microtubule plus-ends, in a "hitch-hiking" mechanism (Honnappa et al., 2009; Lansbergen and Akhmanova, 2006). However, +TIPs can track

microtubule plus-ends using other mechanisms (Carvalho *et al* 2003). Certain +TIPs, like the *S. pombe* protein Tip1, associate with microtubules plus-ends via microtubule motor-driven transport (Busch et al., 2004). Other +TIPs, like the polymerase XMAP215 have weak affinity to the microtubule lattice and can reach the plus-end via one-dimensional diffusion along the microtubule (Brouhard et al., 2008).

The binding of +TIPs to microtubules has been shown to be inhibited upon phosphorylation, most probably due to a reduction in microtubule affinity to negatively charged amino acids (Akhmanova and Steinmetz, 2008; Kumar et al., 2009; Zimniak et al., 2009).

Due to their localization at the microtubule plus-ends together with their multidomain/multisubunit structure, the +TIPs can regulate several biological processes such as microtubules plus-end dynamics, microtubule attachment necessary for vesicle delivery and force generation, and signals for cortical cell polarity (Akhmanova and Hoogenraad, 2005). The interactions of microtubule plus-ends with the cortex via the +TIPs not only allow microtubules to reorient and dwell for longer periods of time, but also promote re-orientation of the cell axis (Gundersen, 2002). The +TIPs bind microtubules, but upon contact with the cell cortex they can be transferred to the cell cortex. In *S. cerevisiae*, microtubule-cortex association is crucial for mitotic spindle alignment. Bim1 (EB1 homologue) present at microtubule plus-ends binds Kar9, a cortex- associated protein, and promotes microtubule re-orientation and mitotic spindle alignment due to pulling forces exerted in actin filaments by the myosin Myo2 (Hwang et al., 2003). In migrating fibroblasts, microtubule contact with the cortex determines the site of polarization of the leading edge due to local activation of the Rho GTPase Rac1 (Fukata et al., 2002; Watanabe et al., 2004). Rac1 activates the actin-binding protein IQGAP1, which is either transported at the microtubule plus-ends together with CLIP-170 or accumulates at the cortex upon microtubule contact in a CLIP-170 dependent manner (Fukata et al., 2002). The formation of the tripartite complex of Rac1/IQGAP1/CLIP-170 at the leading edge stabilizes the microtubule cortex-association. Recently, a redundant mechanism to stabilize microtubules in the leading of motile fibroblasts has been reported (Lansbergen et al., 2006). The membrane-associated protein LL5β binds to CLASPs upon microtubule contact with the cortex. The accumulation of CLASPs promotes microtubule stabilization and actin remodeling at the leading edge of migrating cells (Lansbergen et al., 2006).

In *S. pombe* during interphase there are three to four bundles of microtubules in the cytoplasm, oriented along the long axis of the cell (Figure 1.3) (Drummond and Cross, 2000; Hoog et al., 2007). The bundles contain on average 4.4 microtubules, with lengths ranging 0.7 to 6 µm (Hoog et al., 2007). Interphase microtubules can nucleate from the SPB (Spindle Pole Body) and also from the iMTOCs (interphase Microtubule Organizing Centres). iMTOCs include the nuclear surface and microtubules themselves (Sawin and Tran, 2006). In interphase, the minus-ends of microtubules are generally bundled at the cell centre, leading to an antiparallel and symmetrical microtubule array (Drummond and Cross, 2000). Proper microtubule organization requires Klp2 and Ase1 (Janson et al., 2007). Klp2 is a minus end-directed kinesin-14 motor and Ase1 is an *S. pombe* homolog of the conserved ASE1/PRC1/MAP65 family of microtubule bundling proteins found at the spindle midzone during mitosis (Carazo-Salas et al., 2005; Loiodice et al., 2005). The kinesin Klp2 was shown to slide short microtubules, with the plus-ends oriented towards the cell end, to the bundling area (Carazo-Salas et al., 2005). Antiparallel microtubules are then bundled by Ase1, which cross-links the minus-ends of adjacent microtubules (Janson et al., 2007).

Microtubules plus-ends grow towards the cell ends at a fixed rate until they reach the cell tips, where they slow down (Drummond and Cross, 2000). Upon contact with the cell tip, microtubules pause briefly (between 100 sec and 200 sec) and then initiate catastrophe and shrinkage (Drummond and Cross, 2000). Within a microtubule bundle, only single microtubules contact the cell membrane at a given time (Hoog et al., 2007).

Interestingly, once the cell axis is established, microtubules are not necessary either for cell growth or cell polarity maintenance in *S. pombe* (Sawin et al., 2004). However, during cell polarity establishment, microtubules play a role in defining the growth axis correctly. After cell depolarization, correct polarity reestablishment requires one of two things: either presence of a cortical landmark at the cell tips or microtubules growing, contacting the cell tip and depositing polarity factors at the cell tip (Minc et al., 2009; Piel and Tran, 2009; Sawin and Snaith, 2004; Terenna et al., 2008).

1.3. Tea1 is a key regulator of cell polarity in S. pombe

In *S. pombe*, Tea1 is the key protein linking cell polarity and microtubules.

Tea1 is an 1147 amino acid protein with six N-terminal kelch repeats (aa 78 to aa 370) and a largely alpha-helical coiled-coil C-terminus (aa 609 to aa 1106) (Figure 1.4). The Kelch

repeats and the coiled-coils are common structural features in proteins. Kelch repeats were first identified in the *Drosophila* Kelch protein and consist of four to seven domain repeats, between aa 44 to aa 56 in length. The conserved sequence consists of four hydrophobic residues followed by two glycines and then two aromatic amino acids. The domains fold into a flat β-propeller structure, where each individual domain is a blade of the propeller. Although kelch repeats have very little sequence similarity, they can be found in a wide range of organisms and in proteins playing different functions in the cell (Adams et al., 2000).

Alpha helical coiled-coils are characterized by repetitive units of seven amino-acid. Usually the amino acids in each helix are named *abcdefg* where amino acids *a* and *d* are hydrophobic and amino acids *e* and *g* are polar. When this sequence forms an α-helix, all the hydrophobic amino acids face the same side and the polar amino acids face the other, forming an amphipathic structure. This structure can then interact with other protein domains, either in an inter or intra molecular fashion (Mason and Arndt, 2004). The presence of kelch repeats and extended regions of coiled-coil make it extremely likely that Tea1 has multiple binding partners.

The region between the N-terminal Kelch repeats and C-terminal coiled-coil domains of Tea1 is mainly composed of regions of intrinsic disorder (Dyson and Wright, 2005). The biological role of this Tea1 region is not experimentally characterized and will be further discussed in this thesis.

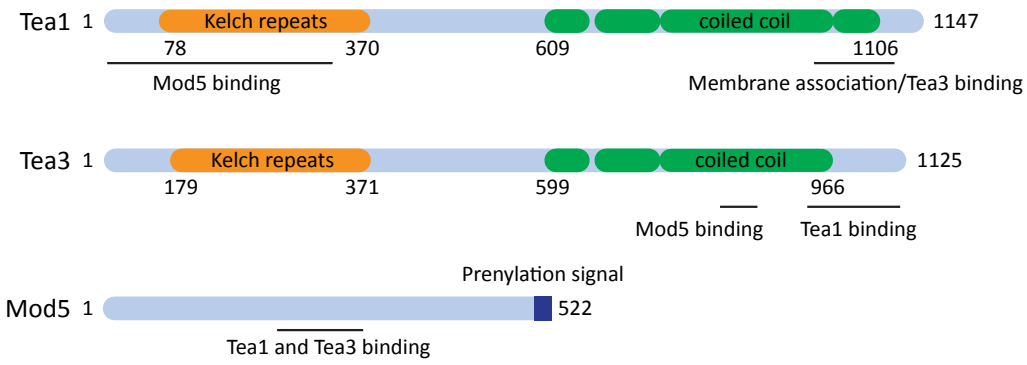

Figure 1.4- Tea1, Tea3 and Mod5 domains. Tea1 and Tea3 share a similar protein structure, with N-terminal Kelch repeats and C-terminal coiled-coil domains. Mod5 is an unstructured protein with a prenylation signal at its C-terminus. Adapted from (Snaith et al., 2005).

Tea1 sequence homologues can be found in all the other yeasts. The protein with highest homology is from *Schizosaccharomyces octosporus*, the closest evolutionarily related yeast to *S. pombe*. Among the experimentally characterized homologues are the *S. cerevisiae* proteins, Kel1 and Kel2. These two proteins were shown to be involved in cell morphogenesis and polarity. Contrary to Tea1, Kel1 and Kel2 play a direct role in the actin cytoskeleton organization (Philips and Herskowitz, 1998). Recently, a Tea1 homologue was characterized in *Aspergillus nidulans* (*A. nidulans*) and named TeaA. It was shown that in *A. nidulan* TeaA is involved in the determination of the growth directionality (Takeshita et al., 2008). Tea1 and its functions in cell polarity are conserved among fungi.

Tea1 was first identified in a screen for cell shape defects (Snell and Nurse, 1994). Under a range of stress conditions, *tea1Δ* mutants form an ectopic site of growth in the medial region of the cell (Sawin and Snaith, 2004; Tatebe et al., 2005). Moreover, Tea1 mutants do not undergo NETO and show monopolar growth throughout the cell cycle (Mata and Nurse, 1997; Snell and Nurse, 1994). Mata and Nurse showed that Tea1 localizes both on the microtubules and also at cell tips. In addition, Tea1 localization to the cell tips is microtubule-dependent (Mata and Nurse, 1997). It was later shown that Tea1 targeting to the cell tip is an extremely dynamic process. Tea1 is transported at the plus-end of growing microtubules in association with other microtubule-associated proteins (Behrens and Nurse, 2002; Feierbach et al., 2004; Snaith and Sawin, 2003). Upon microtubule contact with the cell end, Tea1 is deposited onto the cell cortex and subsequently anchored (Behrens and Nurse, 2002; Feierbach et al., 2004; Snaith and Sawin, 2003). Once at the cell tip, Tea1 plays its role in activating remodeling of the actin cytoskeleton and therefore in promoting directional cell growth (Martin, 2009).

During Tea1 travel from the cytoplasm, on the microtubule lattice and microtubule plus-ends and finally to the cell membrane, Tea1 interacts with a large number of experimentally characterized proteins (Martin, 2009). The formation of several Tea1-containing complexes was confirmed when Feierbach et al showed the presence of Tea1 in several protein complexes with 12S, 20S, 45S and 75S in sucrose gradients (Feierbach et al., 2004). These observations have suggested that Tea1 interacts with distinct sets of proteins at the microtubules and at the cell membrane (Figure 1.5) (Fischer et al., 2008; La Carbona et al., 2006; Martin, 2009).

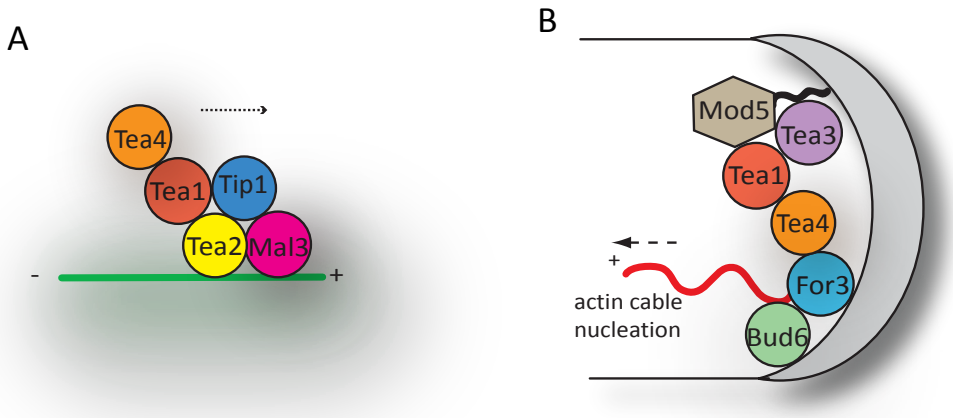

Figure 1.5- Tea1 interacts with several proteins during its travel from the cytoplasm to the cell tip. A) Tea1 binding partners at microtubule plus-ends. Tea1 and Tea4 are transported along the microtubule lattice to the microtubule plus-ends in association with the kinesin Tea2. Tea2 binds Tip1 and Mal3 directly. **B) Tea1 binding partners at the cell tip.** Tea1 anchoring at the cell tip is dependent on the membrane-associated protein Mod5. Tea1, Tea3 and Mod5 bind in a pair-wise manner, independently of the third protein. Tea4 links Tea1-For3 interaction, required for For3 activation and consequent actin cable nucleation. Bud6 relieves For3 auto-inhibition and promotes its tethering to the cell membrane.

1.3.1. Tea1 transport on microtubule plus-ends

Tea1 transport on the microtubules plus-ends is dependent on the microtubule associated-proteins Tea2 (Kip2 homologue), Mal3 (EB1 homologue) and Tip1 (CLIP-170 homologue) (Brunner and Nurse, 2000; Busch and Brunner, 2004; Busch et al., 2004). Mal3 is required to promote the association of the Tip1-Tea1 complex with the microtubule plus-ends (Browning et al., 2003; Busch and Brunner, 2004; Busch et al., 2004).

From cellular and molecular studies it was established that Mal3 tracks microtubules plus-ends independently of the other +TIPs (Bieling et al., 2007; Busch and Brunner, 2004). Mal3 localizes at the microtubule lattice and at the plus-end, both *in vivo* and *in vitro*. The observation that Mal3 association with the microtubules is essential to recruit Tea2-Tip1 to the microtubule plus-ends suggested that Mal3 maintains microtubule growth by providing a binding local for the other +TIPs (Browning et al., 2003; Busch and Brunner, 2004; Sandblad et al., 2006) (Bieling et al., 2007; Busch et al., 2004). *mal3Δ* mutants present shorter microtubules due to increased cytoplasmic catastrophe events. Since microtubules

contacts with the cell tip are less frequent in *mal3Δ* mutants, Tea1 is less frequently delivered to the cell tip, resulting in cell shape defects (Busch and Brunner, 2004).

Tip1 and Tea2 physically interact and move together along the microtubule lattice. The two proteins accumulate at the microtubule plus-ends and are transferred to the cell tip together with Tea1 (Browning et al., 2003; Brunner and Nurse, 2000; Busch and Brunner, 2004; Busch et al., 2004). In *tip1Δ* mutants, microtubules are shorter due to catastrophe upon contact with the cell cortex, which suggested that Tip1 is needed to restrict microtubule catastrophe to the cell tip (Brunner and Nurse, 2000). In *tea2Δ* mutants, microtubules are also shorter. This suggested that Tea2 might be involved in the regulation of microtubule dynamics probably by moving Tip1 and Tea1 along the lattice to the plus-ends (Browning et al., 2003). Although in *tea2Δ* mutant Tea1 does not move along microtubules, it can still bind microtubules (Browning et al., 2003).

Tea1 might not only be transported by microtubules but also have a role in the regulation of their dynamics. It has been shown that in *tea1Δ* mutants a small percentage of microtubules curl around the cell ends (Behrens and Nurse, 2002; Mata and Nurse, 1997; Snaith and Sawin, 2003). Moreover, Tea1 overexpressing cells have shorter microtubules (Mata and Nurse, 1997). Behrens and Nurse shown that the role of Tea1 in microtubules dynamics seems to be independent of its role in cell polarity (Behrens and Nurse, 2002). The *tea1Δ200* protein, in which the C-terminus 200 aa are removed, does not accumulate at the cell tip but continues to bind to microtubules. Although the *tea1Δ200* mutant does not have any microtubule dynamics defects, it does not correctly establish the cell polarity axis (Behrens and Nurse, 2002). This evidence indicates that Tea1 affects microtubule stability directly and not via anchoring microtubules to the cell membrane.

1.3.2. Mod5 is the molecular anchor of Tea1 at the cell tip

Once microtubules contact the cell tip and pause, Tea1 has the opportunity to be deposited and subsequently anchored. One of the most intriguing questions in the field is how Tea1 gets transferred from the microtubule plus-ends to the cell membrane. Mod5, and to a lesser extent Tea3, are critical components on Tea1 anchoring process.

Snaith and Sawin identified Mod5 as the membrane protein, localized at the cell tips, responsible for receiving Tea1 from the microtubules (Snaith and Sawin, 2003). It is a serine-proline rich unstructured protein, with a prenylation signal in its C-terminal (CAAX is

a cysteine, two aliphatic amino acids and X any amino acid). Prenylation is a posttranslational modification where isoprenoid groups are covalently bound to proteins. Isoprenoid chains with 15-carbon (farnesyl) or 20-carbon (geranylgeranyl) form a covalent thioester bound to a cysteine. The reaction is catalyzed by a farnesyltransferase (farnesyl) or by a geranylgeranyltransferase I (geranylgeranyl) (Resh, 2006). Prenylation, like other lipid-based posttranslational modifications, allows proteins to interact with the membrane, either in a reversible or irreversible reaction. Mutation of the cysteine to a serine in the CAAX box of Mod5 delocalizes Mod5 from the membrane. *mod5Δ*CAAX localizes at the microtubule plus-ends, and moves together with Tea1 (Snaith and Sawin, 2003)(H. Snaith, personal communication).

In *tea1Δ*, Mod5 is no longer restricted to the cell tip and instead spreads all over the cell cortex (Snaith and Sawin, 2003). Interestingly, Tea1 localization at the cell tips is also Mod5-dependent. In *mod5Δ* mutants, Tea1 does not accumulate at the cell tip and it is seen increased at the microtubule plus-ends. In *mod5Δ* cells, Tea1 is delivered to the cell tip at the same rate as in wild-type, and contacts with the cell tip during the length of time spent by the microtubule pausing (Snaith and Sawin, 2003). However, in *mod5Δ* cells, Tea1 is not productively anchored at the cell tip. The co-dependency in localization of Tea1 and Mod5 proteins lead to the proposal of a positive feedback loop model, in which the increase of one of the proteins in the cell tip positively recruits more of the other protein to the same localization (Figure 1.6) (Snaith and Sawin, 2003).

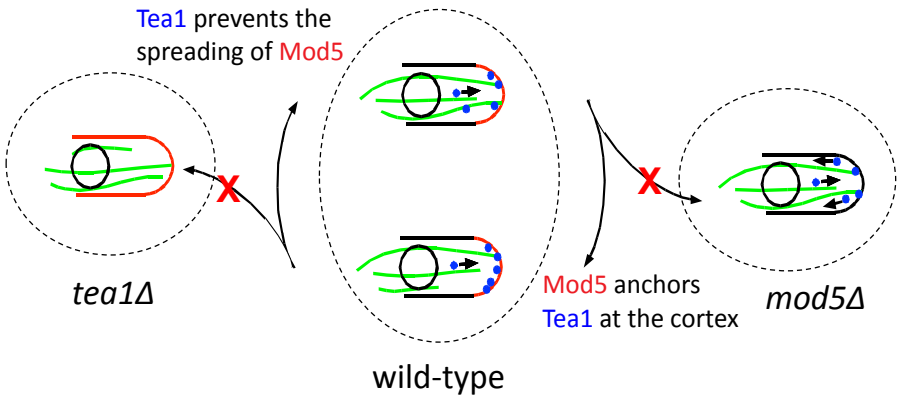

Figure 1.6- Tea1 and Mod5 localization is co-dependent. Cartoon representing Tea1 and Mod5 localizations in wild-type and in *mod5Δ* and *tea1Δ* cells. In wild-type, Tea1 binds Mod5 upon microtubule-based delivery to the cell tip. The positive anchoring of Tea1 recruits more membrane-associated Mod5 to the cell tip, and as a consequence when newly Tea1 arrives it binds Mod5 recruited to the cell tip. Tea1 is represented in blue, Mod5 in red and microtubules in green.

In a yeast two-hybrid screen, Snaith et al identified Tea3 as a Mod5 interacting protein, together with Tea1 (Snaith et al., 2005). Tea3 has high homology with Tea1 and shares a similar domain structure (Figure 1.4) (Arellano et al., 2002). Tea3 localizes at the cell tip in a microtubule-dependent manner and *tea3Δ* mutants present defects in activating growth in the new end (Arellano et al., 2002).

Tea1 and Tea3 physically interact via their C-terminal coiled-coils (Figure 1.4). At the non-growing cell tip of *tea3Δ* mutants there is less Tea1 accumulation, and Tea1 is more rapidly lost upon microtubule depolymerization. Therefore, Tea3 is necessary for correct anchoring of Tea1 to the non-growing tip (Snaith et al., 2005). In *tea1Δ*, Tea3 localizes as foci around the cell membrane, with a pattern similar to Mod5, which strongly supports the interpretation that a Tea3-Mod5 cortical interaction is Tea1-independent (Snaith et al., 2005). However, the Tea3-Tea1 interaction bypasses Mod5, as in *mod5*Δ Tea3 is no longer at the cell tip and instead is co-transported with Tea1 on microtubules plus-ends. Nevertheless, Tea3 is necessary for Mod5 restriction to the cell tip. In *tea3Δ*, although Mod5 accumulates at the cell tip, Mod5 is spread in a wider region than in wild-type cells (Snaith and Sawin, 2003). Both Tea3 and Mod5 are cortically-associated and are involved in Tea1 anchoring process. However, from genetic analysis, protein localization and protein interaction studies it seems that the two proteins work in a parallel mode to ensure the correct cortical anchoring of Tea1 (Snaith et al., 2005).

Snaith et al showed that Tea1, Tea3 and Mod5 all physically interact in a pair wise manner, independently of the third protein (Figure 1.4). This observation has made it difficult to understand the individual role of each protein in the anchoring process of Tea1. Mapping of Mod5 functional regions showed that amino acids 156 to 256 of Mod5 are necessary for its restriction at the cell tip, but not for its binding to the cell membrane. It was also demonstrated that amino acids 156 to 256 of Mod5 are necessary for the localization of both Tea1 and Tea3 at the cell tip. Moreover, it was shown by yeast two-hybrid that Tea3 binds Mod5 within amino acids 156 and 256, and that *mod5Δ(156-256)* does not co-immunoprecipitate Tea1. Therefore, it could not be distinguished if the lack of accumulation of *mod5Δ*(156-256) at the cell tip is directly due to its failure to bind Tea1, Tea3 or to both (Snaith et al., 2005). Although both Tea1 and Tea3 bind to Mod5 in the same region, the binding mechanisms are possibly different because the two proteins bind Mod5 via distinct domains. Tea1 binds Mod5 via the N-terminal Kelch repeats and Tea3 via its coiled-coils at the C-terminal. It remains unknown if Tea1 and Tea3 compete to bind to

Mod5 or if the two proteins bind Mod5 simultaneously. It would also be interesting to understand what are the roles of the three-way interaction for correct Tea1 anchoring, and as a consequence, for positioning of the polarity machinery (Snaith et al., 2005).

1.3.3. Tea1 binding-partners at the cell membrane

Once Tea1 is properly anchored at the cell membrane, it can interact with its downstream effectors and promote actin cytoskeleton remodeling via the formin For3 (Figure 1.5B). For3 is a large protein, with an actin binding domain (FH2), a profilin binding domain (FH1) and also the auto-inhibitory domains DID and DAD (Feierbach and Chang, 2001; Martin and Chang, 2006; Martin et al., 2007). For3 localizes as dots at the cell tip and at the septum, in an actin-dependent manner. For3 mutants have cell shape defects as well as polarity defects. For3 actin cable nucleation activity is tightly regulated by an auto-inhibitory relief mechanism, either by Bud6 or Cdc42 (Martin and Chang, 2006; Martin et al., 2007).

Bud6 was shown to bind Tea1 in a high molecular weight complex. Bud6 plays its role in cell polarity independently of both microtubules and the actin cytoskeleton (Feierbach et al., 2004). Bud6 is localized to the cell tip in a Tea1-dependent manner, where it binds to For3 (Martin and Chang, 2006). Bud6 not only activates the actin-nucleation activity of For3 by relieving its auto inhibition but also promotes For3 tethering at the cell membrane (Martin and Chang, 2006; Martin et al., 2007).

Although Tea1 activates actin cable nucleation via For3, For3 and Tea1 do not bind directly (Martin et al., 2005). A third protein, Tea4, bridges the interaction of Tea1 with For3 (Martin et al., 2005). Tea4 is an SH3-domain protein, with coiled-coil regions in the C-terminus. Tea4 directly interacts both with Tea1 and For3. Tea4 mutants are monopolar and fail to localize For3 at cell tips and to localize Tea1 at the growing cell tip (Martin et al., 2005; Tatebe et al., 2005). Tea4 co-localizes with Tea1 at the microtubule plus ends and at the cell tip. Together with Tea1, Tea4 functions as a linker between the microtubule cytoskeleton and the actin cytoskeleton (Martin et al., 2005; Tatebe et al., 2005).

Recently, Minc et al proposed a new pathway to accumulate polarity factors at the cell membrane, independently of Tea1 (Minc et al., 2009). When cells are forced to acquire a bent shape, the polarity factors known to accumulate at the cell tip are recruited to ectopic

sites at the cell cortex (Minc et al., 2009; Terenna et al., 2008). The accumulation requires microtubules, Mal3 and Moe1 (involved in translation and found to bind Mal3), and bypasses Tea1 in the recruitment of For3 and the actin based machinery (Minc et al., 2009). Although the ectopic sites are competent to accumulate all the components of the polarity machinery they fail to produce cell growth. It remains be to explained what is inhibiting cell growth from ectopic sites in such situation (Minc et al., 2009; Terenna et al., 2008).

1.3.4. Relationship between Tea1 and cell polarity protein kinases

Protein functions can be regulated by many different post-translational modifications. In the case of phosphorylation, a phosphate group is added to serine, threonine or tyrosine, transforming a neutrally-charged region of the protein into a charged region (Lehninger et al., 2000). Phosphorylation can lead to dramatic conformational changes of the protein, as in the classic example of glycogen phosphorylase. In this enzyme, phosphorylation of a single serine induces conformational changes that expose the catalytic site, making it accessible to the substrate (Serber and Ferrell, 2007). However, phosphorylation also affects protein-protein interactions without inducing conformational changes (Serber and Ferrell, 2007). The presence of phosphate in an active site can inhibit substrate binding or create a new epitope to bind to specific protein domains. Recently, multisite phosphorylation has been shown to be a robust and tunable mean of regulating protein-protein interactions (Guimaraes et al., 2008; Kim and Ferrell, 2007; Strickfaden et al., 2007).

Enzymes termed kinases catalyze the attachment of phosphate groups to substrates. Enzymes called phosphatases catalyze the inverse process of dephosphorylation. Both kinases and phosphatases recognize and bind to their substrates via specific amino acid sequences. For some evolutionarily conserved protein kinases, such as the CDKs (Cyclin-dependent kinases), it was possible to determine a consensus sequence that is recognized within the substrate (Ubersax and Ferrell, 2007). However, phospho-regulation is a complex process, as the same substrate residue can be potentially phosphorylated by more than one kinase, while some substrate residues need to have neighbouring residues phosphorylated to become phosphorylated themselves (Lehninger et al., 2000).

Several protein kinases and phosphatases specifically localized at the cell tip are involved in cell polarity (Alvarez-Tabares et al., 2007; Bahler and Pringle, 1998; Kim et al., 2003; Verde et al., 1998).

The Orb2 and Orb6 genes encode protein serine/threonine kinases, and Orb2 belongs to the family of conserved p21-activated kinases (PAK) (Qyang et al., 2002; Verde et al., 1998). Orb6 and Orb2/Pak1/Shk1 mutants are round (Snell and Nurse, 1994). Both Orb2 and Orb6 are essential, and the two proteins localize at the cell tip and at the septum (Loo and Balasubramanian, 2008; Qyang et al., 2002; Verde et al., 1998). It was shown that Orb6 acts downstream of Orb2 (Verde et al., 1998). Orb2 does not play a role in activating cell growth, but instead is required for the cell to recognize its ends as sites of growth (Sawin et al., 1999). Although Orb2 phosphorylates Tea1 *in vitro*, data *in vivo* suggests that Tea1 and Orb2 are not in the same pathway (Kim et al., 2003; Loo and Balasubramanian, 2008).

Pom1 is a dual specificity kinase for serine/threonine and tyrosine (Bahler and Pringle, 1998). Cell shape and polarity defects in *pom1Δ* are very similar to *tea1Δ*. Tea1 and Pom1 seem to act together in cell polarity, but both have additional functions (Bahler and Nurse, 2001; Bahler and Pringle, 1998). It has been shown that Pom1 forms a gradient across the cell membrane, being more concentrated at the cell tips (Celton-Morizur et al., 2006; Padte et al., 2006). The gradient of Pom1, together with Tea1 and Tea4, have been shown to inhibit the division-septum assembly at the cell tip (Huang et al., 2007). Recently two independent studies have reported that the gradient of Pom1 inhibits Cdr2 kinase at the cell middle and consequently inhibits the progression of cell cycle. Pom1 inhibition of Cdr2 links the cell size control with the cell cycle progression (Martin and Berthelot-Grosjean, 2009; Moseley et al., 2009).

Another Tea1 candidate kinase is the MAP kinase kinase kinase (MAPKKK) Win1 and its functional homologue Wis4 (Samejima et al., 1998; Tatebe et al., 2005). Win1 is part of the MAP kinase-signaling cascade that regulates cell responses to a wide range of cellular stresses (Samejima et al., 1998; Tatebe et al., 2005). Tea4 was shown to bind Wis1 directly *in vitro*, but not *in vivo* suggesting that Win1-Tea4 interaction is transient. MAPK mutants as well as *tea1Δ* and *tea4Δ* branch with high frequency under osmotic or temperature stresses. Under stress conditions, Tea1-Tea4 complex acts together with the stress-signaling MAPK cascade and contributes to the maintenance of the cell polarity (Tatebe et al., 2005).

Recently Dis2, one of two type 1 protein phosphatases (PP1) in *S. pombe*, was shown to have a role in cell growth. Dis2 localization at the cell tip is microtubule- and Tea1/Tea4/Tip1/Mal3-dependent. Dis1 interacts directly with Tea4 by binding its PP1 recruit motif (RVXF). However, it still unknown if Dis1 is directly involved in Tea1 cell polarity role (Alvarez-Tabares et al., 2007).

There is a variety of evidence for Tea1 phosphorylation. First, Niccoli and Nurse showed that a Tea1 band-shift seen in anti-Tea1 western-blots is eliminated when the sample is treated with lambda-phosphatase (Niccoli and Nurse, 2002). Second, Kim et al showed that Tea1 is a substrate of the protein kinase Orb2 *in vitro* (Kim et al., 2003). Third, the co-localization of Tea1 and the cell tip-associated kinases suggests that the interactions of Tea1 with its binding partners at the cell tip may be phospho-regulated. In addition, Tea1 phosphorylation could regulate its interactions at microtubule plus-ends. Phosphorylation has been shown to regulate the binding of several microtubule-associated proteins to microtubules. For example, the binding of APC and CLASPs to microtubules is regulated by the kinase GSK-3β (Glycogen synthase kinase-3β) (Akhmanova and Steinmetz, 2008).

Thus, although Tea1 plays a role in localization of protein kinases and protein phosphatases at the cell tip, it remains unclear how Tea1 interacts with these protein kinases and phosphatases and if any of the cell tip-localized kinases and phosphatases plays a role in Tea1 regulation.

1.4. Symmetry-breaking: Extrinsic, Intrinsic and stochastic cues

In this section I will describe the processes by which cells develop polarity. The transition from uniform to polarized distribution of cellular components is usually termed “symmetry-breaking” (Li and Bowerman, 2010; Li and Gundersen, 2008).

Cells polarize in response to extrinsic cues that change the external environment and require adaptation. Among such extrinsic cues are chemical gradients (chemotaxis), mechanical forces or environmental changes such as light or temperature (Iglesias and Devreotes, 2008).

During chemotaxis, chemical cues such as growth factors, chemokines or the yeast matting pheromones, are sensed at the cell membrane and trigger a network of interlinked

signals which feedback upon each other (Elion, 2000; King and Insall, 2009). As a response, the polarity machinery is oriented towards the source of the gradient. In migrating cells, such as leukocytes or the ameba *Dictyostelium discoideum*, directionality in movement requires the orientation of the polar machinery towards the leading edge, in opposition to the trailing end (Petrie et al., 2009). The orientation of the leading edge and persistence in movement is maintained by actin-rich protrusions or lamellipodia (Petrie et al., 2009).

Asymmetry can also be originated by internal cues, from the intrinsically polar cytoskeleton or due to pre-assembled cortical landmarks. The classic example of orientation towards a polarity landmark comes from the budding yeast *S. cerevisiae* (Slaughter et al., 2009). This spherical-shaped unicellular organism grows isotropically until it reaches a certain size in the G1 phase of the cell cycle. At this time the cells form a bud at the presumptive budding site, landmarked from the previous cell cycle. The landmark proteins function as a "spatial cell memory" and vary with the type of polarity to be established. Haploid cells have an axial polarity pattern that is landmarked by proteins such as Bud3, Bud4, Axl1 and Axl2 whereas diploid cells have a bipolar pattern marked by Bud7, Bud8, Bud9, Rax1 and Rax2 (Park and Bi, 2007). Deletion of any of these genes encoding for the cortical landmark leads to random cell axis establishment (Kang et al., 2001; Park and Bi, 2007). The selection of the asymmetry axis requires the association of the cortical marker Bud1/Rsr1 in relation to the landmark proteins. Rsr1/Bud1 is a Ras family GTPase whose activity is regulated by the GAP (GTP-activating proteins) Bud2 and by the GEF (Guanidine nucleotide exchange) Bud5. (Park and Bi, 2007). After the determination of the budding site the polarity machinery, containing the Rho GTPase Cdc42 and its regulatory proteins, is then recruited and the signal amplified and stabilized. Although Rsr1/Bud1 and the polarity landmarks are dispensable for growth, the recruitment of the polarity machinery is essential (Park and Bi, 2007).

In the fission yeast *S. pombe* the sites of growth are also landmarked. However, in comparision with the pre-assembled landmarks found in *S. cerevisiae*, in *S. pombe* landmark proteins are predominantly deposited at the cell membrane due to a microtubule based-transport (Behrens and Nurse, 2002; Feierbach et al., 2004; Snaith and Sawin, 2003).

The cytoskeletal polymers provide cues for symmetry-breaking because they are inherently polar, as a result of their head-to-tail oligomerization (Siegrist and Doe, 2007; Waterman-Storer et al., 1999). In addition, actin and microtubules polymerization is an

autocatalytic reaction, in which the product of the reaction is one of the reagents. Therefore cytoskeleton polymers can amplify their own signal and generate persistent asymmetry (Mullins, 2010). Although actin and microtubules are structurally and kinetically different, both are extremely dynamic polymers, which allows them to respond rapidly to polarity signals (Li and Gundersen, 2008). In fact, it has been shown that the microtubule dynamic instability at the leading-edge of fibroblasts locally activates the small GTPase Rac1 and consequently promotes actin polymerization and lamellipodial protrusion required for cell migration (Waterman-Storer et al., 1999). In addition to their roles in symmetry breaking, the cytoskeleton polymers provide oriented tracks for directed movement of cargo to the polar site once it was established (Hirokawa et al., 2009; Kardon and Vale, 2009). The overall mechanism of cell polarity establishment and maintenance requires a coordinated cross talk between actin and microtubules (Basu and Chang, 2007).

Until recently it has been accepted that cells would orient in response to either intrinsic or extrinsic stimuli. However, observations that cells could polarize in the absence of any spatial cues started to change that view. It has been observed for long time that *S. cerevisiae* could form buds at random locations without landmarks (Nern and Arkowitz, 2000; Shimada et al., 2000), that motile cells polarize even without strong gradients (Petrie et al., 2009) and that spherical neurons polarize their axon and dendrites *in vitro*, where no extracellular cues are present (Li and Bowerman, 2010; Witte and Bradke, 2008).

The most molecularly detailed model of symmetry breaking in the absence of a polarity cue comes from *S. cerevisiae*. As explained above, *S. cerevisiae* asymmetry depends on Cdc42 clustering around a landmark. However, in the absence of landmarks Cdc42 can spontaneously cluster at a random site at the cell membrane. Recently two redundant mechanisms for spontaneous symmetry breaking by Cdc42 in *S. cerevisiae* have been proposed: the first is actin-dependent (Wedlich-Soldner and Li, 2003) and the second is Bem1-dependent (Howell et al., 2009; Kozubowski et al., 2008). In the first mechanism, Cdc42 clustering depends on the stochastic fluctuation of the local concentrations of Cdc42 or actin at the cell membrane. The increase in the local concentration of one of the components recruits the other and works as a positive feedback to reinforce the signal (Marco et al., 2007; Wedlich-Soldner et al., 2003). Its is known that Cdc42 is necessary to activate actin polymerization and in turn the actin cytoskeleton delivers active Cdc42-GTP to the membrane and recycles back inactive Cdc42-GDP to the cytoplasmic pool (Marco et

al., 2007; Wedlich-Soldner et al., 2003). In the second mechanism the membrane clustering of Cdc42 is mediated by the scaffold protein Bem1 (Goryachev and Pokhilko, 2008; Howell et al., 2009; Kozubowski et al., 2008). In this mechanism, Bem1 recruits Cdc24, the only Cdc42 GEF in *S. cerevisiae*, and promotes Cdc42-GTP local activation. The small fluctuations in the local concentration of active Cdc42-GTP promote a positive feedback loop in the recruitment of Bem1 and Cdc24 (Goryachev and Pokhilko, 2008; Howell et al., 2009; Kozubowski et al., 2008).

The polarization of Cdc42 without spatial and temporal cues suggests that establishment and maintenance of cell polarity is likely self-organized (Altschuler et al., 2008; Kozubowski et al., 2008; Wedlich-Soldner et al., 2003). In the context of cell biology, self-organization is the ability of a macromolecular complex or organelle to determine its own architectural and functional features based on interactions among its components (Misteli, 2001; Rafelski and Marshall, 2008). Self-organized structures are at states of non-equilibrium and exhibit oscillatory behaviors due to energy dissipation (Karsenti, 2008; Misteli, 2001). Thus, the intrinsically dynamic properties of self-organization of Cdc42 clustering serve the establishment of cell polarity in *S. cerevisiae* with the necessary flexibility to respond to changes and robustness to fluctuations in the interactions of its components (Park et al., 2009).

The molecular mechanisms of cell polarity establishment and maintenance described for *S. pombe* share characteristics with other examples in higher-eukaryotes (Siegrist and Doe, 2007). In *S. pombe,* symmetry breaking occurs due to the continuous microtubule-based delivery of the landmark protein, Tea1, to the cell cortex. Although some of the proteins involved in Tea1 transport along microtubules and plus-end are well characterized, little is known about Tea1-microtubule association and its role in regulation of microtubule dynamics. In addition, it is known that Tea1 can associate in protein complexes within a range of molecular weights and interact with several binding-partners. However, the regulation of Tea1 interaction with such a diverse set of proteins is still far from being understood. Moreover, despite it being known that Mod5 and, to a lesser extent Tea3, are required for Tea1 cortical anchoring, the molecular mechanisms of Tea1 anchoring are yet to be uncovered. In addition, we still do not understand how the frequent delivery and anchoring of Tea1 promotes its role in cell polarity establishment and maintenance.

Project aims

During my PhD I was interested in understanding the molecular mechanisms of Tea1 anchoring to the cell tip upon its transference from the microtubule plus-ends to the cell membrane. In order to achieve my goals, the work presented in this thesis was divided in three different approaches that cover several aspects of Tea1 anchoring mechanism.

First, Chapter III uses a combination of FRAP, quantitative live-cell imaging and mathematical modeling to understand how the Tea1-Mod5 interaction contributes mechanistically to generate a stable cortical landmark. Second, Chapter IV describes the identification of Tea1 phosphorylated residues, using large-scale protein purification followed by mass spectroscopy, and the role of phosphorylation in dissociation of Tea1 from the cell tip. Third, Chapter V describes the development of a robust SILAC method for *S. pombe*. Finally, Chapter VI describes a systematic mutagenic analysis of Mod5 designed to separate the roles of Tea1, Tea3 and Mod5 in cell polarity.

Chapter II: Material and Methods

2.1. Strains, media and genetic methods

Schizosaccharomyces pombe strains used in this study were grown in yeast extract medium (YE5S) or in Edinburgh minimal medium (EMM2). YE5S medium contains 0.5% (w/v) Difco Yeast Extract, 3.0% (w/v) glucose, 250 mg/l adenine, leucine, histidine, lysine hydrochloride, and uracil. Where 4x applies to all ingredients. In some experiments, 4x YE5S was used to grow cells to higher densities. All components in 4xYE5S, including supplements, are increased by a factor of four. EMM2 medium contains NH_4Cl (2.2 g/l) or L-glutamic acid monosodium salt (3.75 g/l), 14.7 mM potassium hydrogenphthalate, 15.5 mM Na_2HPO_4, 2% glucose, 1 X salts (50 X stock solution: 52.5 g/l $MgCl_2 \bullet 6H_2O$, 0.735 mg/l $CaCl_2 \bullet 2H_2O$, 50 g/l KCl, 2 g/l Na_2SO_4), 1 X vitamins (1000 X stock: 1 g/l pantothenic acid, 10 g/l nicotinic acid, 10 mg/l biotin) and 1 X minerals (10,000 X stock:5 g/l boric acid, 4 g/l $MnSO_4$, 4 g/l $ZnSO_4 \bullet 7H_2O$, 2 g/l $FeCl_2 \bullet 6H_2O$, 0.4 g/l molybdic acid, 1 g/l KI, 0.4 g/l $CuSO_4 \bullet 5H_2O$ and 10 g/l citric acid, plus with appropriate supplements. Solid agar plates are made by adding 2% Difco Bacto agar to the media.

2.2 Genetic crosses

Freshly-grown cells of the strains to be crossed were mixed in 10 µl of distilled water and spotted onto SPA plates (30 g/l glucose, 5 g/l KH_2PO_4, 2% Difco Bacto agar, 1x vitamins plus appropriate supplements). Plates were incubated at 25˚C for 2 O/N to form asci. Asci were streaked in YE5S plates and placed at 32˚C for 1 hr to allow the ascus walls to break down. A Singer dissector was used to separate tetrads from a single cross and the plates placed at a suitable temperature to allow the spores to germinate (32˚C for non-temperature sensitive strains and 25˚C for temperature-sensitive strains). Once colonies appeared, the donor plate was replicated onto selective media to allow identification of specific genotypes.

Random spore analysis was used in place of tetrad analysis for constructing strains where a large number of spores were to be analyzed. 6 µl of Helicase (*Helix pomatia* juice, Life technologies) were diluted in 400 µl of sterile distilled water, and a small amount of

crossed strains was added. The mixture was incubated at 32˚C O/N to digest the ascus and vegetative cell walls. Spore number was counted using a haematocytometer and diluted appropriately in sterile distilled water. The samples were sonicated to separate spores and to prevent the appearance of colonies with mixed genotypes. Spores were plated in YE5S plates at a density of 200-1000 per plate.

2.3. Growth of E. coli strains

All bacterial strains were grown at 37°C on Luria-Bertani broth (10 g/l Difco Bacto tryptone, 5 g/l Difco Bacto yeast extract, 5 g/l NaCl, pH 7.2). For general cloning, XL1-Blue (Stratagene) strain was used, and for Gateway cloning the TOP10 (Invitrogen) strain was used. BL21- CodonPlus® RIL competent *E. coli* cells (Stratagene, USA) were used to express recombinant proteins. BL21- CodonPlus® expresses *argU*, *ileY*, *leuW* tRNA genes from a pACYC based plasmid, and provides extra copies of rare tRNAs which frequently limit translation during high-level expression; expression of T7 phage RNA polymerase is driven by the lacUV5 promoter in response to IPTG (Isopropyl β-D-1-thiogalactopyranoside).

2.4. Preparation of chemically competent cells

Single colonies were used to inoculate 5 ml of LB culture which was grown O/N at 37°C. The resultant stationary phase culture was used to inoculate 500 ml of LB, and grown to OD_{600} 0.5. The culture was incubated on ice for 10 min and centrifuged at 2400 rpm at 4°C for 15 min. The pellet re-suspended in 165 ml of 100 mM RbCl, 50 mM $MnCl_2$, 30 mM potassium acetate, 10 mM $CaCl_2$, 15% (v/v) glycerol, pH 5.8 and incubated on ice for 45 min. Cells were then spun at 2400 rpm at 4°C for 15 min and re-suspended in 40 ml of 10 mM MOPS, 10 mM $RbCl_2$, 75 mM $CaCl_2$, 15% (v/v) glycerol, pH 6.8 and incubated on ice for further 15 min. Aliquots of 200 µl were transferred to a screw-cap tubes, and then frozen in liquid nitrogen and stored at -80°C.

2.5. Transformation of E. coli

200 µl aliquots of frozen competent cells were thawed on ice. 50 – 200 ng of DNA was added to the cells and incubated on ice for 20 min. Cells were incubated at 42°C for 60 sec,

and then were incubated on ice for 2 min. 1 ml of SOC medium (20 g/l Difco Bacto tryptone, 5 g/l Difco Bacto yeast extract, 10 mM NaCl, 2.5 mM KCl, 10 mM $MgCl_2$, 10 mM $MgSO_4$, 20mM glucose) was then added to the cells and incubated with agitation at 37°C for 1 hr. Cells were then centrifuged at 13,000 rpm for 30 sec at RT. Pellet was re-suspended in 200 µl of SOC, and plated in LB-agar plates containing 100 µg/ml of the appropriate antibiotic. Plates were incubated O/N at 37°C.

2.6. Gateway® cloning

The Gateway® cloning technology (Invitrogen) is based on site-specific recombination system used by bacteriophage lambda to integrate DNA into *E. coli* chromosomes. Both phage and *E.coli* DNA contain specific recombination sites, *attP* and *at*tB respectively. Following integration into the bacteria, recombination occurs between *attB* and *attP* sites to generate *attL* and *attR. In vitro*, recombination is catalyzed by the BP clonase enzyme, and the inverse reaction is catalyzed by the LR clonase.

2.6.1 Construction of pDONR Entry clones: Generation of PCR product containing attB1/2-flanking sites

Amplification of DNA containing flanking *attB*1/2 sites required oligonucleotides covering 31 bp of *attB1/2* sequence and ~20 bp of template specific sequence. In order to avoid the use of long (> 50bp) oligonucleotide primers a two-step amplification strategy was used. In step 2 of the amplification reaction, 10 µl of the reaction from the first step were used as well as 40 pmoles of each adaptor primer, OKS1203 and OKS1217. Cycling parameters for the second step were set as follows: 1] 98°C for 30 sec; 2] 98°C for 10 sec; 3] 45°C for 30 sec; 4] 72°C for 20 sec; 5] repeat steps 2 to 4 five times; 6] 98°C for 10 sec; 7] 55°C for 30 sec; 8] 72°C for 20 sec; 9] repeat steps 6 to 8 20 times; 72˚C for 10 min.

2.6.2. BP recombination reaction

Gateway™ BP Clonase™ II enzyme mix was supplied by Invitrogen (USA). The reaction mix contained 50 fmoles of *attB1/2* flanked PCR product and 50 fmoles of pDONR™221 Donor vector and 2 µl BP Clonase™ II enzyme mix in a final reaction volume of 10 µl. The

recombination mix was incubated O/N at RT. The reaction was stopped by adding 1 µl of Proteinase K (Invitrogen) and incubating the mix at 37°C for 1 hr. 5 µl of the reaction was then transformed into TOP10 *E.coli* cells, and the transformed cells were plated onto LB-agar plus kanamycin. Plasmids were isolated and sequenced using appropriated oligonucleotides.

2.6.3. LR recombination reaction

Gateway™ LR Clonase™ II enzyme mix was supplied by Invitrogen (USA). The 10 µl reaction mix was prepared as follows: 150 ng of pDONR™221 containing the insert of interest flanked by *attL1/2* sites, 150 ng of Destination vector containing *attR1/2* sites, 2 µl of LR Clonase™ II enzyme mix, plus sterile distilled water to 10µl. Reactions were incubated O/N at RT. 2 µl of Proteinase K were added to the mixture and incubated for 1 hr at 37°C. 10 µl of the reaction mix was then transformed into TOP10 chemically competent *E. coli* (Invitrogen, USA), which were plated onto LB agar plus ampicilin.

2.7. DNA Sequencing

DNA sequencing was carried out on in-house ABI 3730 capillary sequencing instruments (Applied Biosystems, USA). The sequencing reaction contained 100-250 ng of DNA, 3.2 pmol of oligonucleotide, 2 µl BigDye Terminator 3.1 (Applied Biosystems), 2 µl 5x sequencing buffer (Applied Biosystems) in a final volume of 10 µl. The sequencing reaction was performed as follows: 1] 30 sec at 96˚C, 2] 15 sec at 50˚C, 3] 4 min at 60˚C, 4] repeat steps 1 to 3 25 times. Sequencing samples were sent to the University of Edinburgh sequencing service. Digital output file of the DNA sequence was then further analyzed using Seqman sequence analysis software (DNASTAR Inc.)

2.8. Strain construction using the PCR-based tagging method

N- and C- terminal tagging as well as gene deletions were created using a PCR based method, described in Bahler et al 1996. Oligonucleotides with 80 bp homology to the gene of interest were used to amplify a region of a plasmid that contains: the sequence for antibiotic resistance (kanamycin, hygromycin or nourseothricin), in case of gene tagging or

the *ura4+* gene is case of gene deletion; and the sequence of the tagging gene. Table 2.1 describes all the strains constructed using this method as well as the oligonucleotides used and the template plasmids.

50 µl PCR reactions were prepared as follows: distilled water to 50 µl, 20 ng of plasmid template DNA, 5 µl Buffer IV (10 x stock: 750 mM Tris-HCl pH8.8, 200 mM $(NH_4)_2SO_4$, 0.1% Tween 20), 2.5 µl of 10 mM dNTPs, 7 µl of 25 mM $MgCl_2$, 0.1 µl of each oligonucleotide (100 µM stock), 0.4 units Taq polymerase (Sawin Laboratory), 7.6 units Pwo polymerase (Sawin Laboratory). The PCR program used was as follows: 1] 2 min at 95˚C, 2] 15 sec at 95˚C, 3] 30 sec at 55˚C, 4] 7 min at 72˚C, 5] repeat steps 2-4 29 times, 6] 5 min at 72˚C. 0.5 µl of the PCR reaction was run on a 1% agarose gel to confirm the reaction was successful. The DNA was then cleaned up using phenol/chloroform/ isoamyl alcohol (PCI). 0.5 ml of PCI solution (25:24:1) was added to an equal amount volume of PCR product, vortexed, centrifuged for 5 min at 13,000 rpm and the supernatant recovered. This step was repeated first with PCI and then with chloroform alone. One-tenth volume 3 M NaOAc pH 5.2 and two volumes of ethanol were added to the final recovered supernatant. This mixture was then centrifuged at 4˚C for 10 min at 13,000 rpm. The pellet was washed with 1 ml 70% ethanol and centrifuged for 5 min at 13,000 rpm. The pellet was then air-dried and resuspended in TE (10 mM Tris-HCl pH 7.5, 1 mM EDTA). Samples of the purified DNA were run on an agarose gel to estimate DNA concentration.

The DNA cassettes were then transformed into yeast. Cultures were grown to mid-exponential phase, with 20 ml of culture used per transformation. Cells were harvested by centrifugation for 4 min at 4000 rpm. The cells were then washed in an equal volume of sterile distilled water, spun again before being resuspended in 1 ml of 100 mM LiOAc pH 7.5/ TE. The cells were centrifuged for 1 min at 13,000 rpm, resuspended in 50 µl of 100 mM LiOAc pH 7.5/ TE. ~20 µg of purified PCR product was added per transformation and incubated for 10 min at RT. 260 µl of freshly prepared 40% PEG3350/100 mM LiOAc pH 7.5/ TE was added and gently pipetted to mix before incubating at RT for 30 min. 43 µl of DMSO was then added and the cells heat shocked for 5 min at 42˚C. Cells were centrifuged for 1 min at 13,000 rpm and washed with 1 ml of sterile distilled water. Finally, cells were resuspended in 400 µl sterile distilled water and plated to two YE5S plates, in case of gene tagging, or to two plates of EMM minus uracil, in case of gene deletion. Plates were

incubated O/N at 32˚C, replica plated to YE5S plates supplemented with the appropriate antibiotic (G418, Hygromycin or Nourseothicin, 100 µg/ml) and grown for 2 days. The cells were then replica plated a second time to fresh YE5S/antibiotic plates and incubated O/N. Colonies were streaked to YE5S, incubated for 2 days and then replica plated to YE5S/antibiotic plates to check stable integration.

Table 2.1- List of strains constructed using the PCR based method. The list includes the template plasmid, the oligonucleotides used and the parent strain.

Strain name	Plasmid	Oligonucleotides (FW/REV)	Parent strain
KS3138	pKS393	OKS222/OKS223	KS516
KS3626	pKS108	OKS1261/OKS1262	KS1826
KS4524	pKS715	OKS172/OKS196	KS3892
KS4526	pKS715	OKS172/OKS196	KS3755
KS4528	pKS715	OKS172/OKS196	KS3756
KS5566	pKS112	OKS2026/OKS2027	KS516
KS5655	pKS131	OKS2046/OKS2047	KS1260

2.9. Colony PCR

Colony PCR was used to check that the cassettes had integrated at the correct position in the genome and to prepare genomic DNA for sequencing. To confirm the correct position in the genome one oligonucleotide within a primer pair contained homology to the resistance gene in the cassette and the other contained homology to the 3' region of the tagged gene, in case of C-terminal tagging, or to the 5' region, in case of N-terminal tagging. DNA was prepared from freshly grown cells (1 day old). A pinhead amount (1-2 µl) of cells was added to 25 µl of 0.25% SDS/TE. The cells were boiled for 5 min, centrifuged to pellet cell debris and the supernatant retained. 25 µl PCR reactions were prepared as follows: sterile distilled water to 25 µl, 1 µl DNA, 2.5 µl Buffer IV, 0.5 µl of 10 mM dNTPs, 1.5 µl of 25 mM $MgCl_2$, 1.25 µl of 20% Triton X-100, 0.125 µl each of forward and reverse oligonucleotide (100 µM stock), 5 units Taq polymerase (Sawin Laboratory), 0.075 units Pwo polymerase (Sawin Laboratory). See Table 2.1 for oligonucleotide list used to test each strain. The PCR program used was as follows: 1] 2 min at 94˚C, 2] 30 sec at 94˚C, 3] 30 sec at 47˚C, 4] 3.5 min at 68˚C, 5] repeat steps 2-4 34 times, 6] 10 min at 68˚C. 5µl of the PCR reaction were run on a 1% agarose gel to confirm the DNA fragment size.

2.10. Construction of mod5-155 to mod5-256 mutant strains

Amino acids 155 to 256 of Mod5 were sequentially substituted in blocks of five amino acids by the linker sequence *Ala-Gly-Ser-Ala-Gly* (GCTGGTTCAGCAGGA). Figure 2.1 summarizes the "mega-primer PCR" approach used to construct the 20 Mod5 alleles. To construct each Mod5 allele, two PCR products were generated: PCR product *A* contained the 5' end of the gene and the linker sequence in the 5' end. The forward oligonucleotide (OKS985) had homology to nucleotides 4 to 21 of Mod5; and the reverse oligonucleotides (OKS998 to OKS1017) had homology to the amino acid codon adjacent to the one to be deleted. The reverse oligonucleotides also contained the linker sequence. PCR product *B* contained the 3' end of the gene. The forward oligonucleotides (OKS1018 to OKS1037) also contained the linker sequence and had homology to the amino acid codon adjacent to the one to be deleted. The reverse oligonucleotide (OKS984) had homology to the final 21 nucleotides of Mod5. PCR products *A* and *B* were then mixed together in the same PCR reaction and amplified with OKS984 and OKS985. The two PCR products were 'stitched' together due to hybridization within the linker sequence. The PCR products resulting from the second reaction were cloned into the pGEM-T Easy vector (Promega) and sequenced to confirm the correct nucleotide substitution and no further mutations in the Mod5 gene.

Figure 2.1- Schematic representation of the "mega-primer" PCR method.

The PCR reactions to create PCR products *A* and *B* were as follows: distilled water to 100 µl, 40 ng of pKS456, 10 µl KOD Buffer, 500 µM dNTPs, 3.5 mM $MgCl_2$, 500 nM of each oligonucleotide, 2 units KOD polymerase (Novagen). The PCR program used was as follows: 1] 15 sec at 98˚C, 2] 15 sec at 68˚C, 3] 1 sec at 72˚C. The PCR products were run on an 1%

agarose gel and the bands with the correct size (~750bp for PCR product A and ~1000bp for PCR product B) were gel-purified.

For the second PCR reactions the following conditions were used: sterile distilled water up to 100 µl, 100 ng of each PCR products *A* and *B*, 500 nM of each oligonucleotides OKS984 and OKS985, 10 µl KOD Buffer, 200 µM dNTPs, 3.5 mM $MgCl_2$, 500 nM of each oligonucleotide, 2 units KOD polymerase (Novagen). The PCR program used was as follows: 1] 2 min at 98˚C, 2] 15 sec at 98˚C, 3] 30 sec at 50˚C, 4] repeat steps 2 and 3 5 times, 5] 2 sec at 72˚C, 6] 1 sec at 98˚C, 7] 15 sec at 60˚C, 8] 2 sec at 72˚C, 9] repeat steps 5 and 6 30 times. The resulting PCR products were run on an 1% agarose gel and the bands with the correct size (~1750bp) were gel purified. In order to clone the PCR products in pGEM-T Easy vector, a tail of A was added as follows: 6 µl of insert, 1 µl 25 mM $MgCl_2$, 1 µl 10 x PCR buffer IV, 1 µl 2 mM dATP, 0.25 units Taq polymerase (Sawin Laboratory). The reactions were incubated at 72˚C for 30 min.

In the ligation reaction were used: 1 µl of pGEM-T Easy vector (Promega), 3 µl of gel purified and A-tailed Mod5 fragments, 5 µl 2 x ligase buffer (50 mM Tris-HCl, 10 mM $MgCl_2$, 1 mM ATP, 10 mM Dithiothreitol), 1µl T4 DNA ligase (NEB). The reaction was incubated for 4 hrs at RT. The ligations were transformed into competent *E. coli* XL1-blue cells, as described previously and plated into LB with 50 µg/ml of ampicilin. The plates were incubated at 37˚C ON. Plasmids were recovered, purified and sequenced with OKS312, OKS313, OKS314, OKS989 and OKS990 to confirm the 5 aa substitutions and no other undesired mutations. The resulting plasmids are described in Table 2.2.

Table 2.2- List of plasmid used to construct *mod5-155* to *mod5-256* mutant strains. Plasmids pKS78 to pKS797 were constructed using pKS456 as template and oligonucleotides OKS998 to OKS1037. [a] PCR product using OKS985 as forward oligonucleotide; [b] PCR product using OKS984 as reverse oligonucleotide.

Plasmid number	aa substitution	PCR product A[a]	PCR product B[b]
pKS778	156-160	OKS998	OKS1018
pKS779	161-165	OKS999	OKS1019
pKS780	166-170	OKS1000	OKS1020
pKS781	171-175	OKS1001	OKS1021
pKS782	176-180	OKS1002	OKS1022
pKS783	181-185	OKS1003	OKS1023
pKS784	186-190	OKS1004	OKS1024
pKS785	191-195	OKS1005	OKS1025
pKS786	196-200	OKS1006	OKS1026
pKS787	201-205	OKS1007	OKS1027
pKS788	206-210	OKS1008	OKS1028
pKS789	211-215	OKS1009	OKS1029
pKS790	216-220	OKS1010	OKS1030
pKS791	221-225	OKS1011	OKS1031
pKS792	226-230	OKS1012	OKS1032
pKS793	231-235	OKS1013	OKS1033
pKS794	236-240	OKS1014	OKS1034
pKS795	241-245	OKS1015	OKS1035
pKS796	246-250	OKS1016	OKS1036
pKS797	251-255	OKS1017	OKS1037

Cloned *mod5-155* to *mod5-256* fragments were integrated in Mod5 endogenous locus, via two-step gene replacement. *ura4+* gene was integrated between bp 581 to bp 680 of Mod5, creating the strain KS3626. *ura4+* in KS3626 was then replaced by *mod5-155* to *mod5-256* fragments between bp 401 and bp 1001 of endogenous Mod5. *ura4+* was counter-selected with 5-FOA (5-Fluoroorotic acid). The URA4 gene product (orotine-5'-monophosphate decarboxylase) converts 5-FOA to the toxic metabolic, 5-fluorouracil. *mod5-155* to *mod5-256* fragments cloned in the pGEM-Teasy vector (pKS778 to pKS797) were amplified by PCR and used to transform the strain KS3626. 50 µl PCR reactions were prepared as follows: sterile distilled water to 50 µl, 20 ng of plasmid template DNA (pKS778 to pKS797), 5 µl Buffer IV, 2.5 µl of 10 mM dNTPs, 7 µl of 25 mM $MgCl_2$, 0.1 µl of OKS312 and OKS602 (100 µM stock), 0.4 units Taq polymerase (Sawin Laboratory), 7.6 units Pwo polymerase (Sawin Laboratory). The PCR-program used was as follows: 1] 2 min at 95˚C, 2] 15 sec at 95˚C, 3] 30 sec at 55˚C, 4] 90 sec at 72˚C, 5] repeat steps 2-4 29 times, 6] 5 min at 72˚C. Resulting PCR products were PCI purified and used to transform KS3626, as described above. Transformants were plated on to EMM plates supplemented with 96 mM ammonium chloride, 3.75 mg/l of uracil and 0.1% 5- FOA, to allow *ura4+* counter-selection. Transformants were grown at 32˚C for four or five days, streaked on to YE5S plates and left

to grow for 2 more days. Single colonies were isolated and patched on to YE5S plates. Integration of the Mod5 substitution fragment was confirmed by colony PCR, followed by sequencing across the homologous recombination region and the five aa substitution. To sequence the chromosomal region of Mod5, genomic DNA was prepared as described and colony PCR was performed using OKS328 and OKS323. The PCR products were cleaned-up for sequencing as follows: 12 µl of PCR product were mixed with 1 µl of Exonuclease I (NEB) and 1 µl of Antarctic phosphatase (NEB). The reaction was incubated at 37˚C for 15 min to degrade the excess of oligonucleotide and to cleave 5' phosphatases. The enzymes were inactivated by heating at 80˚C for 15 min. Sequencing reaction were performed as described using 2 µl of cleaned-up PCR product and oligonucleotides OKS312 and OKS602.

2.11. Construction of tea1Δ434-478, tea1Δ479-532, tea1Δ533-586 and tea1Δ434-586 strains

To construct *tea1Δ434-478* (KS4734), *tea1Δ479-532* (KS4736)*, tea1Δ533-586* (KS4738) and *tea1Δ434-586* (KS4740) strains the same approach was taken as above, with minor modifications. KS4530, used as parent strain, has the *ura4+* gene integrated between nucleotides 1200 and 1800 of Tea1, and the C-terminus of Tea1 is GFP-tagged. Tea1 internal deletions were obtained by replacing the deleted amino acids with a linker sequence containing seven alanines (GCTGCCGCAGCGGCTGCCGCA). The following PCR conditions were used: sterile distilled water to 25 µl, 20 ng of pKS235, 2.5 µl Buffer IV, 0.5 µl of 10 mM dNTPs, 7 µl of 25 mM $MgCl_2$, 1.25 µl of each oligonucleotide (100 µM stock, see Table 2.3 for details), 0.4 units Taq polymerase (Sawin Laboratory), 2 units Pwo polymerase (Sawin Laboratory). The PCR program used was as follows: 1] 2 min at 95˚C, 2] 15 sec at 95˚C, 3] 30 sec at 55˚C, 4] 45 sec at 72˚C, 5] repeat steps 2-4 29 times, 6] 3 min at 72˚C. The resulting PCR products were run on 1% agarose gel and the bands with correct size were excised. Subsequently, PCR products *A* and *B* were mixed together and PCR-amplified as follows: sterile distilled water to 25 µl, 25 ng of PCR product *A* and of *B*, 2.5 µl Buffer IV, 0.5 µl of 10 mM dNTPs, 4 µl of 25 mM $MgCl_2$, 0.125 µl of each OKS1863 and OKS422 (100 µM stock), 0.4 units Taq polymerase (Sawin Laboratory), 2 units Pwo polymerase (Sawin Laboratory). The PCR program used was as follows: 1] 2 min at 95˚C, 2] 15 sec at 95˚C, 3] 30 sec at 55˚C, 4] 90 sec at 72˚C, 5] repeat steps 2-4 29 times, 6] 5 min at 72˚C. The resulting PCR products were PCI-purified and used directly to transform KS4530, without the cloning step. Transformation, colony selection and confirmation of gene

insertion and mutation by sequencing were performed as described before. For colony PCR, oligonucleotides OKS422 and OKS687 were used, and for sequencing, OKS421, OKS422, OKS687 and OKS1863 were used.

Table 2.3- List of oligonucleotides used to constructed Tea1 internal-deletions strains. Tea1 was internally deleted using a two-step PCR method. The oligonucleotides used to obtain each the PCR obtained are listed. [a] PCR products using OKS422 as forward oligonucleotide; [b] PCR products using OKS1863 as reverse oligonucleotide.

Strain number	Deleted amino acids	PCR product A[a]	PCR product B[b]
KS4734	434-478	OKS1846	OKS1845
KS4736	479-532	OKS1848	OKS1847
KS4738	533-586	OKS1850	OKS1849
KS4740	434-586	OKS1846	OKS1849

2.12. Construction of tea1Δdimer, tea1Δtrimer and tea1ΔdimerΔtrimer strains

tea1Δdimer (KS5661), *tea1Δtrimer* (KS5980) and *tea1ΔdimerΔtrimer* (KS5664) strains were constructed as before, with minor modifications. The linker sequence used was a five times repeat of the dipeptide *GlySer* (GGTAGCGGAAGTGGTAGTGGAAGCGGCAG). The parent strain (KS5655) has the *ura4+* gene integrated between nucleotides 1200 and 2550 of Tea1 gene and Tea1 GFP-tagged in the C-terminal. Strains KS5661 and KS5664 were obtained by direct transformation of the final PCR product. The PCRs were done as follows: sterile distilled water to 50 µl, 20 ng of pKS235, 5 µl Buffer IV, 1 µl of 10 mM dNTPs, 4 µl of 25 mM $MgCl_2$, 2.5 µl of each oligonucleotide (10 µM stock, see Table 2.4), 0.3 units Taq polymerase (Sawin Laboratory), 4 units Pwo polymerase (Sawin Laboratory). The PCR program used was as follows: 1] 2 min at 95˚C, 2] 15 sec at 95˚C, 3] 30 sec at 55˚C, 4] 1 min at 72˚C, 5] repeat steps 2-4 29 times, 6] 3 min at 72˚C. Resulting PCR products were run on 1% agarose gel and purified. The second PCR was done as follows: sterile distilled water to 25 µl, 25 ng of PCR product A and of B, 2.5µl Buffer IV, 0.5 µl of 10 mM dNTPs, 4 µl of 25 mM $MgCl_2$, 0.125 µl of each OKS420 and OKS2069 (100 µM stock), 0.4 units Taq polymerase (Sawin Laboratory), 2 units Pwo polymerase (Sawin Laboratory). The PCR program used was as follows: 1] 2 min at 95˚C, 2] 15 sec at 95˚C, 3] 30 sec at 55˚C, 4] 3 min at 72˚C, 5] repeat steps 2-4 29 times, 6] 5min at 72˚C. The resulting PCR products were PCI- purified and used directly to transform KS5655, without the cloning step. KS5980 was constructed by transforming the PCR product of pKS1029 amplified with OKS420 and OKS2069. Tea1 allele

in pKS1069 was cloned by the two-step PCR method described before. The PCR reaction was as follows: sterile distilled water to 100 µl, 20 ng of pKS769, 10 µl Phusion HF Buffer, 1 µl of 10 mM dNTPs, 8 µl of 25 mM $MgCl_2$, 2 µl of each oligonucleotide (10 µM stock, see Table 2.4), 1 unit of Phusion polymerase (Finnzymes). The PCR program used was as follows: 1] 30 sec at 98˚C, 2] 10 sec at 98˚C, 3] 5 sec at 52˚C, 4] 3 min at 72˚C, 5] repeat steps 2-4 29 times, 6] 5 min at 72˚C. Resulting PCR products were run on an 1% agarose gel and purified. The second PCR reaction was done as follows: sterile distilled water to 100 µl, 100 ng of each PCR product *A* and *B*, 10 µl Phusion HF Buffer IV, 2 µl of 10 mM dNTPs, 5 µl of 25 mM $MgCl_2$, 5 µl of OKS1203 and OKS1204 (100 µM stock), 1 unit of Phusion polymerase. The PCR program used was as follows: 1] 30 sec at 98˚C, 2] 10 sec at 98˚C, 3] 5 sec at 52˚C, 4] 4 min at 72˚C, 5] repeat steps 2-4 29 times, 6] 10 min at 72˚C. Resulting PCR products were run on 1% agarose gel and purified. The band was excised from the gel and cloned by Gateway recombination in pDONR221, as described above. Tea1 internal deletions were confirmed by sequencing with oligonucleotides OKS254, OKS420, OKS421, OKS423, OKS426, OKS427, OKS684 and OKS6865, as described above. pKS1029 was used as template for *tea1Δ726-762* fragment. 50 µl PCR reactions were prepared as follows: sterile distilled water to 50 µl, 20 ng of plasmid template DNA, 5 µl Buffer IV, 2.5 µl of 10 mM dNTPs, 7 µl of 25 mM $MgCl_2$, 0.1 µl of OKS420 and OKS829 (100µM stock), 0.4 units Taq polymerase (Sawin Laboratory), 7.6 units Pwo polymerase (Sawin Laboratory). The PCR program used was as follows: 1] 2 min at 95˚C, 2] 15 sec at 95˚C, 3] 30 sec at 55˚C, 4] 2 min at 72˚C, 5] repeat steps 2-4 29 times, 6] 5 min at 70˚C. The PCR product was PCI-purified and transformation; clone selection and gene mutation confirmation were performed as described before.

Table 2.4 - List of plasmids and PCR products used to construct strains KS5661, KS5664 and KS5980. [a] PCR product using OKS420 as forward oligonucleotide; [b] PCR product using OKS2107 as forward oligonucleotide; [c] PCR product using OKS829 as reverse oligonucleotide; [d] PCR product using OKS1682 as reverse oligonucleotide.

Strain number	Plasmid number	Deleted amino acids	PCR product A[a]	PCR product B
KS5661	-	697-726	OKS2065[a]	OKS2066[c]
KS5980	pKS1029	727-762	OKS2067[b]	OKS2068[d]
KS5664	-	697-726	OKS2065[a]	2OKS068[c]

2.13. Strain construction using the pDUAL system

The strains listed in the Table 2.5 were constructed using the pDUAL system. This system allows gene tagging with several epitopes in the N and C terminal and its integration in the *leu1+* locus. Gene cloning in pDUAL vectors can be done with Gateway technology. After the gene of interest has been cloned in the vector of interest, it was digested with the restriction enzyme *Not*I (NEB) as follows: 10 µg of DNA, 3 µl of Buffer NEB3, 0.3 µg BSA (Bovine Serum Albumin), 10 units of NotI and sterile distilled water up to 30 µl. The reactions were incubated at 37˚C for 60 min and transformed directly into yeast. The transformations were performed as described, and transformants were plated directly on to EMM minus leucine plates. Selection of stable integrants was performed as described above. Correct tagging was confirmed by fluorescence microscopy for strains KS4344 to KS4638 and by western blotting for strain KS4821.

Table 2.5 – List of strains constructed using the pDUAL system, as well as the plasmids used for transformation.

Strain number	Plasmid	Parent strain
KS4344	pKS771	KS4293
KS4417	pKS818	KS4293
KS4630	pKS865	KS4293
KS4632	pKS866	KS4293
KS4634	pKS867	KS4293
KS4636	pKS869	KS4293
KS4638	pKS871	KS4293
KS4821	pKS914	KS2660

2.14. Site directed mutagenesis

Site Directed Mutagenesis was performed using the QuickChange® Site-Directed Mutagenesis Kit (Stratagene, USA). Table VI shows the plasmids created as well as the oligonucleotides used. The PCR reaction contained: 50 ng of pKS769, 125 ng of each oligonucleotide, 1 µl of the dNTP mix (provided in the kit), 1 X Reaction Buffer (10 mM KCl, 10 mM $(NH_4)_2SO_4$, 20 mM Tris-HCl pH 8.8, 2 mM $MgSO_4$, 0.1% (v/v) Triton X-100, 0.1 mg/ml nuclease-free BSA). The following parameters were used for the PCR reaction: 1] 30 sec at 95°C, 2] 30 sec at 95˚C, 3] 1 min at 55˚C for, 4] 10 min 68˚C, 5] repeat steps 2 to 4 18 times. 10 U of Dpn*I* restriction enzyme were then added to the mix and incubated at 37°C for 1 hr to digest un-mutagenised, methylated dsDNA template. The nicked mutagenised dsDNA

was then transformed into XL1-Blue cells. Correct mutagenesis was confirmed by sequencing the plasmid DNA.

Table 2.6 - List of plasmids created with site directed mutagenesis and multi-site directed mutagenesis, as well as the oligonucleotides and the template plasmids used.

Plasmid	Mutation	Forward oligonucleotide	Reverse oligonucleotide	Template plasmid
pKS819	S586A	OKS1672	OKS1673	pKS769
pKS820	S586D	OKS1674	OKS1675	pKS769
pKS821	Y484F	OKS1676	OKS1677	pKS769
pKS851	S467A	OKS1823	OKS1824	pKS769
pKS852	S467A, S476A, S478A	OKS1819	OKS1820	pKS851
pKS853	S467D, S476D, S478D	OKS1670	--	pKS769

2.15. Multi-site Directed mutagenesis

pKS853 was constructed using the QuickChange Multi Sit-Directed Mutagenesis Kit (Stratgene, U.S.A.). The mutagenesis reaction was performed in a final volume of 25 µl and contained 100 ng of pKS851, 100 ng of OKS1670, 1 µl of the dNTP mix (provided in the kit), 2.5 µl of 10 X Reaction Buffer (10 mM KCl, 10 mM $(NH_4)_2SO_4$, 20 mM Tris-HCl pH 8.8, 2 mM $MgSO_4$, 0.1% (v/v) Triton X-100, 0.1 mg/ml nuclease-free BSA) and 1 µl of the QuickChange® Multi enzyme mix. PCR reaction was done as follows: 1] 1 min at 95°C, 2] 1 min at 95˚C, 3] 1 min at 55˚C for, 4] 20 min 65˚C, 5] repeat steps 2 to 4 30 times. 10 U of Dpn1 restriction enzyme was then added to the mix and incubated at 37°C for 1 hr to digest un-mutagenised, methylated dsDNA template. The nicked mutagenised ssDNA was then transformed into XL1-Blue cells. Correct mutagenesis was confirmed by sequencing of the plasmid DNA.

2.16. Microscopy

Wide-field microscopy used a Nikon 100x/1.40 NA Plan Apo objective on a Nikon TE300 inverted microscope. This was connected to a CoolSnap HQ CCD camera (Photometrics). For spinning-disc confocal microscopy, a Nikon 100x/1.45 NA Plan Apo objective was used on a TE2000 inverted microscope, connected to a Yokogawa CSU-10 spinning disc confocal head (Visitech) and an Andor Du888 EMCCD camera. Image acquisition, processing and analysis were carried out using Metamorph software (Molecular Devices). Maximal projections are shown for all imaging. Microscope images were adjusted using only linear

contrast enhancement with Metamorph (Molecular Devices). Time-lapse images to compare samples were imaged under identical illumination conditions; the brightness and contrast were later scaled using consistent values, to allow accurate comparisons of intensity.

Cells for live-cell imaging were grown in EMM2 medium at 25˚C, for 2 O/N and diluted 1:100 and grown for one O/N. Expression of *nmt1* or *nmt81* was induced for 2 x O/N at 25˚C in EMM2 plus 15 µM and 150 nM thiamine, respectively. Cultures were diluted 1:100 in EMM2 plus appropriate amount of thiamine and grown 1 x O/N at 25˚C prior to imaging. Cells were imaged at room temperature in 2% EMM2 agarose pads.

2.17. FRAP experiments

FRAP experiments used a Deltavision RT system (Applied Precision) with an Olympus IX70 microscope and a Cascade II EMCCD camera (Roper Scientific). Pre- and post-bleach images were acquired with 600 ms exposure time. Cell tips were bleached with a 488 nm laser pulse for 0.3 sec. Fluorescence recovery was measured either every 5 sec for 5 min or every 30 sec for 50 min. Recovery curves were obtained using a script written in-house (Dr. David Kelly) using Image Pro Analyzer (Media Cybernetics).

2.18. Immunofluorescence

Samples were collected for immunofluorescence using rapid filtration, the filter then being immersed into methanol at -80˚C. Samples were further processed by washing twice in PEM (0.1 M NaPipes pH 6.8, 1 mM EGTA, 1 mM $MgCl_2$), the cell wall digested by incubation with 1 ml freshly prepared PEMS (PEM+1.2 M sorbitol) with 1 mg/ml zymolyase (ICN) for 30 min at 37˚C. Digestion was confirmed by mixing a sample of cells with 10% SDS and observing loss of refractility using phase contrast microscopy. Cells were then washed twice with PEM, once with PEM + 1% Triton X-100, and washed twice more with PEM, before being incubated with PEMBAL (PEM + 1% BSA, 0.1% NaN_3, 100 mM lysine (monohydrochloride)), rotating, for 1 hr. Anti-Tea1 staining used affinity purified anti-Tea1 antibody (Snaith and Sawin, 2003, followed by three extended (1-2 hr) washes in 500 µl PEMBAL. Alexa 568 labeled donkey anti-goat secondary antibody (Molecular Probes Europe BV) was used at 1:50 dilution, followed by three further extended washes with PEMBAL.

For imaging, cells were spun onto coverslips previously coated with poly-L-lysin (10 mg/ml). Samples were observed using spinning disc confocal microscopy.

2.19. Morphology Assay

Strains were grown to stationary phase in YE5S liquid medium for 3 days at 25°C before dilution 1:20 into fresh medium at 32°C, in the presence or absence of 50 µg/ml MBC. Cells were fixed with formaldehyde and branching was scored by light microscopy.

2.20. Tea1-TAPS large-scale immunoprecipitation

Native extracts for tandem affinity purification were purified from cell pellets frozen in liquid nitrogen then ground to a powder. 25 g of cell powder for each strain were resuspended in 50 ml of a buffer of 15 mM Na_2HPO_4, 10 mM NaH_2PO_4, 150 mM NaCl, 2 mM EDTA, 1 mM DTT, 2 mM Benzamidine, 1 mM PMSF, 2 mM AEBSF, 1% Igepal CA-630 5 µg/ml chymostatin, leupetin, antipain, aprotinin, pepestatin, E64, 60 mM β-glycerol phosphate, 15 mM PNPP (*p*-Nitrophenyl Phosphate), 10 mM sodium orthovanadate, 10 mM sodium azide, 50mM sodium fluoride. Cell powder was incubated for 20 min at 4˚C. The extract was centrifuged at 4000 rpm for 4 min at 4˚C to remove insoluble cellular debris. The supernatant was re-centrifuged at 13,000 rpm for 30 min at 4˚C. Purification was either performed with 10 µl of in-house coupled IgG-Dynabeads or 40 µl (bed volume) of in-house coupled IgG-Fractogel beads per gram of cell powder. Rotating incubation was performed for 2 hrs at 4˚C. Beads were washed with 5 x 15 ml of a buffer of 25 mM Tris-HCl pH 8.0, 150 mM NaCl, 0.1% NP-40, 1 mM DTT. The beads were recovered in 1 ml of a buffer of 25 mM Tris-HCl pH 8.0, 150 mM NaCl, 0.1% Igepal-630, 1 mM DTT, 0.5 mM EDTA and 100 µl of recombinant TEV protease (Tobacco Etch Virus, Sawin Lab) were added. The slurry was incubated with end-over-end rotation for 2 hrs at 4˚C and the supernatant was recovered. The recovered material was precipitated with 10% TCA (Trichloroacetic acid) for 30 min at 4˚C. The pellet was washed twice with 70% acetone, 20% ethanol, 10 mM Tris-HCl pH 7.5 and 0.0025% bromophenol blue. The pellet was air-dried for 10 min at 4˚C and then resuspended in 40 µl of Laemmli sample buffer (0.0625 M Tris-HCl pH 6.8, 2% SDS, 10% glycerol). Sample equivalent to 2 g of cells was loaded onto a 8% acrylamide gel and silver

stained with a home-made kit. Briefly, the gel was incubated with 50% (v/v) methanol for 10 min at RT and then with 5% (v/v) methanol for 10 min at RT. 3.2 µl of 1 M DTT was added to 100 ml of dH_2O and gel was added to the reducing solution and washed for 10 min at RT and then transferred to a solution 0.2% (w/v) $AgNO_3$ for 10 min at RT. The gel was then washed in distilled water three times for 5 sec. The gel was then developed with 3% (w/v) Na_2CO_3, 50 µl 37% (v/v) formaldehyde in 100 ml) until adequate contrast was observed between gel and protein bands. The developing reaction was quenched by incubating the gel in 5% (v/v) acetic acid for 10 min. The remaining recovered material was run onto a 8% acrylamide gel and colloidal coomassie stained (Pierce) and processed to MS analysis. Sample preparation for MS was performed by Dr Flávia Alves from the Rappsilber group from the Wellcome Trust Center for Cell Biology, University of Edinburgh.

2.21. Immunoprecipitation

Native extracts for immunoprecipitation were prepared from cell pellets frozen in liquid nitrogen then ground to powder. Extracts were made with extract buffer (20 mM NaHEPES pH 7.5, 50 mM K-acetate, 200 mM NaCl, 1 mM EDTA, 0.2% TritonX-100, and a protease inhibitor cocktail: 5 µg/ml CLAAPE, 2 mM AEBSF, 1 mM benzamidine); 1ml of buffer was added to 500 mg of ground cell powder and incubated for 15 min at 4˚C. Samples were centrifuge at 4000 rpm for 2 min to remove insoluble cellular debris. The supernatant was retained and re-centrifuged at 13000 rpm for 15 min. Protein concentration was determined with BCA assay (Bicinchoninic acid) and sample concentration was adjusted to be the same. 10 µl of ProteinG-Dynabeads were pre loaded with antibody prior to extract incubation. Table VII describes the antibodies used, as well as the concentrations. Extracts were incubated with beads for 2 hrs at 4˚C with end-over-end rotation. Next, beads were washed five times with 1 ml of extract buffer without protease inhibitors. The beads were resuspended in 40 µl of Laemmli sample buffer and eluted by heating the beads at 50˚C for 15 min. 40 µl of 2x Laemmli buffer with 5% of β-mercaptoethanol and 0.01% bromophenol blue were added to the sample prior to SDS-PAGE and Western blotting. 20 µl of sample and 5 µl of whole cell extract were loaded per lane.

2.22. Western blot

Proteins were run on an acrylamide gel in running Laemmli buffer (25 mM Tris-base, 192 mM Glycine, 0.1% SDS, pH 8.3). Mini-gels (Biorad) were run at 35 mA per gel and low-wide gels (Scie-Plas) were run at 80 mA per gel. Proteins were transferred to a nitrocellulose membrane in 10 mM CAPS and 10% methanol. Mini gels were transferred at 60 V for 60 min and low-wide gels at 50 V for 90 min. Protein transfer and equal loading were observed with Ponceau staining. Membranes were blocked with 2% non-fat dried milk and 0.2% Tween20 in TBS for 6 min. Membrane to be probed with anti-GFP (Sawin Lab) and anti-Tea3 blocked with 5% non-fat dried milk and 0.01% Tween20 in TBS for 60 min. Membranes were then incubated O/N at 4˚C with primary antibody diluted in the same blocking solution. Antibody concentrations are described in Table 2.7. Membranes were washed 3 times for 10 min with TBS/0.02% Tween20 or TBS/0.01% Tween20, in case of anti-GFP (Sawin Lab) or anti-Tea3 incubations and then incubated with secondary antibodies in blocking solution for 60-120 min at RT. Membranes were either incubated with HRP conjugated secondary antibodies or IRDye conjugated antibodies. HRP conjugated were ECL (Enhanced Chemiluminesence) detected by incubating the membrane with 100 mM Tris-HCl pH 8.5, 2.5 mM luminol, 0.4 mM p-coumaric acid, 0.02% (v/v) H_2O_2 for 1 min and x-ray film exposure. When incubated with IRDye conjugated antibodies protein detection was obtained by scanning the membranes in Odyssey scanner (LI-COR Biosciences) either at 800 or 700 nm.

Table 2.7 – List of primary antibodies used in this study.

Antibody	Description	WB[a]	IP[b]	IF[c]	Source
Tea1	Sheep, polyclonal, affinity purified	1:2,000		1:1000	Sawin Lab
Tea3	Sheep, polyclonal, serum	1:2,000			Nurse Lab
Mod5	Sheep, polyclonal, serum	1:2,000			Sawin Lab
Mod5	Sheep, polyclonal, Affinity purified	1:200			Sawin Lab
Cdc13	Mouse, monoclonal	10 µg/ml			CRUK
Bip1	Rabbit, polyclonal	1:10,000			Dr Alison Pidoux
GFP	Sheep, polyclonal affinity purified	1:300	3 µg		Sawin Lab
GFP	Mouse, monoclonal	1:2,000			Roche
FLAG2	Mouse, monoclonal	1:500	3 µg		Sigma
tdimer2	Rabbit, polyclonal, affinity purified	1:500	5 µg		Sawin Lab
TAT1	Mouse, monoclonal	1:1000			Gull Lab

[a] Western Blot, [b] Immunoprecipitation, [c] Immunofluorescence

2.23. Boiled protein extracts from yeast

Cultures were grown O/N to mid-exponential growth in appropriate media. The cultures were centrifuged for 4 min at 4000 rpm to pellet the cells. The supernatant was removed and the cell pellet ressuspended in 1 ml TBS. Samples were centrifuged 1 min at 13000 rpm, the supernatant removed and the cell pellets boiled for 5 min. The samples were bead-beaten with zirconium beads in a Rybolyser (Hybaid) at room temperature, using 2 cycles of 30 sec at the maximum setting ("6.5"). A hole was pierced in the bottom of each tube and the liquid collected by brief centrifugation into a second tube containing 150 µl of 2x Laemmli buffer. The samples were then boiled for 5 min and centrifuged for 10 min at 13000 rpm to remove insoluble cell debris. Protein concentration was determined via BCA assay. 50 µg of total protein were loaded per lane of SDS-PAGE analysis.

2.24. Protein expression in E. coli and purification

Tea1-6xHis (pKS1102) and 6xHis-MBP-*mod5(28-477)* (pKS1103) were expressed in *E. coli* BL21-CodonPlus (DE3)-RIL cells (Stratagene). Cells were grown in LB medium at 37˚C O/N, and diluted to OD_{600} 0.1. When cultures reached OD_{600} 0.5, protein expression was induced with 1 mM IPTG (Isopropyl β-D-1-thiogalactopyranoside) and cells were grown O/N at 18˚C. Cells were harvested and 400 mg of pelleted cells were resuspended in 1600 µl of lysis buffer (6 M guanidine-HCl, 25 mM Tris-HCl pH8, 0.3 M NaCl). Cells were disrupted by sonication, 4x 10 sec cycles at 30% output, duty cycle of 3, using a Branson sonicator. The soluble fraction was obtained after centrifugation at 4˚C at 55,000 rpm for 30 min in a TLS-55 rotor (Beckman). 2 ml of soluble extract were incubated with 200 µl slurry of nickel-activated His-bind Fractogel beads (Merck) for 60 min at 4˚ C. Beads were washed 4 times with 5 ml of wash buffer (8 M urea, 25 mM Tris-HCl pH 8, 0.3 M NaCl, 10mM imidazole). Proteins were eluted from beads with elution buffer (8 M urea, 25 mM Tris-HCl pH8, 0.3 M NaCl, 300 mM imidazole) and 2x Laemmli sample buffer was added. Proteins were stored at -80˚C.

Table 2.8- List of oligonucleotides used in this thesis

Oligonucleotide	Sequence
OKS312	CGTCAGAGGATATTAGCATTG
OKS313	TTCTTCCGCGAAGGCTCGACC
OKS314	CAGGAGTCAGATATTCCTCAA
OKS330	TTTGTCGACCTCTAATTTGGAACCTTTCTTTT
OKS421	CCTCCACCAGCTCGTGCTGG
OKS422	AATTGGGGGGAAACAAGGG
OKS602	TTGATTGCGTCTGCGCGCCAA
OKS687	GTCAGGAACATCGTATGGGTAAAAGATATCACGATACAATGACTCGATTTC
OKS989	AAAGGTTCCTGCTGAACCAGC
OKS990	CTCACTTCCTGCTGAACCAGC
OKS998	AAAGGTTTCCTGCTGAACCAGCAAAAGATGATCTAGCTCCCTT
OKS999	CTCACTTCCTGCTGAACCAGCTCGAAAATTACTATTAAAAGA
OKS1000	AAAGGTTTCCTGCTGAACCAGCTCCAATGTCAAAGGTTCGAAA
OKS1001	CTCACTTCCTGCTGAACCAGCCCTTCGGCGCTCACTTCCAAT
OKS1002	AAAGGTTTCCTGCTGAACCAGCTGCTTCCAATATTCTCCTTCG
OKS1003	CTCACTTCCTGCTGAACCAGCAGATGAGTCCTGTGATGCTTC
OKS1004	AAAGGTTTCCTGCTGAACCAGCGTATCTTCCCGGACGAGATGA
OKS1005	CTCACTTCCTGCTGAACCAGCTTTTGTCCTATAAGAGTATCT
OKS1006	AAAGGTTTCCTGCTGAACCAGCTGCTGGAGATGCGCTTTTTGT
OKS1007	CTCACTTCCTGCTGAACCAGCCGAAGTATCAATTAATGCTGG
OKS1008	AAAGGTTTCCTGCTGAACCAGCCCTAGAATCCAAGGTCGAAGT
OKS1009	CTCACTTCCTGCTGAACCAGCCATAGTAAAATTCAACCTAGA
OKS1010	AAAGGTTTCCTGCTGAACCAGCTCGTTCCAAGCGTCCCATAGT
OKS1011	CTCACTTCCTGCTGAACCAGCAACTGAGCAATGGATCGTTC
OKS1012	AAAGGTTTCCTGCTGAACCAGCCATCGTATTTTTGGATAACTG
OKS1013	CTCACTTCCTGCTGAACCAGCATGCGACACAGCGCGCATCGT
OKS1014	AAAGGTTTCCTGCTGAACCAGCTGGCGGATTTTCCAAATGCGA
OKS1015	CTCACTTCCTGCTGAACCAGCCAACGTTATGTCCTTTGGCGG
OKS1016	AAAGGTTTCCTGCTGAACCAGCAACGTTTAATTTTGGCAACGT
OKS1017	CTCACTTCCTGCTGAACCAGCCCAAGCAGAATTCTTAACGTT
OKS1018	AAAGGTTTCCTGCTGAACCAGCACCTTTGACATTGGAAGTGAG
OKS1019	CTCACTTCCTGCTGAACCAGCAGTGAGCGCCGAAGGAGAATA
OKS1020	AAAGGTTTCCTGCTGAACCAGCAGAATATTGGAAGCATCACAG
OKS1021	CTCACTTCCTGCTGAACCAGCTCACAGGACTCATCTCGTCCG
OKS1022	AAAGGTTTCCTGCTGAACCAGCCGTCCGGGAAGATACTCTTAT
OKS1023	CTCACTTCCTGCTGAACCAGCTCTTATAGGACAAAAAGCGCA
OKS1024	AAAGGTTTCCTGCTGAACCAGCAGCGCATATACAGCATTAATT
OKS1025	CTCACTTCCTGCTGAACCAGCTTAATTGATACTTCGACCTTG
OKS1026	AAAGGTTTCCTGCTGAACCAGCACCTTGGATTCTAGGTTGAAT
OKS1027	CTCACTTCCTGCTGAACCAGCTTGAATTTTACTATGGGACGC
OKS1028	AAAGGTTTCCTGCTGAACCAGCGGACGCTTGGAACGATCCATT
OKS1029	CTCACTTCCTGCTGAACCAGCTCCATTGCTCAGTTATCCAAA

OKS1030	AAAGGTTTCCTGCTGAACCAGCTCCAAAAATACGATGCGCGCT
OKS1031	CTCACTTCCTGCTGAACCAGCCGCGCTGTGTCGCATTTGGAA
OKS1032	AAAGGTTTCCTGCTGAACCAGCTTGGAAAATCCGCCAAAGGAC
OKS1033	CTCACTTCCTGCTGAACCAGCAAGGACATAACGTTGCCAAA
OKS1034	AAAGGTTTCCTGCTGAACCAGCCCAAAATTAAACGTTAAGAAT
OKS1035	CTCACTTCCTGCTGAACCAGCAAGAATTCTGCTTGGCCGTTG
OKS1036	AAAGGTTTCCTGCTGAACCAGCCCGTTGCAGCCATATTCACCA
OKS1037	CTCACTTCCTGCTGAACCAGCTCACCACCTGCCAATGAAACG
OKS1203	GGGGACAAGTTTGTACAAAAAAGCAGGCT
OKS1204	GGGGACCACTTTGTACAAGAAAGCTGGGT
OKS1670	CGGTCGAGCAGACAATGATCTGCCTGACCCTGTTGTGCCAACTCGGTCAAATGACTCTTCCATC TTAC
OKS1672	CACTAGATCTATCAACGCTATATCCGAGGTGTCAG
OKS1673	CTGACACCTCGGATATAGCGTTGATAGATCTAGTG
OKS1674	CACTAGATCTATCAACGATATATCCGAGGTGTCAG
OKS1675	CTGACACCTCGGATATATCGTTGATAGATCTAGTG
OKS1676	CATCTTACAACCTAGTTTTAACTTGAATTCACAC
OKS1677	GTGTGAATTCAAGTTAAAACTAGGTTGTAAGATG
OKS1819	CGGTCGAGCAGCCAATGATCTGCCTGCACCTGTTGTG
OKS1820	CACAACAGGTGCAGGCAGATCATTGGCTGCTCGACCG
OKS1823	CTCGGTCAAATGCGTCTTCCATCTTAC
OKS1824	GTAAGATGGAAGACGCATTTGACCGAG
OKS1843	TCTACTGGTAACACAAATCCCAGTGCCTTTAACGGTCTTTTGACTTCATCCCGTATCCCATCTTA TAATGGGTCGAAAGTCGCCAGGGTTTTCCCAGTCACGAC
OKS1844	GTTAACGAATCTATTTTAGAAGCGGAATCTCGAAGAATCTCATAAAGTTTACTCTTAAACCATT CAACGATTTGTTGCTT AGCGGATAACAATTTCACACAGGA
OKS1845	GCTGCCGCAGCGGCTGCCGCAATCTTACAACCTAGTTATAAC
OKS1846	TGCGGCAGCCGCTGCGGCAGCGGGATGACTAGTAGAACGAAC
OKS1847	GCTGCCGCAGCGGCTGCCGCAGAACAAGGGAACGGTTCCGTC
OKS1848	TGCGGCAGCCGCTGCGGCAGCGGAAGACGAATTTGACCGAGT
OKS1849	GCTGCCGCAGCGGCTGCCGCAGTCACTCTAGAAACACTTGTT
OKS1863	CTGACAACTTATTGTGCTTTGC
OKS1883	GGGGACAAGTTTGTACAAAAAAGCAGGCTTCATGTCGGCTTTATCTGAAAGCCCTGCT
OKS1884	GGGGACCACTTTGTACAAGAAAGCTGGGTCCTACATCAAAATACAACAAAACTTCTCTAA
OKS2030	CGAAAAAGGAAAAATTCGGCTCTTTAAGGACTTTACACAGTTTTGAAAGTAGTATGAGGAGA GTATCTACTTCTGCAGCACGGATCCCCGGGTTAATTAA
OKS2031	TAAGCAGAATTTACTGCGTTCATAAAGTTGCGAAAGCATAGTCTTCAAAATCTTTCGTTTGCTT CTTAGCCAAAATTCAAGAATTCGAGCTCGTTTAAAC
OKS2065	ACTGCCGCTTCCACTACCACTTCCGCTACCAGAAGTCTCACGCATGACCTCAAG
OKS2066	GGTAGCGGAAGTGGTAGTGGAAGCGGCAGTGAACGAGAACGGCACAATGCTATA
OKS2067	ACTGCCGCTTCCACTACCACTTCCGCTACCTTCCACTAATTCCTTTTGGAAAGA
OKS2068	GGTAGCGGAAGTGGTAGTGGAAGCGGCAGTCAAACGGTAACCATTAACAAGTTT

Table 2.9- List of plasmids used in this thesis

Name	Vector	Insert	Source
pKS112	pFA6a-GFP(S65T)-kanMX6	-	Sawin Lab
pKS131	pBS	Ura4	Sawin Lab
pKS235	pGEMT	Tea1	Sawin Lab
pKS393	pFA6a-tdTomato-natMX6	-	Sawin Lab
pKS456	pGEMT easy	*mod5(2-523)*	This study
pKS535	pDONR221	-	Invitrogen
pKS544	pHMGWA	-	(Busso et al., 2005)
pKS547	pDONR221	*mod5(28-447)*	Sawin Lab
pKS715	pFA6a-natMX6-P81nmt1-GFP	-	Sawin Lab
pKS769	pDONR221	Tea1	Sawin Lab
pKS771	pDUAL-GFH81c	Tea1	This study
pKS778	pGEMT-easy	*mod5Δ(156-160)*	This study
pKS779	pGEMT-easy	*mod5Δ(161-165)*	This study
pKS780	pGEMT-easy	*mod5Δ(166-170)*	This study
pKS781	pGEMT-easy	*mod5Δ(171-175)*	This study
pKS782	pGEMT-easy	*mod5Δ(176-180)*	This study
pKS783	pGEMT-easy	*mod5Δ(181-185)*	This study
pKS784	pGEMT-easy	*mod5Δ(186-190)*	This study
pKS785	pGEMT-easy	*mod5Δ(191-195)*	This study
pKS786	pGEMT-easy	*mod5Δ(196-200)*	This study
pKS787	pGEMT-easy	*mod5Δ(201-205)*	This study
pKS788	pGEMT-easy	*mod5Δ(206-210)*	This study
pKS789	pGEMT-easy	*mod5Δ(211-215)*	This study
pKS790	pGEMT-easy	*mod5Δ(216-220)*	This study
pKS791	pGEMT-easy	*mod5Δ(221-225)*	This study
pKS792	pGEMT-easy	*mod5Δ(226-230)*	This study
pKS793	pGEMT-easy	*mod5Δ(231-235)*	This study
pKS794	pGEMT-easy	*mod5Δ(236-240)*	This study
pKS795	pGEMT-easy	*mod5Δ(241-245)*	This study
pKS796	pGEMT-easy	*mod5Δ(246-250)*	This study
pKS797	pGEMT-easy	*mod5Δ(251-256)*	This study
pKS818	pDONR221	Tea1-(S556A)	This study
pKS819	pDONR222	Tea1-(S556A)	This study
pKS820	pDONR223	Tea1-(S556D)	This study
pKS821	pDONR224	Tea1-(Y484F)	This study
pKS851	pDONR225	Tea1-(S462A)	This study
pKS852	pDONR226	Tea1-(S462A,S467A,S476A)	This study
pKS853	pDONR227	Tea1-(S462D,S467D,S476D)	This study
pKS865	pDUAL-GFH1c	Tea1-(S556A)	This study
pKS866	pDUAL-GFH1c	Tea1-(S556D)	This study
pKS867	pDUAL-GFH1c	Tea1-(Y484F)	This study
pKS869	pDUAL-GFH1c	Tea1-(S462A,S467A,S476A)	This study
pKS871	pDUAL-GFH1c	Tea1-(S462D,S467D,S476D)	This study

pKS912	pDONR221	*mod5(2-523)*	This study
pKS914	pDUAL- HFF41c	Mod5	This study
pKS1025	pDONR221	*tea1Δ(697-726)*	This study
pKS1026	pDONR221	*tea1Δ(697-762)*	This study
pKS1027	pDUAL-GFH1c	*tea1Δ(697-726)*	This study
pKS1028	pDUAL-GFH1c	*tea1Δ(697-762)*	This study
pKS1029	pDONR221	*tea1Δ(726-762)*	This study
pKS1030	pDUAL-GFH1c	*tea1Δ(726-762)*	This study
pKS1102	p0GWA	Tea1	This study
pKS1103	pHMGWA	*mod5(28-477)*	This study
pKS1104	pDUAL- HFF41c	-	(Matsuyama et al., 2004)
pKS1105	pDUAL-GFH1c	-	(Matsuyama et al., 2004)

Table 2.10- List of strains used in this study

Name	Genotype	Source
KS515	*h+ ade6-M216 ura4-D18 leu1-32*	Sawin Lab
KS516	*h- ade6-M210 ura4-D18 leu1-32*	Sawin Lab
KS706	*h- kanMX6:nmt81GFP-mod5 ade6-M210 leu1-32 ura4-D18*	(Snaith and Sawin, 2003)
KS714	*h- kanMX:nmt81:GFP- mod5 tea1Δ::ura4+ ura4-D18 leu1-32 ade6-M216*	(Snaith and Sawin, 2003)
KS780	*h+ mod5Δ::kanMX6 ade6-M216 leu1-32 ura4-D18*	(Snaith and Sawin, 2003)
KS1259	*h- tea1GFP:kanMX ura4-D18 leu1-32 ade6-M216*	Sawin Lab
KS1259	*h- tea1-GFP:kanMX ura4-D18 leu1-32 ade6-M210*	(Snaith and Sawin, 2003)
KS1260	*h+ tea1-GFP:kanMX ura4-D18 leu1-32 ade6-M210*	Sawin Lab
KS2223	*h- tea3GFP::kanMX6 tea1Δ::ura4+ mod5Δ::kanMX6 ade6-M210 leu1-32 ura4-D18*	Sawin Lab
KS2739	*h- tea1-TAPS:kanMX6 ade6-M210 leu1-32 ura4-D18*	Sawin Lab
KS2958	*h- mod5Δ::hphMX6 tea1-TAPS:kanMX6 ade6-M210 leu1-32 ura4-D18*	This study
KS3138	*h- tea1-tdTomato:natMX6 ade6-210 leu1-32 ura4-D18*	This study
KS3316	*h- arg1-230*	Sawin Lab
KS3626	*h+ mod5Δ::ura4+ kan+ ade6-M216 leu1-32 ura4-D18*	This study
KS3695	*h+ mod5Δ-(196-200) kan+ ade6-M216 leu1-32 ura4-D18*	This study
KS3696	*h+ mod5Δ-(201-205) kan+ ade6-M216 leu1-32 ura4-D18*	This study
KS3697	*h+ mod5Δ-(206-210) kan+ ade6-M216 leu1-32 ura4-D18*	This study
KS3698	*h+ mod5Δ-(211-215) kan+ ade6-M216 leu1-32 ura4-D18*	This study
KS3699	*h+ mod5Δ-(216-220) kan+ ade6-M216 leu1-32 ura4-D18*	This study
KS3700	*h+ mod5Δ-(221-225) kan+ ade6-M216 leu1-32 ura4-D18*	This study
KS3701	*h+ mod5Δ-(226-230) kan+ ade6-M216 leu1-32 ura4-D18*	This study
KS3702	*h+ mod5Δ-(231-235) kan+ ade6-M216 leu1-32 ura4-D18*	This study
KS3703	*h+ mod5Δ-(241-245) kan+ ade6-M216 leu1-32 ura4-D18*	This study
KS3745	*h+ tea1-tdTomato:natMX6 tea3-GFP:hph ade6-210 leu1-32 ura4-D18*	This study
KS3746	*h- tea1-tdTomato:natMX6 tea3-GFP:hph ade6-210 leu1-32 ura4-D18*	This study
KS3747	*h- tea1-tdTomato:natMX6 tea3-GFP:hph mod5Δ: kan MX6(500bp) ade6-210 leu1-32 ura4-D18*	This study
KS3748	*h? tea1-tdTomato:natMX6 tea3-GFP:hph mod5Δ: kan MX6(500bp) ade6-210 leu1-32 ura4-D18*	This study
KS3749	*h- mod5Δ-(196-200aa) kanMX6 tea1-tdTomato: natMX6 tea3-GFP:hph ade6-M216 leu1-32 ura4-D18*	This study
KS3750	*h- mod5Δ-(201-205aa) kanMX6 tea1-tdTomato: natMX6 tea3-GFP:hph ade6-M216 leu1-32 ura4-D18*	This study
KS3751	*h- mod5Δ-(206-210aa) kanMX6 tea1-tdTomato: natMX6 tea3-GFP:hph ade6-M216 leu1-32 ura4-D18*	This study
KS3752	*h+ mod5Δ-(211-215aa) kanMX6 tea1-tdTomato: natMX6 tea3-GFP:hph ade6-M216 leu1-32 ura4-D18*	This study
KS3754	*h+ mod5Δ-(221-225aa) kanMX6 tea1-tdTomato: natMX6 tea3-GFP:hph ade6-M216 leu1-32 ura4-D18*	This study
KS3755	*h- mod5Δ-(226-230aa) kanMX6 tea1-tdTomato: natMX6 tea3-GFP:hph ade6-M216 leu1-32 ura4-D18*	This study
KS3756	*h- mod5Δ-(231-235aa) kanMX6 tea1-tdTomato: natMX6 tea3-GFP:hph*	This study

	ade6-M216 leu1-32 ura4-D18	
KS3756	*h- mod5Δ-(231-235aa) kanMX6 tea1-tdTomato: natMX6 tea3-GFP:hph ade6-M216 leu1-32 ura4-D18*	This study
KS3757	*h+ mod5Δ-(241-245aa) kanMX6 tea1-tdTomato: natMX6 tea3-GFP:hph ade6-M216 leu1-32 ura4-D18*	This study
KS3892	*h-mod5Δ-(156-160) kan+ tea1-tdT:natMX6 tea3-GFP:hph ade6-M216 leu1-32 ura4-D18*	This study
KS3893	*h+ mod5Δ-(161-165) kan+ tea1-tdT:natMX6 tea3-GFP:hph ade6-M216 leu1-32 ura4-D18*	This study
KS3894	*h+ mod5Δ-(166-170) kan+ tea1-tdT:natMX6 tea3-GFP:hph ade6-M216 leu1-32 ura4-D18*	This study
KS3895	*h- mod5Δ-(176-180) kan+ tea1-tdT:natMX6 tea3-GFP:hph ade6-M216 leu1-32 ura4-D18*	This study
KS3896	*h+ mod5Δ-(181-185) kan+ tea1-tdT:natMX6 tea3-GFP:hph ade6-M216 leu1-32 ura4-D18*	This study
KS3897	*h- mod5Δ-(186-190) kan+ tea1-tdT:natMX6 tea3-GFP:hph ade6-M216 leu1-32 ura4-D18*	This study
KS3898	*h+mod5Δ-(191-195) kan+ tea1-tdT:natMX6 tea3-GFP:hph ade6-M216 leu1-32 ura4-D18*	This study
KS3899	*h+mod5Δ-(236-240) kan+ tea1-tdT:natMX6 tea3-GFP:hph ade6-M216 leu1-32 ura4-D18*	This study
KS3900	*h+ mod5Δ-(246-250) kan+ tea1-tdT:natMX6 tea3-GFP:hph ade6-M216 leu1-32 ura4-D18*	This study
KS3901	*h+ mod5Δ-(251-256) kan+ tea1-tdT:natMX6 tea3-GFP:hph ade6-M216 leu1-32 ura4-D18*	This study
KS3995	*h+ pom1Δ::ura4+ tea1-TAPS:kanMX6 ade6-M216 leu1-32 ura4-D18*	This study
KS3997	*h- orb2-34 tea1-TAPS:kanMX6 ade6-M210 leu1-32 ura4-D18*	This study
KS3999	*h- tea1Δ200-TAPS:kanMX6 ade6-M210 leu1-32 ura4-D18*	This study
KS4001	*h+ tip1Δ299:hphMX6 mod5Δ::natMX6 tea1-TAPS:kanMX6 ade6-M210 leu1-32 ura4-D18*	This study
KS4018	*bud6Δ::hphMX6 tea1-TAPS:kanMX6 tea3Δ::kanMX6 tea4Δ::hphMX6 ade6-M216 leu1-32 ura4-D18*	This study
KS4029	*h+ win1Δ::LEU2 wis4Δ::ura4 tea1-TAPS:kanMX6 ade6-M21(?) leu1-32 ura4-D18(?)*	This study
KS4116	*h? tea3-GFP:hph tea1Δ::ura4+ ade6-210 leu1-32 ura4-D18*	This study
KS4117	*tea1Δ::ura4+ mod5Δ-(196-200aa):kanMX6 tea3-GFP:hph ade6-M216 leu1-32 ura4-D18*	This study
KS4118	*tea1Δ::ura4+ mod5Δ-(201-205aa):kanMX6 tea3-GFP:hph ade6-M216 leu1-32 ura4-D18*	This study
KS4119	*tea1Δ::ura4+ mod5Δ-(206-210aa):kanMX6 tea3-GFP:hph ade6-M216 leu1-32 ura4-D18*	This study
KS4120	*tea1Δ::ura4+ mod5Δ-(211-215aa):kanMX6 tea3-GFP:hph ade6-M216 leu1-32 ura4-D18*	This study
KS4121	*tea1Δ::ura4+ mod5Δ-(216-220aa):kanMX6 tea3-GFP:hph ade6-M216 leu1-32 ura4-D18*	This study
KS4122	*tea1Δ::ura4+ mod5Δ-(221-225aa):kanMX6 tea3-GFP:hph ade6-M216 leu1-32 ura4-D18*	This study
KS4123	*tea1Δ::ura4+ mod5Δ-(226-230aa):kanMX6 tea3-GFP:hph ade6-M216 leu1-32 ura4-D18*	This study
KS4124	*tea1Δ::ura4+ mod5Δ-(231-235aa):kanMX6 tea3-GFP:hph ade6-M216 leu1-32 ura4-D18*	This study
KS4125	*tea1Δ::ura4+ mod5Δ-(241-245aa):kanMX6 tea3-GFP:hph ade6-M216 leu1-32 ura4-D18*	This study

KS4126	*tea1Δ::ura4+ mod5Δ-(156-160aa):kanMX6 tea3-GFP:hph ade6-M216 leu1-32 ura4-D18*	This study
KS4127	*tea1Δ::ura4+ mod5Δ-(161-165aa):kanMX6 tea3-GFP:hph ade6-M216 leu1-32 ura4-D18*	This study
KS4128	*tea1Δ::ura4+ mod5Δ-(166-170aa):kanMX6 tea3-GFP:hph ade6-M216 leu1-32 ura4-D18*	This study
KS4129	*tea1Δ::ura4+ mod5Δ-(176-180aa):kanMX6 tea3-GFP:hph ade6-M216 leu1-32 ura4-D18*	This study
KS4130	*tea1Δ::ura4+ mod5Δ-(181-185aa):kanMX6 tea3-GFP:hph ade6-M216 leu1-32 ura4-D18*	This study
KS4131	*tea1Δ::ura4+ mod5Δ-(186-190aa):kanMX6 tea3-GFP:hph ade6-M216 leu1-32 ura4-D18*	This study
KS4132	*tea1Δ::ura4+ mod5Δ-(191-195aa):kanMX6 tea3-GFP:hph ade6-M216 leu1-32 ura4-D18*	This study
KS4133	*tea1Δ::ura4+ mod5Δ-(236-240aa):kanMX6 tea3-GFP:hph ade6-M216 leu1-32 ura4-D18*	This study
KS4134	*tea1Δ::ura4+ mod5Δ-(246-250aa):kanMX6 tea3-GFP:hph ade6-M216 leu1-32 ura4-D18*	This study
KS4135	*tea1Δ::ura4+ mod5Δ-(251-256aa):kanMX6 tea3-GFP:hph ade6-M216 leu1-32 ura4-D18*	This study
KS4293	*h+ tea1Δ::ura4+ leu1-32*	This study
KS4344	*h- tea1Δ::ura4+ leu1-32:p[leu1+:nmt81:tea1-GFP-FLAG-6His] ade6-M210 ura4-D18*	This study
KS4417	*h+ tea1Δ::ura4+ leu1-32:p[leu1+:nmt1:tea1-GFP-FLAG-6His] ade6-M210 ura4-D18*	This study
KS4417	*h+ tea1Δ::ura4+ leu1-32:p[leu1+:nmt1:tea1-GFP-FLAG-6His] ade6-M210 ura4-D18*	This study
KS4524	*h+ NatMX6:nmt81:GFPmod5Δ(156-160) kan+ ade6-M216 leu1-32 ura4-D18*	This study
KS4526	*h+ NatMX6:nmt81:GFPmod5Δ(226-230) kan+ ade6-M216 leu1-32 ura4-D18*	This study
KS4528	*h+ NatMX6:nmt81:GFPmod5Δ(231-236) kan+ ade6-M216 leu1-32 ura4-D18*	This study
KS4530	*h+ tea1(Δ400-600)GFP::kanMX::ura4+ ura4-D18 leu1-32 ade6-M210*	This study
KS4630	*h- tea1Δ::ura4+ leu1-32:p[leu1+:nmt1:tea1-S556A-GFP-FLAG-6His] ade6-M210 ura4-D18*	This study
KS4632	*h- tea1Δ::ura4+ leu1-32:p[leu1+:nmt1:tea1-S556D-GFP-FLAG-6His] ade6-M210 ura4-D18*	This study
KS4634	*h- tea1Δ::ura4+ leu1-32:p[leu1+:nmt1:tea1-Y484F-GFP-FLAG-6His] ade6-M210 ura4-D18*	This study
KS4636	*h- tea1Δ::ura4+ leu1-32:p[leu1+:nmt1:tea1-S462AS467AS476A-GFP-FLAG-6His] ade6-M210 ura4-D18*	This study
KS4638	*h- tea1Δ::ura4+ leu1-32:p[leu1+:nmt1:tea1-S462D S467D S476D-GFP-FLAG-6His] ade6-M210 ura4-D18*	This study
KS4684	*h+ mod5Δ::kanMX6 tea1-tdTomato:natMX6 hphMX6:nmt81GFP-atb2 leu1-32ade6-M210 ura4-D18*	This study
KS4703	*h- car1Δ::kanMX4 arg1-230*	This study
KS4706	*h- aru1Δ::kanMX4 arg1-230*	This study
KS4709	*h- car2Δ::kanMX4 arg1-230*	This study
KS4731	*h- car1Δ::kanMX4 aru1Δ ::kanMX4 arg1-230*	This study
KS4734	*h+ tea1Δ(434-478)-GFP:kanMX ura4-D18 leu1-32 ade6-M210*	This study
KS4736	*h+ tea1Δ(479-532)-GFP:kanMX ura4-D18 leu1-32 ade6-M210*	This study

KS4738	*h+ tea1Δ(533-586)-GFP:kanMX ura4-D18 leu1-32 ade6-M210*	This study
KS4740	*h+ tea1Δ(434-586)-GFP:kanMX ura4-D18 leu1-32 ade6-M210*	This study
KS4774	*h? tea1-tdTomato:natMX6 leu1-32:p[leu1+:nmt1:tea1-GFP-FLAG-6His] ade6-M210 ura4-D18*	This study
KS4776	*h? tea1Δ(434-478)-GFP:kanMX mod5Δ::hphMX6 ade6-M210 leu1-32 ura4-D18*	This study
KS4778	*h? tea1Δ(479-532)-GFP:kanMX mod5Δ::hphMX6 ade6-M210 leu1-32 ura4-D18*	This study
KS4780	*h? tea1Δ(533-586)-GFP:kanMX mod5Δ::hphMX6 ade6-M210 leu1-32 ura4-D18*	This study
KS4782	*h? tea1Δ(434-586)-GFP:kanMX mod5Δ::hphMX6 ade6-M210 leu1-32 ura4-D18*	This study
KS4821	*h- mod5Δ::hphMX6 leu1-32:p[leu1+:nmt41:6His-FLAG2-mod5] ade6-M210 ura4-D18*	This study
KS4825	*h? tea1Δ(434-478)-tdTomato:natMX6 ura4-D18 leu1-32 ade6-M210 KanMX::nmt81::GFP-atb2*	This study
KS4827	*h? tea1Δ(479-532)-tdTomato:natMX6 ura4-D18 leu1-32 ade6-M210 KanMX::nmt81::GFP-atb2*	This study
KS4829	*h? tea1Δ(533-586)-tdTomato:natMX6 ura4-D18 leu1-32 ade6-M210 KanMX::nmt81::GFP-atb2*	This study
KS4831	*h? tea1Δ(434-586)-tdTomato:natMX6 ura4-D18 leu1-32 ade6-M210 KanMX::nmt81::GFP-atb2*	This study
KS4889	*h- kanMX6:nmt81GFP-mod5 leu1-32:p[leu1+:nmt41:6His-FLAG2-mod5] ade6-M210 ura4-D18*	This study
KS4891	*h- KanMX6:nmt81:GFP-mod5 leu1-32:p[leu1+:nmt41:6His FLAG2-mod5] tea1Δ::ura4+ ade6-M210 ura4-D18*	This study
KS4893	*h? KanMX6:nmt81:GFP-mod5 leu1-32:p[leu1+:nmt41:6His FLAG2-mod5] tea3Δ::natMX6 ade6-M210 ura4-D18*	This study
KS4895	*h? KanMX6:nmt81:GFP-mod5 leu1-32:p[leu1+:nmt41:6His FLAG2-mod5] tea3Δ::natMX6 tea1Δ::ura4+ ade6-M210 ura4-D18*	This study
KS5036	*h- lys3-37*	Sawin Lab
KS5042	*h- car2Δ::kanMX4 arg1-230 lys3-37*	This study
KS5344	*h+ cdc25-22 car2Δ::kanMX4 hphMX6:nmt81:GFP-atb2 arg1-230 lys3-37*	This study
KS5566	*h- Uds1-GFP:KanMX6 ade6-M210 ura4-D18 leu1-32*	This study
KS5570	*h? Uds1-GFP cdc25-22 leu1-32 ade6-? ura4-?*	This study
KS5655	*h+ tea1Δ(600-850aa)GFP::ura4+ :kanMX ura4-D18 leu1-32 ade6-M210*	This study
KS5661	*h+ tea1Δ(697-726aa)GFP:kanMX ura4-D18 leu1-32 ade6-M210*	This study
KS5664	*h+ tea1Δ(697-762aa)GFP:kanMX ura4-D18 leu1-32 ade6-M210*	This study
KS5811	*h? tea1Δ(697-726aa)tdTomato:NatMX6 leu1-32:p[leu1+:nmt1:tea1-GFP-FLAG-6His] ade6-M210 ura4-D18*	This study
KS5813	*h? tea1Δ(697-762aa)tdTomato:NatMX6 leu1-32:p[leu1+:nmt1:tea1-GFP-FLAG-6His] ade6-M210 ura4-D18*	This study
KS5905	*h? tea1Δ(697-726aa)tdTomato:NatMX6 leu1-32:p[leu1+:nmt1:tea1Δ(697-726)GFP-FLAG-6His] ade6-M210 ura4-D18*	This study
KS5906	*h? tea1Δ(697-726aa)tdTomato:NatMX6 leu1-32:p[leu1+:nmt1:tea1Δ(697-726)GFP-FLAG-6His] ade6-M210 ura4-D18*	This study
KS5907	*h? tea1Δ(697-762aa)tdTomato:NatMX6 leu1-32:p[leu1+:nmt1:tea1Δ(697-762)GFP-FLAG-6His] ade6-M210 ura4-D18*	This study
KS5908	*h? tea1Δ(697-762aa)tdTomato:NatMX6 leu1-32:p[leu1+:nmt1:tea1Δ(697-762)GFP-FLAG-6His] ade6-M210 ura4-D18*	This study
KS5980	*h+ tea1Δ(726-762aa)GFP:kanMX ura4-D18 leu1-32 ade6-M210*	This study

Chapter III: Molecular analyses of Tea1-Mod5 interaction at the cell tip

3.1. Introduction

Previous work has shown that Tea1 and Mod5 physically interact with each other and that their localizations at the cell tip are co-dependent (Snaith et al., 2005; Snaith and Sawin, 2003). These observations lead to the proposal of a model in which Tea1 and Mod5 accumulate at the cell tip in a positive feedback mechanism (depicted in Figure 1.6) (Snaith and Sawin, 2003). In such mechanism, upon microtubule-based delivery of Tea1 to the cell tip, Tea1 recruits membrane-associated Mod5 specifically to the cell tip. Thus, the increase in Mod5 molecules at the cell tip is Tea1-dependent and would result on an increased accumulation of Tea1 at the same location, upon its microtubule-based delivery. The proposed positive feedback mechanism suggests that Mod5 could act as a molecular-receptor for Tea1 at the cell membrane (Martin, 2009; Snaith and Sawin, 2003). Although, a positive feedback mechanism for Tea1 and Mod5 localization has been proposed, the molecular basis of Tea1-Mod5 interactions at the cell tip are still poorly understood. Moreover, it stills unclear how Tea1-Mod5 interaction contributes for cell polarity.

FRAP (Fluorescence Recovery After Photo bleaching) was used to determine Tea1 and Mod5 dynamics at the cell tip. FRAP was developed in 1970s, and mainly used as a technique to determine diffusion constants of biomolecules in membranes (Sprague and McNally, 2005). However, with the discovery of naturally fluorescent proteins, FRAP became a widely used experimental approach in studying proteins dynamics within the cell (Lippincott-Schwartz et al., 2003). In a FRAP experiment, proteins are fused to a fluorescent protein or a fluorescent dye and a small region of the cell is bleached with a high-powered laser beam. The recovery of the fluorescence from the surrounding areas is followed with low light intensity. With FRAP it is possible to measure protein kinetic parameters, such as rate of mobility and the mobile fraction of the protein, and also the protein kinetics of binding (Lippincott-Schwartz et al., 2001; Sprague and McNally, 2005). Moreover, the qualitative analysis of the recovery curve is informative about the binding and unbinding properties of the protein to its substrate(s) (Sprague and McNally, 2005). Unlike *in vitro* measurements, FRAP allows the determination of protein kinetic parameters in different subcellular compartments.

Mathematical modeling in cell biology attempts to recapitulate *in silico* the properties of *in vivo* systems. Mathematical modeling can formalize complex mechanisms, such as cell cycle regulation, with simple reactions with the minimal number of components (Tyson et al., 2003). Thus, mathematical modeling allows the testing of hypothesis related with a particular system, and consequently the *in silico* analysis of the physiological consequences. Modeling is of significant relevance when the hypothesis to be tested is technically challenging to be shown experimentally. Moreover, mathematical models not only describe the properties of a given system but can also predict unforeseen properties of such system. During the modeling process, the system to be modeled is mathematically formalized and described with a set of equations and a set of variables. Then, the model is parameterized and the numerical values of the variables are defined. These values can either be experimental measured or can be fitted parameters. Finally, the mathematical model is numerically simulated to generate the output solutions (Tyson et al., 2003).

This chapter describes a molecular mechanism of Tea1-Mod5 interaction at the cell tip. Tea1-Mod5 interaction was dissected using a combination of FRAP and quantitative imaging approaches, in combination with mathematical modeling. Dr Andrew Goryachev, from the Center for Systems Biology at University of Edinburgh did the mathematical modeling described in this chapter. The simulations obtained with the mathematical model of Tea1-Mod5 interaction were then used to understand Tea1 function as a cortical polarity landmark.

3.2. Results

3.2.1. Cell tip associated Tea1 does not turn over

To better understand Tea1-Mod5 interaction at the cell tip I used FRAP to determine the dynamics of both proteins.

Figure 3.1A shows the schematic diagram of the experimental design used to determine the turn over of tip-associated Tea1-GFP with the cytoplasm. Tea1-GFP was photobleached from the entire cell tip (hereafter designated by “full-tip FRAP”) and after 5 min the fluorescence intensity was only recovered to ~ 20% of its initial intensity. This shows that tip-associated Tea1-GFP turns over extremely slowly with the cytoplasm.

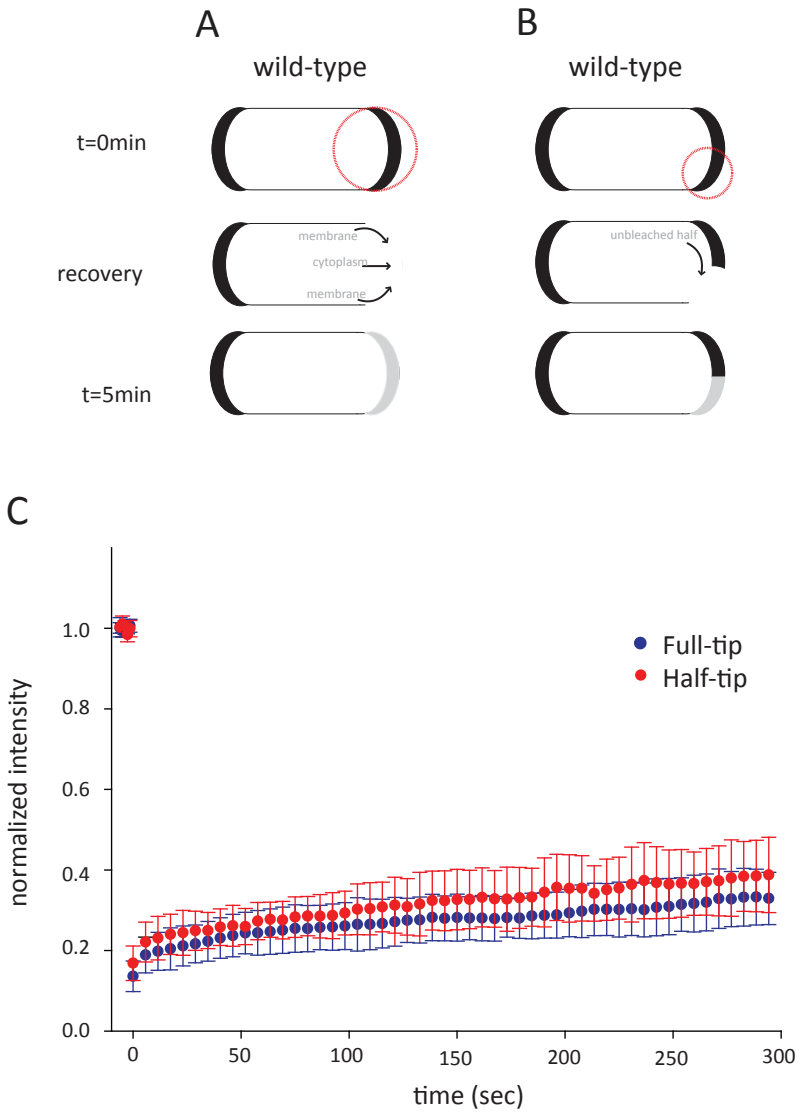

Figure 3.1-Tea1-GFP FRAP. A and B) Diagram of FRAP experimental design and result. A) Tea1-GFP (KS1260) was bleached from the entire cell tip and **B)** from half of the cell tip. Red circle represents position and width of bleaching laser beam. Arrows represent Tea1-GFP movement during recovery. **C) Tea1-GFP recovery curves.** Tea1-GFP fluorescence recovery when it is bleached from the entire cell tip (blue curve, n= 20 cell tips) and from half the cell tip (red curve, n= 13 cell tips). Fluorescence recovery was recorded every 5 sec for 5 min. Error bars are standard deviation.

Next, I determined the turnover rate of Tea1 within the cell tip by photobleaching only half of the cell tip (hereafter designated by "half-tip FRAP"). With the full-tip FRAP it was established that Tea1 does not exchange with the cytoplasm, thus in a half-tip FRAP all the fluorescence recovery will be due to exchange between bleached and unbleached proteins within the cell tip. Figure 3.1B shows the schematic diagram of the half-tip FRAP experimental design, as well as the experiment result. Figure 3.1C shows that when Tea1-GFP is photobleached from half of the cell tip, after 5 min, it recovers to only ~ 20% of its initial fluorescence intensity. This means that Tea1-GFP turn over within the cell tip is very slow, demonstrating that Tea1 is stably associated at the cell tip. Therefore, despite Tea1 is targeted to the cell tip at a high and permanent rate on microtubule plus-ends, a fraction of delivered Tea1 do not accumulate at the cell tip.

3.2.2 Mod5 is dynamic within the cell tip

Next, GFP-Mod5 dynamics at the cell tip were analyzed using the same experimental approach as for Tea1-GFP. Figure 3.2A shows the schematic diagram of the experimental design and experiment outcome and Figure 3.2D shows the curve of GFP-Mod5 fluorescence recovery after photobleaching. After 5 min, the fluorescence recovers to ~ 20% of its initial value. This indicates that when GFP-Mod5 is tip-associated it exchanges slowly with the cytoplasm and with the rest of the cell membrane.

To examine Mod5 diffusion within the cell membrane, GFP-Mod5 was photobleached from the entire cell tip in a *tea1Δ* background (Figure 3.2B). In *tea1Δ* mutants, GFP-Mod5 does not accumulate at the cell tip and spreads around the entire cell membrane (Snaith et al., 2005; Snaith and Sawin, 2003). Figure 3.2D shows that in *tea1Δ* cells the fluorescence of GFP-Mod5 completely recovers after 5 min. Thus, in the absence of Tea1, GFP-Mod5 diffuses freely within the cell membrane.

GFP-Mod5 turnover within the cell tip was then examined by photobleaching half the cell tip, as depicted in Figure 3.2C. Figure 3.2E shows that after 5 min, within the cell tip, GFP-Mod5 fluorescence intensity recovers to half of its initial value. Half of the initial intensity is the expected recovery if GFP-Mod5 is mobile within the cell tip. Thus, although cell tip-associated GFP-Mod5 does not turnover with the cytoplasm and the rest of the cell membrane, it is mobile within the cell tip.

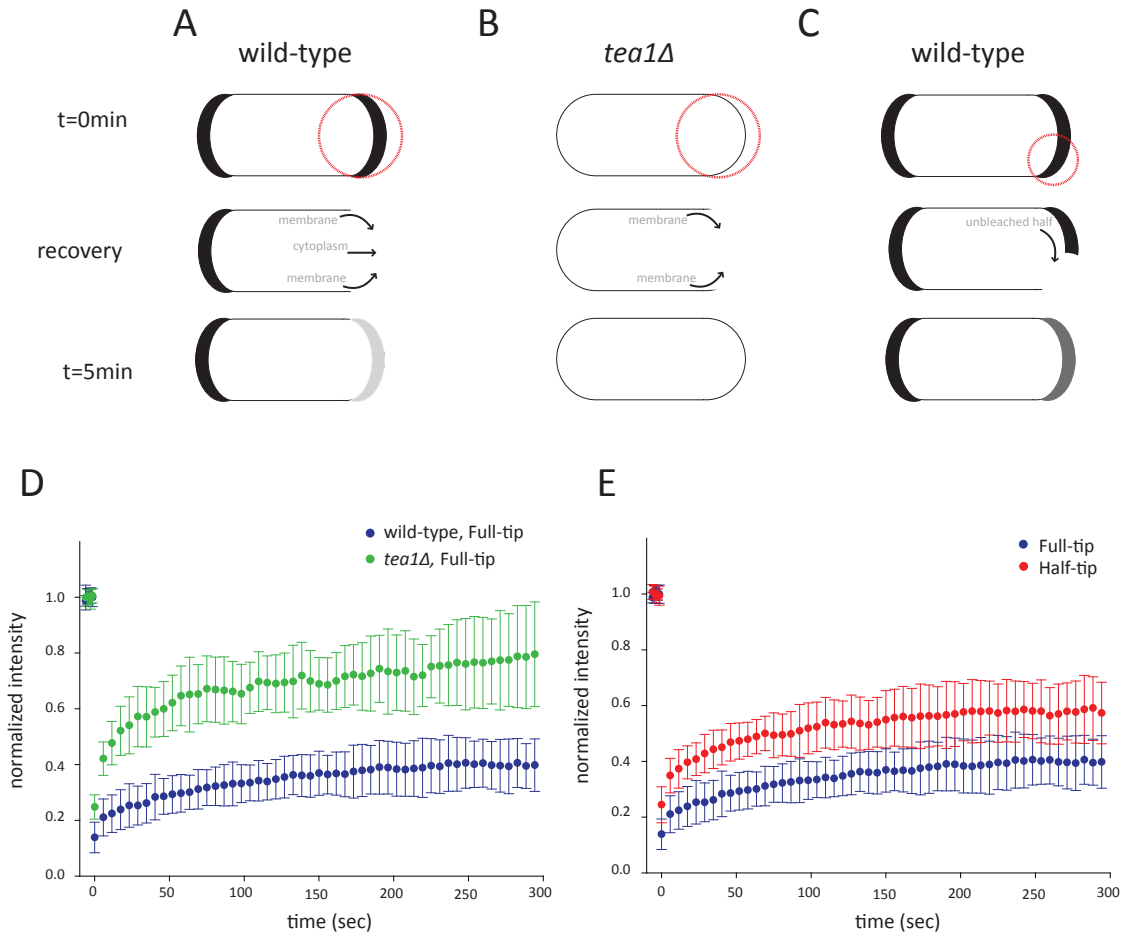

Figure 3.2-GFP-Mod5 FRAP. A-C) Diagram of FRAP experimental design and result. GFP-Mod5 was photobleached from **A)** the entire cell tip in wild-type (KS706), **B)** the entire cell tip in *tea1Δ* (KS714) cells, and **C)** from half the cell tip in wild-type cells. Red circle represents position and width of bleaching laser beam. Arrows represent GFP-Mod5 movement during recovery. **D) GFP-Mod5 recovery curves**. GFP-Mod5 fluorescence recovery when it is bleached from the entire cell tip from wild-type (blue curve, n= 16 cell tips) and from *tea1Δ* cells (green curve, n= 19 cell tips). **E) GFP-Mod5 recovery curves.** GFP-Mod5 fluorescence recovery when it is bleached from the entire cell tip (blue curve) and from half-tip (green curve, n= 19 cell tips) from wild-type. The fluorescence recovery was recorded every 5 sec for 5 min. Error bars are standard deviation.

FRAP results showed that once Tea1 and Mod5 are present at the cell tip, they exchange only very slowly with the cytoplasm. This indicates that the cortical structure where Tea1 and Mod5 are incorporated is very stable. Importantly, FRAP analysis also demonstrated that, within the cell tip, Tea1 and Mod5 turnover at different rates. While Tea1 is largely immobile, Mod5 is mobile, which suggests that Tea1 and Mod5 interact transiently.

3.2.3. Tea1 forms a stable cluster-network at the cell tip

How can a stable complex be formed as a result of transient interactions? In order to reconcile this apparent contradiction we aimed to dissect the molecular details of Tea1 and Mod5 dynamic interaction.

First, we focused on understanding Tea1 stability at the cell tip. The immobility of Tea1 observed in the FRAP experiments suggests that it binds to a stable cortical structure, of unknown molecular composition. Proteins can become immobile either due to binding to a pre-existent cortical network, like the Fascin-Actin interaction in the lamellipodia (Aratyn et al., 2007), or due to *de novo* self-assembly of an immobile structure, like the clustering of the membrane-associated protein SyntaxinI (Sieber et al., 2007).

We began by analyzing the hypothesis of Tea1 binding to a pre-existent stable cortical network. In *S. pombe*, the cell cortex is rich in polymeric actin, which could provide the necessary scaffold for Tea1 binding (Siegrist and Doe, 2007). Thus, the role of cortical actin in Tea1 stability at the cell tip was tested. Actin cytoskeleton was depolymerized with latranculin B (LatB) and the fluorescence intensity of Tea1-GFP was used as readout of its stability at cell tip. Figure 3.3A and 3.3B show that the decay of Tea1-GFP fluorescence at the cell tip after actin depolymerization is kinetically similar to untreated cells. This shows that actin does not play a role in Tea1 stability at the cell tip.

If actin does not provide the cortical scaffold for Tea1 binding, what does? Deletion of any of the described Tea1-interactors, with the exception of Mod5, does not completely prevent Tea1 accumulation to the cell tip. Although Tea1 accumulation in the *tea4Δ* mutant is monopolar, nevertheless Tea1 can localize at the cell tip. This indicates that Tea1-Tea4 interaction is not completely essential for Tea1 accumulation *per se* (Martin et al., 2005; Tatebe et al., 2005). This suggests that Tea1 stability at the cell tip might depend on Tea1 itself. Previously Martin *et al* have shown *in vitro* that Tea1 interacts with itself via its C-

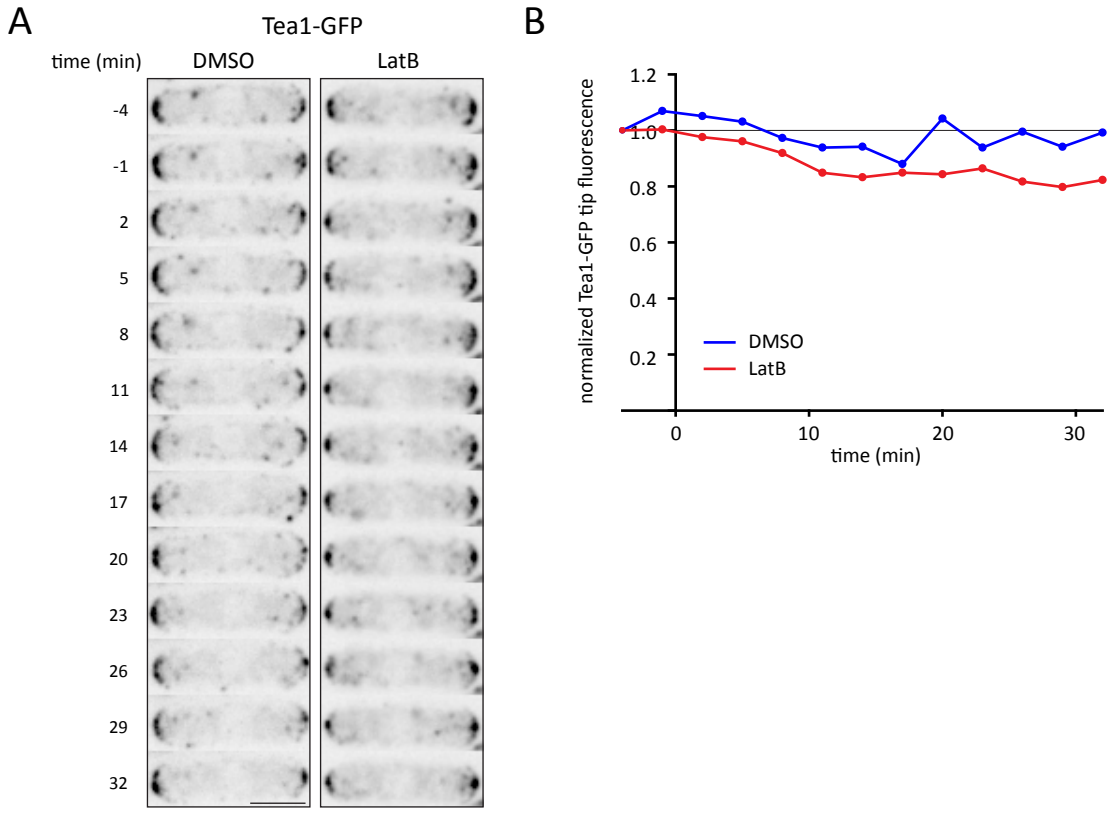

Figure 3.3- Tea1-GFP stability at the cell tip after actin cytoskeleton depolymerization. A) Actin cytoskelteon was depolymerized with LatB and Tea1-GFP (KS1260) was imaged every 3 min. Cells were treated with DMSO as a control for drug solvent. **B)** Tea1-GFP fluorescence intensity at the cell tip over 32 min after DMSO and LatB treament at the cell tip was quantified and normalized. Actin cytoskelteon depolymerization does not affect Tea1-GFP stability at the cell tip. Time zero indicates 7 min after drug addition. This figure was contributed by Dr Hilary Snaith. Bar, 5 µm.

terminus (Martin et al., 2005). Therefore, Tea1 may form a stable complex at the cell tip due to Tea1-Tea1 interactions.

Next, I aimed to demonstrate that Tea1 binds Tea1 *in vivo*. Therefore, Tea1-GFP and Tea1-tdTomato were co-expressed in a haploid strain and their interaction was tested. Figure 3.4A shows that when Tea1-GFP and Tea1-tdTomato are co-expressed they co-localize at the microtubule plus-ends and at the cell tip. Moreover, Figure 3.4B shows that Tea1-tdTomato and Tea1-GFP co-immunoprecipitate, demonstrating that Tea1 interacts with itself *in vivo.*

To further confirm Tea1-Tea1 interaction I sought to identify regions necessary for such interaction. Figure 3.5A shows the Multi-Coil prediction of Tea1 oligomerization domains (Wolf et al., 1997). Multi-Coil predicts domains of oligomerization based in protein sequence. As described in the Chapter I, protein dimerization and trimerization occur via coiled-coil domains that have a repetitive and predictable pattern. Multicoil predicts with high probability a dimeric region (aa 697 to 726, ~ 70% probability) and a trimeric region (aa 727-762, ~ 70% probability).

To examine the consequences of disrupting Tea1-Tea1 interaction, I constructed three putative Tea1 oligomerization mutants. Figure 3.5B shows a schematic diagram of the three Tea1 oligomerization mutants: *tea1Δdimer* (deletion of aa 697 to 726), *tea1Δtrimer* (deletion of aa 727 to 762), and *tea1ΔdimerΔtrimer* (deletion of aa 697 to 762). Figure 3.5C shows that Tea1 oligomerization mutants are expressed at similar levels as wild-type Tea1-GFP.

Figure 3.6A shows localization of Tea1 oligomerization mutants. Tea1Δdimer-GFP localizes at the cell tip and at the microtubules plus-ends. Tea1Δtrimer-GFP and Tea1ΔdimerΔtrimer-GFP do not accumulate at the cell tip, and are only observed at the microtubule plus-ends. The localization patterns of *tea1Δtrimer* and *tea1ΔdimerΔtrimer* resemble Tea1 localization in *mod5Δ*, suggesting an anchoring defect.

The reduced accumulation of Tea1 oligomerization mutants at the cell tip could be due to a decreased in their association with microtubules, which would reduce microtubule-based delivery and consequently Tea1 accumulation. Figure 3.6B shows that Tea1Δdimer, Tea1Δtrimer, Tea1ΔdimerΔtrimer microtubule-based delivery to the cell tip is similar to wild-type Tea1.

Lack of accumulation of Tea1 oligomerization mutants at the cell tip could also be due to the disruption of their interactions with Mod5, as Tea1-Mod5 interaction had been

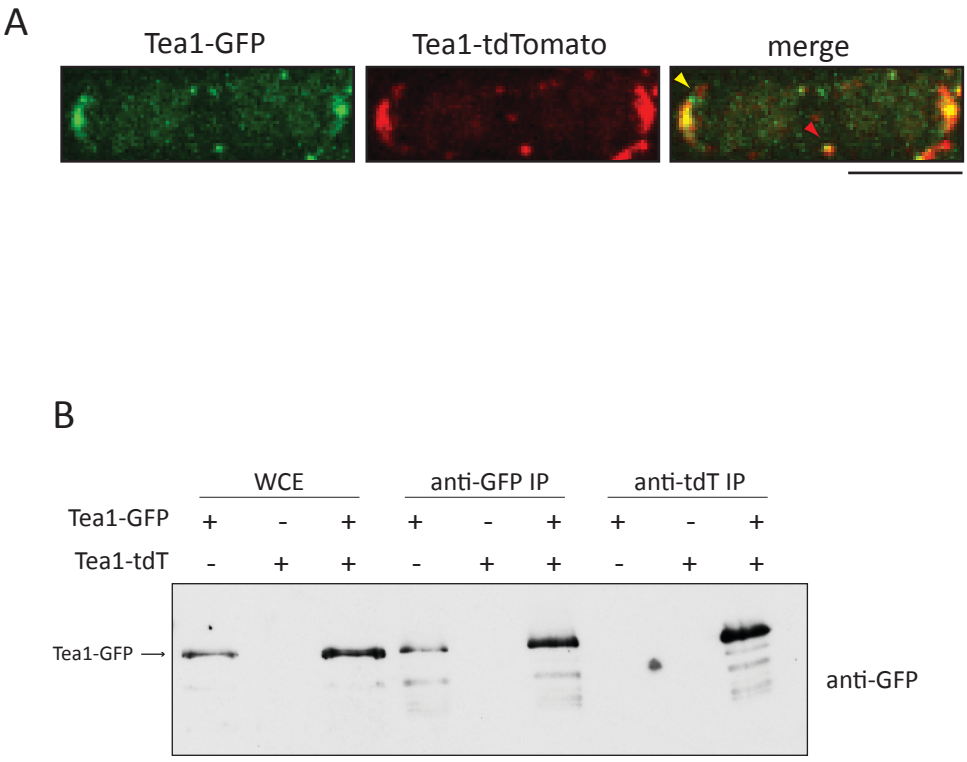

Figure 3.4- Analysis of Tea1-Tea1 interaction *in vivo*. A) Confocal microcopy images of live cells co-expressing Tea1-GFP and Tea1-tdTomato (KS4474). Tea1-GFP and Tea1-tdTomato co-localize at the cell tips (yellow arrowhead) and at the microtubule plus-ends (red arrowhead). **B) Tea1-GFP immunoprecipitates Tea1-tdTomato.** anti-GFP and anti-tdTomato immunoprecipitation from cells expressing Tea1-GFP (KS4417), Tea1-tdTomato (KS3138) or both proteins (KS4474). The samples were probed with anti-GFP. Bar, 5 µm.

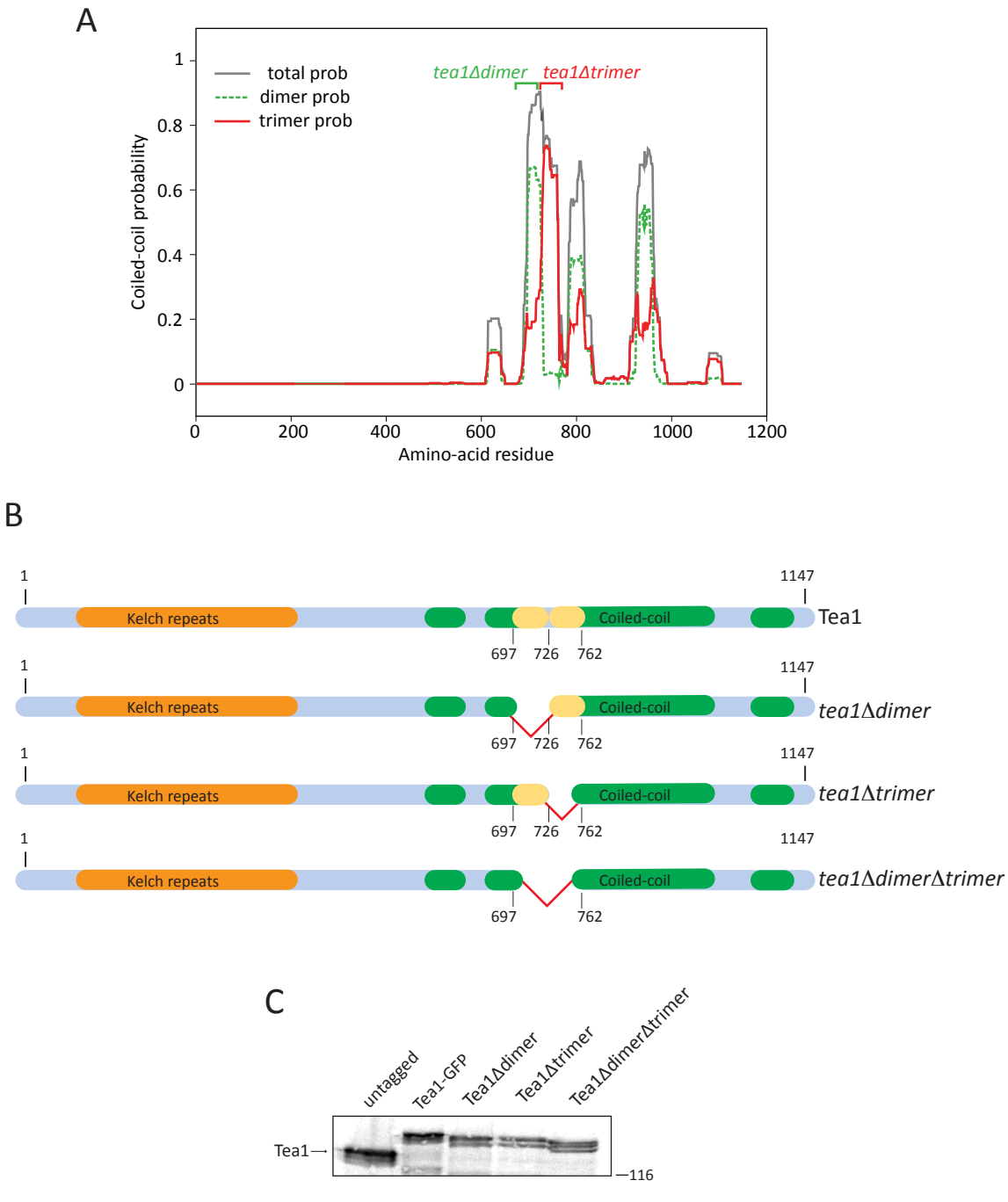

Figure 3.5-Tea1 oligomerization mutants. A) Multicoil prediction of Tea1 region with high probability to form dimers (dashed green line) and trimers (solid red line). **B) Diagram of Tea1 oligomerization mutants.** Three Tea1 oligomerization mutants were constructed: *tea1Δdimer* (aa 697 to 726), *tea1Δtrimer* (aa 727 to 762) and *tea1ΔdimerΔtrimer* (aa 697 to 762). The mutants were expressed in Tea1 locus and are GFP tagged. **C) Protein stability of Tea1 oligomerization mutants.** Protein levels of Tea1Δdimer-GFP (KS5661), Tea1Δtrimer-GFP (KS5980) and Tea1ΔdimerΔtrimer-GFP (KS5664) were compared with Tea1-GFP (KS1260) and Tea1 (KS516) wild-type by immnunoblotting. Samples were probed with anti-Tea1 antibody.

previously shown to play a role in Tea1 anchoring (Snaith et al., 2005; Snaith and Sawin, 2003). Figure 3.6C shows that the interaction of GFP tagged Tea1Δdimer, Tea1Δtrimer and Tea1ΔdimerΔtrimer with Mod5 is not disrupted.

Data shown here indicated that polymerized actin does not provide a scaffold for Tea1 accumulation at the cell tip. However, our results show that Tea1 can interact with itself, which suggested that Tea1-Tea1 interactions could account for Tea1 stability at the cell tip. Moreover, deletion of a uniquely predicted trimeric region of Tea1 prevents its accumulation at the cell tip. The failure of Tea1Δtrimer to accumulate at cell tip occurs despite its delivery on microtubule-plus ends and its interaction with Mod5. This means that Tea1 trimerization is required for Tea1 accumulation at the cell tip. It has been shown that protein oligomerization beyond dimers is required for the formation of stable polymeric networks (Scott et al., 2009; Yin and Lai, 2000). Therefore, Tea1 stability at the cell tip might be due to the *de novo* formation of a structure based in Tea1 self-oligomerization. We propose that Tea1 forms a polymeric structure at the cell tip that we termed of the Tea1 "cluster-network".

3.2.4. Role of Mod5 in the formation of the cluster-network

In the FRAP experiments it was shown that Tea1-Mod5 interaction is transient. The next step was to understand how could Mod5 contribute for the accumulation of Tea1 at the cell tips, despite Mod5 only transiently interacts with Tea1. The transient Tea1-Mod5 interaction indicates that Mod5 must frequently bind to and release from the Tea1 cluster-network. This suggests that Mod5 may be restricted to the cell tip by a diffusion-capture mechanism, similar to what was initially proposed for the *B. subtilis* bacteria protein SpoIVFB (Rudner et al., 2002).

The iterative binding and the mobility of Mod5 suggest that it interacts with the cluster-network as individual molecules. Therefore, I analyzed evidences for Mod5-Mod5 interaction *in vivo* by co-expressing two tagged versions of Mod5 in haploid cells. Figure 3.7A shows that FLAG-Mod5 cannot co-immunoprecipitate GFP-Mod5, but can pull down its known binding partner, Tea1. This result shows that Mod5 does not interact with itself, and therefore suggests that Mod5 may interact with Tea1 cluster-network as individual molecules.

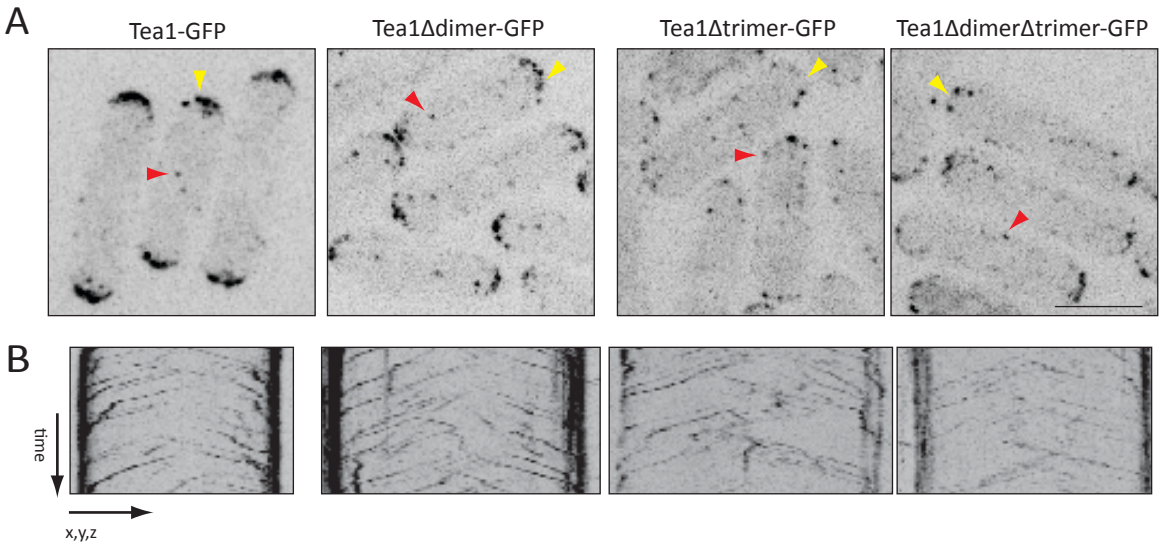

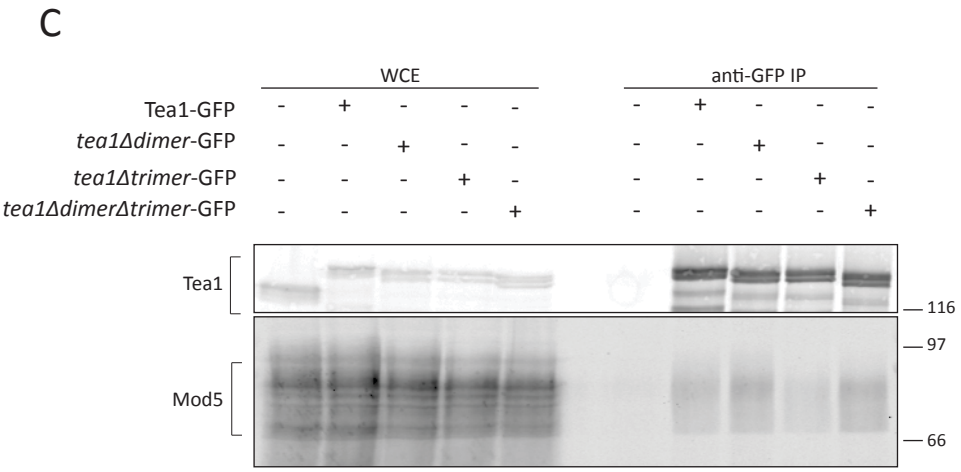

Figure 3.6- Analysis of Tea1 oligomerization mutants. A) Confocal microscopy images of live cells expressing Tea1 oligomerization mutants tagged with GFP. *tea1Δtrimer* (KS5980) and *tea1ΔdimerΔtrimer* (KS5664) mutants localize at the microtubule plus-ends (red arrow heads) and fail to accumulate at the cell tip (yellow arrow head). *tea1Δdimer* (KS5661) accumulates at the cell tip (yellow arrow-head) like wild-type Tea1-GFP. **B)** Tea1 movements towards the cell tip are shown by a representative kymographs. **C) aa 697 to 762 are not required for Tea1-Mod5 interaction.** Tea1Δdimer, Tea1Δtrimer and Tea1ΔdimerΔtrimer-GFP were immunoprecipitated with anti-GFP antibody. The samples were probed with anti-Tea1 and anti-Mod5 antibodies. Bar, 5 µm.

Because Mod5 binds to Tea1 transiently we ruled out the idea of Mod5 playing a structural role in Tea1 cluster-network. However, the absolute requirement of Mod5 for the existence of Tea1 cluster-network suggests that Mod5 might be directly involved in promoting Tea1-Tea1 interaction. Figure 3.7B shows the microtubule delivery and membrane deposition of Tea1-tdTomato in a *mod5Δ* cell, where no Tea1 cluster-network is present. After microtubule depolymerization, Tea1-tdTomato is left behind and stays associated with the cell membrane on average for 120 sec, until it eventually dissipates. This shows that even though Tea1 has a reasonable affinity to the cell membrane it does not form a cluster-network in the absence of Mod5.

Figure 3.7C shows a representative kymograph used to determine the delivery frequency of Tea1-packets in wild-type. In my measurement, Tea1 is delivered at a rate of one packet per min, in agreement with work done by others (Behrens and Nurse, 2002). On average, the time spent by a Tea1-packet at the cell tip (~2 min) is longer than the frequency of arrival of Tea1-packets. In principle, this would give time for Tea1 to form a cluster-network, even in the absence of Mod5. This shows that Tea1 from packets is competent to form Tea1-Tea1 interactions at cell tip only in the presence of Mod5. This suggests that Mod5 function is to facilitate the formation of Tea1 cluster-network at the cell tip.

3.2.5. Mathematical model of Tea1-Mod5 interaction

Figure 3.8 shows a simplified schematic diagram of the model for Tea1 and Mod5 transient interaction at the cell tip based on the observations described in the sections 3.2.2 to 3.2.4. In the diagram, for simplicity, Tea1 cluster-network is represented in one dimension, rather than the real two dimensions structure. In A), Tea1 is stably associated with itself in the form of clusters-networks. Mod5 is restricted to the cell tip, due to binding and unbinding to the Tea1 cluster-network. In B) an incoming Tea1 binds free Mod5. In C), Mod5 facilitates the formation of Tea1-Tea1 bonds between the newly arrived Tea1 and the cluster-network. In D), newly-arrived Tea1 is bound to the cluster-network and Mod5 returns to transiently interacting with the cluster-network.

Because the model described above is difficult to test experimentally, we decided to mathematically formalize these ideas using the minimal components and simulate the

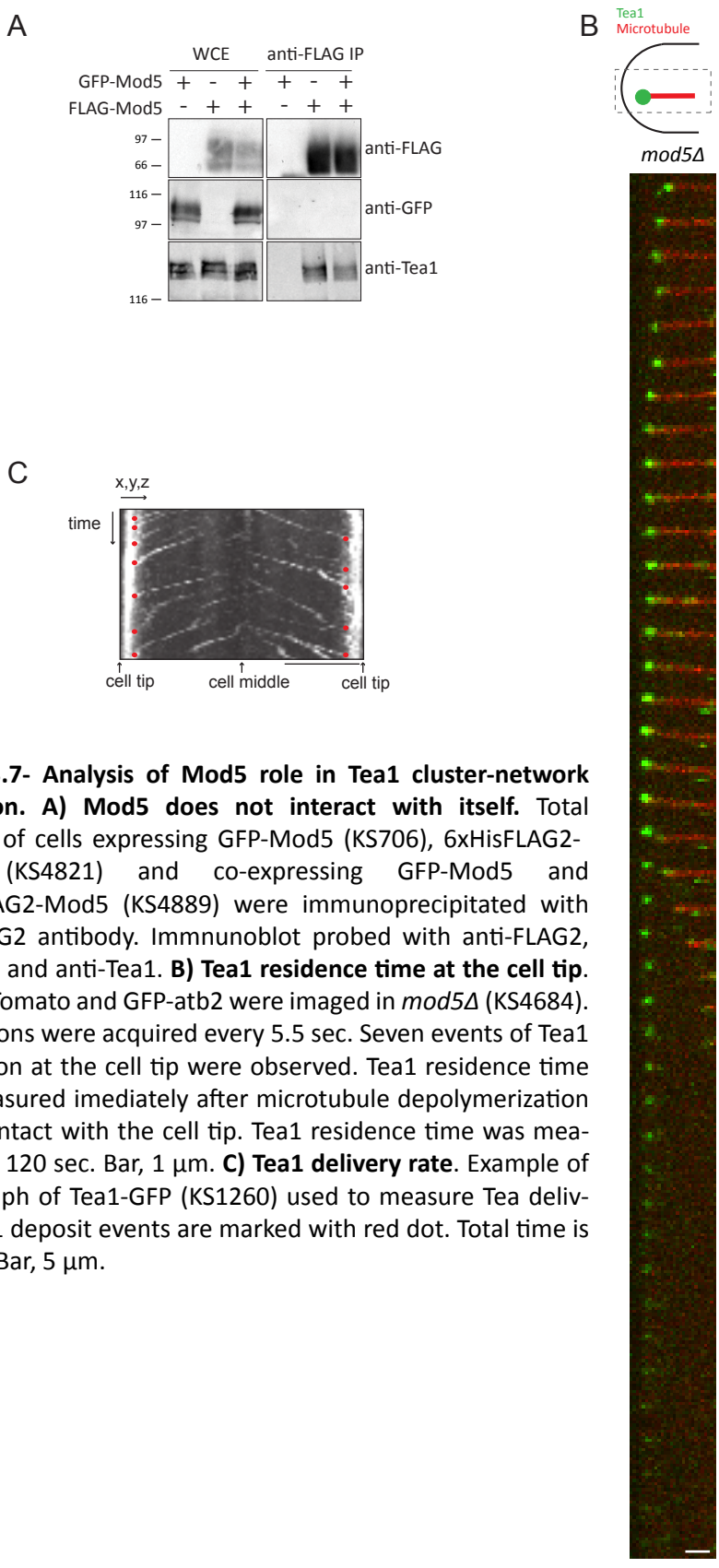

Figure 3.7- Analysis of Mod5 role in Tea1 cluster-network formation. A) Mod5 does not interact with itself. Total extracts of cells expressing GFP-Mod5 (KS706), 6xHisFLAG2-Mod5 (KS4821) and co-expressing GFP-Mod5 and 6xHisFLAG2-Mod5 (KS4889) were immunoprecipitated with anti-FLAG2 antibody. Immnunoblot probed with anti-FLAG2, anti-GFP and anti-Tea1. **B) Tea1 residence time at the cell tip**. Tea1-tdTomato and GFP-atb2 were imaged in *mod5Δ* (KS4684). 8 z-sections were acquired every 5.5 sec. Seven events of Tea1 deposition at the cell tip were observed. Tea1 residence time was measured imediately after microtubule depolymerization upon contact with the cell tip. Tea1 residence time was measured as 120 sec. Bar, 1 µm. **C) Tea1 delivery rate**. Example of kymograph of Tea1-GFP (KS1260) used to measure Tea delivery. Tea1 deposit events are marked with red dot. Total time is 10 min. Bar, 5 µm.

system behavior. Tea1-Mod5 interaction at the cell tip was mathematically modeled by Dr. Andrew Goryachev, from the Centre for Systems Biology at the University of Edinburgh.

Figure 3.9 shows the kinetic scheme used to describe Tea1 and Mod5 interaction at the cell tip. Here and throughout the description of the model the term "bond" will be used to formally describe protein-protein interactions. "Bonds" does not necessarily describe a direct interaction and, for example, if other proteins form "bridges" between Tea1 molecules these can also be counted as Tea1-Tea1 "bonds". The minimal model for cluster-network formation is based on two distinct reversible interactions. First, it describes the properties of Tea1-Mod5 "bonds" as rapidly formed but relatively unstable, with a rate constant k_1, k_{-1} (Figure 3.9 Bi). In the kinetic scheme, Mod5 forms "bonds" both with Tea1 monomers and with Tea1 in the polymeric form. Second, it describes the slowly-formed but more stable Tea1-Tea1 "bonds", with a rate constant k_3,k_{-3} (Figure 3.9Bi). Although Tea1 has several binding partners at the cell tip, these interactions are not critical for the model behavior. Therefore, they can be subsumed within the model, by contributing to the average rate constant (see Appendix II for detailed description of the mathematical model).

Figure 3.9B and 3.9C show that in the model Tea1 and Mod5 associate to form polymeric networks with variable stoichiometry. The association and dissociation of Mod5 from these complexes occurs with the formation and breakage of Tea1-Mod5 "bonds". On other hand, incorporation of Tea1 into the polymeric network requires its presentation by Mod5 in the context of the short-lived Tea1·Mod5 bimolecular complex. According to thermodynamic reversibility, individual molecules of Tea1 can be removed from the polymer due to the breakage of Tea1-Tea1 "bonds" via dissociation of Tea1·Mod5 complexes.

In Figure 3.9C, the cluster-network dynamics are depicted. The changes in the cluster-network connectivity, size and stability at the cell tip are a consequence of formation and dissociation of Tea1-Tea1 and Tea1-Mod5 "bonds".

The proposed mechanism for Tea1-Mod5 interaction at the cell tip, described in Figure 3.9, was converted into a predictive computational model by constraining its kinetic parameters with experimentally measured parameters. The number of Tea1 and Mod5 molecules per cell were determined using quantitative immunoblotting, as described in Appendix II. I measured approximately 8000 molecules of Tea1 and 2000 molecules of Mod5 per cell, and therefore in a cell there are on average ~ 4 Tea1 molecules for each

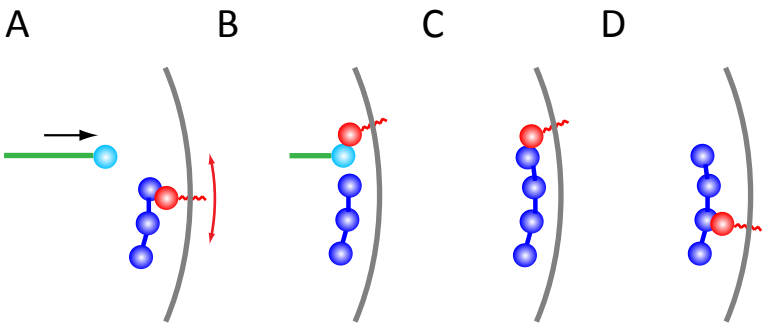

Figure 3.8- Schematic model for Tea1 anchoring by Mod5 at cell tips. This model is a 1D simplification of the 2D mechanism. **A)** New Tea1 (light blue) is delivered by microtubules (green). Mod5 (red) diffuses in membrane but is restricted to cell tips by transient interactions with anchored Tea1 (dark blue); **B and C)** Interaction of Tea1 with Mod5 results in new Tea1 anchoring; **D)** Mod5 diffuses in membrane as before.

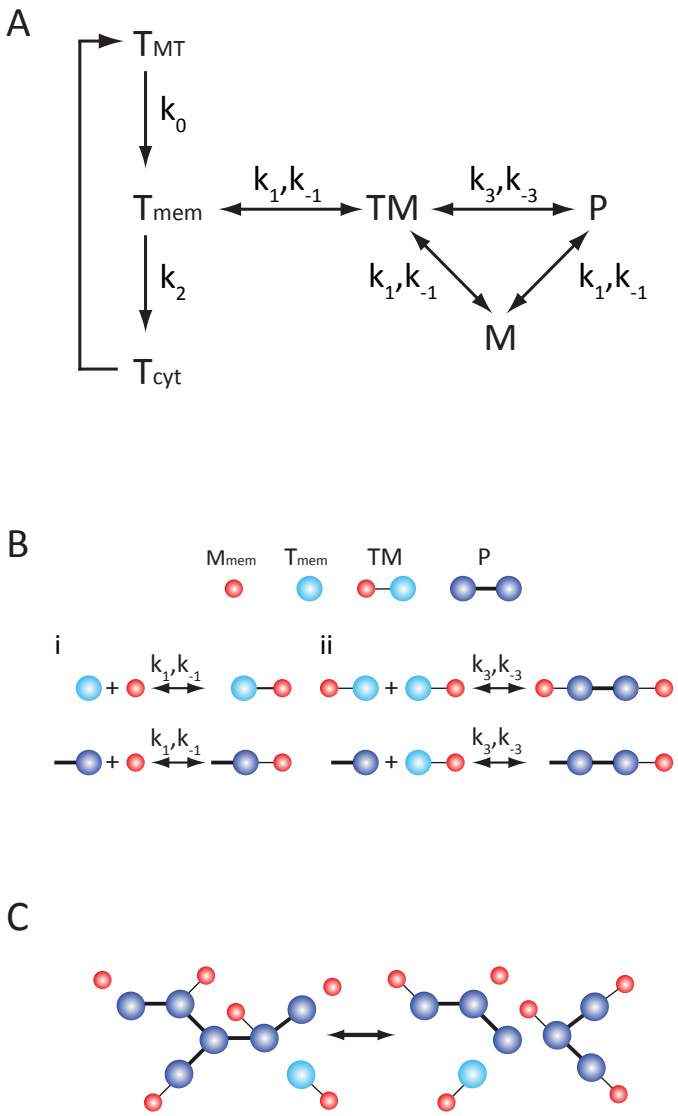

Figure 3.9- Mathematical model formalization and reactions description. A) Kinetic scheme used in computational model. **B)** Proposed molecular interactions described in the model. Molecular species are described as well as kinetic constants for each reaction. **i)** describes reactions with k_1,k_{-1} and **ii)** describes reactions with k_3,k_{-3}. **C)** Diagram of Tea1 cluster network dynamics and connectivity. Light blue is Tea1 not present in polymeric form (T_{mem} and *TM*), purple is Tea1 in the polymer (P) and red is Mod5 (M_{mem} and M_{pol}). This figure was contributed by Dr. Andrew Goryachev.

Mod5 molecule. The number of Tea1 and Mod5 molecules present at the cell tip was measured using a fluorescence quantitation method (details in Appendix I). At the cell tip, Tea1 to Mod5 ratio measured is the same as for the entire cell, with 1510 ± 500 molecules of Tea1 and 380 ± 200 molecules of Mod5. Moreover, fluorescence quantification was also used to determine that Tea1-packets transported on microtubule plus-ends contain ~ 80 molecules of Tea1. The diffusion rate of Mod5 at the cell membrane was calculated from the FRAP data shown in Figure 3.2B, as described in Appendix II.

Preliminary computational simulated FRAP curves suggested that if longer recovery times were allowed, the cytoplasm pool of Tea1-GFP and GFP-Mod5 would continue to turn over with the cell tip and tip-associated Tea1 and Mod5 would turn over within the cell tip (details of FRAP simulation in Appendix II, section A2.3). Tea1 and Mod5 FRAP experiments were therefore repeated but the fluorescence recovery was followed for 50 min or 30 min, instead of for only 5 min. Figure 3.10 shows the fitting of *in silico* FRAP curves, generated using optimized kinetic parameters (described in Table A2.1), with Tea1 and Mod5 FRAP curves obtained experimentally. The fitting of FRAP curves was used to manually constrains the model kinetic parameters, that could not be directly measured with the experimental data. Therefore, this demonstrates that the kinetic constraints used in the computational model can describe Tea1 and Mod5 dynamics with a good approximation. Moreover, the longer FRAP further confirms the stability of Tea1 and Mod5 cluster-network. The parameters used in the model are summarized in Table A2.1 of Appendix II.

3.2.6. In silico recapitulation of de novo cluster-network formation

Figure 3.11 shows a simulation of *de novo* formation of a Tea1 cluster-network, which recapitulates *in silico* the accumulation of Tea1 in the polymeric form (T_{pol}) and Mod5 bound to the cluster-network (M_{pol}). At time zero, Mod5 diffuses freely at the cell membrane (M_{mem}) and Tea1 is localized at the cytoplasm. The simulation begins when Tea1 influx starts. At time zero, 116 molecules of Tea1 per minute are targeted to the cell membrane, where the only molecular species present is M_{mem}. Figure 3.11A shows a plot of M_{mem}, M_{pol} and T_{pol} concentration across the cell membrane at the tip, 1 min after the beginning of Tea1 delivery. The inlay in Figure 3.11A shows that M_{mem} is the most abundant molecular species and its concentration is slightly decreased at the cell tip center. Figure 3.11B shows the molecular species concentration 10 min after start. At this time, 800

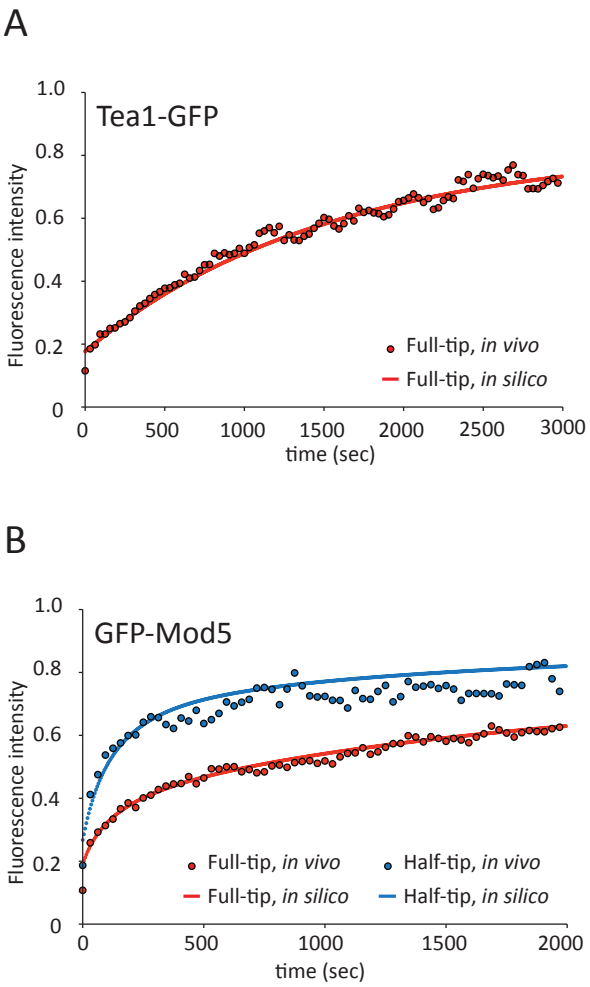

Figure 3.10- *In vivo* and *in silico* long term FRAP curves used to constrain kinetic parameters of the mathematical model. A) Full-tip FRAP curve of Tea1-GFP (KS1260) from *in vivo* data (red dots, n= 8 cell tips) and *in silico* simulation (red line). **B)** Full-tip (red, n= 13 cell tips) and half-tip (blue, n= 12 cell tips) FRAP curves of GFP-Mod5 (KS706) from *in vivo* data (dots) and *in silico* simulation (lines). Proteins were photobleached and recovery of fluorescence was recorded every 30 sec for 50 min for Tea1 and for 30 min for Mod5. The *in silico* FRAP curves were contributed by Dr. Andrew Goryachev.

molecules of Tea1 were delivered to the cell tip and $Tea1_{pol}$ and $Mod5_{pol}$ are already the most abundant molecular species at the cell tip. After 180 min (Figure 3.11D), the cluster-network is close to steady state. The simulation resulted in 1200 molecules of Tea1 and 400 molecules of Mod5 at the cell tip at steady state, in good agreement with experimental data (1510 ± 500 molecules of Tea1 and 380 ± 200 molecules of Mod5, see Appendix I for details).

The evolution of *de novo* formation of the cluster-network shows that although a large number of molecules of Tea1 are targeted to the cell tip over 180 min, only a small fraction (1510 molecules per tip) becomes part of the Tea1 cluster-network.

3.2.7. Incorporation efficiency of Tea1 in the cluster-network

Next, we wanted to understand why Tea1 targeting to the cell tip is such an inefficient mechanism. Therefore, we used *in silico* targeting experiments to determine efficiency of Tea1 incorporation into cluster-network at the cell tips. The proportion of Tea1 deposited at the cell tip that becomes part of the cluster-network was determined using an approach similar to that of FRAP and is described in Appendix II. To do so, the total area of the cell tip was divided in different concentric sub-zones and the efficiency of Tea1 incorporation into the cluster-network upon microtubule-based delivery was simulated.

The results of the simulation of Tea1 incorporation efficiency are presented in Figure 3.12. Figure 3.12A shows that Tea1 incorporation into the cluster-network is higher (64%) at the central disc with ~ 1/8 of total cell tip area (Figure 3.12Ai) and lowest at the periphery of the cell tip area (18%) (Figure 3.12Aiii). In Figure 3.12B incorporation efficiencies in each concentric sub-zone of the cell tip are plotted together, which allows an approximated reconstruction of the underlying continuous probability density of Tea1 incorporation across the entire cell tip. In this reconstruction the highest incorporation occurs at the very center of the cell tip, with a value of ~ 80%.

This analysis showed that efficiency of Tea1 incorporation into the cluster-network is dependent on where on the membrane Tea1 is deposited. At the center of the cell tip Tea1 is efficiently incorporated into the cluster-network, and at the cell tip periphery Tea1 is recycled back to the cytoplasm upon microtubule catastrophe.

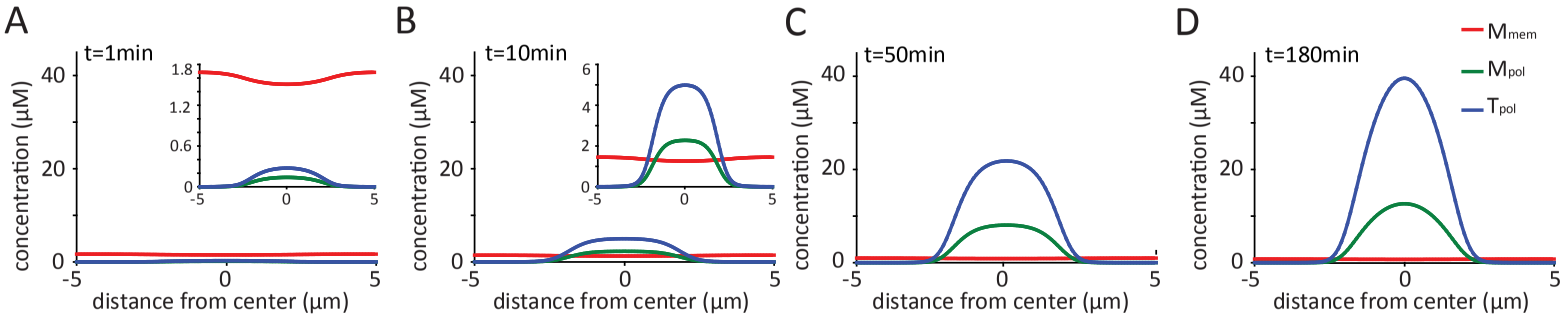

Figure 3.11- *In silico* recapitulation of *de novo* formation of Tea1 cluster-network. The *y*-axis represents concentrations of M_{mem} (red, $Mod5_{membrane}$), M_{pol} (green, $Mod5_{polymer}$) and T_{pol} (blue, $Tea1_{polymer}$). The *x*-axis represents the membrane of the cell tip in 1D of half of a cell, where zero represents cell tip center. Time zero represents no Tea1 influx. Figure represents four time points until steady state: **A)** 1 min, **B)** 10 min, **C)** 50 min and **D)** 180 min. This figure was contributed by Dr. Andrew Goryachev

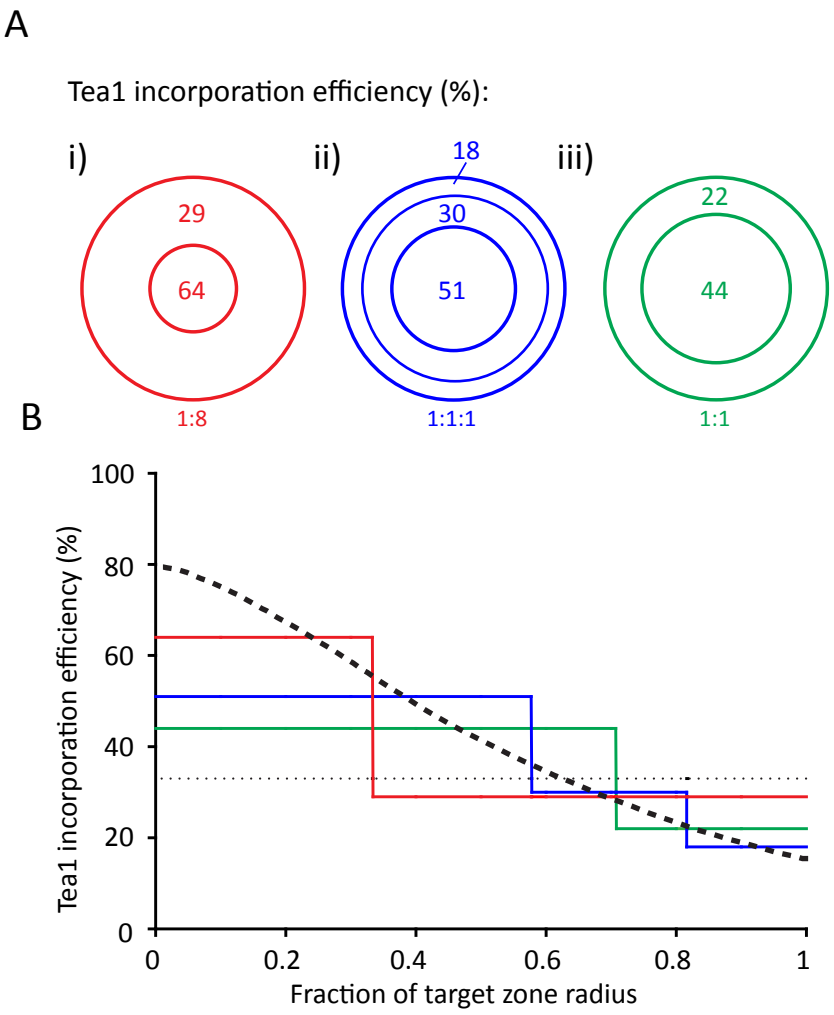

Figure 3.12- Simulation of Tea1 incorporation efficiency into the cluster-network. A) Tea1 incorporation efficiency in different concentric sub-zones of the cell tip. Circles represent a top-view of the cell tip in 2D. **i)** The cell tip divided into central disc and surrounding annulus, with area ratio 1:8. **ii)** The cell tip divided into central disc and two surrounding annulis, with area ratio 1:1:1. **iii)** The cell tip divided into central disc and surrounding annulus, with area ratio 1:1. Numbers inside the sub-zones indicate average Tea1 incorporation efficiency within that sub-zone. **B) Plot of Tea1 incorporation efficiency in different cell tip sub-zones.** Stepped lines in graph show average values of Tea1 incorporation efficiency for the different sub-zones as a function of the fractional radius of the sub-zone relative to the target zone, color-coded as in i, ii and iii. Dotted line represents average Tea1 incorporation efficiency over the entire target zone. Dashed line represents estimated Tea1 incorporation efficiency as a continuous function of distance from center of target zone. This figure was contributed by Dr. Andrew Goryachev.

3.2.8. Tea1 cluster-network formation is an autocatalytic reaction

What is the reason in the model that Tea1 incorporation at the center of the cell tip is four times more efficient than at the cell tip periphery? In the model formalism (Figure 3.9A and 3.9B), formation of Tea1 polymer is an autocatalytic reaction. That is, two species react and the product of the reaction is also one of the reactants. In this case, Tea1 in the polymeric form ($Tea1_{pol}$) and Mod5 are the reactants and the product is more Tea1 in the polymeric form. It is shown in the Figures 3.11A to 3.11D, that $Tea1_{pol}$ concentration is higher at the center of the cluster, where Tea1 incorporation is more efficient. Moreover, simulation in Figures 3.11A to 3.11D also show that $Mod5_{pol}$ is enriched at the cell tip. However, $Mod5_{pol}$ is bound to the cluster-network, and therefore not available to facilitate Tea1 polymerization. In the mathematical model, the concentration of free Mod5 ($Mod5_{mem}$), the molecular species that facilitates Tea1 polymerization, is almost uniform across the cell membrane. This demonstrates that the incorporation efficiency of Tea1 at the center of the cell tip is not dependent on $Mod5_{mem}$ concentration.

Because Tea1 polymerization is an autocatalytic reaction, Tea1 incorporation efficiency depends only on the magnitude of polymeric Tea1 concentration. Therefore, Tea1 is incorporated at the center of the cluster-network, where $Tea1_{pol}$ concentration is the highest, and is recycled back to the cytoplasm at the cluster-network periphery.

3.2.9. Tea1 cluster-network is narrower than Tea1 delivery area

Next we wanted to investigate if the autocatalytic polymerization of Tea1 at the center of the cluster-network and its recycling back to the cytoplasm at the periphery could define the width of the cluster-network.

Figure 3.13A shows the progression of Tea1 cluster-network width over time. Despite the overall increase in the amount of Tea1 at the cluster-network (see Figure 3.11A to 3.11D), the width of the cluster-network continuously decreases until it reaches steady state. The progressive decrease of Tea1 cluster-network width, until steady state, is also shown in Figure 3.14A. This figure shows that even after the maximum concentration of total Tea1 associated with the cluster-network had reached a plateau, the maximum Tea1 in the polymeric form continuously increases over time, until it reaches steady state. Therefore, the conservation of mass would imply that the cluster-network width should

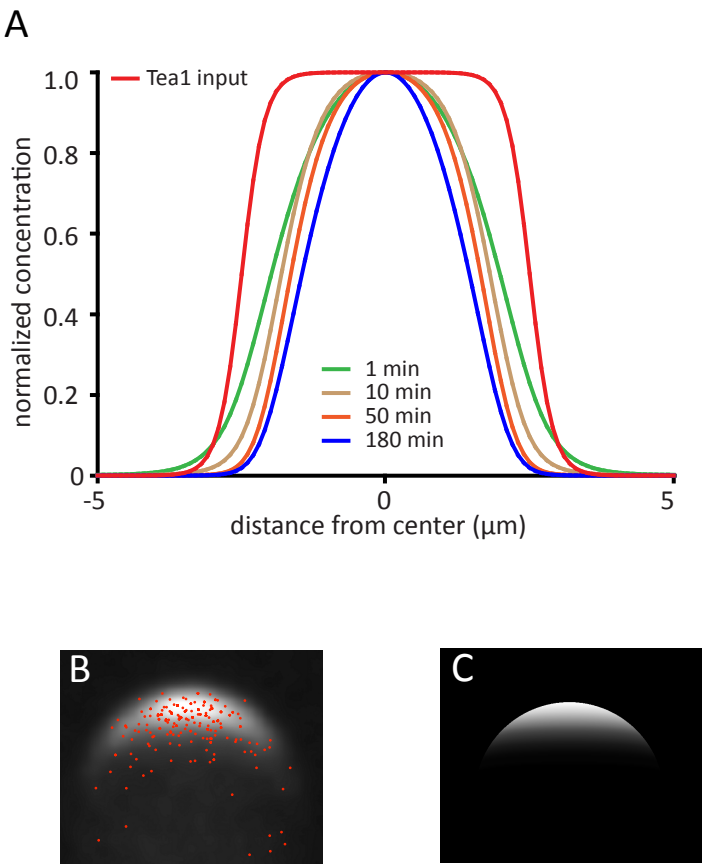

Figure 3.13- Tea1 delivery area is wider than Tea1 cluster-network. A) Normalized concentration of Tea1 incorporated at the cluster-network ($Tea1_{pol}$) during time-evolutions of the network. The normalized profile of Tea1 deposition (input, red line) at the cell tip is also shown. Tea1 cluster-network becomes progressively narrower over time. In the plot *x*-axis indicates distance from the cell tip center along cell perimeter. **B) Average Tea1 target zone *in vivo*.** 60 cell tips of cells expressing Tea1-GFP (KS1260) were superimposed to create the average Tea1-GFP ocupancy at the cell tip. Red dots represent 200 events of Tea1 delivery. Each *x,y* position was normalized and overlayed with average Tea1 accumulation. **C) *In silico* Tea1-GFP acumulation at cell tip**. Accumulation of Tea1 is sharper than *in vivo* because out of focus fluorescence is not present. A) and C) were contributed by Dr. Andrew Goryachev.

simultaneously decrease as the polymerization of Tea1 continues. This indicates that at later stages of cluster-network formation, Tea1 polymerization at the center must occur at the expense of Tea1 depolymerization at the periphery.

In order to demonstrate that at steady state Tea1 polymerizes at the center and depolymerizes at periphery of the cluster-network, the reaction fluxes across the cluster-network were determined (see details in Appendix II). Because $Mod5_{mem}$ concentration is uniform across the cell membrane (shown in Figure 3.11), acceleration of Tea1-Tea1 "bond" formation and dissociation can occur across the entire cluster-network. Figure 3.14B shows the plot of normalized $Tea1_{pol}$ concentration together with the reaction fluxes at steady state (180 min) across the cluster-network. At steady state, the cluster-network is continuously polymerizing Tea1 at the center (maximum of reaction flux), and continuously dissociating Tea1-Tea1 "bonds" at the periphery (negative reaction flux). Figure 3.14c represents the reaction flux of $Mod5_{mem}$ promoting the formation of Tea1-Tea1 "bonds" and Figure 3.14D represents the reaction flux of $Mod5_{mem}$ promoting Tea1-Tea1 "bonds" dissociation.

Figures 3.13 and 3.14 demonstrate that Tea1 cluster-network at steady state is dynamic, and maintains its width by continuous polymerization of Tea1 at the center of the cluster-network and dissociation of the polymer at the periphery.

We next wanted to know why although the cluster-network continuously polymerizes Tea1 it does not became infinitely narrower. Figure 3.15 shows a plot of Tea1 in the polymeric form ($Tea1_{pol}$) normalized concentration at steady state, computed with different diffusion coefficients (D_{pol} =10^{-4}, 10^{-5} and 10^{-6} $\mu m^2/s$). The increase in the diffusion rate results in a wider cluster-network, and decrease in D_{pol} makes a narrower cluster-network. This indicates that at steady steady, Tea1 autocatalysis at the center of the cluster-network is balanced by diffusion of the polymer.

The progressive decrease of Tea1 cluster-network width during *de novo* formation suggests an emergent property of self-focusing, i.e. Tea1 cluster-network can find its own center (see discussion for details). Figure 3.13A shows that at any given time Tea1 delivery zone is wider than Tea1 cluster-network. This means that although Tea1 is delivered in a wide area of the cell tip, it only become part of the cluster network in a significantly narrower area. Moreover, Figure 3.13C also presents *in vivo* evidence for a wider Tea1 delivery zone than the Tea1 cluster-network at steady state. In the *in vivo* reconstitution of

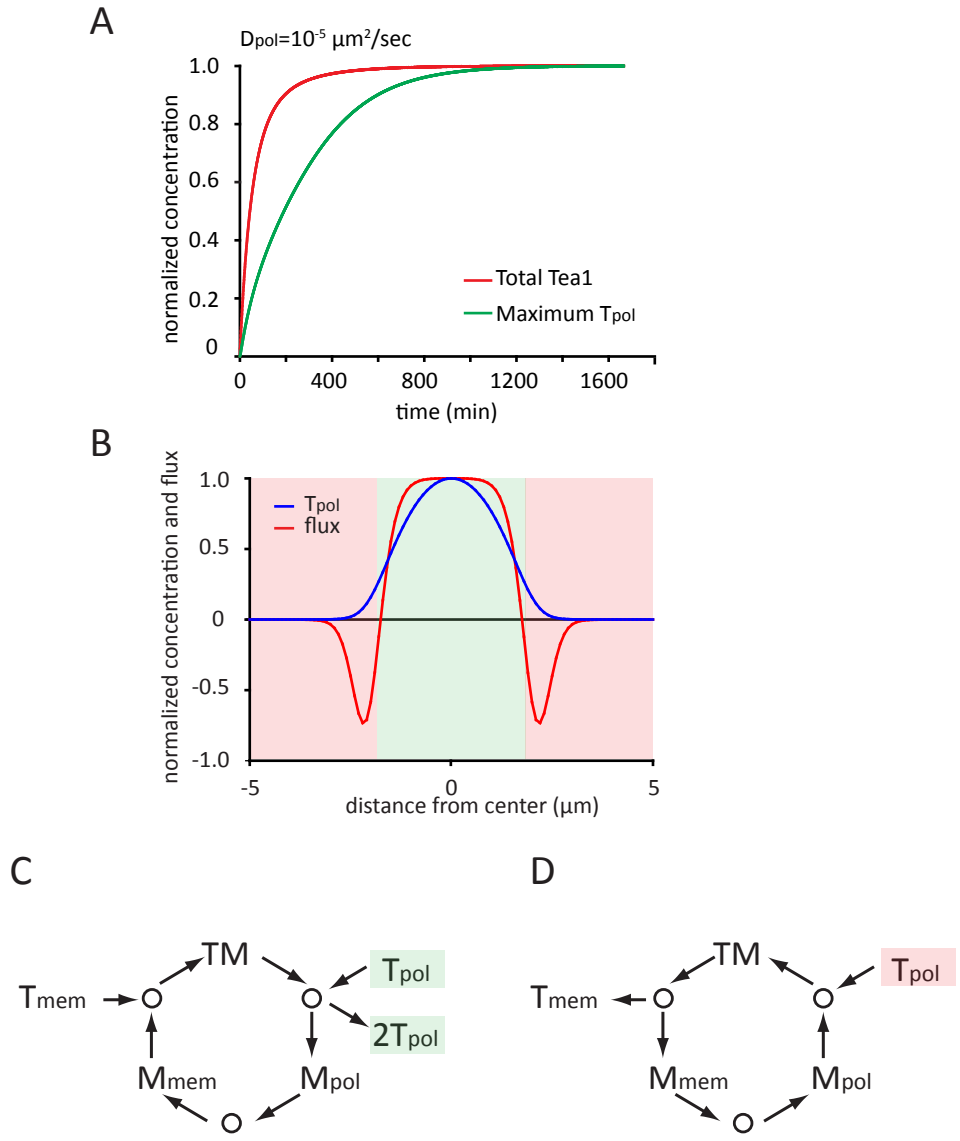

Figure 3.14- Tea1 cluster-network is assembled at the center and disassembled at the periphery. A) Continued increase in maximum concentration of polymeric Tea1 (i.e. local concentration of T_{pol} at center of microtubule-targeting zone; green line) even after total cluster network-associated Tea1 (red line) reaches a plateau. **B)** Plot of normalized $Tea1_{pol}$ concentration (blue line) and reaction fluxes (red line) at 180 min (steady state) across the cell membrane. **C) Reaction flux in green shadowed part of plot in B)**. At the cell tip center the reaction flux in the direction of Tea1 polymerization (clockwise arrows) and Mod5 promotes Tea1 cluster-network assembly. **D) Reaction flux in red shadowed area in B)**. At cell periphery the reaction flux is in the direction of Tea1 cluster-network disassembly (anti clockwise arrows). Mod5 promotes Tea1 dissociation from the cluster-network. This figure was contributed by Dr. Andrew Goryachev.

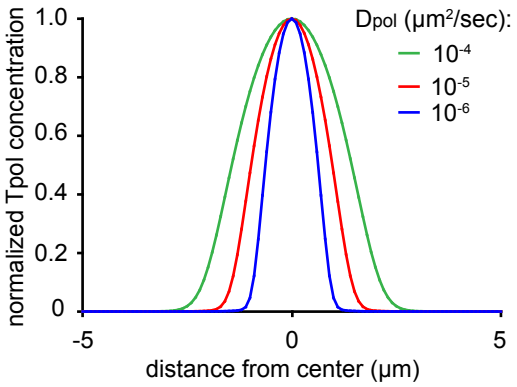

Figure 3.15- Tea1 cluster width is a balance between Tea1 autocatalysis and cluster-network diffusion. Plot of normalized Tea1 in the polymeric form (*Tea1*$_{pol}$) concentration at steady-state, using three different diffusion coefficients to recapitulate *in silico* Tea1 cluster-network formation. This figure was contributed by Dr. Andrew Goryachev.

the “average Tea1 cluster-network” area at steady state, the delivery area of Tea1 by microtubules is wider than the accumulation of Tea1 at the cell tip. Figure 3.15D shows the same area of highest accumulation of Tea1 in an *in silico* simulation. Thus, the cluster-network maybe able to find its center, by continuous incorporation of Tea1 at the center of the cluster-network and recycling Tea1 back to the cytoplasm at the periphery.

3.3. Discussion

This chapter describes the molecular interactions and dynamics of Tea1 and Mod5 at the cell tip, using a combination of quantitative experimental approaches and mathematical modeling.

After observing that Tea1 and Mod5 turn over at different rates, we proceeded to investigate how a transient interaction between Tea1 and Mod5 could nevertheless lead to a stable cortical Tea1 structure. Our results indicate that Tea1 polymerizes in some way and thus is present at the cell tip as a cluster-network. As with other proteins, the clustering of Tea1 may reduce protein mobility, which might be necessary for Tea1 functions at the cell tip (Sieber et al., 2007). Protein association in clusters can provide a lattice necessary to regulate protein-protein interactions both spatially and temporally (Yin and Lai, 2000). As an example, the central spindle and midbody protein complex Centralspindlin needs to form higher-order clusters in order to stabilize the microtubules at the spindle midzone (Hutterer et al., 2009). Moreover, because clusters are maintained due to weak protein-protein interactions they are responsive to changes, as can be seen in processes such as membrane signaling or stabilization of the spindle midzone (Hutterer et al., 2009; Scott et al., 2009; Sieber et al., 2007).

Our data suggests that Mod5 facilitates the formation of Tea1-Tea1 “bonds”. In our model, Mod5 is by definition a catalyst, Mod5 is not modified during polymerization and one molecule of Mod5 can catalyze the formation of several Tea1-Tea1 bonds (Lehninger et al., 2000). Moreover, we have shown that Mod5 available to facilitate Tea1 polymerization (free $Mod5_{mem}$) is uniformly distributed across the entire cell tip. Therefore Mod5 does not alter the balance of Tea1 polymerization and disassembly.

In our model, Mod5 is confined to the cell tip due to a diffusion-capture mechanism. Mod5 diffuses freely in the cell membrane until it encounters the Tea1 cluster-network,

and becomes restricted due to frequent binding to and release from Tea1. Recently a similar binding and unbinding mechanism was described to the fascin-actin interaction in the lammelapodia (Aratyn et al., 2007). Moreover, other membrane-associated proteins present in clusters, like LL5β or SyntaxinI, also have differential turnover rates depending if they are localized within the cluster or diffusing in the cell membrane (Lansbergen et al., 2006; Sieber et al., 2007).

Our experimental observations were formalized in a mathematical model. The model describes three molecular features of Tea1-Mod5 interaction. First, it is based in Tea1 targeted delivery to the cell tip, on the microtubule plus-ends, and formation of Tea1-Tea1 "bonds" in the form of a cluster-network. Second, Mod5 acts to facilitate the formation of Tea1-Tea1 "bonds". And finally, Mod5 is restrained to the cell tip due to a diffusion-capture mechanism.

It has been previously proposed that Tea1 and Mod5 reinforce each others' localization at the cell tip due to a positive feedback mechanism. In such mechanism the accumulation of one of the proteins at the cell tip would recruit more of the other. Therefore, the accumulation of Tea1 at the cell tip should be dependent of Mod5 concentration and vice-versa (Snaith and Sawin, 2003). Contrary to what has been proposed, the *in silico* analysis of Tea1 cluster-network demonstrated Tea1 and Mod5 do not reinforce each others' localization due to a positive feedback mechanism (Snaith and Sawin, 2003). The mathematical model formalizes that Tea1 polymerization at the cell tip is an autocatalytic reaction. Therefore, Tea1 accumulation at the cell tip depends on the magnitude of Tea1 concentration and not on Mod5 concentration. In addition, the concentration of free Mod5 across the cluster-network is essentially uniform during *de novo* formation.

In the model, the Tea1 cluster-network is narrower than Tea1 delivery zone, and the width of the cluster-network decreases progressively until it reaches steady state. Thus, the cluster-network is able to find its center by iteratively pruning away the periphery while accumulating at center. The ability of the cluster-network to find its center represents an emergent property of self-focusing (see description below). The self-focusing property of Tea1 cluster-network can explain its role as a polarity landmark. During cell polarity establishment, self-focusing provides orientation because the cell can find the center of the tip. Moreover, during maintenance of polarized growth, self-focusing is a robust

mechanism to filter-out microtubule deposition errors or even transient microtubule depolymerization. That is if a Tea1-packet is deposited at the periphery of the cluster-network, it is likely to be recycled back. On the other hand, if a Tea1-packet is deposited at the center of the cell tip it is likely to be incorporated and reinforce the cluster-network. This mechanism represents a dynamic structure and yet is robust.

The self-focusing mechanism proposed here might have general relevance for cellular processes that require establishment and maintenance of directional growth or mark specific sites within the cell. For example, during neuronal polarization and directed migration the microtubule-associated protein APC regulates cell extension and migration due to microtubule-cortex attachments. APC is transported on microtubules towards the cell cortex, where it stably accumulates as clusters. Once at the cell cortex, APC stabilizes microtubules and directs cell movement or growth cone growth direction. In this case microtubules establish a positive feedback for their own stabilization, by transporting the protein necessary for stability towards the correct localization (Barth et al., 2008). Recently it has been shown that CLASPs proteins promote microtubule-cortex cross-talk near focal adhesion formation. Microtubule-transported CLASPs bind the membrane-associated protein LL5β and concentrate it next to focal adhesions in HeLa cells and in the leading edge of fibroblasts (Lansbergen et al., 2006). The CLASPs-LL5β-ELKS interaction forms clusters in the cortex responsible for microtubule attachments and subsequent stabilization.

In addition, self-focusing can be used to mark specific sites, such as the cell middle during cytokinesis. It has been shown in *C. elegans* embryos that the Rho GTPase RhoA is spread in a wide zone of the cytokinesis ring**.** However, active RhoA is focused in a narrow area in a microtubule-dependent manner, which involves targeting of Ect2 (a RhoGEF) and Cyk4 (a centralspindlin subunit) (Bement et al., 2005; Yuce et al., 2005).

The mechanism of Tea1 cluster-network formation described here is an example of cellular self-organization (Karsenti, 2008; Misteli, 2001). Several self-organizing mechanisms have been described in cell biology and are thought to be as critical for cell organization (Misteli, 2001; Mullins, 2010; Sieber et al., 2007). In order to a system to self-organize, its components must be continuously exchanging due to energy dissipation and the system must have a symmetry-breaking stimulus (Anderson, 2002; Misteli, 2001). In Tea1 cluster-network, the microtubule-based transport of Tea1 provides both the energy dissipation, by

GTP hydrolysis during microtubule polymerization, and the symmetry breaking, because tubulin-dimers are intrinsically polar, necessary for self-organization. Tea1 cluster-network described here shares some properties with the formation of the Cdc42-cluster during symmetry breaking in *S. cerevisiae* (Goryachev and Pokhilko, 2008; Howell et al., 2009). Like Tea1, can Cdc42 self-focus at the presumptive budding site, due to continuous GTP hydrolysis.

Self-organized mechanisms are characterized by their emergent properties, which arise from the interaction of the system components but are not immediately apparent from the system formalization (Anderson, 2002; Coffey, 1998). In the case of Tea1 cluster-network, it emergent property of self-focusing arises from the non-linearity of Tea1 autocatalytic polymerization.

In this chapter is proposed a model in what Tea1 is stably associated with the cell tip due to self-oligomerization and formation of a cluster-network. In the model, Mod5 is restricted to the cell tip due to frequent binding and unbinding to Tea1 within the cluster-network. In the mathematical model described here, the Tea1 cluster-network has an emergent self-focusing property, which might explain Tea1 cell polarity landmark behavior. The self-focusing property of Tea1 cluster-network proposed in this chapter might describe a basic mechanism of directional growth or intercellular-based landmark positioning observed in other organisms or/and cellular structures.

Chapter IV: Analysis of Tea1 phosphorylation

4.1. Introduction

Despite the evidence that Tea1 is phosphorylated *in vivo*, phosphorylated residues of Tea1 have never been mapped. Further, the biological significance of Tea1 phosphorylation remains to be studied. It is plausible that Tea1 phosphorylation could regulate the formation of differential Tea1 complexes at the microtubule plus-ends and/or at the cell membrane.

Until very recently, mapping of phosphorylated residues was not directed to specific residues, making it very laborious and time consuming (Mann and Jensen, 2003). In recent years, mass spectroscopy (MS) has emerged as a more straightforward and effective strategy for mapping phosphorylated amino acid residues. MS identifies peptides by their mass-to-charge ratio (m/z) and by the fragmentation pattern of peptides derived from proteins (Steen and Mann, 2004).

Prior to MS phospho-mapping, the protein of interest is isolated from a complex mixture of proteins. It is then digested with a protease, usually trypsin, to obtain smaller peptides. These peptides are then run in the mass spectrometer and identified by their m/z. The identification of proteins is done by comparing the mass of the identified peptides with a database containing the theoretical masses of all tryptic peptides of the organism analysed (Steen and Mann, 2004). In tandem MS, after the determination of the m/z of the peptides, they are fragmented again, resulting in the MS/MS spectra. Using the MS/MS spectra, it is possible to identify post-translational modifications, because the m/z of the peptide fragments containing the modification varies from the predicted m/z for the unmodified proteins. Phosphorylated residues are identified by an 80 Da increase in their predicted m/z, due to the presence of the phosphoryl group. However, if the phosphorylation is relatively labile, as is the case for phopho-serine and phospho-threonine, it can also be identified by the presence of a 'satellite mass' of -98 Da, due to the elimination of phosphoric acid (Mann and Jensen, 2003).

To study the role of phosphorylation in Tea1 function, I purified Tea1-TAPS from *S. pombe* cells and the samples were analysed by MS to identify phosphorylated residues. The

role of the phosphorylated residues in Tea1 function was further characterized using mutagenic approaches and comparative proteomics.

4.2. Results

4.2.1. Tea1-TAPS purification using IgG-Dynabeads

To purify Tea1 I used a TAPS tag, which has two Z domains from Protein A (from *Staphylococcus aureus*), which are minimal IgG binding domains. It also has one TEV (Tobbaco Etch Virus) cleavage site, to elute the protein of interest from the IgG binding, and the S-peptide sequence from Ribonuclease A. The S-peptide binds specifically to S-protein from ribonuclease A (Cheeseman et al., 2001; Kim and Raines, 1993).

TAPS-purification using IgG-Dynabeads was established in the lab by Dr Hilary Snaith (Sawin et al., 2009). This method was modified to meet the requirements of a large-scale purification for subsequent identification of phosphorylated residues. I aimed to prevent protein dephosphorylation by carrying out the purification under native conditions in the presence of phosphatase inhibitors. Moreover, Tea1-TAPS was purified using only the binding of the Z domains to IgG. This strategy shortens the purification time allowing less time for endogenous phosphatases to dephosphorylate Tea1-TAPS.

Figure 4.1 shows purified Tea1-TAPS separated in a SDS-PAGE gel and silver stained, used to evaluate the purification yield. Tea1-TAPS was enriched in the TEV cleaved fraction, when compared to the total cell lysate. This means that isolated Tea1-TAPS was pure enough for the band to be excised and processed for MS analysis.

MS analysis was performed by the Rappsilber group, at the Wellcome Trust Centre for Cell Biology, University of Edinburgh.

4.2.2. The central region of Tea1 is highly phosphorylated

The MS analysis of Tea1-TAPS identified 24 phospho-serines and one phospho-threonine. In this analysis, 574 peptides of Tea1 were identified (covering 92% of the amino acid sequence), 44 of which were phosphorylated. Figure 4.2A shows the amino acid sequence of Tea1, with phosphorylated residues identified by MS highlighted in red.

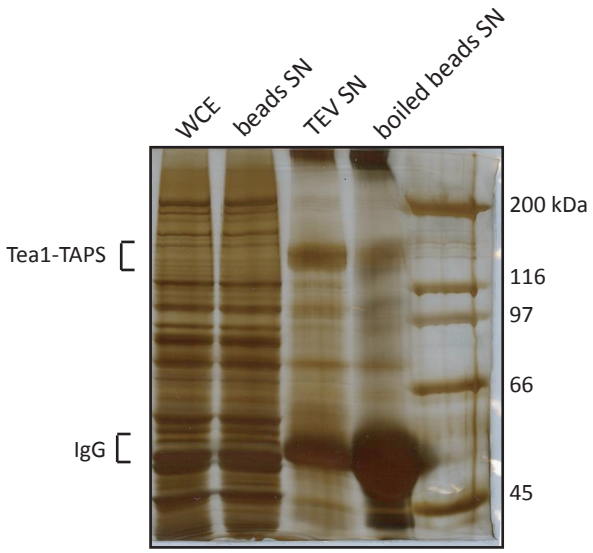

Figure 4.1- Tea1-TAPS purification using IgG-Dynabeads. Tea1-TAPS (KS2739) was purified from *S. pombe* whole cell extract (WCE), using IgG-Dynabeads. The silver stained gel shows the following samples: WCE, beads supernatant (SN) after Tea1-TAPS binding and TEV cleavage supernatant, supernatant of beads boiled in Laemmli sample buffer. Tea1-TAPS is enriched in the TEV cleaved fraction, compared to WCE. The boiled beads fraction shows that only a small fraction of Tea1-TAPS remains bound to the beads after TEV cleavage.

Figure 4.2B shows a schematic representation of Tea1 and the relative position of its phosphorylated residues. The identified phosphorylated residues are mainly localized between aa 434 and aa 586 (20 out of 25 phosphorylated residues), away from both the Kelch repeats and coiled-coil domains. The region between aa 434 and aa 586 has never been experimentally examined, and its role, if any, in Tea1 function remains unknown. Therefore, the location of phosphorylated residues within the Tea1 primary structure provides no information regarding the biological significance of Tea1 phosphorylation However, the large concentration of phosphorylated residues between aa 434 and aa 586 may correspond to a particular phospho-rich region with regulatory functions.

The next step was to study the role of the 25 phosphorylated residues identified by MS in the regulation of Tea1 function. In order to examine as many phosphorylated residues as possible, three different approaches were designed to further study Tea1 phosphorylation. In the first approach, the differential phosphorylation of Tea1 was compared using a combination of MS analysis and mutants defective in Tea1 localization. In the second approach, five phosphorylated residues were single-point mutated, based on the information from the MS results. Finally, a broader approach was taken and aa 434 to aa 586 of Tea1 were internally deleted. In the next sections I will describe the results of the three approaches used to study the role of Tea1 phosphorylation.

4.2.3. Analysis of Tea1 differential phosphorylation

The first approach to understand the role of Tea1 phosphorylation was to examine if Tea1 was differentially phosphorylated, using comparative phospho-proteomics. The goal was to differentiate phosphorylated residues associated with different steps of Tea1 localization and/or function. To compare the phosphorylated residues, Tea1 was enriched at specific locations, using different “cell states”, depicted in Figure 4.3. Subsequently, the phosphorylated residues were identified by MS and compared with wild-type. In principle, this approach should allow the direct matching of specific phosphorylated residues with the localization of Tea1.

First, Tea1 was purified from a *mod5*Δ strain treated with MBC for 30 min. In this mutant, Tea1 is absent from the cell membrane and from microtubules (except for any remaining microtubules) {Figure 3A; Snaith, 2005 #82;Snaith, 2003 #87}. Second, Tea1 was

A

```
1     MSFLFKRNKG SAHKPTKPNF SKTSTTPSTS QLKHSHESNV KMSTSTVTEH RKKPTGSGSH  60
61    ITASPWSKLT VRGSSNVLPR YSHASHLYAE GGQEIYIFGG VASDSQPKND LWVLNLATSQ 120
121   FTSLRSLGET PSPRLGHASI LIGNAFIVFG GLTNHDVADR QDNSLYLLNT SSLVWQKANA 180
181   SGARPSGRYG HTISCLGSKI CLFGGRLLDY YFNDLVCFDL NNLNTSDSRW ELASVVNDPP 240
241   PARAGHVAFT FSDKLYIFGG TDGANFFNDL WCYHPKQSAW SKVETFGVAP NPRAGHAASV 300
301   VEGILYVFGG RASDGTFLND LYAFRLSSKH WYKLSDLPFT PSPRSSHTLS CSGLTLVLIG 360
361   GKQGKGASDS NVYMLDTSRF RLGSVPTTSG RQRNTSFFSN STGNTNPSAF NGLLTSSRIP 420
421   SYNGSKVRST SHPSRQQYIG SSNSRFNTRH QTISTPVSGR ASNDLPSPVV PTRSNSSSIL 480
481   QPSYNLNSHS SDRRNTNDDD QSSLNSQQLS NQAKAQGEVS PTLSFVPSSH SMEQGNGSVA 540
541   SANNAQSEAA TRSINSISEV SEVRFPEQSS VKTVDERKSL DGRITSVTLE TLVEKYSELS 600
601   KQQIVEWFKS KLYEILRDSA SKIDSLTEKL KVANAEKNAA LCEAALEKVP LAKHNKLSDG 660
661   TFSTPDKENV QSTNDAHIMQ ENFSLHKALE VMRETSSDLD KQLKDATASQ KELIVQTSSF 720
721   QKELVEERER HNAISKRLQE IESLYRDREL LVTNLEDQLV DQTVTINKFA FERDQFRERS 780
781   MGFENTIKDL TRKMEATDML NVSLHESLRS VQTENSELVT EMALLKAELV KKQAIIDANA 840
841   NIYDKLTADH TNYETVSADI NQNLKETLDK LLNGSSDFKN NEIELLHDQI RITNAKLEKR 900
901   EKLINASKYI EDTLRSEIQE AAEKVSNLEF SNFNLKEENS NMQLQLMKAL EQRNTGAKQL 960
961   VNLRMQLSTA TSELDMLKLK LRTTALALEE SPDDYSDILS ILRADMSPFH DLHKQCGVLI 1020
1021  DTLNGVKRGF GIFEKKFTDY HKFLENISDK LKSEEDTSLE TPIHENQSIQ SDQIKEVGEV 1080
1081  LSAIKSLSDS VMLLKNQIDD LAKEKLPLSS SDDEKVNIKE KTDFMKLLVK SGLSNPPAKE 1140
1141  PVHDNEN
```

B

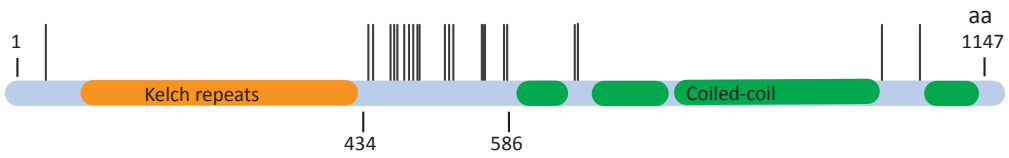

Figure 4.2- Tea1 phosphorylated residues identified by MS. A) Tea1 protein sequence with the phosphorylated residues identified by MS marked in red. **B)** Tea1 protein diagram showing the location of phosphorylated residues. N-terminal Kelch repeats (aa 78-370) are in orange and the C-terminal coiled-coils (aa 609-1106) are in green. aa 434 to aa 586 mark the boundaries of the Tea1 phospho-rich region. Black vertical lines mark the phosphorylated residues identified by MS.

enriched at microtubules but kept away from the cell membrane. To create this situation two different mutants, *tipΔ299 mod5Δ* and *tea1Δ200*, were used (Figure 4.3C). In these mutants, Tea1 associates with the microtubules but fails to be transferred to the cell membrane upon microtubule contact with the cell tip (Behrens and Nurse, 2002; Brunner and Nurse, 2000). Third, the *tea3Δtea4Δbu6Δ* triple mutant was used to maintain Tea1 at the cell membrane, without interacting with its downstream effectors (Figure 4.3D). At the cell tip Tea1 promotes actin cytoskeleton remodelling, *via* the formin For3. However, the Tea1-For3 interaction is indirect and is bridged by Tea4. Moreover, Tea3 is required for Tea1 proper anchoring at the non-growing cell tip and Bud6 activates For3 by relieving its auto-inhibition (Martin et al., 2007). Therefore, in principle, deletion of Tea3, Tea4 and Bud6 prevents Tea1-mediated remodelling of the actin cytoskeleton. Finally, Tea1 is a potential substrate for three cell membrane-associated protein kinases, which have previously been shown to be involved in cell polarity: Pom1, Orb2 and Win1 (see Chapter I). Tea1 phosphorylation was examined in *pom1Δ*, *orb2-34* and *win1Δwin4Δ* mutants and compared with wild-type (Figure 4.3E). This approach could in principle identify specific target residues of each kinase.

4.2.4. Purification of Tea1-TAPS using IgG-Fractogel beads

To purify Tea1-TAPS from the mutant backgrounds described above, IgG-Fractogel beads were used rather than IgG-Dynabeads. Dynabeads present relatively low non-specific binding of proteins to the beads' surface. However, Dynabeads are considerably expensive, especially for large-scale purifications with multiple samples. Fractogel beads are a methacrylate-based resin in which functional groups are linked to beads by linear polymer chains. Sawin et al describe method of coupling Fractogel beads with IgG that results in the isolation of the protein of interest with a purity which is comparable with Dynabeads (Sawin et al., 2009).

Before proceeding to the large-scale purification of Tea1-TAPS, the method was optimized for IgG-Fractogel beads. First, I tested the amount of IgG-Fractogel beads necessary for the complete depletion of Tea1-TAPS from the cell lysate. After the first incubation, the bead supernatant was re-incubated with fresh IgG-Fractogel beads (same amount as in first incubation). The re-incubation step allows an evaluation of how much unbound Tea1-TAPS is still available to bind IgG-Fractogel beads. Figure 4.4A shows the

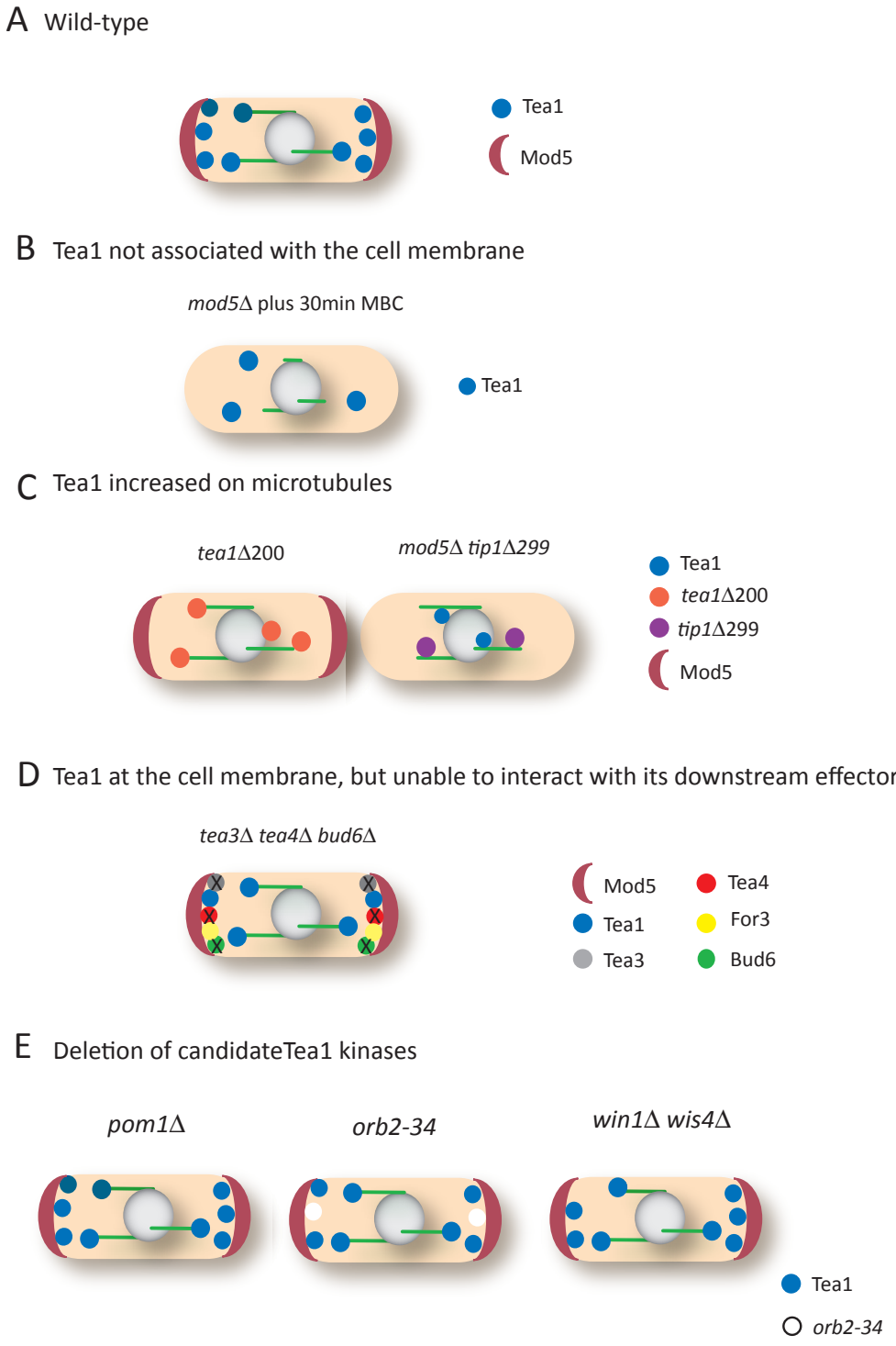

Figure 4.3 (A-E)- Mutants used for the comparative analysis of Tea1 phosphorylated residues. Schematic diagrams representing different conditions used for proteomic comparision of Tea1 phosphorylation. Tea1 localization is shown in each mutant.

immunoblot analysis of the experiment. Tea1-TAPS depletion from the cell lysate is proportional to the amount of beads used. This experiment shows that 40 µl of IgG-Fractogel beads were sufficient to deplete Tea1-TAPS from native cell extracts prepared from 2 g of cells.

Next, it was tested if TEV could efficiently cleave Tea1-TAPS from IgG-Fractogel beads. Figure 4.4B shows that TEV cleavage elutes Tea1-TAPS from the IgG-Fractogel beads, and only a small fraction of Tea1-TAPS remains bound to the beads. The resulting purity of Tea1-TAPS is comparable with the purity obtained with IgG-Dynabeads. Therefore, IgG-Fractogel beads can be used to isolate Tea1-TAPS from *S. pombe* cells.

4.2.5. Tea1 is differentially phosphorylated

Once the purification method with IgG-Fractogel was established, I proceeded to the large-scale purification of Tea1-TAPS necessary for the identification of phosphorylated residues by MS. Tea1-TAPS was isolated from the following cell backgrounds: wild-type, *mod5Δ* treated with MBC for 30 min, *tip1Δ299 mod5Δ, tea1Δ200*, *tea3Δ tea4Δ bud6Δ*, *pom1Δ*, *orb2-34* and *win1Δ wis4Δ.* Figure 4.4C shows a silver-stained SDS-PAGE with Tea1-TAPS purified from cells with different mutant backgrounds. A parallel gel was stained with colloidal coomassie blue and the bands corresponding to Tea1-TAPS were excised and processed for MS analysis.

The summary of all phosphorylated residues identified in wild-type and in the different mutants is shown in Table 4.1 and in Figure 4.5. Figure 4.5 also shows the phosphorylated residues identified in the first MS analysis of Tea1, described in the section 4.2.2. The phosphorylated residues identified in the two wild-type experiments vary significantly, both in number and in position. Because these two samples are biological replicates, some variation might be expected, but we did not expect this much. The differences between samples could be because in the second MS run the sequencing of Tea1 had low protein coverage compared with the first experiment (574 peptides identified, 44 phosphorylated vs. 184 peptides identified, 16 phosphorylated). This led to fewer phosphorylated residues identified in the second experiment (25 phosphorylated residues in experiment #1 compared with 11 in experiment #2). The decrease in protein coverage could be due to a failure either during protein purification or during the MS analysis. However, five of the

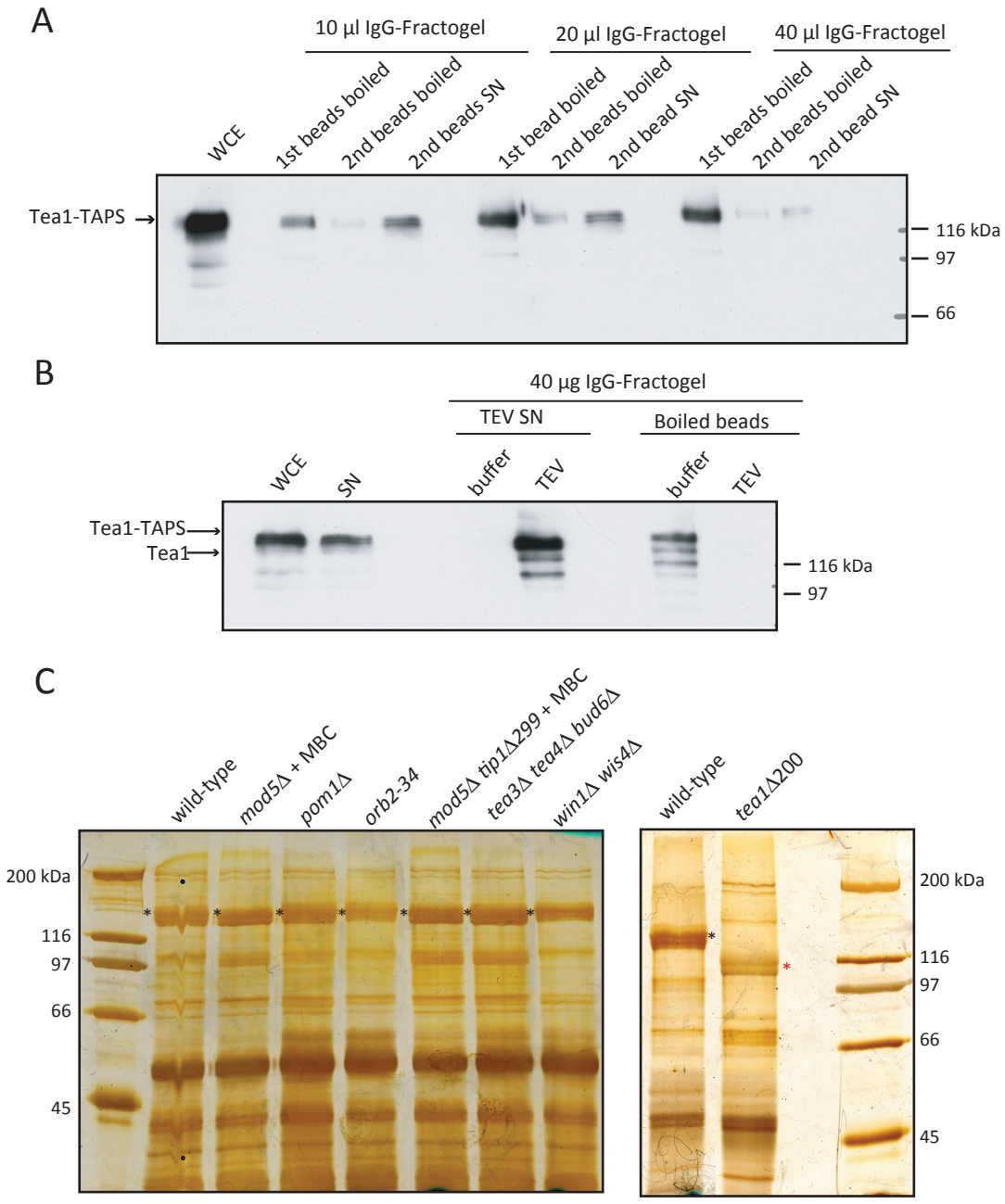

Figure 4.4- Tea1-TAPS purification with IgG-Fractogel beads. A) WCE from 2 g of cells expressing Tea1-TAPS (KS2739) was incubated with 10 µl, 20 µl and 40 µl of IgG-Fractogel beads. The bead supernant was subsequently incubated with fresh IgG-Fractogel beads in the same amounts as in the first incubation. Beads from first and second incubation were boiled in Laemmli sample buffer to elute Tea1-TAPS. **B)** WCE from cells expressing Tea1-TAPS was incubated with IgG-Fractogel beads. Tea1-TAPS was eluted either by TEV cleavage or by boiling the beads in Laemmli sample buffer. **C)** Silver-stained SDS-PAGE showing Tea1-TAPS from wild-type cells, *mod5Δ* plus MBC (KS2958), *pom1Δ* (KS3995), *orb2-34* (KS3997), *mod5Δ tip1Δ299* (KS4001), *tea3Δ tea4Δ bud6Δ* (KS4018), *win1Δ wis4 Δ* (KS4029) and *tea1Δ200* (KS3999). Each sample equals 2 g of cells. * indicates Tea1-TAPS and * indicates *tea1Δ200*-TAPS.

residues (S458, S462, S467, S476 and S586), all of which are in the region between aa 434 to aa 586, identified in the first MS run of Tea1 were confirmed in the second MS run.

The variation in the identification of phosphorylated residues between two biological replicates makes comparison with the mutants less informative because any potential differences in phosphorylated residues between wild-type and mutant cells, could be either biologically significant or technical artifacts.

Although the comparison of wild-type and mutants strains is compromised due to technical issues, some conclusions can be drawn if comparing the mutants amongst themselves. A few residues appear phosphorylated only in certain mutants. The residue Y484 only appeared phosphorylated when Tea1 was present in the cytoplasm (*mod5Δ* plus 30 min MBC), and not in any other situation. This suggests that the phosphorylation of Y484 is cytoplasm-specific. On the other hand, S556 was phosphorylated in the two mutants where Tea1 was localized only to microtubules plus-ends and not at the cell tip (*tip1Δ299 mod5Δ* and *tea1Δ200*). This indicates that S556 may be specifically phosphorylated while Tea1 is microtubule-associated. The residues S462, S474 and S476 were identified as phosphorylated in all samples, suggesting that they are constitutively phosphorylated. Phosphorylation of these three residues could either be essential for Tea1 function or irrelevant and a by-product of cellular metabolic noise. Although these experiments are very preliminary and need further experimental support they suggest that Tea1 might be differentially phosphorylated according to its localization within the cell.

The statistical variability of MS results could be overcome by increasing the number of biological replicates. However, the repetition of MS runs was not an option, especially due to the large number of samples (eight at a time) and cost. Moreover, the number of necessary repetitions to increase confidence in each observation is uncertain, because it depends on the quality of the sample preparation. Due to this technical constraint, a different approach was taken. Instead of repeating the experiments an unknown number of times, we decided to develop a method that decreases statistical variability and allows direct comparison between samples. The development of such method for *S. pombe* is described in detail in Chapter V.

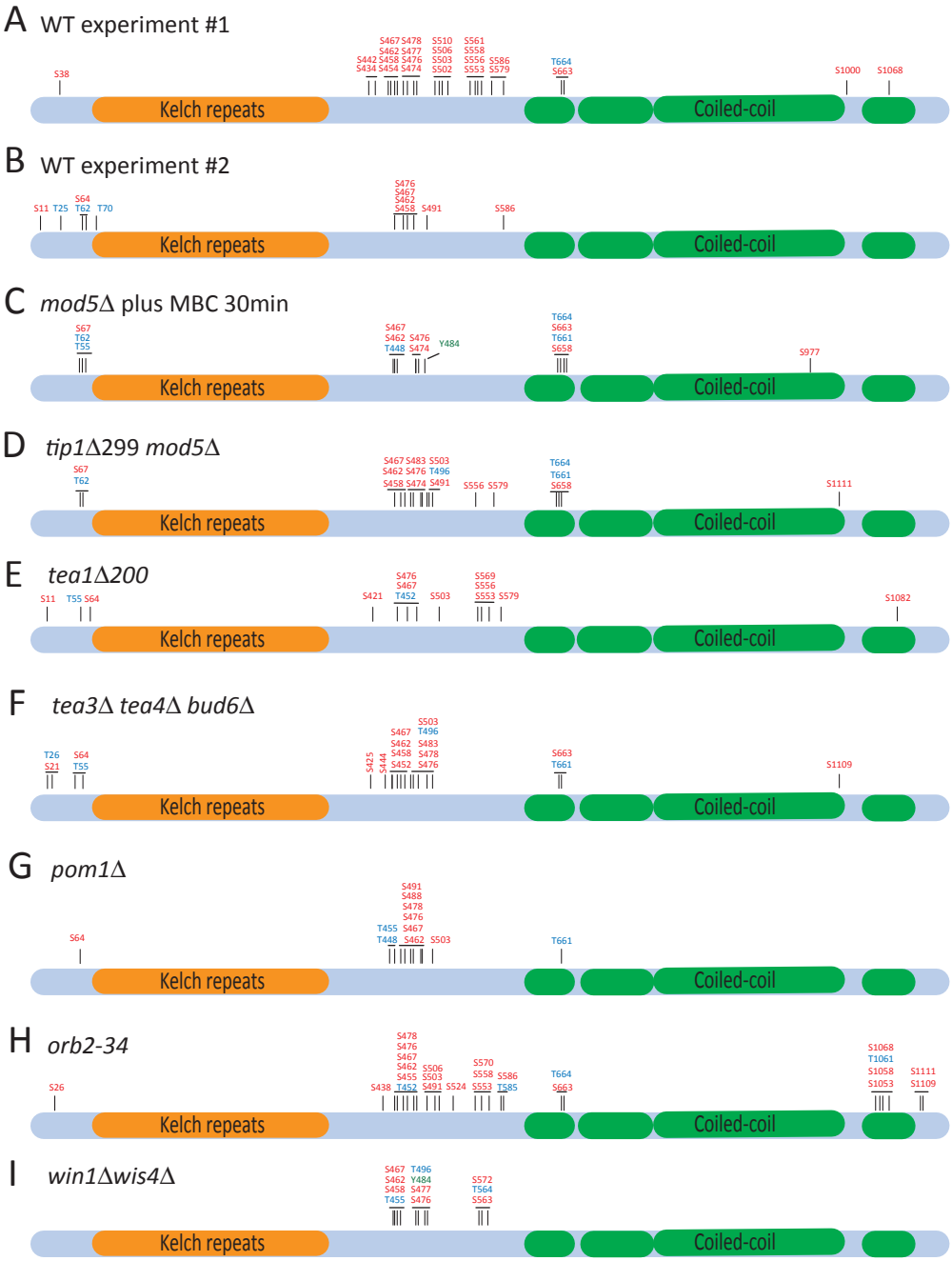

Figure 4.5 (A-I)- Tea1 phosphorylated residues identified by MS. Schematic diagrams representing Tea1. The phosphorylated residues identified by MS are represented by vertical black lines. The amino acid residues are labbeled as follows: serines in red, threonines in blue as tyrosines in green.

4.2.6. Analysis of Tea1 over-expression phenotypes

Next, the phosphorylated residues with a potential role in Tea1 function were studied using point mutations. To express Tea1 point-mutations in *S. pombe* I decided to use the pDUAL system (Matsuyama et al., 2004). This system allows easy integration of the cloned gene at the *LEU1* locus. This is a Gateway cloning based system and the gene of interest can be easily transferred into different destination vectors. This expression system was chosen because it allows a simple and fast expression of different mutants (Matsuyama et al., 2004).

Tea1 mutants were integrated at the *LEU1* locus under control of an exogenous promoter. The pDUAL system has three different promoters available, with *nmt1* being the strongest, and *nmt81* the weakest. In addition, *nmt* promoters can be repressed with thiamine, adding an extra layer for fine-tuning gene expression. Tea1 mutants were tagged at the C-terminus with the GFH tag. GFH is a combination of three different protein tags: GFP, the FLAG epitope and 6xHis. This combination allows analysis of the mutants by live-cell imaging with GFP and biochemical analysis using GFP, FLAG or 6xHis.

In the pDUAL system, Tea1 expression was not under the control of its endogenous promoter. Therefore, before analysing Tea1 point-mutants it was necessary to test the effects of Tea1 expression under different promoter strengths and expression conditions. The effects of the exogenous expression of Tea1-GFH in *tea1Δ* mutants were evaluated by live-cell imaging and Tea1 protein levels were determined by immunoblot.

Figure 4.6A shows an immunoblot of *nmt81*:Tea1-GFH expressed under different repressing conditions. Under the control of unrepressed *nmt81* promoter, Tea1 is only mildly over-expressed. Figure 4.7A shows the localization of Tea1-GFH when expressed under unrepressed *nmt81* promoter. The mild over-expression of Tea1-GFH increases its localization along microtubules but has no effect on the cell tip association. Cell morphology is normal when Tea1 is mildly over-expressed.

Figure 4.7A shows the abnormal cell shape after strong over-expression of Tea1, under the un-repressed *nmt1* promoter. Tea1-GFH accumulates in aggregates in the cytoplasm and along microtubules. Figure 4.7B shows a kymograph of *nmt1*:Tea1-GFH, used to analysed over-expressed Tea1 dynamics. In large excess, Tea1-GHF is no longer seen tracking along the microtubule plus-ends and is immobile.

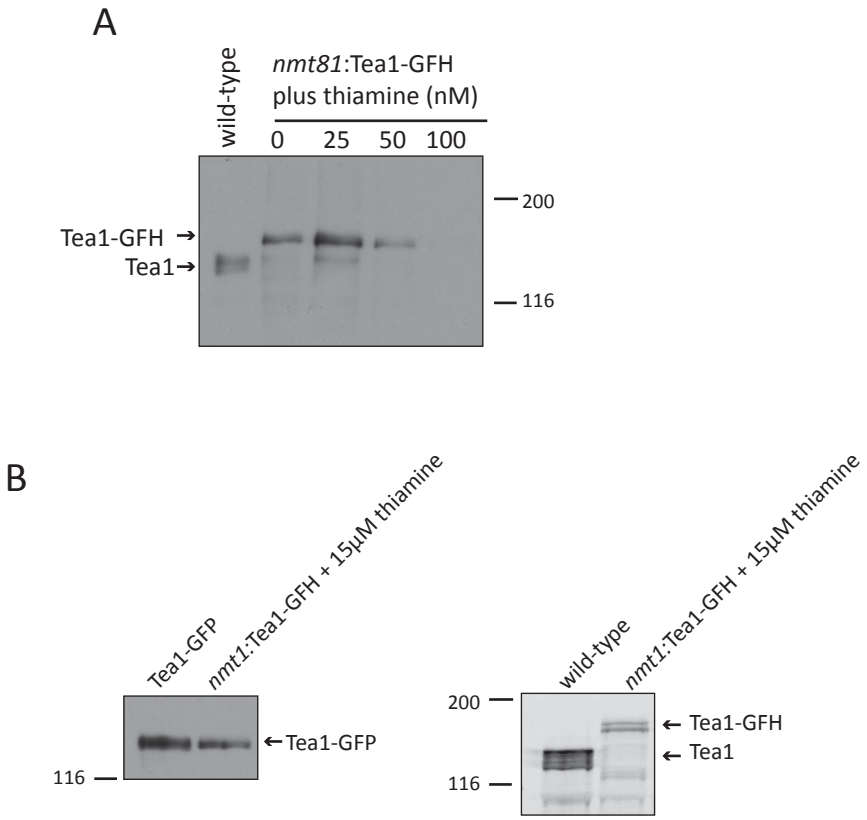

Figure 4.6- Analysis of Tea1-GFH expression under *nmt1* and *nmt81* promoters. A) *nmt81*:Tea1-GFH expression levels. Total cell extracts from cells expressing Tea1-GFP (KS1260) and from cells expressing *nmt81*:Tea1-GFH (KS4344) were analyzed by western blot. Cells expressing *nmt81*:Tea1-GFH were grown in the absence of thiamine and in the presence of 25, 50 and 100 nM of thiamine. Cells were grown in the presence of thiamine for two O/N at 25˚C, then diluted 1:100 and grown under the same conditions for one O/N. Samples were probed with anti-Tea1 antibody. **B) *nmt1*:Tea1-GFH expression levels.** Total cell extracts were prepared from wild-type cells (KS516), Tea1-GFP cells and *nmt1*:Tea1-GFH (KS4417) cells repressed with 15 µM of thiamine. Samples were probed with anti-Tea1 antibody.

In order to have Tea1-GFH expression closer to the levels observed when Tea1 is expressed under its endogenous promoter, *nmt81* and *nmt1* promoters were repressed with thiamine. 25 nM and 15 µM of thiamine were added to cells expressing *nmt81*:Tea1-GFH and *nmt1*:Tea1-GFH, respectively. Figure 4.6A and 4.6B show the expression levels of Tea1-GFH under the two experimental conditions. In both situations, addition of thiamine reduced Tea1-GFH expression closer to wild-type levels. Moreover, addition of 100 nM of thiamine completely shut down *nmt81:*Tea1-GFH expression (Figure 4.6A). Figures 4.7A and 4.7B show that when both *nmt81* and *nmt1* promoters are repressed the localization of Tea1-GFH is similar to wild-type.

Based on the results described, I decided to express Tea1 phospho-mutants under the *nmt1* promoter repressed with 15 µM thiamine. This option was favoured because over time at intermediate thiamine levels (25 nM) the regulation of *nmt* expression is not under tight control.

4.2.7. Construction of Tea1 non-phosphorylatable and phospho-mimetic point mutants

Next, the Tea1 phospho-mutants were constructed and expressed in *S. pombe* cells. To construct Tea1 phospho-mutants, Tea1-pDONR was mutated using the Quikchange kit (Quiagen) and subsequently cloned into the expression vector, pDUAL-GFHc (GFH C-terminal tag). All the mutants were integrated at the *leu1+* locus of a *tea1*Δ strain and were expressed under the *nmt1* promoter repressed with 15 µM of thiamine.

The incorporation of a phosphate group in a side chain transforms a neutrally charged part of the protein into a charged one. By substituting serine and tyrosine residues with alanine and phenylalanine, respectively, the protein charge is altered. It goes from highly charged (due to phosphorylation) to two neutral amino acids. The substitution with aspartic acid has the opposite effect, because this amino acid introduces charge and mimics the incorporation of a phosphoryl group. Based on the results obtained in the comparative phospho-analysis (section 4.2.5), three Tea1 non-phosphorylatable mutants and two Tea1 phospho-mimetic mutants were constructed. The residues Y484 and S556 were mutated because they are differentially phosphorylated. The triple combination S462, S474 and S476 was mutated because these residues seem to be constitutively phosphorylated, suggesting that the phosphorylation of these three residues could be important for Tea1 function. Figure 4.8A shows the position of the mutated residues in Tea1 sequence. Y484

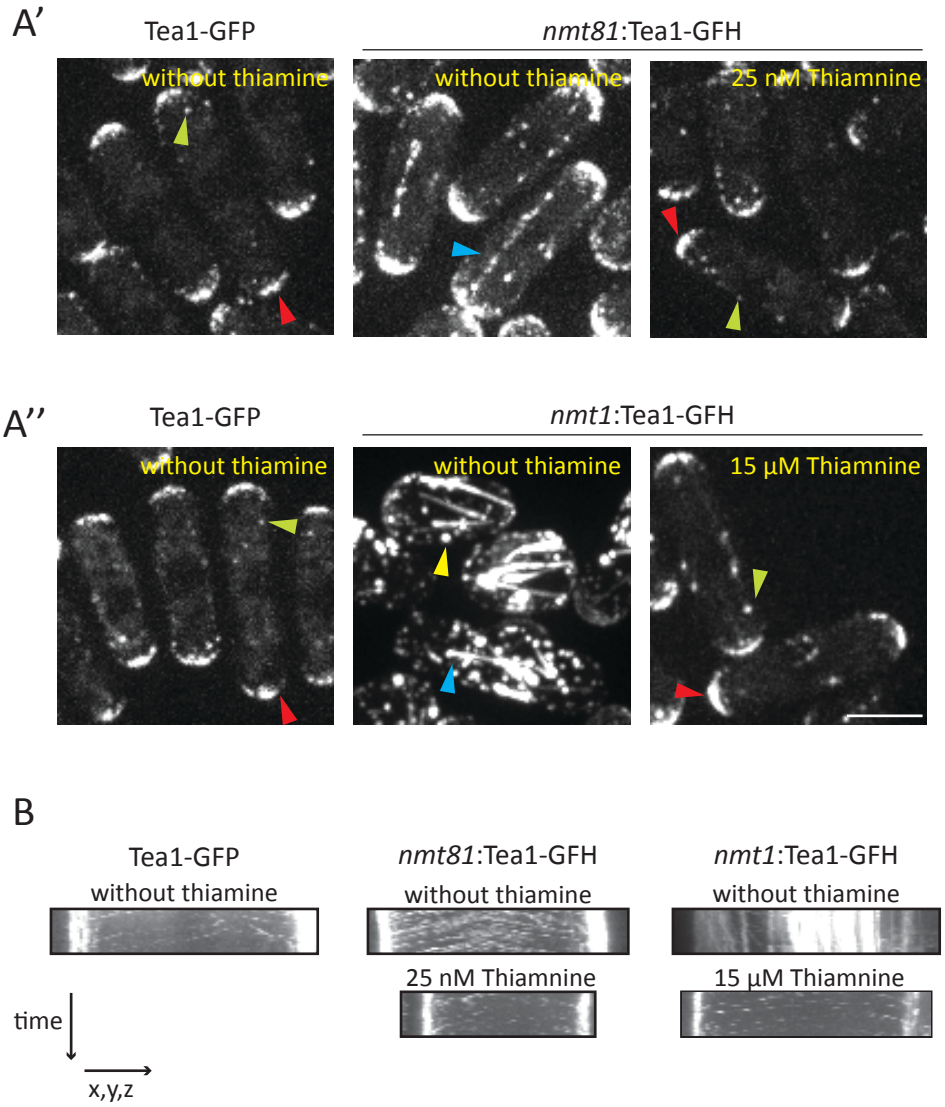

Figure 4.7- Localization of Tea1-GFH when over expressed. A) Tea1-GFP (KS1260), *nmt81*:Tea1-GFH (KS4344) without thiamine or with 25 nM of thiamine, and *nmt1*:Tea1-GFH (KS4417) without thiamine or with 15 µM of thiamine were imaged on a wide-field microscope. Both unrepressed *nmt81*:Tea1-GFH and *nmt1*:Tea1-GFH localize more abundantly along microtubules than wild-type levels of Tea1-GFP (blue arrowheads). When expressed under the unrepressed *nmt1* promoter, Tea1-GFH forms aggregates in the cytoplasm (yellow arrowheads). Thiamine repression of *nmt81*:Tea1-GFH and *nmt1*:Tea1-GFH reduces the protein expression levels and restores the protein localization at microtubule plus-ends (green arrowheads) and at the cell tip (red arrow heads). The set of images in A' and in A'' were acquired using the same imaging conditions and can be directly compared among themselves. **B) Tea1-GFH movements towards the cell tips.** Kymographs of Tea1-GFP, *nmt81*:Tea1-GFH grown without or with 25 nM thiamine; and *nmt1*:Tea1-GFH grown without or with 15 µM thiamine. Kymographs result from time-lapse microscopy. Each strain was imaged for 5 min every 15 sec. At each time point 5 z-sections with 0.6 µm intervals were acquired. Bar, 5 µm.

residue was mutated to phenylalanine (F) to become non-phosphorylatable while S556 and the triple mutant were mutated to alanine (non-phosphorylatable mutant) and to aspartic acid (phospho-mimetic).

4.2.8. Analysis of Tea1 phospho-mutants

Next, the localization of Tea1 phospho-mutant proteins was analyzed, in order to link the amino acid(s) mutated with differential Tea1 localization.

Figure 4.8B shows live-cell images of the five Tea1 phospho-mutant proteins tagged with GFH. Figure 4.8C contains kymographs showing Tea1 packets moving towards the cell tip. The localization of the five Tea1 phospho-mutants was comparable with wild-type Tea1, both at the cell tip and at the microtubule plus-ends. Moreover, all Tea1 phospho-mutants move directionally towards the cell tip. Live-cell imaging of Tea1 phospho-mutants showed that the residues tested do not play a major role in Tea1 localization and as a consequence in Tea1 function.

Although the mutated residues did not show an effect on Tea1 localization, the hypothesis that phosphorylation plays a role in Tea1 regulation cannot be ruled out. There are still 20 candidate phospho-residues to be tested, as well as the combinatory effect of multisite phosphorylation.

4.2.9. Deletion of aa 434 to aa 586 reduces Tea1 targeting to the cell tip

Next, the phospho-rich region (aa 434 to aa 586) of Tea1 was internally deleted, in order to examine its biological relevance to Tea1 function. If phosphorylation did not play any role in regulating Tea1 function, the deletion of all phosphorylated residues would not affect Tea1 localization.

Tea1-GFP was internally deleted in three sequential fractions. In Tea1 internal-deletion mutants, the deleted amino acids were replaced with seven alanine residues, in order to create a linker region. Each internal deletion aimed to delete individual phospho-rich clusters within the larger region. Figure 4.9A contains a schematic diagram of the mutants *tea1Δ(434-478)*, *tea1Δ(479-532)*, *tea1Δ(533-586)* and *tea1Δ(434-586)*.

Figure 4.9B shows Tea1 expression levels of each internal-deletion determined by immunoblotting. The expression levels of each internal-deletion are comparable to the

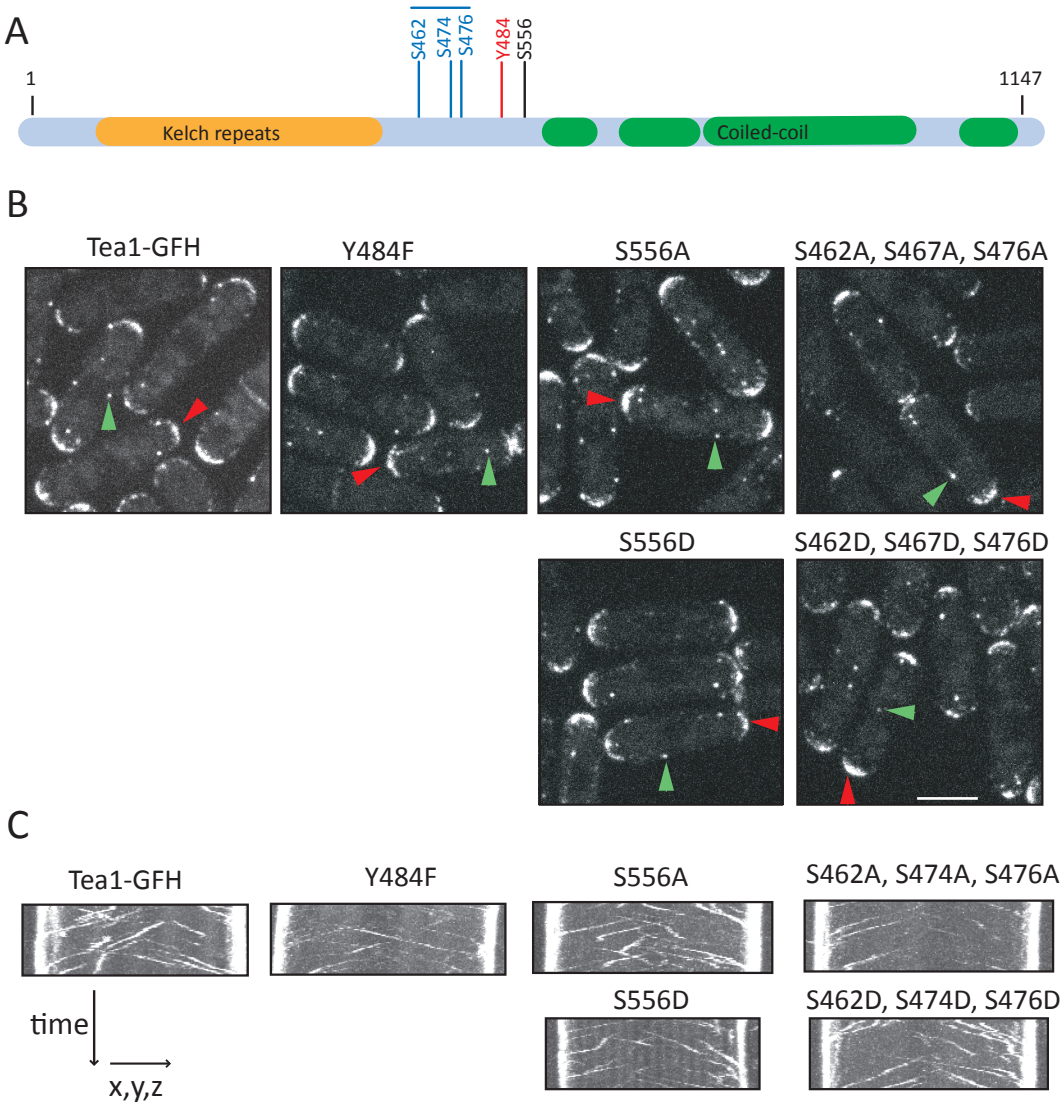

Figure 4.8- Analysis of Tea1 phospho-mutants localization and dynamics. A) Diagram of Tea1 domains and the relative localization of the mutated phosphorylated residues. Five Tea1 phospho-mutants were constructed: Tea1(Y484F) (KS4634) (red), Tea1(S556A) (KS4630) (black), Tea1(S556D) (KS4632) (black), Tea1(S434/474/476A) (KS4636) (blue) and Tea1(S434/474/476D) (KS4638) (blue). The mutants were GFH tagged at the C-terminus and expressed under the *nmt1* promoter from the *leu1+* locus. **B) Localization of Tea1-GFH non-phosphorylatable and phospho-mimetic mutants.** The localization of Tea1 phospho-mutants was analyzed in a spinning disc microscope. All the five tested phospho-mutants localize at microtubule plus-ends (green arrow-heads) and at the cell tip (red arrow-heads), with comparable similarity to Tea1-GFH wild-type. **C) Analysis of Tea1 phospho-mutants movement towards the cell tips.** Kymographs of Tea1-GFH, Tea1(Y484F)-GFH, Tea1(S556A)-GFH, Tea1(S556D)-GFH, Tea1(S434/474/476A)-GFH and Tea1(S434/474/476D)-GFH. Kymographs result from time-lapse microscopy. Each strain was imaged for 5 min every 5 sec. At each time point 5 z-sections with 0.6 µm interval were acquired. Bar, 5 µm.

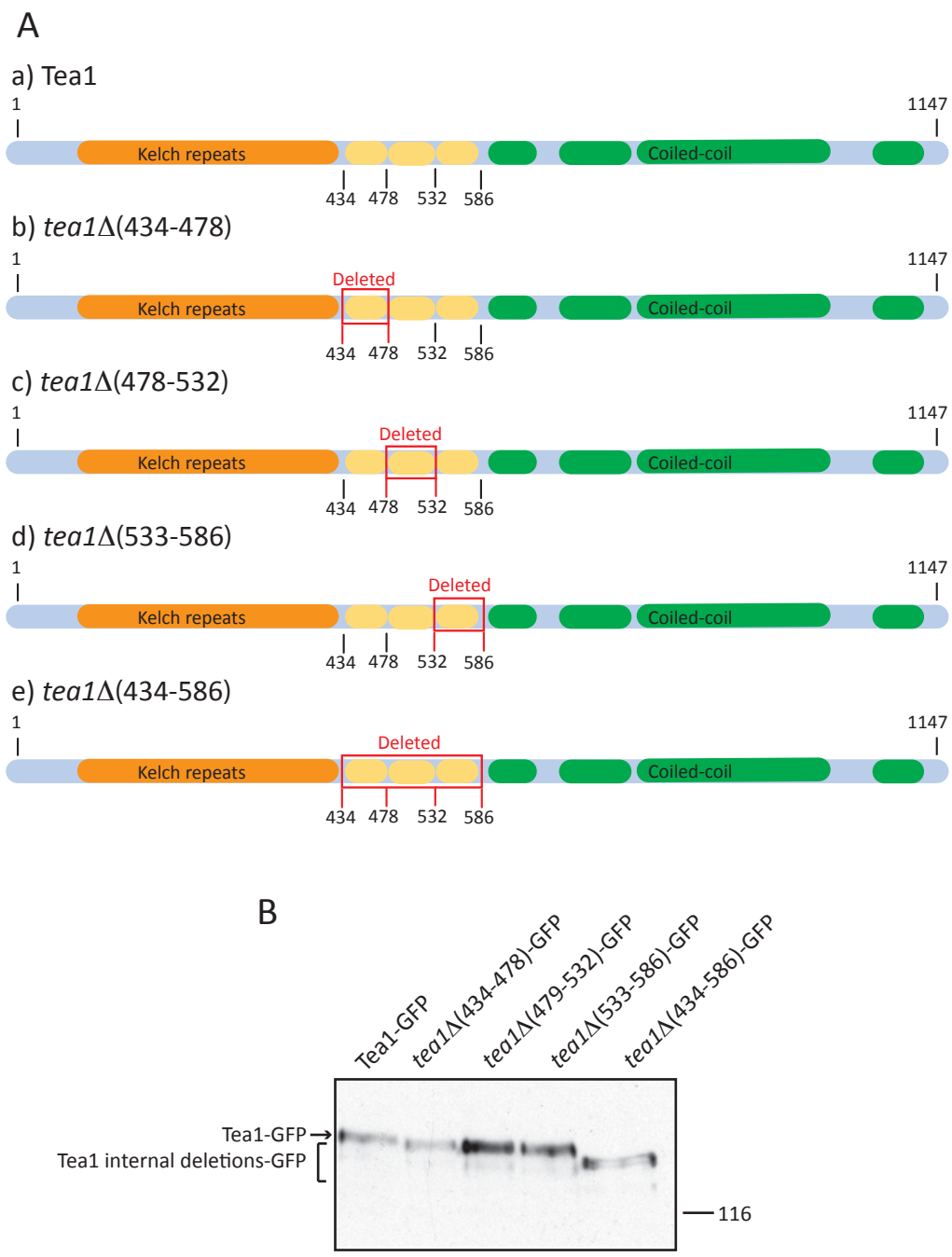

Figure 4.9- Tea1 internal-deletion mutants. A) Diagram of Tea1 internal deletion. Four Tea1 internal deletions were constructed: a) Tea1 wild-type (KS1260), b) *tea1 Δ*(434-478) (KS4734) (ten phosphorylated residues deleted), c) *tea1Δ*(478-532) (KS4736) (four phosphorylated residues deleted), d) *tea1Δ*(533-586) (KS4738) (six phosphorylated residues deleted) and e) *tea1Δ*(434-586) (KS4740) (20 phosphorylated residues deleted). Internal-deletion mutants were expressed from the endogenous locus and tagged with GFP at the C-terminal. **B) Protein stability of internally deleted Tea1.** The expression levels of Tea1 internal-deletion mutant are comparable to wild-type Tea1-GFP. Samples were probed with anti-Tea1 antibody.

levels of wild-type Tea1-GFP. Thus, subsequent observations are not an artefact resulting from changes in protein stability.

Figure 4.10 shows that *tea1Δ(434-478), tea1Δ(479-532)*, *tea1Δ(532-586)* and *tea1Δ(434-586)* localize at the cell tip as in wild-type cells. However, *tea1Δ(479-532)*, *tea1Δ(532-586)* and especially *tea1Δ(434-586)* do not localize to microtubule plus-ends as abundantly as in wild-type cells. This suggests that the binding of Tea1 to the microtubules is perturbed in the internal-deletion *tea1Δ479-532, tea1Δ533-586* and *tea1Δ434-586.*

Next, the association of Tea1 internal-deletions with microtubules was characterized by quantifying the number of Tea1 packets delivered to the cell tip per unit time (Figures 4.11B and 4.11C). The frequency of arrival of *tea1Δ(478-532)* (1.01±0.32 packets/min/tip) is similar to wild-type (1.12±0.39 packet/min/tip). However, the excursions in *tea1Δ(478-532)* (0.49±0.31 packet/min/tip) and *tea1Δ(532-586)* (0.6±0.41 packet/min/tip) and *tea1Δ(434-586)* (0.13±0.24 packet/min/tip) are significantly reduced when compared with wild-type.

The deletion of the phospho-rich region (aa 434 to aa 586) of Tea1 significantly reduces Tea1 delivery to the cell tip. This could mean that aa 434 to aa 586 are necessary for Tea1 association with microtubules, and consequently their deletion makes Tea1 delivery to the cell tip defective. Another hypothesis is that aa 434 to aa 586 may be involved in Tea1 dissociation from the cell tip. In this case, when these amino acids are deleted, Tea1 turnover at the cell tip is slower. Thus, Tea1 is sequestered at the cell tip and is not available to bind to microtubules in the cytoplasm.

4.2.10. tea1Δ434-586 is more stably associated at the cell tip than wild-type Tea1

The reduced number of Tea1 excursions in *tea1Δ(479-532)*, *tea1Δ(533-586)* and *tea1Δ(434-586)* could be because these mutants are sequestered within the cell membrane. Thus, once at the cell tip, these mutants do not recycle back to the cytoplasm and less cytoplasmic Tea1 is available to become microtubule-associated. To test this hypothesis, the localization of *tea1Δ(434-478), tea1Δ(479-532)*, *tea1Δ(533-586)* and *tea1Δ(434-586)* was analysed in a *mod5*Δ background. In the *mod5*Δ mutant, Tea1 does not accumulate at the cell tip, and therefore the cytoplasm pool of Tea1 increases (Snaith and Sawin, 2003). Thus, in a *mod5Δ* mutant, *tea1Δ(434-478), tea1Δ(479-532)*, *tea1Δ(533-586)* and *tea1Δ(434-586)* could be biased towards association with microtubules because their cytoplasm pool is increased.

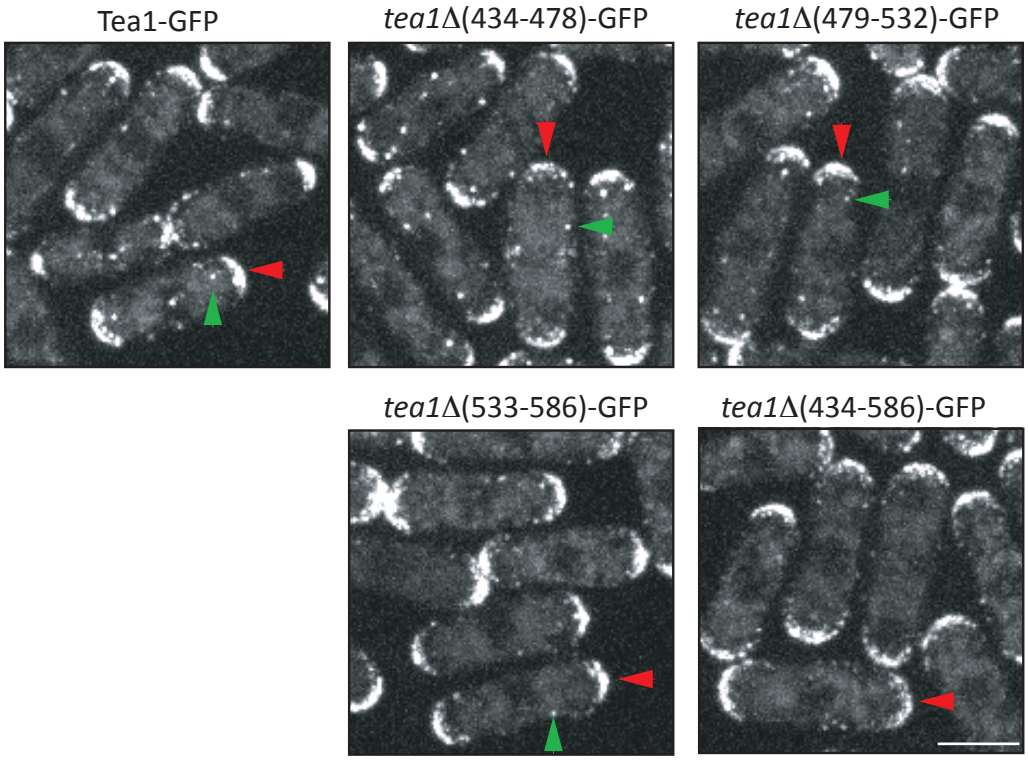

Figure 4.10- Localization of Tea1 internal-deletion mutants. The localization of Tea1 internal-deletion mutants was analyzed with a spinning disc microscope. All Tea1 internal-deletion mutants (KS4734, KS4736, KS4738 and KS4740) localize at the cell tip (red arrow-heads), with comparable intensity to wild-type Tea1-GFP (KS1260). Localization at the microtubule plus-ends (green arrow-heads) is less abundant in *tea1Δ533-586* and *tea1 Δ434-586*. Bar, 5 µm.

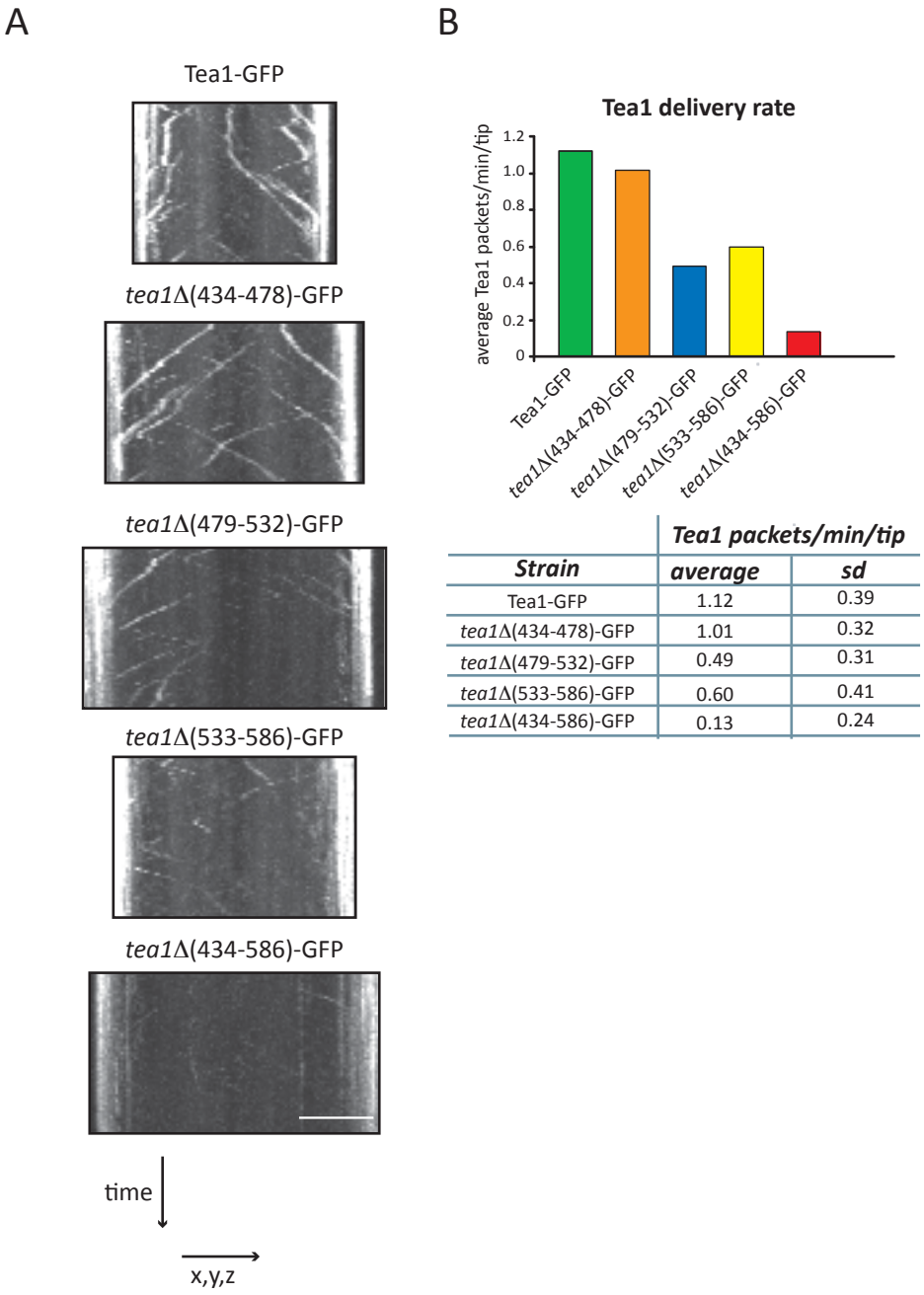

	Tea1 packets/min/tip	
Strain	**average**	**sd**
Tea1-GFP	1.12	0.39
*tea1*Δ(434-478)-GFP	1.01	0.32
*tea1*Δ(479-532)-GFP	0.49	0.31
*tea1*Δ(533-586)-GFP	0.60	0.41
*tea1*Δ(434-586)-GFP	0.13	0.24

Figure 4.11- Analysis of the movement of Tea1 internal-deletion mutants. **A)** Kymographs of Tea1-GFP (KS1260), *tea1 Δ*(434-478) (KS4734), *tea1Δ*(478-532) (KS4736), *tea1Δ*(533-586) (KS4738) and *tea1Δ*(434-586)-GFP (KS4740), obtained from time-lapse microscopy. Each strain was imaged for 5 min every 5 sec. At each time point 5 z-sections with 0.6 µm intervals were acquired. **B) Quantification of Tea1 packets delivery rate**. Kymographs were used to determine the number of Tea1 packets delivered to the cell tip per minute. 15 cells were quantified for each strain in a total of 150 min/strain. sd is standard deviation. Bar, 5 µm.

Figure 4.12A shows the localization of Tea1 internal deletion mutants expressed in a *mod5Δ* background and Figure 4.12B shows the representative kymographs. In the *mod5*Δ background, *tea1Δ(434-478), tea1Δ(479-532)*, *tea1Δ(533-586)* and *tea1Δ(434-586)* are microtubule-associated and are transported to the cell tip as in wild-type (Figures 4.12A and 4.12B). This result shows that *tea1Δ(434-478), tea1Δ(479-532)*, *tea1Δ(533-586)* and *tea1Δ(434-586)* can be transported by association with microtubule plus-ends, but only when Tea1 anchoring to the cell membrane is compromised. In a *mod5+* strain, *tea1Δ(434-478), tea1Δ(479-532)*, *tea1Δ(533-586)* and *tea1Δ(434-586)* are sequestered at the cell tip and do not recycle back to the cytoplasm.

Taken together, these results suggest that aa 434 to aa 586 of Tea1 are important for Tea1 to dissociate from the cell tip. Moreover, the evidence presented here suggests that Tea1 turnover at the cell tip might be regulated by phosphorylation within aa 434 and aa 586. The implications of Tea1 phosphorylation on its dissociation from the cell tip are discussed below.

4.3. Discussion

This chapter describes the analysis of Tea1 phosphorylation. Although, there were some indications in the literature supporting Tea1 phosphorylation, no phospho-mapping or functional analysis has been performed before.

A total of 25 phosphorylated residues were identified in Tea1 by MS. 20 out of 25 phosphorylated residues were identified in the central region of Tea1, from aa 434 to aa 586, which is not part of either the Kelch repeats or the coiled-coils. This suggests that the folded tertiary structures of the Kelch repeats and the coiled-coils make them inaccessible for modification.

Because there was no obvious potentially relevant phosphorylated residue to be analysed, two different experimental approaches were designed to study Tea1 phosphorylation. First, a comparative phospho-mapping study was designed to identify differential Tea1 phosphorylation. Second, the phosphorylated residues of Tea1 were mutagenized and their roles in Tea1 function were examined.

The comparison of Tea1 phosphorylated residues between wild-type and the different mutants of Tea1 interacting proteins suggested that differential Tea1 localization correlates with differential Tea1 phosphorylation. However, because there was variation from sample

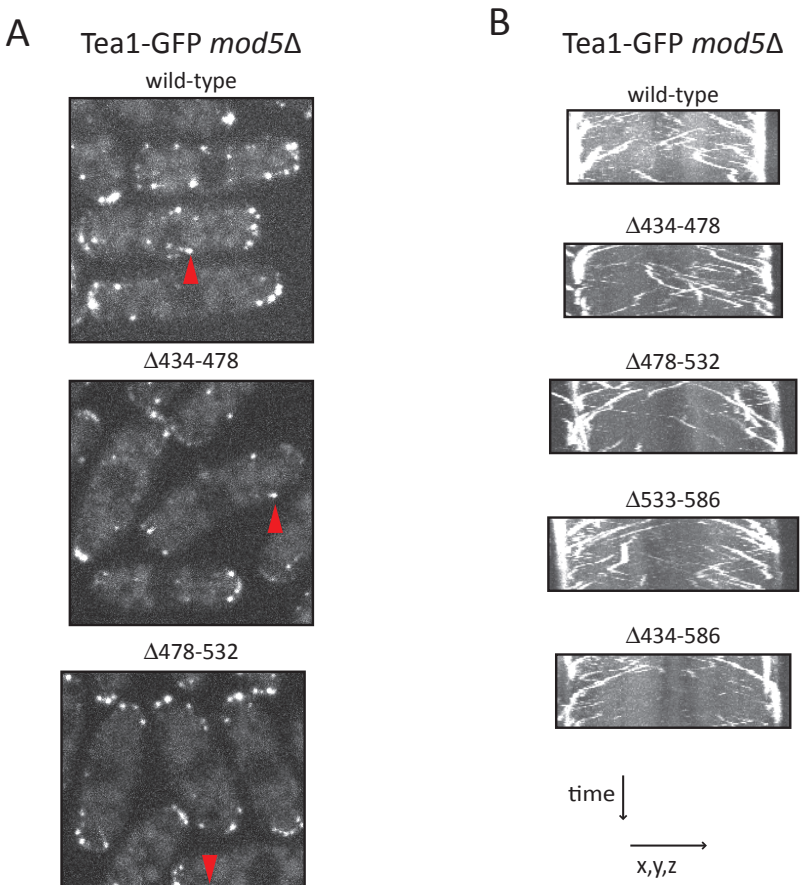

Figure 4.12- Localization and dynamics of Tea1 internal-deletion mutants in *mod5Δ* background. **A)** Confocal microscopy of live cells expressing *tea1*Δ(434-478) (KS4776), *tea1*Δ(479-532) (KS4778), *tea1*Δ(533-586) (KS4780) and *tea1*Δ(434-586)-GFP (KS4782) in a *mod5Δ* background. Red arrows indicate Tea1 localization at the microtubule plus-end. **B) Analysis of the movement of Tea1 internal-deletion mutants towards the cell tips.** Kymographs of Tea1-GFP and Tea1 internal-deletion mutants in *mod5Δ* background. Bar, 5 µm.

to sample, interpretation of data was difficult. The variation could have been originated from biological sample preparation or from MS sample handling.

Five residues (Y484, S556 and the combination S467/S476/S478) were mutated by site-directed mutagenesis, to either non-phosphorylatable or phospho-mimetic amino acids. None of the mutated residues appear to affect Tea1 function. However, the number of phosphorylated residues tested was far from comprehensive. The hypothesis that other single amino acid residue or even a combination of residues can play a role in Tea1 function cannot be ruled out.

The internal-deletion of the phospho-rich region of Tea1 showed that aa 434 to aa 586 are important for Tea1 dissociation from the cell tip. This could be because Tea1 needs to be phosphorylated before it dissociates from the cell tip. There are several candidate membrane-associated kinases involved in cell polarity, such as Pom1 and Orb2, which could indeed phosphorylate Tea1. In order to demonstrate this hypothesis it would be interesting to make non-phosphorylated and phospho-mimetic versions of all the Tea1 phospho-residues.

How could aa 434 to aa 586 be involved in Tea1 dissociation from the cell tip? The region of Tea1 spanning aa 434 to aa 586 does not fold into a predictable tertiary protein structure, such as the Kelch repeats or the coiled-coils. FoldIndex, which predicts protein folding based on amino acid hydrophobicity and the absolute value of their net charge, was used to predict Tea1 folded and unfolded regions (Prilusky et al., 2005). Figure 4.13 shows the FoldIndex prediction for Tea1 and amino acids 397 to 525 of Tea1 are predicted not to fold. Unfolded or intrinsically disordered regions are characterized by having a low complexity in the amino acid sequence, a low content in bulky hydrophobic amino acids and a high content in polar amino acids (Dyson and Wright, 2005). Due to their amino acid content, unfolded regions do not have sufficient hydrophobic cores that are necessary to form organized 3D structures. Therefore, these regions can provide a linear linker between domains with bulky tertiary structure. In the case of Tea1, the unfolded region spanning aa 397 to aa 525 could link the N-terminal Kelch repeats and the C-terminal coiled-coils.

Unfolded regions have been shown to function not only as linkers, but also as regulatory regions. In these regions, amino acids are exposed and therefore accessible to kinases (Serber and Ferrell, 2007; Zimniak et al., 2009). Thus, it is not surprising that aa 434 to aa 586 of Tea1 were found to be heavily phosphorylated. In fact, it is known that unfolded regions can be multisite-phosphorylated and act as regulators of global protein structure

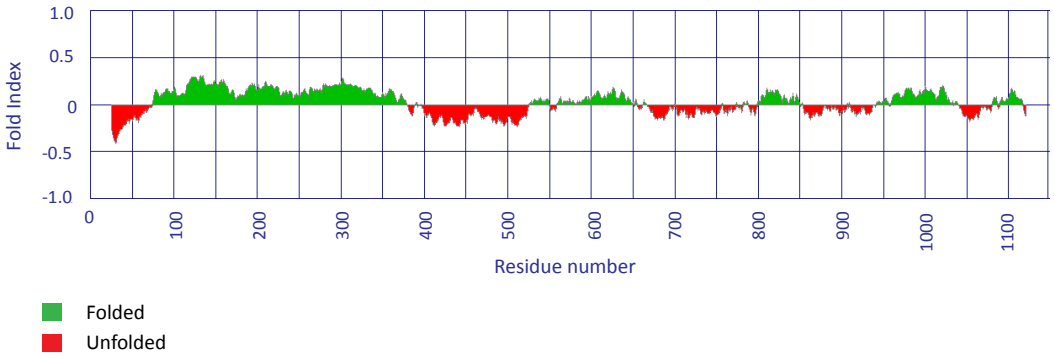

Figure 4.13- FoldIndex prediction of Tea1 folded and unfolded sequences. In the plot green means folded and red unfolded. FoldIndex predicts aa 397 to 525, aa 701 to aa 798 and aa 854 to aa 936 to be largely unfolded. FoldIndex provides single scores for the entire sequence, predicting if it is folded or not. Therefore, FoldIndex prediction of folded regions is not successful if their global physical chemical properties are borderline between folded and unfolded (Prilusky et al., 2005). Paircoil predictions of coiled-coil regions show that aa 695 to aa 730 and aa 783 to aa 829 have a high probability of folding into a coiled-coil tertiary structure (Wolf et al., 1997).

(Kim and Ferrell, 2007; Serber and Ferrell, 2007; Zimniak et al., 2009). Protein regulation by multisite phosphorylation has been shown for proteins such as Ste5 (Strickfaden et al., 2007), Bim1 (Zimniak et al., 2009), CLASP (Kumar et al., 2009) or Hec1 (Guimaraes et al., 2008). Multisite phosphorylation creates a highly negatively charged region in the protein and can disrupt protein interactions. Disruption can be due either to changes in protein bulk electrostatic characteristics (creating repulsion) or to conformational changes (Zimniak et al., 2009).

In Chapter III, Tea1 was proposed to form polymers and to be associated as a cluster-networks at the cell tip. Once at the cluster-network, Tea1 is packed in a polymeric form and is stably bound in a higher ordered structure. The results shown in this chapter suggest that the stability of Tea1 in the cluster-network increases when Tea1 aa 434 to aa 586 are deleted. This suggests that Tea1 phosphorylation might play a role in the dissociation of Tea1 from the cluster-network. Figure 4.14 shows a schematic diagram with a proposed hypothesis for the role of phosphorylation in Tea1 dissociation from the cluster-network. In Figure 4.14A Tea1 is present at the cell tip, adjacent to the cell membrane, embedded in the cluster-network. In Figure 4.14B a membrane-localized kinase(s) multi-phosphorylates the unfolded region of Tea1, leading to an increase in negative charge. Figure 4.14C represents two possible mechanisms for Tea1 dissociation from the cluster-network. In Figure 4.14C i), Tea1 multisite phosphorylation promotes a structural change in the linker region. Therefore, multisite phosphorylated Tea1 cannot fit in the packed structure of the cluster-network and will dissociate. In Figure 4.14Cii) the added negative charges create electrostatic bulk repulsion with the negatively charged membrane and Tea1 dissociates from the cluster-network. Both phosphorylation outcomes lead to a change of phosphorylated Tea1 connectivity with the cluster-network (Figure 4.14D). The change in connectivity can create a window of opportunity during which Tea1 could interact with its binding partners (Misteli, 2001). Moreover, because multisite phosphorylation requires accumulation of signalling it makes the system regulation sensitive to changes and highly tuneable (Serber and Ferrell, 2007).

In summary, the phosphorylated residues of Tea1 were identified mainly in a region of Tea1 (aa 434 to aa 586) predicted to be unfolded. Mutagenic analysis indicated that Tea1 dissociation from the cell tip requires amino acids 434 to 586. This suggests that Tea1 phosphorylation by membrane-localized kinase(s) changes Tea1 connectivity within the cluster-network and therefore promotes its dissociation.

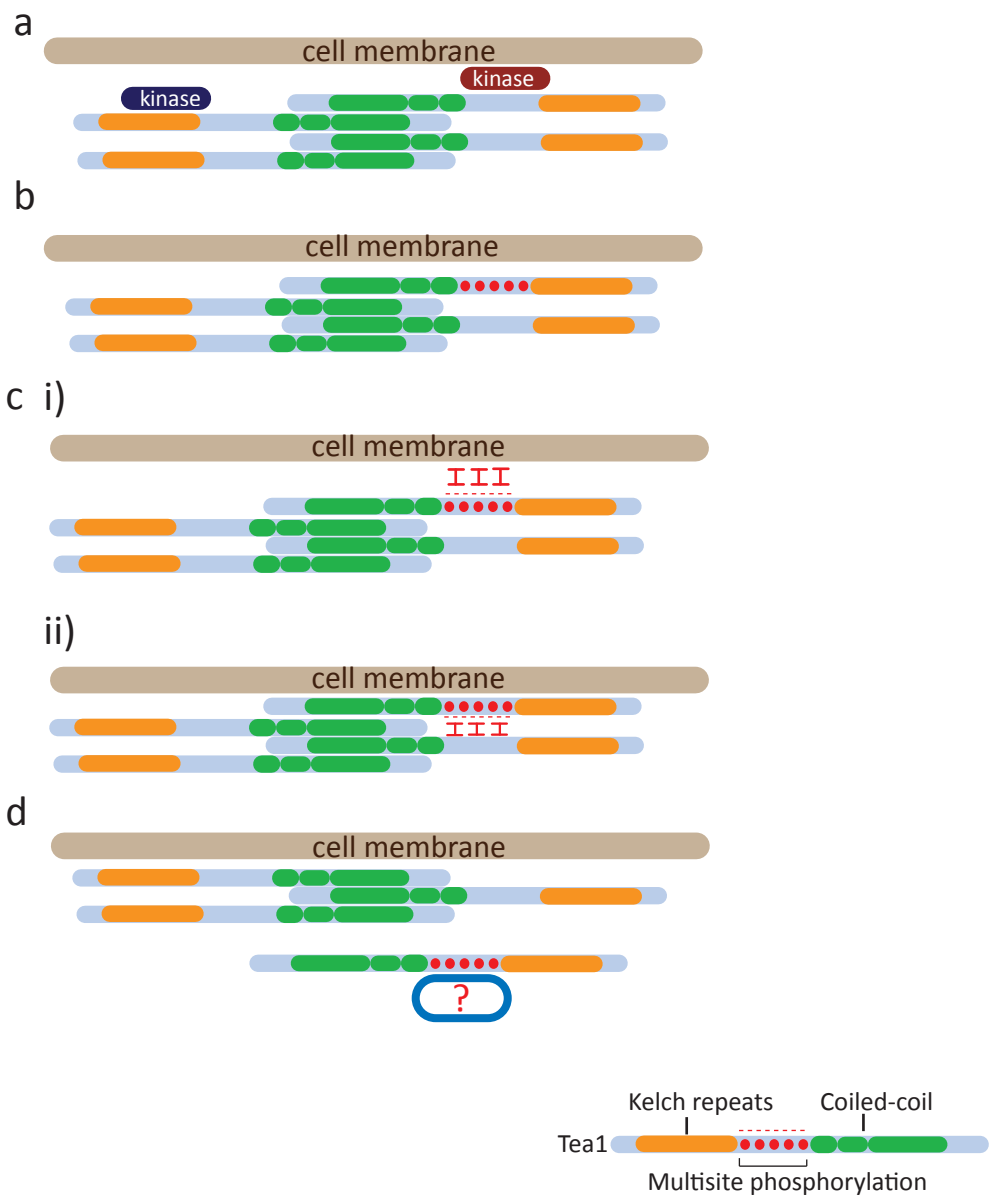

Figure 4.14- Model for phospho-regulation of Tea1 connectivity changes within the cluster-network. a) Tea1 is incorporated in the cluster-network at cell membrane. Kinases are present at the cell membrane. (Protein kinases interactions in the schematic diagram do not represent their position in relation to the Tea1 cluster-network). **b)** Tea1 is multisite phosphorylated in the unfolded region spanning aa 434 to aa 586. **c)** After phosphorylation Tea1 dissociates from the cluster-network, due to: **i)** bulky electrostatic repulsion with the membrane; **ii)** conformational changes that make it unsuitable to fit the tightly packed cluster-network. **d)** Changes in cluster-network connectivity could give Tea1 the chance to interact with other proteins before it is recycled back to cytoplasm.

Chapter V: Development of a robust SILAC method for S. pombe

5.1. Introduction

Experiments described in Chapter IV (Section 4.2.5) demonstrated that comparison between MS samples is associated with high statistical variability, which makes data analysis very challenging. Therefore we decided to develop SILAC (Stable Isotope Labelling by Amino acids in Cell Culture) for *S. pombe,* a method that allows relative quantitation of protein expression between samples.

SILAC was first described in 2002 by the Mathias Mann group (Ong et al., 2002), and since then several studies have successfully used this approach to obtain quantifiable data from MS analysis (Bonaldi et al., 2008; de Godoy et al., 2008; Gruhler et al., 2005). SILAC can be used to quantify differential post-translational modifications (Gruhler et al., 2005), differential interacting proteins as well as differential expression levels in proteome-wide analysis (Bonaldi et al., 2008; de Godoy et al., 2008).

SILAC experiments require *in vivo* incorporation of isotopically labelled amino acids into all expressed proteins. Lysine and arginine are widely used as the amino acids of choice in SILAC, because trypsin, the protease used to digest proteins into smaller peptides, cleaves after lysine and arginine. Labelling with heavy arginine and lysine therefore ensures that all tryptic peptides labelled contain at least one labelled amino acid residue (Ong et al., 2003).

In SILAC, cell cultures are grown separately in the presence of different isotopically labelled amino acids and then mixed in a 1:1 ratio. All the subsequent sample processing is done once the samples are mixed. Peptides from each sample are distinguishable in the MS spectra. For example, in the case of $^{13}C_6$-labelled amino acids, peptides from the heavy labelled sample will be shifted 6 Da relative to the same peptide from the light-labelled sample (Figure 5.1).

Although SILAC is a powerful quantitative method, it faces two main constraints. First, it requires complete incorporation of isotopically labelled lysine and arginine into proteins. The extent of heavy amino acids incorporation varies with the model organism of choice. In mammalian culture cells, for example, although heavy amino acid incorporation is incomplete, it is described as occurring at high levels (Ong et al., 2003). In *S. cerevisiae*, complete incorporation of heavy lysine and arginine was made possible by using lysine and arginine auxotrophic mutants (Gruhler et al., 2005).

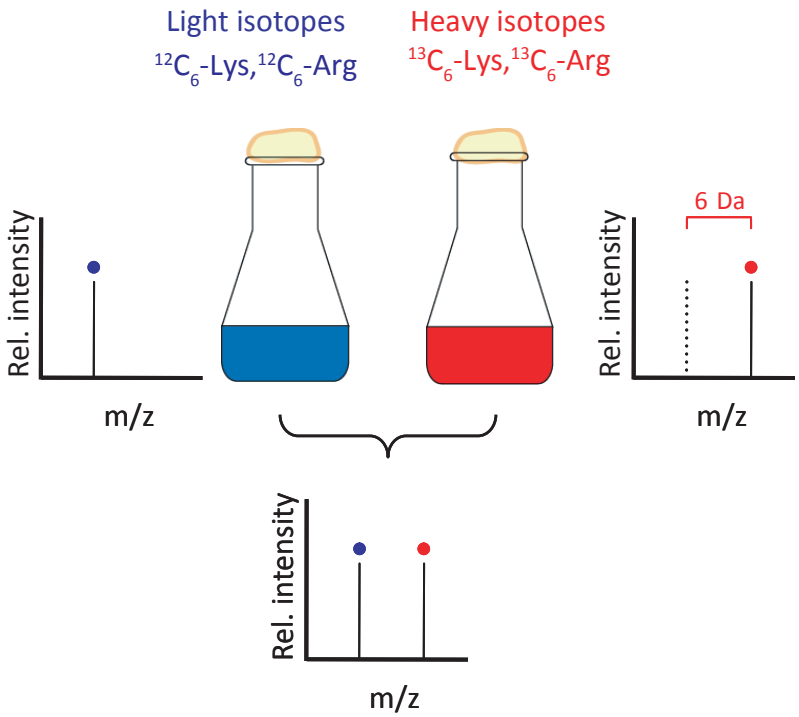

Figure 5.1- SILAC experimental set-up. In a SILAC experiment, two cultures are grown separately. One of the cultures is grown in the presence of light lysine and arginine (blue); and the other is grown in the presence of heavy lysine and arginine (red). The cultures are mixed in a 1:1 ratio and the resulting mixture is processed for MS analysis. Peptides from each sample can be differentiated in the MS spectra, due to a 6Da m/z shift.

Second, it has been observed that arginine is converted into proline, which can cause problems (Bendall et al., 2008; Gruhler et al., 2005). Arginine conversion to proline in SILAC experiments has been described in *S. cerevisiae*, *D. melonogaster* and mammalian cultured cells (Bonaldi et al., 2008; Gruhler et al., 2005; Ong et al., 2003). Several approaches have been proposed to deal with arginine conversion. Arginine catabolism can be metabolically manipulated either by reducing the concentration of heavy labelled arginine or by supplementing the media with light proline (Bendall et al., 2008; Ong et al., 2003). Both approaches have drawbacks. Reducing the arginine concentration could starve cells and means that experiments are not performed under physiological conditions, while an excess of proline could be back-converted to light arginine. Arginine conversion can also be corrected using computational methods (Park et al., 2009; Van Hoof et al., 2007) or by omitting arginine labelling (de Godoy et al., 2008). Lysine-only labelling is in principle possible, but significantly reduces the number of peptides available for quantification. In all of the methodologies proposed to avoid arginine conversion, arginine still has the potential to be catabolised into other amino acids.

My aim was to genetically engineer a *S. pombe* strain that ensures complete incorporation of heavy lysine and arginine, without arginine conversion. I also aimed to find the most cost-effective growth conditions that would give robust growth with the lowest concentration of lysine and arginine.

5.2. Results

5.2.1. Analysis of $^{13}C_6$-Lysine incorporation in lys3-37

The first goal was to find lysine and arginine auxotrophic mutants able to completely incorporate heavy labelled amino acids into proteins.

There are several lysine mutants in *S. pombe* and I selected *lys3-37* to be analysed. Lys3 is a saccharopine dehydrogenase and catalyzes the last step of the lysine biosynthesis pathway (Figure 5.2A).

The growth of the *lys3-37* mutant was tested in the presence of decreasing concentrations of lysine. Figure 5.2B shows the growth curves of *lys3-37* cells grown with a broad range of lysine concentrations (0-120 mg/l). Although the mutant grows at the same

rate within a wide lysine concentration range (30 to 120 mg/l), the final growth density is lysine-concentration dependent.

To test if $^{13}C_6$-lysine is incorporated into proteins, *lys3-37* cells were grown for seven generations in EMM2 medium supplemented with 120 mg/l of $^{13}C_6$-lysine. A total protein extract was prepared, and the proteins were separated in a SDS-PAGE gel and coomassie stained. An abundant band was excised from the gel and was analysed by MS for heavy lysine incorporation. Figure 5.2C shows the MS spectra of representative peptides with a lysine residue. In the peptides *a* to *c*, the monoisotopic peak observed has the m/z predicted if $^{13}C_6$-lysine is incorporated. This shows that *lys3-37* cells completely incorporate $^{13}C_6$-lysine. The peptide shown in *d* does not contain any lysine residues. The monoisotopic peak has the m/z ratio expected for light amino acids incorporation only. Thus, *lys3-37* cells do not convert lysine to any other amino acid.

The MS analysis demonstrated that the *lys3-37* cells are suitable for SILAC. *Lys3-37* cells show robust growth within a wide range of lysine concentrations, have complete incorporation of $^{13}C_6$-lysine, and they do not show any amino acid conversion.

5.2.2. Analysis of $^{13}C_6$-arginine incorporation in arg1-230

Next, the arginine auxotrophic mutant was analysed. From the wide range of arginine auxotrophic mutants available in *S. pombe,* the *arg1-230* mutant was selected for examination. Arg1 is an acetylornithine aminotransferase and catalyses the conversion of N-acetyl-γ-glutamate 5-semialdehyde and glutamate into $^{\alpha}$N-acetyl-ornithine and α-ketoglutarate (Figure 5.3A).

To determine the minimum amount of arginine necessary for robust cell growth, the *arg1-230* strain was grown in the presence of a range of arginine concentrations (0-120 mg/l). Figure 5.3B shows the resulting growth curves. *arg1-230* cells present a lag phase of ~ 15 hrs when grown in the presence of 20-40 mg/ml and grow robustly within a narrow range of arginine concentration (60-120 mg/ml).

To test for the incorporation of arginine, *arg1-230* cells were grown for seven generations in EMM2 medium supplemented with 120 mg/l of $^{13}C_6$-arginine. The total protein extract was separated in a SDS-PAGE gel and an abundant band was excised for MS analysis. Figure 5.3C shows the mass spectrum of a representative peptide. In this spectrum, the isotope cluster with the predicted m/z of light arginine incorporation is not

A

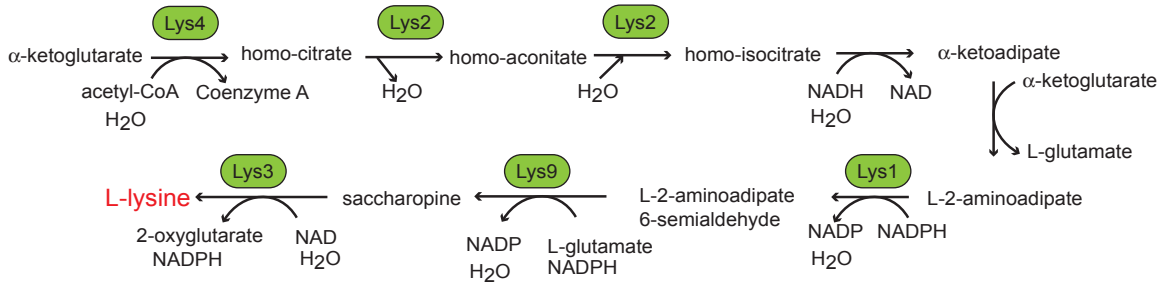

B

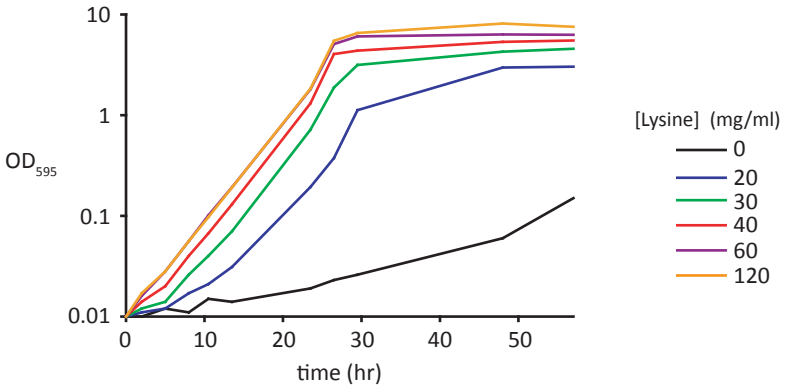

Figure 5.2- *lys3-37* fully incorporates $^{13}C_6$-lysine into proteins, without conversion to other amino acids. A) Lysine biosynthesis pathway, adapted from *S. cerevisiae*. **B) *lys3-37* growth curves**. *lys3-37* (KS5036) was grown in EMM2 medium supplemented with a range of lysine concentration (0-120 mg/l). Cell cultures OD_{595} were measured every 3 hrs, until the cultures reached stationary phase. **C) *lys3-37* fully incorporates $^{13}C_6$-lysine.** *lys3-37*was grown in EMM2 medium supplemented with 120 mg/l of $^{13}C_6$-lysine and 96 mM ammonium chloride. The incorporation of the heavy isotope was analyzed by MS. Peptides shown: NLQDEVDDERLK (a), FTAADLAAVPEESRK (b), GWPETTADLKNMIAAAR (c), and CVQTFEGHSR (d). Blue ovals indicate monoisotopic peaks of peptides. In peak annotations, the peptide sequence was reduced to the potential labelled amino acids; red denotes labelled amino acids. All peaks show absence of labelling for amino acids other than lysine

C

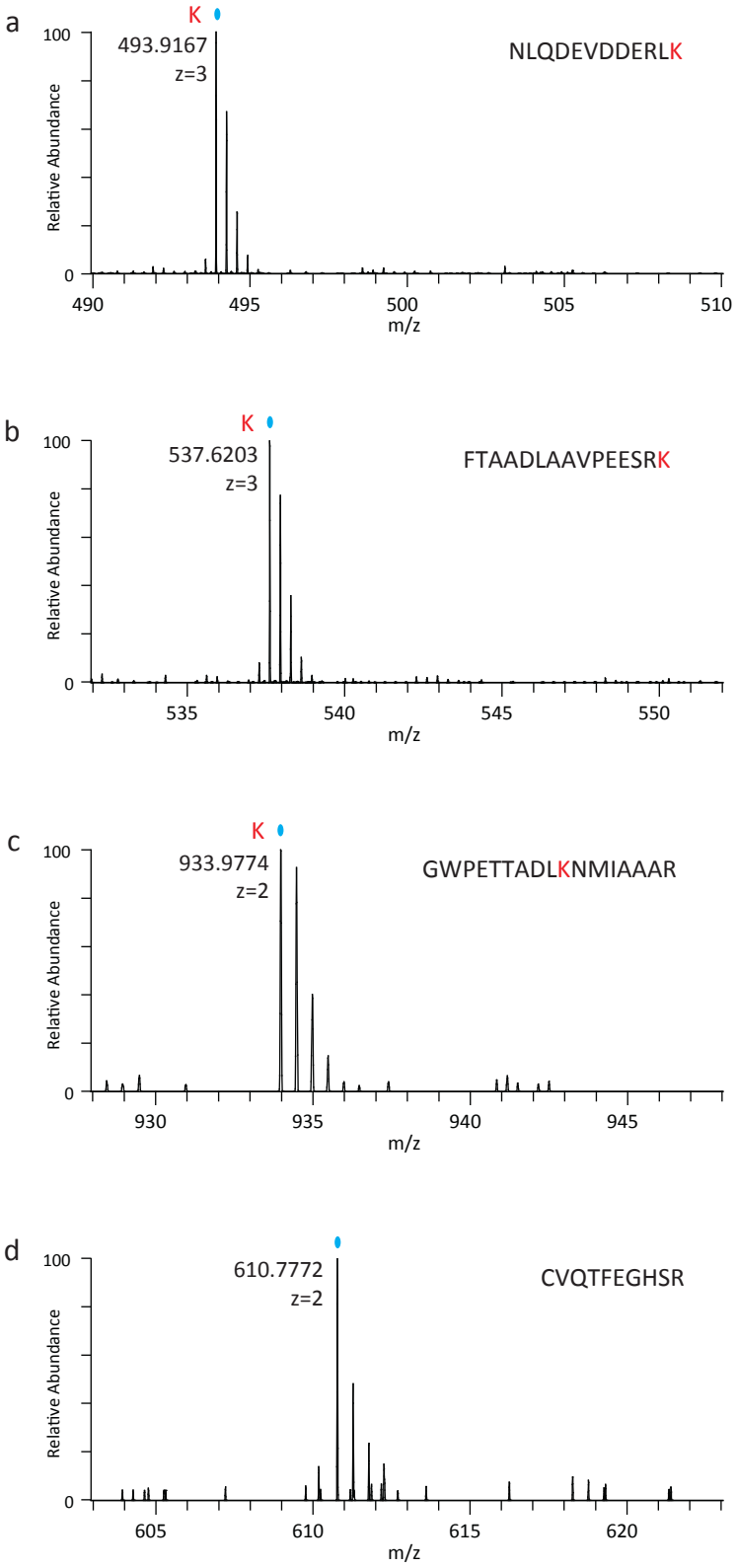
a
K
493.9167
z=3
NLQDEVDDERLK
Relative Abundance
100
0
490
495
500
505
510
m/z
b
K
537.6203
z=3
FTAADLAAVPEESRK
Relative Abundance
100
0
535
540
545
550
m/z
c
K
933.9774
z=2
GWPETTADLKNMIAAAR
Relative Abundance
100
0
930
935
940
945
m/z
d
610.7772
z=2
CVQTFEGHSR
Relative Abundance
100
0
605
610
615
620
m/z

observed. This demonstrates that only heavy labelled arginine, and no light arginine, is incorporated into proteins. However, the isotope cluster of the expected m/z of heavy arginine incorporation is not observed either. Instead, the peptide shows a complex mixture of isotope clusters, which corresponds to the incorporation of not only heavy arginine but also several other heavy-labelled amino acids. After analysis of arginine incorporation in *arg1-230* cells we concluded that arginine is fully incorporated into proteins, but is extensively converted into other amino acids.

Next, we determined the set of amino acids to which arginine is converted. To do so, spectra of peptides with different amino acid combinations and a single arginine residue were analysed (Figure 5.4). Figure 5.4A and 4B show MS spectra of peptides containing only heavy labelled arginine. In the two spectra, the observed isotope clusters have the predicted m/z of heavy arginine presence. This demonstrates that all heavy arginine is incorporated in proteins. Moreover, peptides in Figures 4A and 4B show that arginine is not converted to leucine, glycine, isoleucine, valine, serine, methionine, threonine, tyrosine, alanine, aspartic acid, asparagine and cysteine. Figure 5.4C shows a proline-containing peptide and Figure 5.4D the corresponding fragmentation spectrum. The observed isotope cluster corresponds to both heavy-labelled arginine and heavy-labelled proline. The predicted isotope cluster corresponding to light proline and heavy-labelled arginine was not observed. The fragmentation spectrum in Figure 5.4D gives further evidence for heavy labelling of proline. In Figure 5.4 D the *b* and *y* ions are marked and they have a 5 Da shift relative to what would be expected if proline were not heavy- labelled. The lack of the light proline peak demonstrates that the entire pool of cellular proline is obtained from arginine conversion in *S. pombe*. Figures 5A to 5C show that for glutamine, glutamate and lysine there are isotope clusters indicative of heavy glutamine, glutamate and lysine but also light glutamine, glutamate and lysine. The relative height of the light-labelled and heavy-labelled isotope clusters indicate that 25-30% of glutamine, glutamate and lysine are heavy-labelled.

Spectra in Figure 5D to 5F demonstrate how the complexity of the spectra increases markedly as a result of partial labelling of multiple amino acids. In the spectra the monoisotopic peaks corresponding to mixtures of heavy and light labelled amino acids are marked.

From the MS analysis we concluded that in the *arg1-230* mutant the entire cellular pool of proline is heavy labelled when grown in heavy-labelled arginine. In addition, around 25% of the glutamine, glutamate and lysine pools are heavy-labelled. This means that although

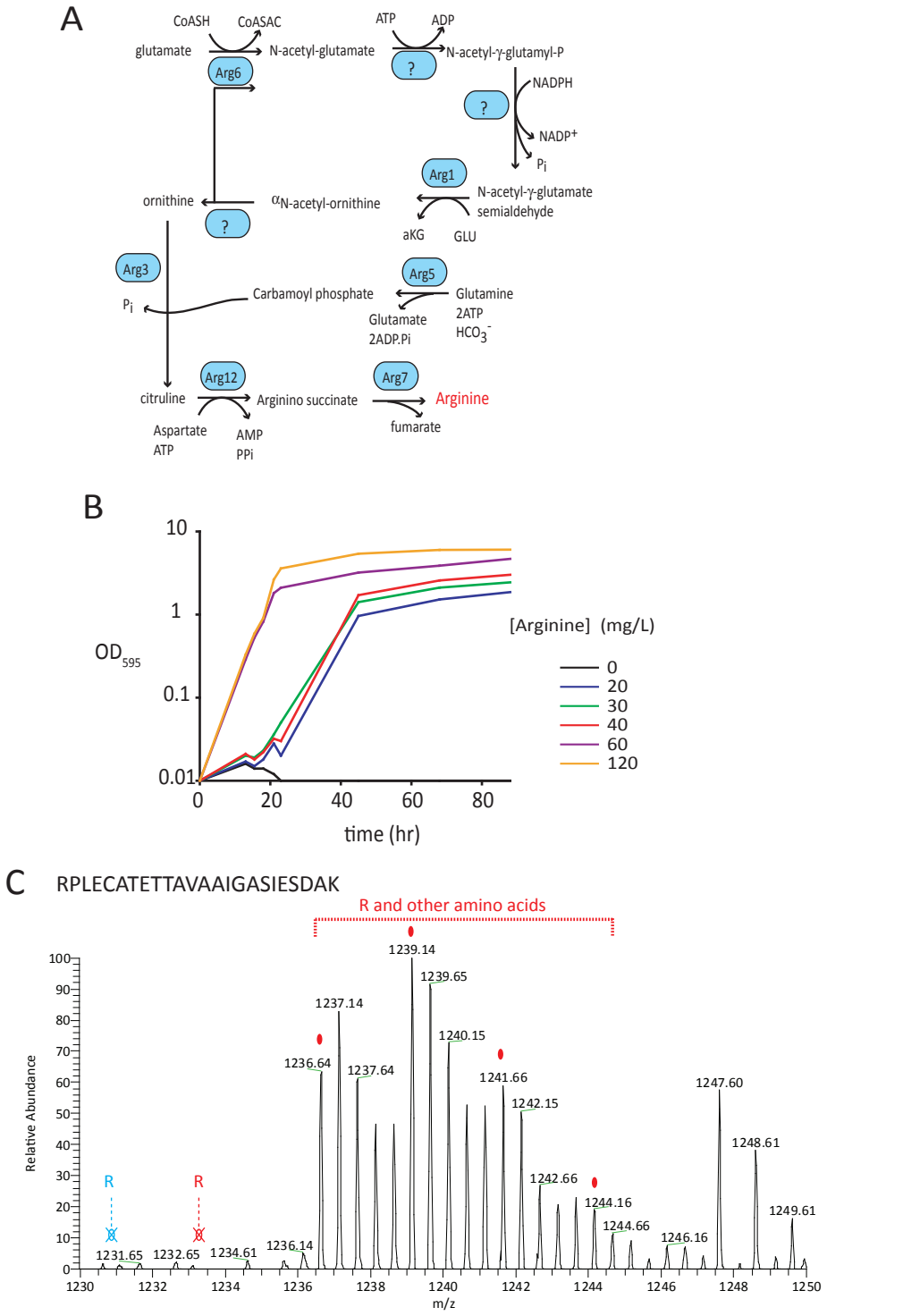

Figure 5.3- Arginine is converted into several amino acids. A) Arginine biosynthetic pathway, adapted from *S. cerevisiae*. **B) *arg1-230* growth curves.** *arg1-230* (KS3316) was grown in EMM2 medium supplemented with a range of arginine concentrations (0-120 mg/l). Cell cultures OD_{595} were measured every 3 hrs, until the cultures reached stationary phase. **C) Arginine is converted into several amino acids**. *arg1-230* mutant was grown in EMM2 with 120 mg/l $^{13}C_6$ -Arginine and 96 mM ammonium chloride. Incorporation of the heavy arginine was analyzed by MS. A representative peptide is shown as an example (Peptide sequence: RPLECATETTAVAAIGASIESDAK). Blue R is light labelled arginine and red R is heavy labelled arginine. Ovals indicate monoisotopic peaks of labelled amino acids different from arginine. Crossed ovals indicate predicted but not observed m/z ratios.

the cells can *de novo* synthesize these four amino acids, a large pool is obtained by arginine conversion. The extensive arginine conversion to amino acids other than proline has not been reported in SILAC experiments in other organisms and will be discussed below. Due to the extensive arginine conversion, the resulting MS spectra are so complex that the current analysis software is not able to interpret them easily. It would be very limiting to obtain meanful data after arginine labelling under these experimental conditions.

Because arginine conversion in *S. pombe* was found to be a large obstacle in SILAC experiments, it was necessary to develop an experimental strategy to abolish arginine conversion into other amino acids.

5.2.3. Reducing the arginine concentration does not prevent conversion

The first experimental approach to abolish arginine conversion was to reduce the supplemented arginine in the growth medium. As described previously, lowering the concentration of supplemented arginine can prevent arginine conversion in mammalian cultured cells. Therefore, the same approach was taken and the arginine concentration was reduced to six times less than initially used (20 mg/l).

Figure 5.5 shows the MS spectrum of the same peptide as in Figure 5.3C. The observed isotope clusters are the same when supplementing with 20 or 120 mg/l of arginine. Although the reduction of arginine concentration diminished the conversion it was not prevented entirely. Moreover, a low arginine concentration compromises cell growth (see growth curve in Figure 5.3A).

The observation of arginine conversion is not unexpected, as it was described in other organisms. But, contrary to what is observed in other organisms, reducing the arginine concentration does not alleviate its conversion. To perform SILAC in *S. pombe* and use arginine labelling, another strategy was necessary.

5.2.4. Prevention of arginine conversion by genetically engineering arginine catabolism

We reasoned that arginine conversion could be prevented by genetically re-engineering the arginine catabolic pathway.

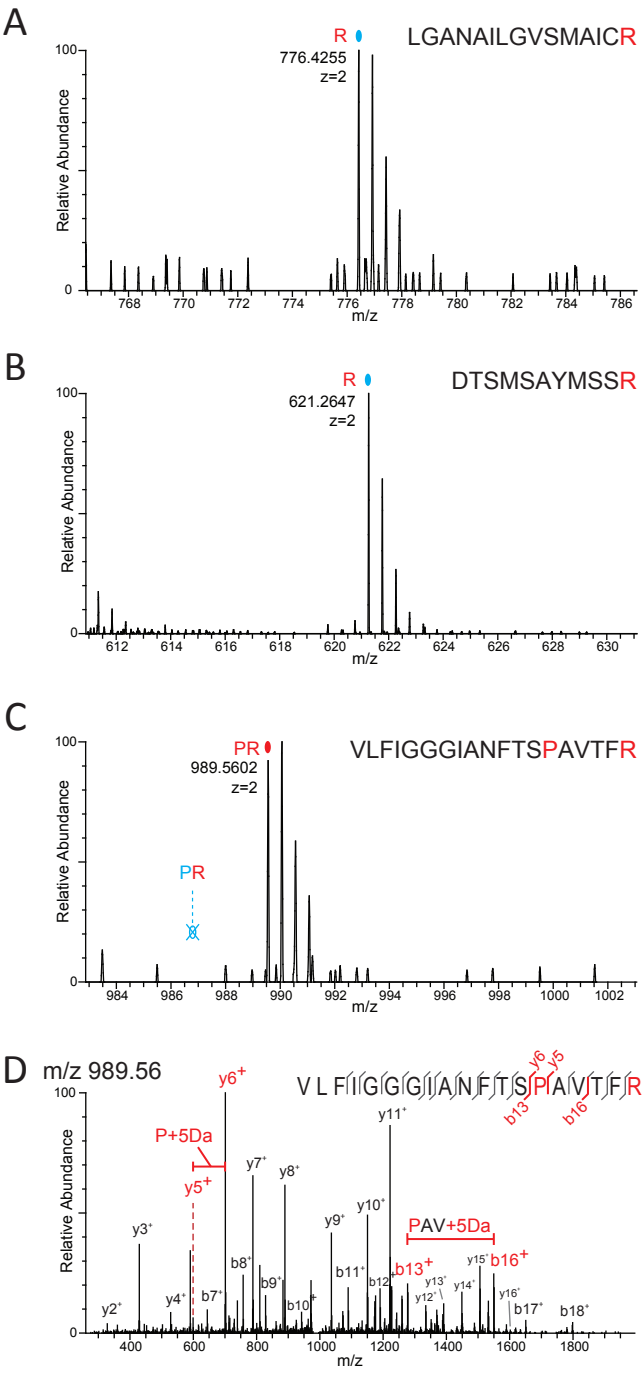

Figure 5.4- Labelled arginine is converted into proline. Mass spectrometric detection of peptides isolated from *S. pombe arg1-230* (KS3316) cells grown in 120 mg/l $^{13}C_6$-labelled arginine and 96 mM ammonium chloride. **A and B-** Peptides containing arginine as the only labelled amino acid. **C and D-** Proline-containing peptide **(C)** and its fragmentation spectrum **(D)**, showing complete labelling of proline. In the peptide sequences, red letters denote incorporation of heavy amino acids. Blue ovals indicate monoisotopic peaks of peptides in which only heavy arginine is incorporated. Red ovals indicate monoisotopic peaks of peptides version in which heavy arginine and heavy proline are incorporated. Hollow blue crossed-out oval indicates the absence of a peak containing only labelled arginine. In peak annotations, the peptide sequence was reduced to the potentially labelled amino acids; red denotes labelled amino acids, and blue denotes unlabelled amino acids.

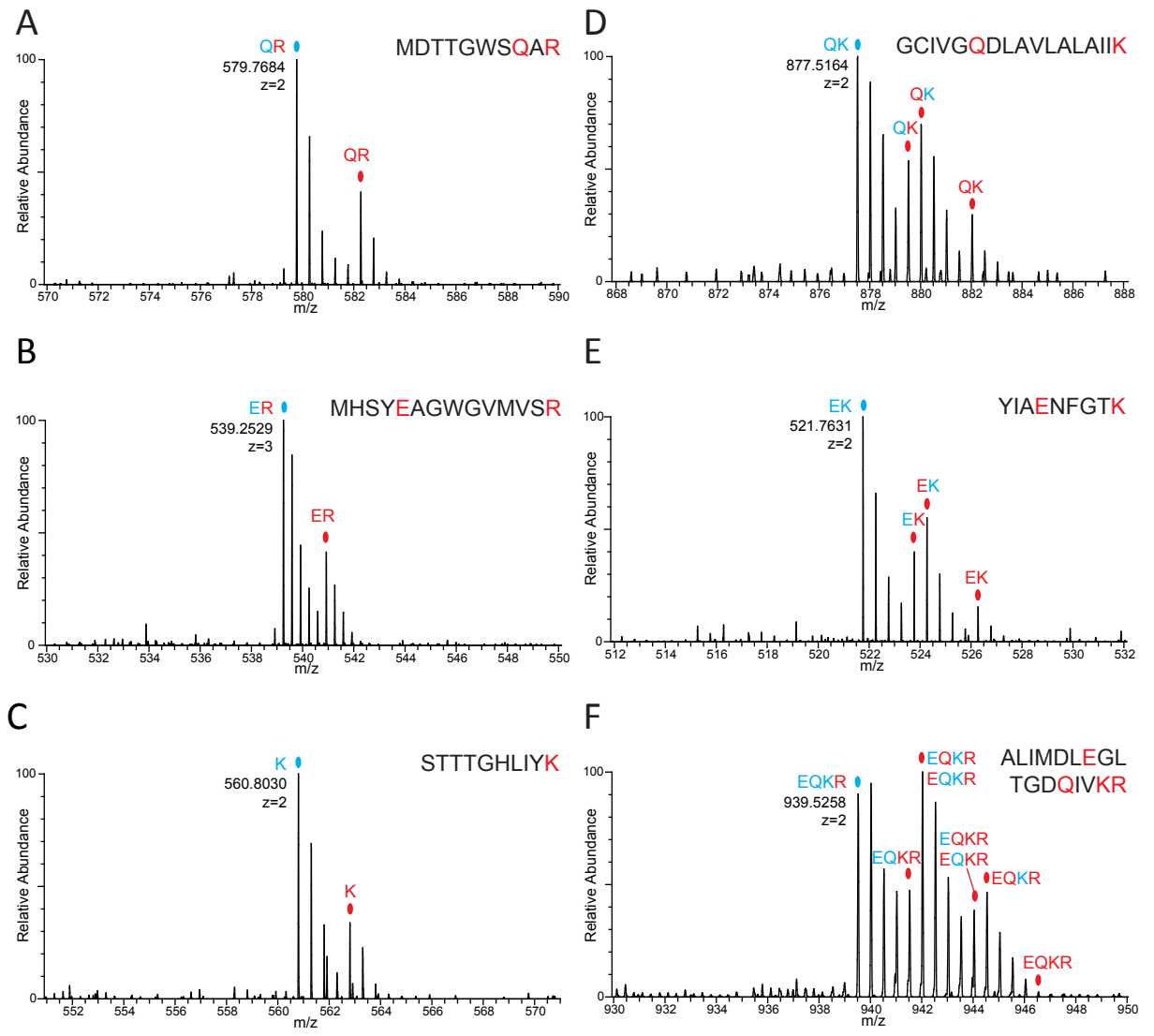

Figure 5.5- Labelled arginine is converted into glutamate, glutamine, and lysine. Mass spectrometric detection of peptides isolated from *S. pombe arg1-230* (KS3316) cells grown in 120 mg/l $^{13}C_6$-labelled arginine and 96 mM ammonium chloride. **A to C**- Peptides showing partial labelling of glutamine **(A)**, glutamate **(B)**, and lysine **(C). D to E**- Peptides showing the increasing complexity of spectra when multiple amino acids are partially labelled. In the peptide sequences, red letters denote incorporation of heavy amino acids. Blue ovals indicate monoisotopic peaks of peptides in which only heavy arginine is incorporated. Red ovals indicate monoisotopic peaks of peptides version in which heavy arginine and other heavy amino acids are incorporated. Hollow blue crossed-out oval indicates the absence of a peak containing only labelled arginine. In peak annotations, the peptide sequence was reduced to the potentially labelled amino acids; red denotes labelled amino acids, and blue denotes unlabelled amino acids.

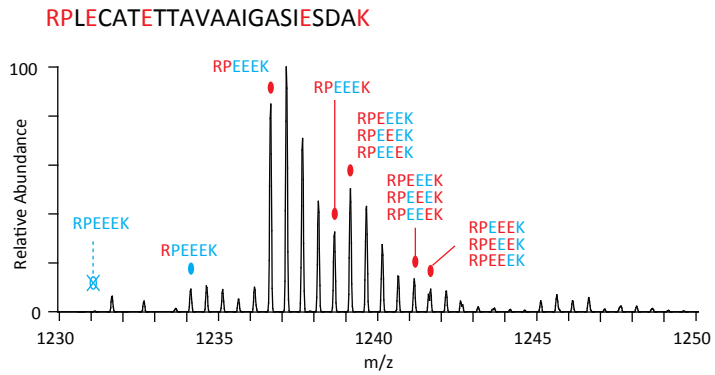

Figure 5.6- Titrating down supplemented arginine does not reduce arginine conversion. *arg1-230* (KS3316) was grown in EMM2 medium supplemented with 20 mg/l instead of 120 mg/ml $^{13}C_6$-arginine. Incorporation of heavy arginine was analyzed by MS. A representative example peptide is shown as example. Blue crossed hollow oval indicates the absence of a peak containing only heavy-labelled arginine. Blue oval corresponds to heavy arginine-labelled peptide. Red ovals correspond to labelled arginine, glutamine, glutamate and lysine monoisotopic peaks.

The catabolic pathway of arginine has not been extensively examined in *S. pombe*. However, the pathway is well studied in other organisms, such as *S. cerevisiae*. One difference is that *S. pombe* has two arginases in opposition to only one in *S. cerevisiae*. We found that the genes that encode enzymes of the arginine catabolic pathway in *S. cerevisiae* are well-conserved in *S. pombe* (Figure 5.7). This indicates that arginine catabolism in *S. pombe* is likely similar to that in *S. cerevisiae.*

We decided to genetically manipulate the arginine catabolic pathway by deleting the enzymes involved in the two first steps. Two putative arginase (CAR1 and ARU1) and one putative ornithine transaminase (CAR2) were identified in the *S. pombe* genome (Figure 5.7) (http://old.genedb.org/genedb/pombe/, {Van Huffel, 1994 #518)}.

First, I analyzed the growth rates of single deletions of each of the three genes as well as the double deletion of CAR1 and ARU1, all in *arg1-230* backgrounds. Figures 5.8 and 5.9 show the growth curves of each mutation in the presence of a range of arginine concentrations. CAR1 and ARU1 single deleted cells show robust growth when arginine is supplemented to the medium at low concentrations (Figures 5.8A and 5.8C). CAR2 single deleted cells present a lag phase similar to what was observed in *arg1-230* cells (see Figure 5.3A) and CAR1 ARU1 double deleted cells show robust growth in a wide range of arginine concentrations (Figures 5.9A and 5.9C).

Next, the mutants in arginine catabolism were examined for arginine conversion. As before, the mutant strains were grown in EMM2 medium supplemented with $^{13}C_6$-arginine and analysed by MS. Although conversion was slightly reduced in both CAR1 and ARU1 single deletions, they did not prevent arginine conversion (compare Figure 5.3C with Figures 5.8B and 5.8D). On the other hand, in *car1*Δ *aru1*Δ *arg1-230* and *car2*Δ *arg1-230* strains the same peptide has an isotope cluster containing only heavy labelled arginine (Figures 5.9B and 5.9D). Both *car2*Δ and *car1*Δ*aru1*Δ can prevent arginine conversion into other amino acids. Moreover, arginine conversion is blocked only when ARU1 and CAR1 are both deleted, indicating that the enzymes Aru1 and Car1 act redundantly in arginine conversion.

Because genetic manipulation is more easily done in a single deletion than a double deletion, *car2Δ* rather than *car1Δaru1Δ* was chosen as the strain for SILAC experiments.

The best strain to be used in SILAC experiments is *car2*Δ *lys3-37 arg1-230*. This strain fulfils all SILAC requirements: it completely incorporates arginine and lysine into proteins and blocks the conversion of arginine into other amino acids.

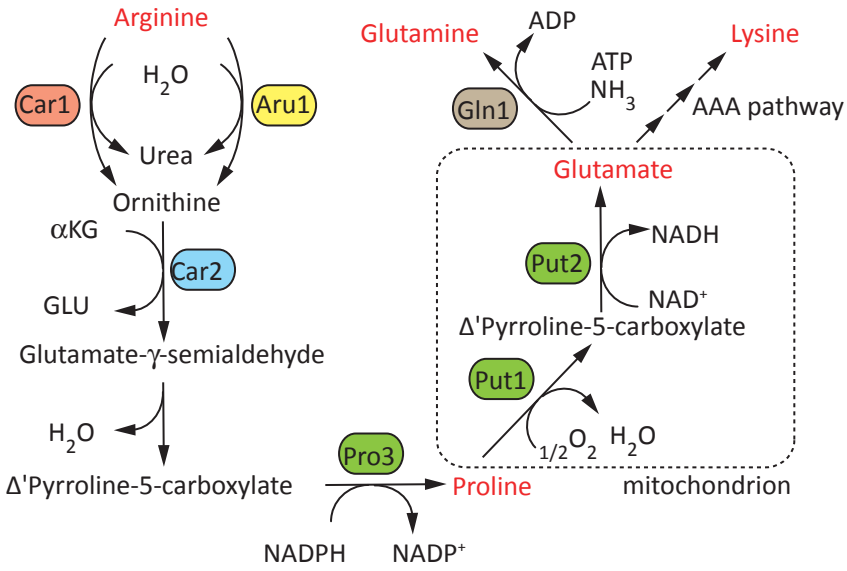

Figure 5.7- Arginine catabolic pathway adapted from *S. cerevisiae*. In *S. pombe,* the first catalytic step of arginine catabolic pathway is predicted to be catalysed by two paralogue arginases, Car1 and Aru1. The second step is predicted to be catalysed by Car2, the *S. cerevisiae* ornithine transaminase homologue. Arginine is converted to proline and proline to glutamate. Glutamine is synthetized from glutamate in a reaction catalysed by glutamine-synthase Gln1 (glutamate-ammonia ligase; EC 6.3.1.2). Lysine is synthetized from glutamate in *S. pombe* via the AAA pathway.

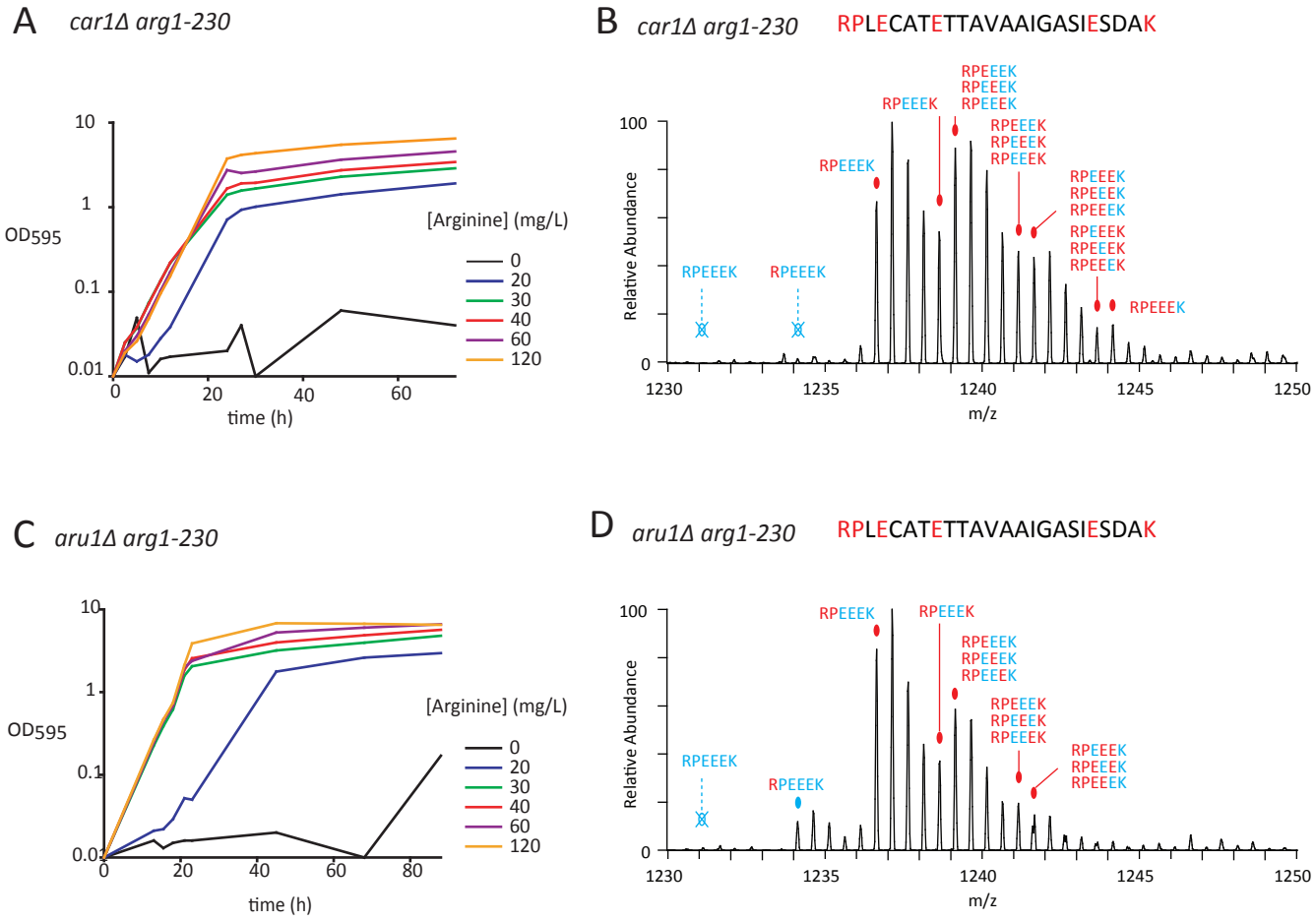

Figure 5.8- Car1 and Aru1 single deletions do not prevent arginine conversion into other amino acids. A) *car1Δ arg1-230* growth curves. *arg1-230 car1Δ* (KS4703) was grown in EMM2 medium supplemented with a range of arginine concentrations (0-120 mg/l) and with 96 mM ammonium chloride. Cell culture OD_{595} were measured every 3 hrs, until cultures reached stationary phase. **B) *car1Δ* does not prevent arginine conversion**. *car1Δ arg1-230* was grown in EMM2 medium supplemented with 120 mg/l $^{13}C_6$–arginine and incorporation of heavy arginine was analyzed by MS. Same peptide as in Figure 3C is shown as an example. **C) *aru1Δ arg1-230* growth curves.** *aru1Δ arg1-230* (KS4706) was grown in EMM2 medium supplemented with a range of arginine concentrations (0-120 mg/l) and with 96 mM ammonium chloride. Cell culture OD_{595} were measured every 3 hrs, until cultures reached stationary phase. **D) *aruΔ* does not prevent arginine conversion.** *aru1Δ arg1-230* was grown in EMM2 medium supplemented with 120 mg/l $^{13}C_6$–arginine and incorporation of heavy arginine was analyzed by MS. Same peptide as in Figure 3C is shown as an example. Spectra are labelled as follows: Blue crossed hollow oval indicates the absence of a peak containing only heavy-labelled arginine. Blue oval corresponds to heavy arginine peptide. Red oval correspond to labelled arginine, glutamine, glutamate and lysine monoisotopic peaks.

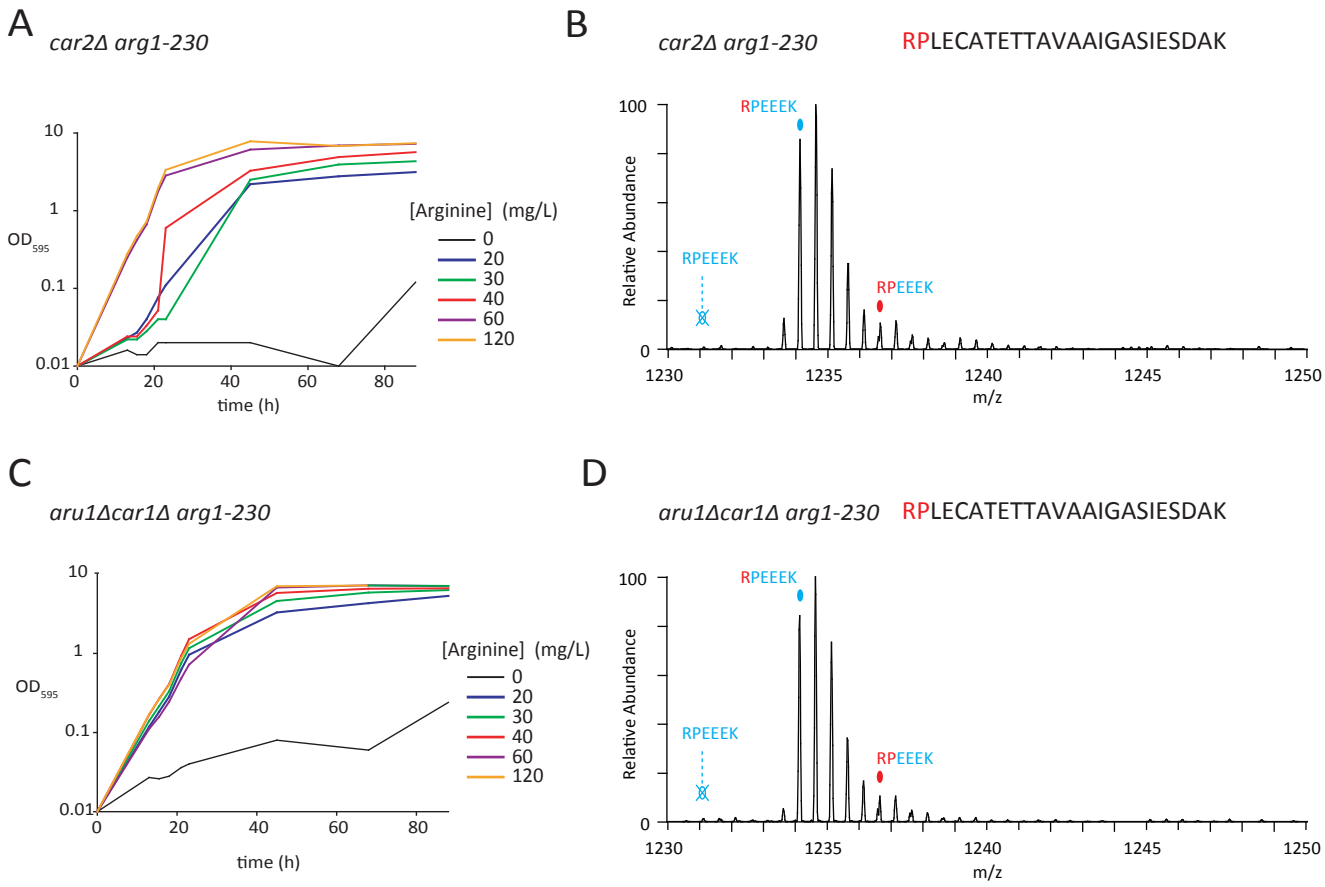

Figure 5.9- Car2 single deletion and Aru1 Car1 double deletion prevent arginine conversion. A) *car2Δ arg1-230* growth curves. *arg1-230 car2Δ* (KS4709) was grown in EMM2 medium supplemented with a range of arginine concentrations (0-120 mg/l) and with 96 mM ammonium chloride. Cell culture OD_{595} were measured every 3 hrs, until cultures reached stationary phase. **B) Car2 single deletion prevents arginine conversion**. *car2Δ arg1-230* was grown in EMM2 medium supplemented with 120 mg/l $^{13}C_6$–arginine and the incorporation of heavy arginine was analyzed by MS. The same peptide as in Figure 3C is shown as an example. **C) *aru1Δ car1Δ arg1-230* growth curves.** *aru1Δ car1Δ arg1-230* (KS4731) was grown in EMM2 medium supplemented with a range of arginine concentrations (0-120 mg/l) and with 96 mM ammonium chloride. Cell cultures OD_{595} were measured every 3 hrs, until cultures reached stationary phase. **D) Aru1 Car1 double deletion prevents arginine conversion.** *aru1Δ car1Δarg1-230* was grown in EMM2 medium supplemented with 120 mg/l $^{13}C_6$ –arginine and incorporation of heavy arginine was analyzed by MS. The same peptide as in Figure 3C is shown as an example. Spectra are labelled as follows: Blue crossed hollow oval indicates the absence of a peak containing only heavy-labelled arginine. Blue oval corresponds to heavy arginine peptide. Red oval correspond to labelled arginine and proline monoisotopic peaks.

5.2.5. Optimization of the growth medium for SILAC experiments

In order to ensure complete incorporation of heavy-labelled amino acids the cells need to grow at for least seven generations in 'heavy medium', which result in extremely diluted starting cultures. Although the *car2*Δ *lys3-37 arg1-230* mutant has a doubling time similar to wild-type cells (~3 hrs), when it is highly diluted it has an extremely long lag phase (~48 hrs, in EMM2 medium supplemented with 96 mM ammonium chloride and 40 mg/l arginine and lysine, grown at 30˚C) (Figure 5.10C). In contrast to the known doubling time, the duration of the lag phase is difficult to predict. Thus, the long lag phase makes it difficult to correctly time and monitor the cell growth. Some *S. pombe* mutants are known to have long lag phases when cultured in extremely diluted conditions. Often, the poor growth of such mutants can be restored when glutamate is used as the nitrogen source, instead of ammonium chloride (Peter Fantes, personal communication). Although glutamate is a poorer nitrogen source than ammonium chloride, it does not inhibit cell growth. However, because glutamate is involved in arginine biosynthesis and catabolism it was decided not to use glutamate as a nitrogen source, and an alternative solution was pursued.

Fantes and Creanor proposed the existence of two arginine uptake mechanisms in *S. pombe*, summarized in Figure 5.10A (Fantes and Creanor, 1984). One of the mechanisms specifically takes up basic amino acids (arginine and lysine); the other is a general amino acid permease and is inhibited by ammonium ions. In the first mechanism might occur competition between basic amino acids for the uptake (including arginine and lysine) (Figure 5.10A). In the *car2*Δ *arg1-230 lys3-37* mutant, uptake of arginine can be compromised due to inhibition of both arginine uptake mechanisms: the general uptake mechanism is inhibited by ammonium ions, and the specific mechanism is inhibited by lysine. We hypothesized that reduction of the ammonium concentration could relieve the arginine specific uptake inhibition and improve *car2*Δ *arg1-230 lys3-37* growth.

Therefore, I grew the *car2Δ arg1-230 lys3-37* mutant in the presence of decreasing amounts of ammonium chloride and also with the standard amount of glutamate (20 mM). Wild-type cells start doubling from time point zero, independently of the ammonium chloride concentration in the medium (Figure 5.9B). However, the *car2*Δ *arg1-230 lys3-37* mutant only starts doubling at time zero when in the presence of low amounts of

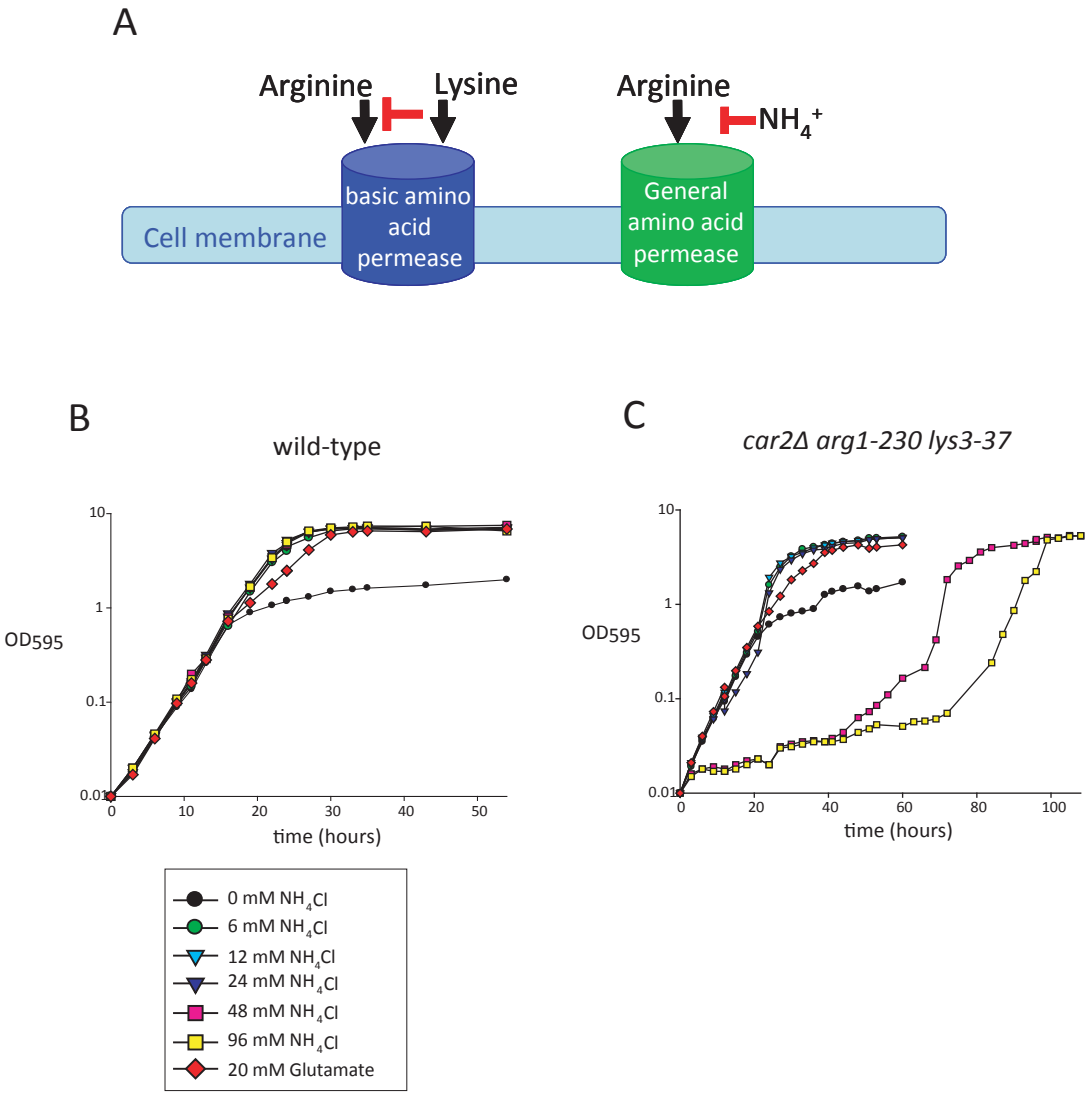

Figure 5.10- 15-fold decrease in ammonium chloride concentration is optimal for *car2Δ arg1-230 lys3-37* growth. A) Diagram of the two arginine uptake mechanisms, as proposed by Fantes and Creanor, 1984. Arginine was proposed to be taken up by two distinct mechanisms: a specific mechanism for basica amino acids; and a general mechanism, inhibited by ammonium ions. In the first mechanism, arginine and lysine compete to be taken up. **B)** Wild-type (KS2) and *car2Δ arg1-230 lys3-37* (KS5042) were grown in EMM2 medium supplemented with 40 mg/l of lysine and 40 mg/l arginine. Ammonium chloride concentrations, ranging from 0 to 96 mM, were added to cells. Cultures OD_{595} were measured every 3 hours until stationary phase.

ammonium chloride (starting from 24 mM of ammonium chloride and decreasing) (Figure 5.9C). The same effect is observed when glutamate is used as the nitrogen source.

The reduction of the ammonium concentration was enough to restore the growth of *car2*Δ *arg1-230 lys3-37* strain at time zero, demonstrating that the inhibition hypothesis was correct.

Optimal growth condition for SILAC experiments were established, achieving robust cell growth with reduced amounts of isotopically labeled amino acids. All subsequent SILAC experiments were performed with the *car2*Δ *arg1-230 lys3-37* strain grown in EMM2 medium supplemented with 40 mg/l of arginine and lysine and 6 mM of ammonium chloride.

5.2.6. Analysis of the effect of heavy isotopes on protein expression levels

Next, it was necessary to confirm that the growth of the *car2*Δ *arg1-230 lys3-37* strain in the presence of heavy amino acids did not affect protein expression levels. To evaluate if the *car2*Δ *arg1-230 lys3-37* mutant could be used for SILAC, the mutant was grown in two separate cultures, under the same experimental conditions. However, one of the cultures was grown with heavy lysine and arginine, and the other with light lysine and arginine. The two cultures were grown separately for seven generations and were combined before harvesting. Therefore, the processing of the two samples (protein extraction and MS analysis) was done after the samples were combined. The combined protein extract was prepared and separated by SDS-PAGE and stained with colloidal coomassie. A gel slice was excised and the sample was then analysed by MS, to identify the heavy/light pairs in the sample.

Figure 5.11 shows a plot with the $\log_2$ of protein ratio between heavy and light cultures at the *x*-axis, and the summed peptide intensity at the *y*-axis. In this small-scale experiment, 106 proteins were identified and quantified (Table 5.1 and Figure 5.11) demonstrating that it is possible to do SILAC in *S. pombe*. In this experiment the heavy and light cultures were grown under the same experimental conditions. Thus, the protein expression levels are not expected to change between heavy and light cultures.

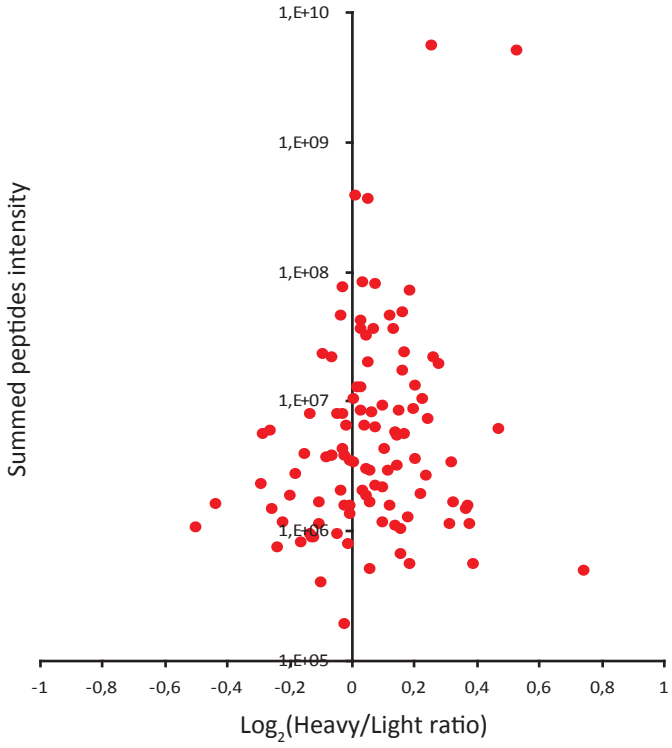

Figure 5.11- Heavy labelling does not affect protein expression levels. *car2Δ arg1-230 lys3-37* (KS5042) was grown in two separated cultures: one supplemented with 40 mg/l $^{12}C_6$-arginine and lysine; and other with $^{13}C_6$-arginine and lysine. Protein extracts were prepared, fractionated by SDS-PAGE separation and analysed by MS. Log_2 of the protein heavy/light ratio (x-axis)is plotted against the summed peptide intensity (y-axis).

5.2.7. Proof-of-principle experiment: Proteome-wide comparison between late G2 and G1/S

In order to demonstrate that the developed method has wide range applicability we decided to compare the entire proteome of cells in late G2 with cells in G1/S.

A *cdc25-22* block-and-release was used to arrest cells in late G2 and then release them into a synchronized mitosis. Cdc25 is a phosphatase and regulates Cdc2 activation by dephosphorylation on tyrosine 15. At the permissive temperature (25˚C), the growth of *cdc25-22* mutants is indistinguishable from wild-type. When the *cdc25-22* mutant is grown at the restrictive temperature (36˚), Cdc2 is not dephosphorylated and cells do not progress into mitosis (Murray and Hunt, 1993).

The SILAC experiment was performed using the *car2Δ arg1-230 lys3-37 nmt81:GFP:atb2 cdc25-22* strain. The *cdc25-22* allele was used to arrest cells in late G2 at the restrictive temperature (36˚C), followed by a shift back to 25˚C to release cells into a synchronized mitosis. The *atb2+* gene was tagged with GFP in order to visualize the mitotic spindle, and thus facilitate the scoring of the cell cycle stage during optimization of the experiment.

5.2.8. Cdc25-22 block and release optimization under SILAC growth conditions

To reliably compare protein expression levels between G2 and G1/S, the *cdc25-22* block-and-release experimental conditions were optimized. Typically, in a *cdc25-22* block-and-release 100% of the cell population is expected to be arrested at late G2, and around 70% of the population is expected to go through synchronized mitosis (Yamano et al., 1996). *cdc25-22* block-and-release is widely used to arrest cells in the late G2 phase of the cell cycle and it is mostly performed under rich medium growth conditions (YE5S). The *cdc25-22* block-and-release has never been performed using the SILAC growth conditions (i.e. EMM2 medium with low ammonium chloride and low arginine and lysine concentrations). Thus, it was necessary to find a suitable experimental design to achieve a complete arrest in late G2 and a synchronized release into mitosis. First, it was decided to test the most conventional block-and-release protocol, under SILAC conditions. Cells were grown in EMM2 supplemented with 6 mM ammonium chloride and 40 mg/l of lysine and arginine. Figure 5.12A depicts the experimental design that was used. Cells were grown asynchronously at 25˚C until they reached OD_{595} 0.2. Then the culture was shifted to 36˚C, to arrest cells in late G2. After 3 hr 40 min at 36˚C, cells were shifted back to 25˚C, to allow

synchronized progression into mitosis. Cell cycle progression after late G2 release was monitored by quantification of Cdc13/CyclinB levels, morphological analysis of the mitotic spindle and septation index. Cdc13/CyclinB is degraded at the anaphase-metaphase transition (Murray and Hunt, 1993). The mitotic spindle was visualized by expression of GFP-Atb2 and used to classify the cell cycle stage at every time point after release from late G2. Cells were stained with calcofluor to determine the septation index (All cytology analysis was performed by Dr Ken Sawin). In *S. pombe* cells, the G1/S transition and septation occur essentially at the same time. Therefore, septation index is often used to monitor the G1/S transition (Murray and Hunt, 1993). Cdc13/CyclinB expression levels were normalized against Bip1, except in the experiment in Figure 5.12B, where tubulin was used. Bip1 and tubulin expression levels are known to be constant throughout the cell cycle.

Figure 5.12C summarizes the cytological analysis of the mitotic spindle morphology, after cells were released from late G2. Under the experimental condition tested, blocked cells do not show a mitotic spindle and therefore are all arrested in late G2 (Figure 5.12C). However, the peak of cells in anaphase was very broad, meaning that the degree of synchronization was not ideal (Figure 5.12C). Figure 5.12B shows CyclinB/Cdc13 levels, after late G2 release. As cells progress into mitosis, CyclinB/ Cdc13 protein levels decrease and reach their lowest (~ 30% of initial value) at 70 min (Figures 12B and 12C). This pilot experiment showed that a higher degree of synchronization during mitosis progression was necessary.

In order to maximize the number of cells synchronized at G1/S, cells were pre-arrested in S-phase, before the G2 block. The S-phase arrest was achieved with addition of 11 mM of hydroxyurea (HU). HU is an inhibitor of ribonucleotide reductase and inhibits DNA replication, due to the lack of deoxyribonucleotides (Boddy and Russell, 1999).

The *car2Δ arg1-230 lys3-37 nmt81:GFP:atb2 cdc25-22* strain was grown as described above. When the culture reached OD_{595} 0.2, 11 mM HU was added and cells were grown for 5 hr at 25˚C. Cells were then washed once with pre-warmed EMM2 medium and shifted up to 36˚C. In order to monitor progression into mitosis after release from late G2 was monitored by CyclinB/Cdc13 protein levels, septation index and mitotic spindle morphology. Figure 5.13 shows the analysis performed in this experiment. Figure 5.13B and D show that CyclinB/Cdc13 levels decrease as cells progress into mitosis. CyclinB/Cdc13 levels are the lowest (around 20% of initial value) 90 min after the release. Figure 5.13D shows the quantification of the septation index, demonstrating that septation peak occurs

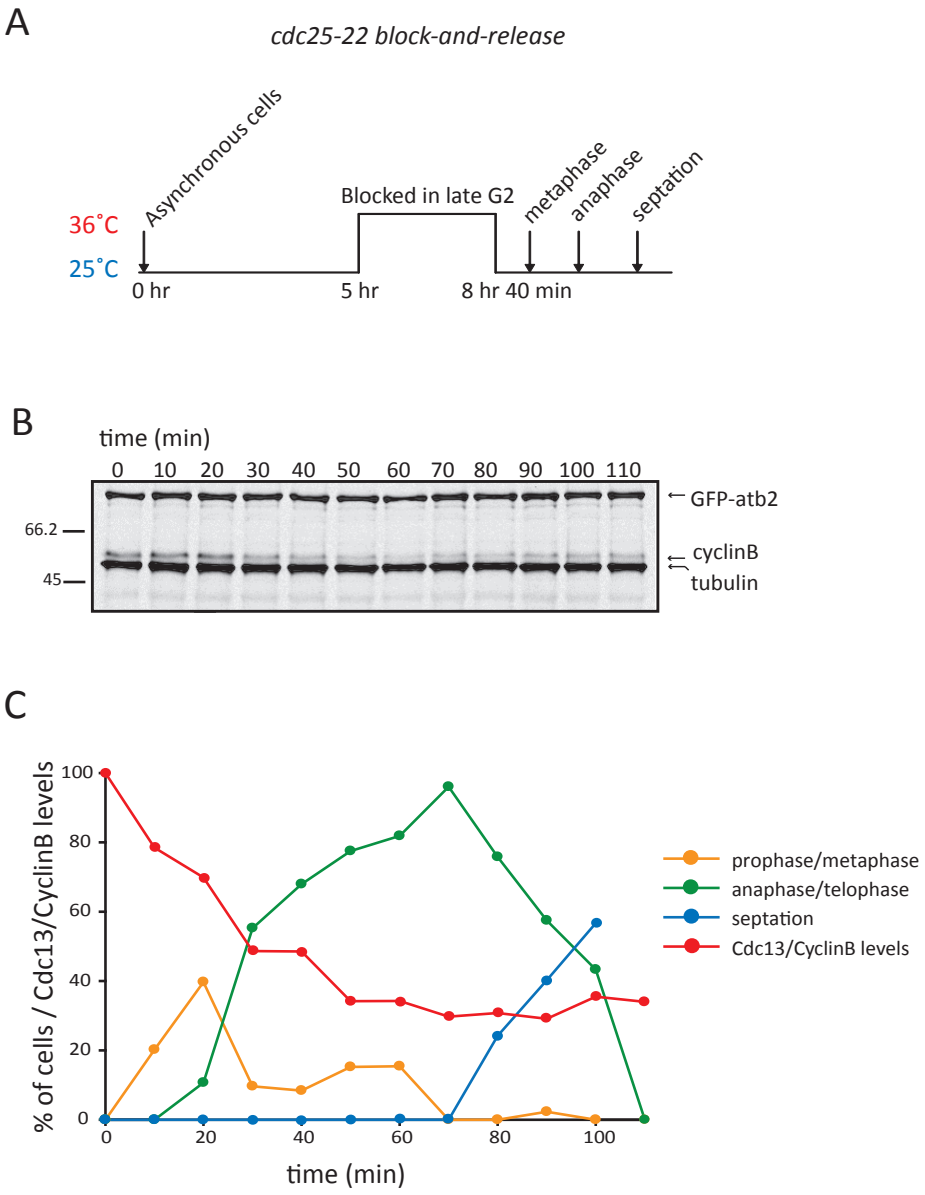

Figure 5.12-*cdc25-22* block-and-release optimization. A) Diagram of experimental design of *cdc25-22* block-and-release. **B) CyclinB levels after release from G2**. After cells (KS5344) were released from G2 block, samples were collected every 15 min. Total protein extracts were prepared and CyclinB/Cdc13 levels were analysed by immunoblotting. Tubulin was used as loading control. **C) Quantification of cell cycle stages.** Spindle morphology was used to indicate mitotic stage. Septation index was determined using calcoflour staining. CyclinB/Cdc13 expression is also shown.

at 90 min and thus coincides with the time at which CyclinB/Cdc13 levels are at a minimum. These experimental conditions result in a complete arrest of cells in late G2. Moreover, a large fraction of the population (~ 70%) undergoes synchronized septation 90 min after release from G2. The cell cycle synchrony obtained is consistent with what is obtained by others using rich medium conditions (Yamano et al., 1996).

5.2.9. Comparison of protein expression levels between late G2 with G1/S

To compare protein expression levels between late G2 and G1/S, two separate cultures of the *car2Δ arg1-230-lys3-37 cdc25-22 nmt81:GFP-atb2* strain were grown in EMM2 medium supplemented with 6 mM ammonium chloride. Cells to be blocked in late G2 were grown with 40 mg/l of $^{13}C_6$-arginine and lysine ("heavy culture"), and cells to be released into mitosis were grown with 40 mg/l of $^{12}C_6$-arginine and lysine ("light culture"). The two cultures were grown at 25˚C, until OD_{595} 0.2. Both cultures were first arrested in S-phase with 11 mM HU and then blocked in late G2 by a shift to 36˚C. The "heavy culture" was harvested at time zero (late G2 block), and the "light culture" was released into mitosis and harvested 90 min later (septation peak, previously determined).

The protein extracts of the two experimental conditions were prepared separately. After determining the protein concentration, the two samples were combined in a 1:1 ratio and were MS analysed. The Rappsilber group then carried out MS analysis of the samples.

5.2.10. SILAC can quantify changes in protein expression at the proteome level

The experiment was independently repeated three times, and in one these biological replicates the heavy/light labelling was inverted. This labelling inversion ensured that heavy labelling does not affect cell progression into mitosis. Table 5.2 summarizes the sample preparation for the four MS runs. The replicate corresponding to experiment one was analysed twice by MS, using two different fractionation methods. The replicates corresponding to experiments two and three were analysed by MS once.

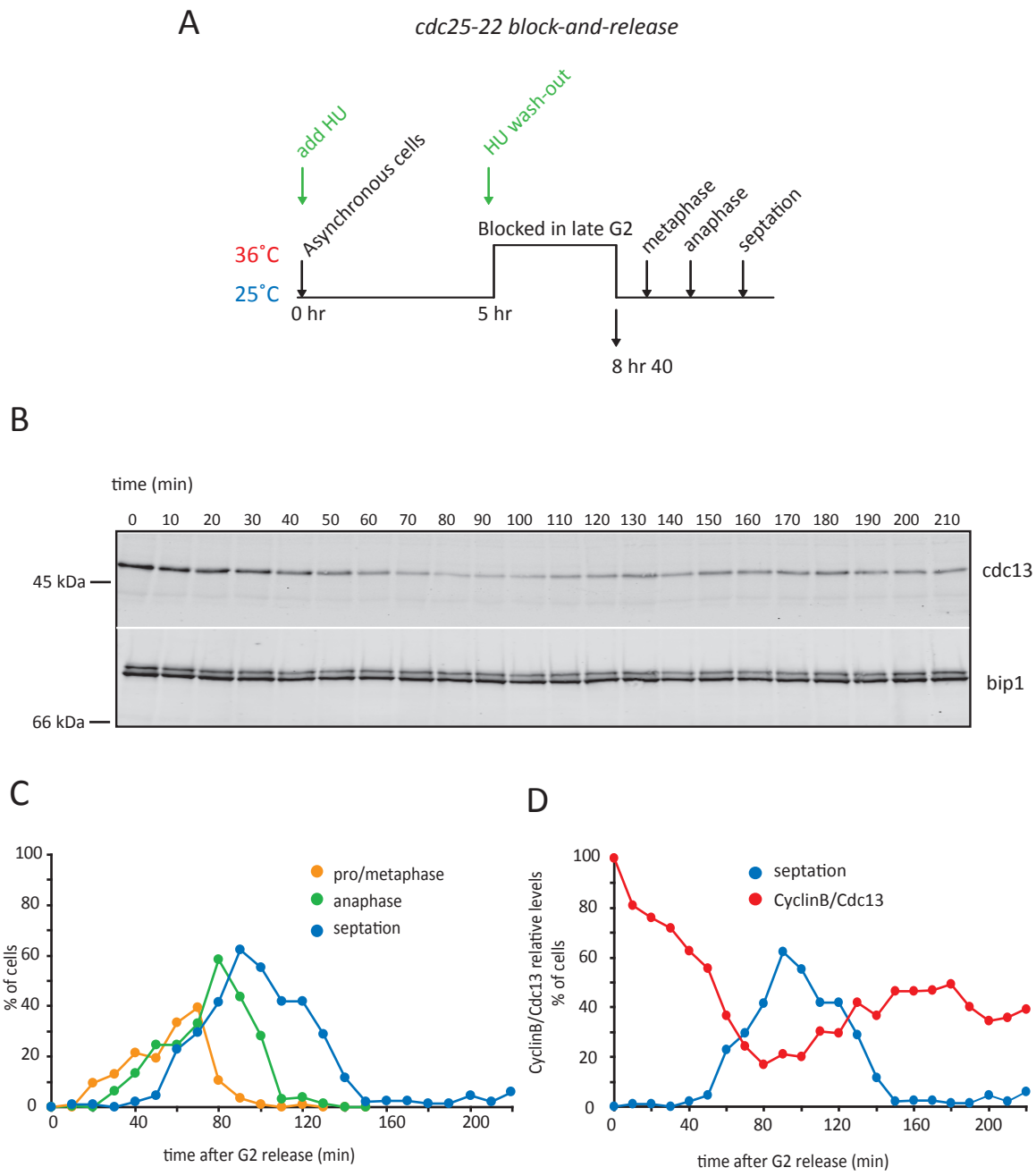

Figure 5.13- *Cdc25-22* block and release experiment. A) Diagram of experimental design of the *cdc25-22* block and release. **B) CyclinB/Cdc13 levels after release from G2.** After cells (KS5344) were released from G2 block, samples were collected every 10 min. Total protein extracts were prepared and CyclinB/Cdc13 levels were analysed by western blot. Bip1 was used as loading control. **C) Morphological analysis of cell cycle progression.** Prometaphase and anaphase/metaphase spindles were scored by GFP-Atb2 imaging. **D) Septation index and CyclinB/Cdc13 levels.** Septation index was determined by imaging the septum after calcoflour staining. CyclinB/Cdc13 levels were determined by immunoblotting.

Table 5.2- Summary of sample preparation for different MS runs.

Sample	G2	G1/S	Fractionation	Biological replicate?
1	Heavy	Light	SCX[1]	Yes
2	Light	Heavy	SCX[1]	Yes
3	Heavy	Light	OFFGEL[2]	Yes
4	Heavy	Light	OFFGEL[2]	No, same as Sample 1

[1] SCX- Strong Cation Exchange
[2] OFFGEL- pI based fractionation from Agilent Technologies

The data from the SILAC experiments was analysed using the MaxQuant software (Cox and Mann, 2008). This software allows quantification of heavy/light pairs, based on protein identification using MASCOT software. In addition, MaxQuant performs statistical analysis on the quantified proteins, in order to identify the ones with a significant variation between compared samples.

Proteins identified in the four MS runs were pooled and ~73% (Table 5.3 in Appendix DVD_01) of the predicted *S. pombe* proteome was identified (3659 proteins identified out of 5027 predicted) (http://old.genedb.org/genedb/pombe/). The group of identified proteins was then filtered to select the proteins quantified in at least two biological replicates. Thus, the expression levels between late G2 and G1/S were quantified in 2964 out of 3659 identified proteins. The plot in Figure 5.14A represents the Log_2 of the ratio between G1/S and late G2 of the proteins quantified with high confidence (Table 5.4). In the plot of Figure 5.14A, proteins are coloured according to the *p* value of their significanceB. SignificanceB is a statistical parameter calculated by MaxQuant, and describes how much a given ratio is significantly different from the distribution of all ratios. To calculate significanceB proteins are binned into groups of different intensities because proteins with higher intensity can be measured with higher accuracy then proteins with lower intensity (Cox and Mann, 2008).

The majority (95%) of the proteins quantified do not change between late G2 and G1/S. However, 65 proteins were quantified as downregulated (left part of plot) and 94 proteins were up-regulated (right part of plot), between late G2 and G1/S.

As expected, the positive control, Cdc13, was identified as being degraded. The majority of the identified downregulated proteins are not experimentally characterized (~70%) (http://old.genedb.org/genedb/pombe/). From the proteins with experimentally characterized functions, none, except Cdc13, is described in the literature as cell cycle

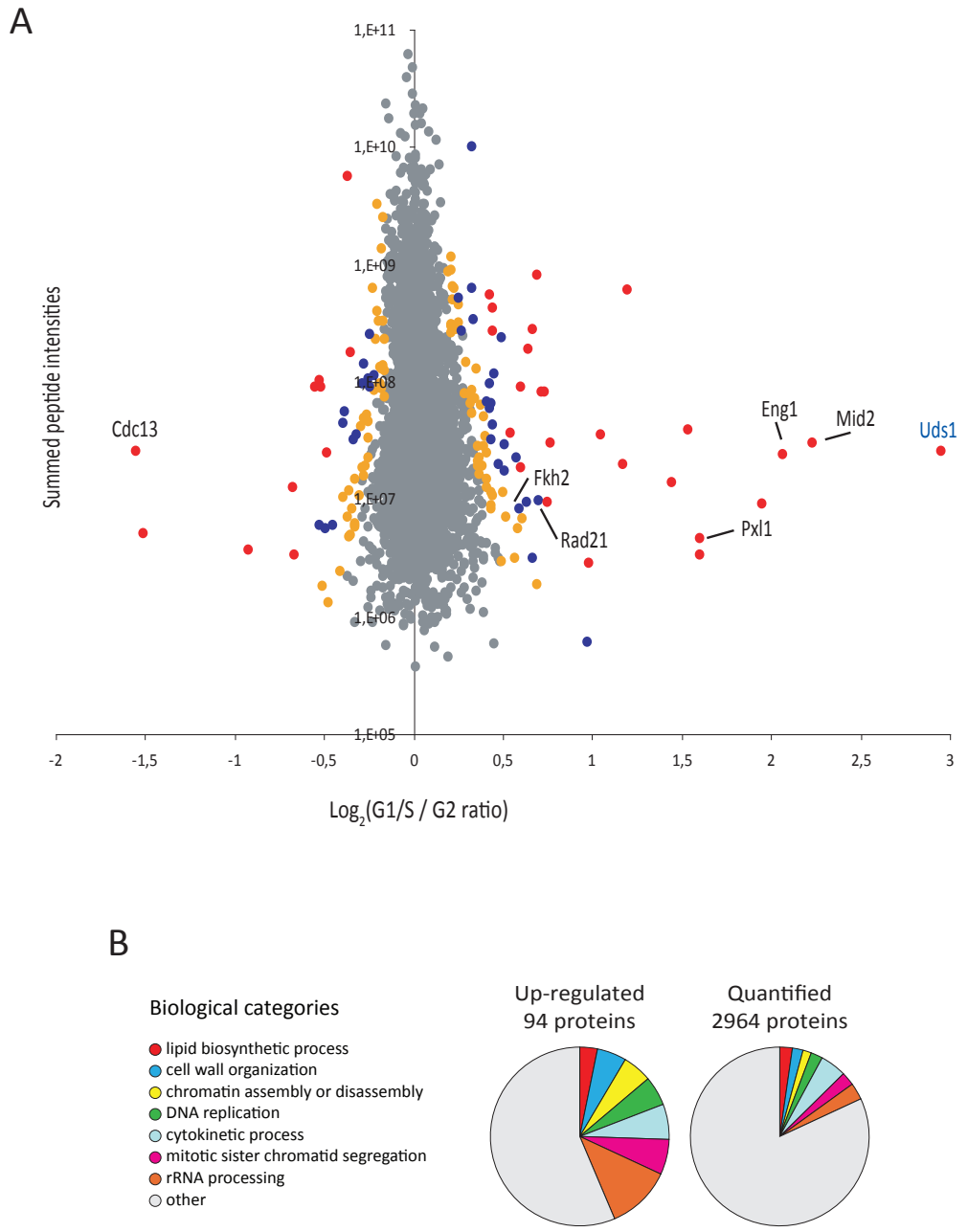

Figure 5.14- SILAC can quantify changes in protein levels between late G2 and G1/S. A) Plot of Log_2 of the protein ratio between late G1/S and G2 vs. the sum of the peptide intensities for 2965 proteins. Each quantified protein is represented by a dot. Proteins coloured in grey do not significantly vary between late G2 and G1/S. Proteins coloured in grey have a significance (B) $>10^{-2}$; orange, 10^{-3} < Significance(B) < 10^{-2}; blue, 10^{-5} < Significance(B) < 10^{-3}; red, Significance(B) < 10^{-5}. Proteins previously described in the literature as being cell cycle-regulated are labelled. 65 proteins are significantly degraded and 94 are significantly up-regulated between late G2 and G1/S. **B) Distribution of up-regulated proteins in different biological categories.** GO terms were assigned to each up-regulated protein. Proteins were grouped according to their biological category. Each biological category was compared with the 2964 quantified proteins.

regulated. The most abundant biological function among the degraded proteins is cellular stress response, represented by ~ 30% of the characterized and uncharacterized proteins.

Around 60% of the 94 up-regulated proteins are not experimentally characterized (http://old.genedb.org/genedb/pombe/). Among the 94 up-regulated proteins we identified five proteins already experimentally characterized as cell cycle regulated (Figure 5.14A, labelled in the plot). The identification of proteins known to be cell cycle-regulated confirms that this SILAC method is able to quantify changes in protein expression levels.

To get a better understanding of the up-regulated proteins, they were classified according to the biological process in which they are involved. The classification was done by assigning a biological process GO term (http://www.geneontology.org/) to each up-regulated protein. For each up-regulated protein the highest GO term in the hierarchy was chosen. Figure 5.14B shows the pie chart with the GO terms distribution of the 94 up-regulated proteins in G1/S compared to representation of the 2964 quantitated proteins. When compared, the up-regulated proteins show increased representation in cellular processes occurring at the G1/S phase, such as DNA replication (e.g. Fkh2), cytokinesis (e.g. Mid2) and cell wall organization (e.g. Eng1) (Figure 5.14B).

The proof-of-principle experiment shows that the developed method can quantify changes at the proteome level in *S. pombe*. In addition, we identified some new candidate proteins that may be cell cycle regulated.

5.2.11. Study of a novel protein up-regulated during septation

To confirm that the method developed can indeed identify new cell cycle regulated proteins, a previously uncharacterized protein was studied. In the SILAC experiment, SPBC27.04 was identified and quantified as the top up-regulated protein during septation. SPBC27.04 is a *S. pombe* orphan sequence which was previously uncharacterized (http://old.genedb.org/genedb/pombe/). SPBC27.04 was named Uds1, 'Up-regulated During Septation'.

Uds1 was tagged with GFP to analyse its localization and its expression levels during the cell cycle. Figure 5.15A shows time-lapse video-microscopy of a cell expressing Uds1-GFP. At time zero no Uds1-GFP is observable in the cell. As the cell undergoes mitosis, Uds1-GFP starts accumulating at the septation site. Once the two daughter cells are separated, Uds1-

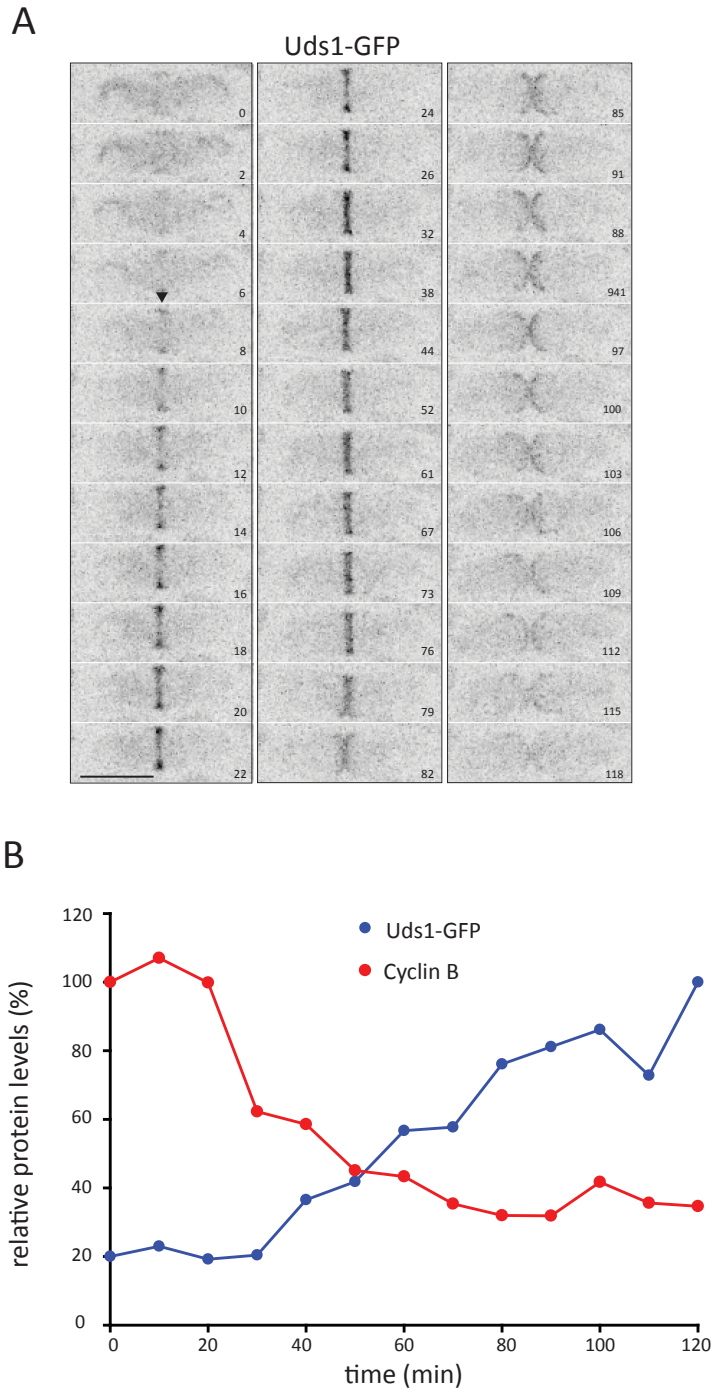

Figure 5.15- Uds1 protein expression is cell cycle-regulated. A) Uds1-GFP accumulates at the septation site. Uds1-GFP (KS5566) was imaged for 118min in a cell undergoing mitosis. The protein is not observed in interphase cells and accumulates at the cell middle (black arrow head) when cells undergo septation. **B) Uds1-GFP expression levels increases from G2 to septation**. Uds1-GFP (KS5570) expression levels during mitosis was determined in a *cdc25-22* block and release experiment. Uds1 expression levels are lowest in late G2, increasing to a peak in septation.

GFP diffuses away from the septation site. Uds1-GFP localization during septation indicates that protein expression is cell-cycle regulated.

To analyse Uds1 expression levels during the cell cycle, cells expressing Uds1-GFP were blocked in late G2 and released in mitosis using a *cdc25-22* block-and-release. Figure 5.15B shows Uds1-GFP expression levels after release from late G2,using Bip1 as a loading control (data not shown). The levels of Uds1-GFP increase from late G2 until septation, where they peak at 90 min.

These results show that Uds1 is a cell cycle-regulated protein. It localizes at the septum and its expression increases as cells progress into mitosis and peaks during septation.

5.3. Discussion

Because the current SILAC methodologies presented some limitations, such as arginine conversion into other amino acids, we decided to develop a new method to perform robust SILAC in *S. pombe*.

We have shown that in *S. pombe,* arginine is converted to proline, glutamine, glutamate and lysine. In contrast to *D. melonogaster*, mammalian cultured cells and *S. cerevisiae,* in which the conversion of arginine to proline is only partial, the conversion of arginine to proline in *S. pombe* is complete. It has also been found that, in *S. pombe*, around 25% of glutamine, glutamate and lysine pools are obtained from arginine conversion. These amino acid conversions have never been observed in SILAC experiments using other organisms. However, analysis of the biosynthetic pathways of glutamine, glutamate and lysine demonstrate (shown in Figure 5.6) that they can be obtained from arginine conversion (http://old.genedb.org/genedb/pombe/). Whereas the conversion of arginine to lysine is expected in *S. pombe,* it is not expected in mammalian cells. The conversion of arginine to lysine in *S. pombe* is due to the enzymes of the AAA pathway (α-aminoadipate), which are not found in mammals (Xu et al., 2006).

The differences observed in arginine conversion between mammalian cells and *S. pombe* can be attributed to differences in the organisms' physiology. In mammals, arginine synthesis is tissue-specific; while some tissues synthesize and catabolise arginine, others only catabolise (Flynn et al., 2002). Therefore, arginine is limited in some tissues and abundant in others. When the availability of arginine is limited, it is expected to become incorporated into proteins, rather than being degraded into metabolites, such as glutamine

or glutamate (Flynn et al., 2002). Therefore, in mammalian cells, proline, glutamate, glutamine and lysine may be exclusively obtained from diet or growth media, but not from arginine conversion.

In this study, the conversion of arginine to other amino acids has been prevented by genetically re-engineering the arginine catabolism. The double deletion of CAR1 and ARU1 or the single CAR2 deletion completely abolished arginine conversion to other amino acids.

Interestingly, while optimizing the growth conditions for the SILAC strain it was demonstrated that the arginine uptake is most probably inhibited by lysine and ammonium ions. Based on the work of Fantes and Creanor it was hypothesized that arginine uptake via the basic amino acid mechanism was inhibited by lysine, and arginine uptake via the general amino acid uptake mechanism was inhibited by ammonium ions. The reduction of the concentration of ammonium chloride to 15 times less prevented arginine uptake inhibition and restored robust cell growth.

As proof-of-principle of the developed method we decided to perform a proteome-wide comparison. Therefore, we compared the expression levels of the entire proteome between the late G2 phase and the G1/S transition of the cell cycle, using a *cdc25-22* block-and-release. It was expected that the proteins identified in this experiment would show the same degradation kinetics as Cdc13. There are few *S. pombe* proteins described in the literature as being degraded from late G2 to G1/S transition. However, some expected candidates, such as the APC activator, Slp1 or the securin Cut2, were not identified in this dataset. Both Slp1 and Cut2 are expressed in very low abundance, and identification by MS is biased towards high abundance proteins. Moreover, the expression of some proteins could be out-of-phase with the analysed cell cycle stages (late G2 and G1/S transition). In order to have a complete dataset of all proteins that are degraded during mitotic progression, the identification by MS needs to be improved either with more sensitive equipment or with different fractionation methods (de Godoy et al., 2008). In addition, the analysis of degraded proteins during mitosis will only be comprehensive once all phases of the cell cycle are analysed.

Among the 94 up-regulated proteins, five have been shown by others to be periodically expressed: Fkh2, which is involved in DNA replication (Buck et al., 2004); Eng1 and Mid2, which participate in cell separation (Martin-Cuadrado et al., 2003; Tasto et al., 2003); Pxl1, which is involved in cell wall synthesis (Pinar et al., 2008); and Rad21, one of the subunits of

the cohesin complex (Birkenbihl and Subramani, 1995). When compared with the entire *S. pombe* proteome, the up-regulated proteins in our data set are enriched in GO terms of biological processes associated with the G1/S transition. Previously uncharacterized proteins assigned with enriched GO terms are good candidates to be periodically expressed during cell the cycle.

Finally, a new cell cycle regulated protein is described in this chapter. Uds1 was a previously uncharacterized protein. Here, it was shown that Uds1 localizes at the septum and its expression levels are cell cycle regulated. The timing of Uds1 localization suggests that it may play a role in cell separation, but not in the assembly of the septum. However, further characterization is necessary to determine the exact timing of Uds1 appearance at the septum.

In summary, we found that performing SILAC in *S. pombe* could be challenging because arginine is converted to proline, glutamine, glutamate and lysine. However, arginine conversion can be prevented by genetically re-engineering the arginine catabolism pathway. Finally, the usefulness of the robust SILAC method developed was proved by a large-scale quantitative analysis of the protein expression levels between the late G2 phase of the cell cycle and the G1/S transition.

Chapter VI: Analysis of Tea1 and Tea3 binding to Mod5

6.1. Introduction

It has been shown that both Tea1 and Mod5 interact with a third cell tip-localized protein, Tea3 (Snaith et al., 2005). The localization of Tea1 and Mod5 at the cell tip is Tea3-dependent, but is not as extreme as in *mod5Δ* and *tea1Δ*, respectively. In *tea3Δ* mutants, Mod5 localization at the cell tip is more spread out than in wild-type cells (Snaith and Sawin, 2003). Tea1, on the other hand, localizes to the cell tip in a *tea3Δ* background. However, the amount of Tea1 at the cell tip is reduced, and upon MBC treatment Tea1 is lost from the non-growing cell tip more rapidly than in wild-type cells (Snaith et al., 2005). Consistently, Tea3 localization is also Tea1 and Mod5-dependent. In *tea1Δ* mutants, Tea3 localizes as foci around the entire cell membrane, because it binds to delocalized-Mod5. In *mod5Δ* mutants, Tea3 no longer accumulates at the cell tip and instead localizes to microtubule plus-ends and is co-transported with Tea1 towards the cell tip (Snaith and Sawin, 2005).

It has been previously shown that Tea1, Tea3 and Mod5 physically interact in a pair-wise fashion, with each pair independent of the third protein (Snaith et al., 2005). This has made it difficult to dissect the individual contribution of each protein to cell polarity. Moreover, Tea1 and Tea3 were shown directly to bind the same 100 aa region of Mod5 (aa 156 to aa 256) (Snaith et al., 2005). These observations raised the question of how the interaction of the three proteins at the cell tip is structurally and stoichiometrically organized. From the data available, two possible scenarios can be suggested: either Tea1, Tea3 and Mod5 could simultaneously interact to form a three-way complex, or Tea1 and Tea3 could compete for binding to Mod5. However, based in the current knowledge these two scenarios cannot be distinguished.

In this chapter I will describe the dissection of Tea1 and Tea3 binding sites to Mod5, using a mutagenic approach. Moreover, I will describe the study of the contribution of Tea3 in the establishment and maintenance of *S. pombe* cell polarity.

6.2. Results

6.2.1. Construction of the mod5-mutants

The region between amino acids 156 and 256 of Mod5 has been identified as the binding site of both Tea1 and Tea3 (Snaith et al., 2005). In order to determine if the binding site of Tea1 and Tea3 could be separated, I constructed a series of mutants within this region. Dr Hilary Snaith performed the experimental design and the initial cloning of the *mod5 mutants*. The 100 amino acids spanning aa 156 to aa 256 were sequentially deleted and substituted by a random linker sequence (*Ala-Gly-Ser-Ala-Gly*), creating a total of twenty *mod5-mutants*. For simplicity, the *mod5-mutants* were named *mod5-156* to *mod5-251*. For example, in *mod5-156* amino acids 156 to 160 are substituted; in *mod5-161* amino acids 161 to 165 are substituted, and so on. The mutant *mod5-171* (aa 171 to aa 175 substituted) could not to be constructed and thus this mutant was not analyzed. In this chapter nineteen *mod5-mutants* are described.

mod5-mutants were expressed under the Mod5 endogenous promoter. These strains also had Tea1 and Tea3 tagged with tdTomato and GFP, respectively, under their endogenous promoters. Because the localizations of Tea1 and Tea3 in *mod5Δ* are easily distinguishable from wild-type (see this chapter introduction for details), the localization and dynamics of Tea1 and Tea3 were planned to be used as reporters of the interaction of Tea1 and Tea3 with the Mod5-mutant proteins. If interaction occurs between *mod5-mutants* and Tea1/Tea3, Tea1/Tea3 would be expected to localize as in wild-type cells. In the absence of interaction, Tea1/Tea3 would be expected to localize as in *mod5Δ*.

6.2.2. Localization screen of Tea1-tdTomato in the mod5-mutants

First, I examined the localization of Tea1-tdTomato in the nineteen *mod5-mutants* as well as in wild-type and *mod5Δ*. The localization of Tea1-tdTomato in each *mod5-mutant* was classified either as wild-type-like or as *mod5Δ*-like by comparison with its localization in wild-type and *mod5Δ* cells (Figure 6.1, row A). In mutants *mod5-156* to *mod5-191* and *mod5-231* to *mod5-251* (Figure 6.1, rows B and D), Tea1-tdTomato localization is mostly wild-type-like. This means that Tea1-tdTomato accumulates in a crescent at the cell tip, and

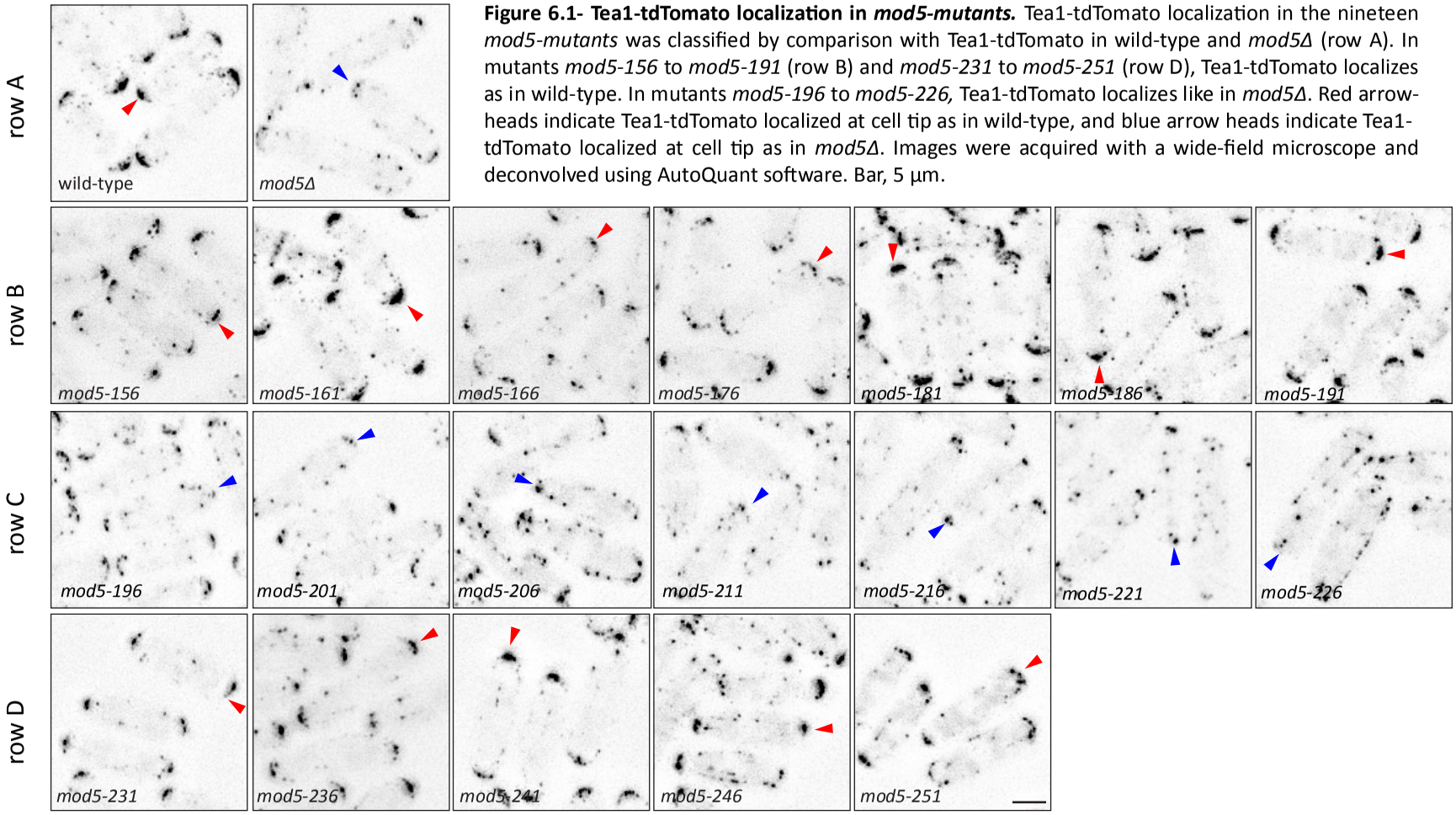

Figure 6.1- Tea1-tdTomato localization in *mod5-mutants.* Tea1-tdTomato localization in the nineteen *mod5-mutants* was classified by comparison with Tea1-tdTomato in wild-type and *mod5Δ* (row A). In mutants *mod5-156* to *mod5-191* (row B) and *mod5-231* to *mod5-251* (row D), Tea1-tdTomato localizes as in wild-type. In mutants *mod5-196* to *mod5-226,* Tea1-tdTomato localizes like in *mod5Δ*. Red arrow-heads indicate Tea1-tdTomato localized at cell tip as in wild-type, and blue arrow heads indicate Tea1-tdTomato localized at cell tip as in *mod5Δ*. Images were acquired with a wide-field microscope and deconvolved using AutoQuant software. Bar, 5 µm.

is transported on microtubules plus-ends to the cell tips. In *mod5-196* to *mod5-226* mutants (Figure 6.1, row C), Tea1-tdTomato localization is *mod5Δ*-like. In these *mod5-mutants* Tea1 does not accumulate at the cell tip and is present in higher amounts at the microtubules plus-ends.

From the analysis of Tea1-tdTomato localization, the region encompassing aa 196 to aa 230 was determined as necessary for Tea1 tip-localization, and interpreted as being necessary for Tea1-Mod5 interaction.

6.2.3. Localization screen of Tea3-GFP in the mod5-mutants

The same screening approach as above was also used to examine Tea3 localization at the cell tip in the *mod5-mutants*. Figure 6.2 shows Tea3-GFP localization in the nineteen *mod5-mutants* (rows B to D) as well as in wild-type and in *mod5Δ* (row A). In mutants *mod5-156* to *mod5-191* (row B) and mutants *mod5-231* to *mod5-251* (row D), Tea3-GFP localizes as in wild-type (row A), and is only present at the cell tip. In the mutants *mod5-196* to *mod5-226* (row c), Tea3-GFP localizes as in *mod5Δ* (row A), that is, Tea3 does not accumulate at the cell tip and localizes in cytoplasmic dots that co-localize with Tea1 (Snaith et al., 2005).

After screening for Tea1-tdTomato and Tea3-GFP localization in the nineteen *mod5-mutants*, the putative interacting-region of Tea1 and Tea3 in Mod5 was narrowed down to 35 amino acids, from aa 196 to aa 230. Tea1 and Tea3 interacting-regions in Mod5 appear to overlap, meaning that most probably Tea1, Tea3 and Mod5 do not bind in a ternary complex formed with one copy of each protein. This result either suggests that Tea1 and Tea3 may compete in binding to Mod5 or that although Mod5, Tea1 and Tea3 can bind simultaneously they do not form a 1:1:1 complex.

6.2.4. Mutants mod5-196 to mod5-226 as well as mutants mod5-231 to mod5-251 present defects in cell polarity establishment

Next, the *mod5-mutants* were analyzed using an assay for cell morphology defects (Sawin and Snaith, 2004; Snaith and Sawin, 2003), in order to examine how Tea1 and Tea3 localization in the *mod5-mutants* was correlated with the establishment of cell polarity. In

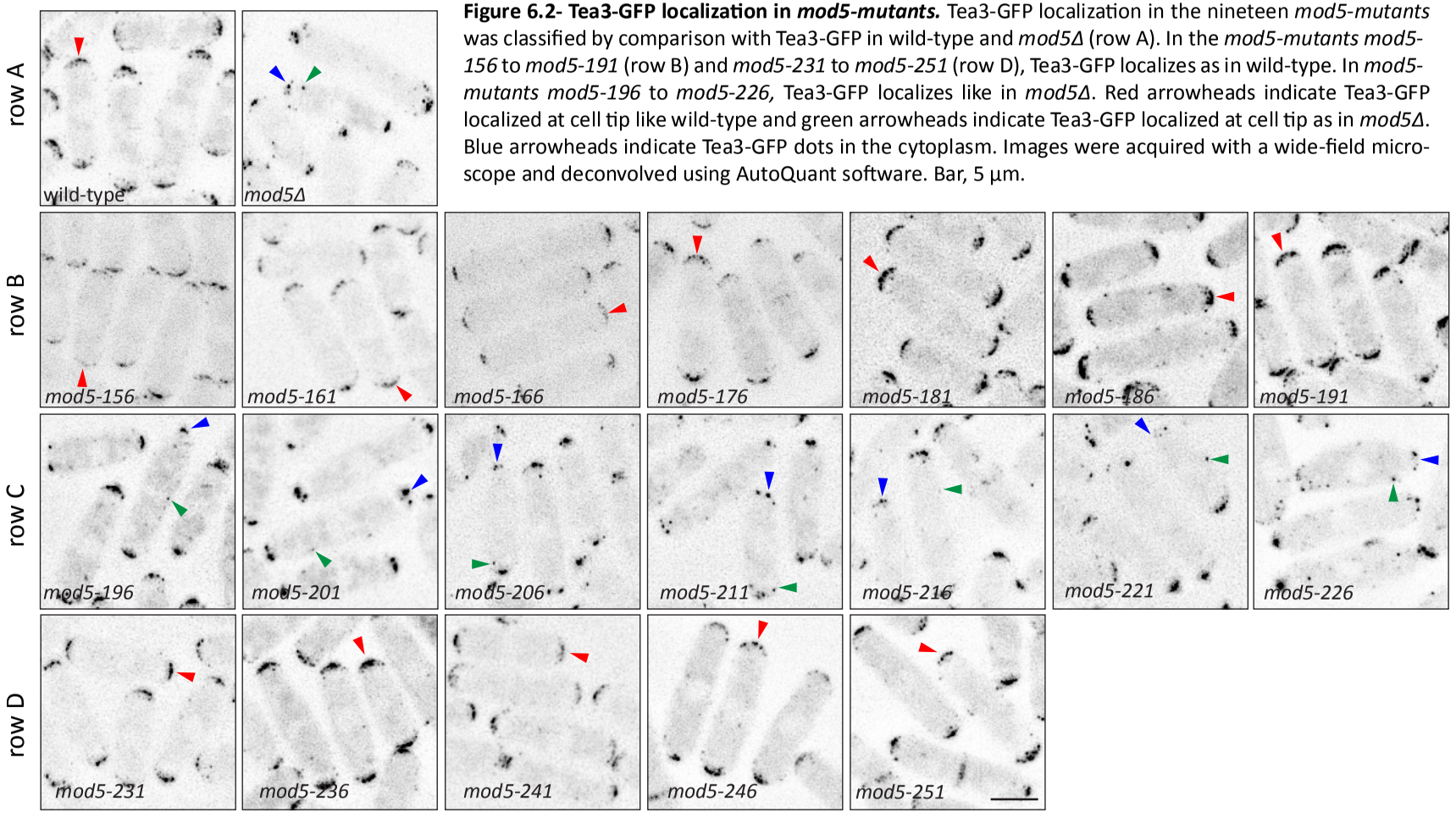

Figure 6.2- Tea3-GFP localization in *mod5-mutants.* Tea3-GFP localization in the nineteen *mod5-mutants* was classified by comparison with Tea3-GFP in wild-type and *mod5Δ* (row A). In the *mod5-mutants mod5-156* to *mod5-191* (row B) and *mod5-231* to *mod5-251* (row D), Tea3-GFP localizes as in wild-type. In *mod5-mutants mod5-196* to *mod5-226,* Tea3-GFP localizes like in *mod5Δ*. Red arrowheads indicate Tea3-GFP localized at cell tip like wild-type and green arrowheads indicate Tea3-GFP localized at cell tip as in *mod5Δ*. Blue arrowheads indicate Tea3-GFP dots in the cytoplasm. Images were acquired with a wide-field microscope and deconvolved using AutoQuant software. Bar, 5 µm.

this morphology assay, *tea1Δ*, *tea3Δ* and *mod5Δ* mutants present defects in cell polarity establishment (Sawin and Snaith, 2004; Snaith et al., 2005; Snaith and Sawin, 2003).

In the cell morphology assay in the presence of MBC, cells are grown until stationary phase and as a result the cells lose their polarity cues. The cells are then released-to-growth in fresh medium in the presence of the microtubule depolymerising drug, MBC. The presence of MBC disrupts microtubules and therefore no microtubule-based signals for positioning polarity (re)establishment are present. Therefore, the polarity machinery will be recruited only if residual cortical landmarks are left at pre-existing cell tips (Sawin and Snaith, 2004). This means that cells with mild polarity defects will branch at high frequency, while cells with no polarity defects will grow straight.

Figure 6.3 shows the plot of the branching frequencies found for each *mod5-mutant* as well as for wild-type and *mod5Δ* cells. Wild-type cells do not branch (~ 5% of branched cells), meaning that Tea1 function as a cell polarity landmark is intact (Sawin and Snaith, 2004). *mod5Δ* mutants branch at high frequency (~ 70%), because Tea1 is not properly anchored at the cell membrane in the absence of Mod5 (Snaith and Sawin, 2003). The mutants *mod5-156* to *mod5-191* branch with a frequency higher (~ 30%) than wild-type (~ 5%), but lower than *mod5Δ* (~ 70%). This result could indicate that Tea1 and/or Tea3 anchoring in mutants *mod5-156* to *mod5-186* is mildly perturbed. However, overall it is enough to ensure proper cell tip localization of Tea1 and Tea3 during exponential cell growth. The mutants *mod5-196* to *mod5-226* branch with high frequency (~ 80%), similar to *mod5Δ*. In this set of mutants the high branching frequency was expected because Tea1 and Tea3 did not show cell tip accumulation (see Figures 6.1 and 6.2). Interestingly, mutants *mod5-231* to *mod5-251* also branch at high frequency (~80%), although Tea1 and Tea3 localize at the cell tip (see Figures 6.1 and 6.2). The high branching frequency of the mutants *mod5-231* to *mod5-251* suggests that Tea1 and/or Tea3 anchoring to the cell tip might be perturbed. However, based in Tea1 and Tea3 localizations in these mutants it is not possible to determine whether or not the cell polarity defects are due to defects in Tea1 or in Tea3 behaviors.

6.2.5. Tea1 localization in the morphology assay

In the morphology assay in the presence of MBC, *mod5Δ* cells branch, and Tea1 does not accumulate at the ectopic site of growth (Sawin and Snaith, 2004). However, in some

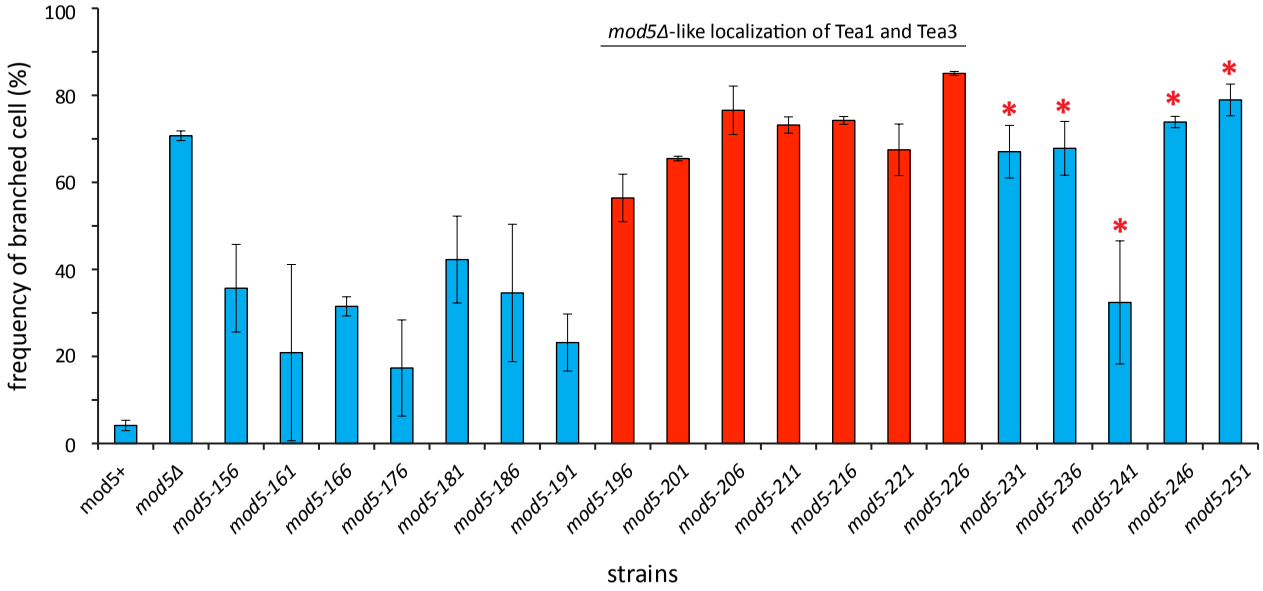

Figure 6.3- Analysis of *mod5*-mutants defects in cell polarity establishment. *mod5*-mutants were analysed using a morphology assay in the presence of MBC. High branching frequency is observed when cells have polarity defects, such as in *mod5Δ*. *mod5*-mutants in which Tea1 and Tea3 localize like wild-type are in blue. *mod5*-mutants in which Tea1 and Tea3 localize as in *mod5Δ* are in red. Asterisks mark mutants with high branching frequency, although Tea1 and Tea3 localize like wild-type. Results from two independent experiments and n=200 for each strain, in each experiment. Error bars are standard deviation.

other polarity mutants where Mod5 is present, such as *tea2-1*, Tea1 retains its ability to interact with the cell cortex and eventually accumulates at the ectopic site of growth, even in the absence of robust microtubule-based delivery (Sawin and Snaith, 2004). This observation was utilized to report the binding of Tea1 to the cell cortex in the *mod5-mutants*. In the event of Tea1 positive-interaction with the *mod5-mutants,* Tea1 is expected to localize at the ectopic-site of growth in the morphology assay in the presence of MBC.

Figure 6.4 shows Tea1 immuno-localization in the morphology assay in the presence of MBC. In mutants *mod5-156* to *mod5-191* (Figure 6.4, row B) and mutants *mod5-231* to *mod5-251* (Figure 6.4, row C) Tea1 either localizes at the cell tip or at the ectopic site of growth. By contrast, Tea1 does not accumulate at ectopic sites of growth in mutants *mod5-196* to *mod5-226* (Figure 6.4, row C) similar to what is observed in the *mod5Δ* mutant (Figure 6.4, row A) (Sawin and Snaith, 2004). Tea1 is localized to ectopic sites of growth in the mutants *mod5-231* to *mod5-251* (Figure 6.4, row D). Because Tea1 retains the ability to localize at the cell cortex in these *mod5-mutants*, this suggests that Tea1 can interact with Mod5-231 to Mod5-251.

I conclude that the molecular basis for branching is different in mutants *mod5-196* to *mod5-226* and in mutants *mod5-231* to *mod5-251*. In the mutants *mod5-196* to *mod5-226*, cells branch but Tea1 does not localize at the ectopic site of growth. This means that Tea1 did not retain its cell polarity landmark function (Sawin and Snaith, 2004), most probably because its interaction with Mod5-196 to Mod5-226 is perturbed. However, mutants *mod5-231* to *mod5-251* exhibit branching as well as Tea1 localization to ectopic sites of growth. In this set of *mod5-mutants* the branching seems to be independent of Tea1 interaction with the cell cortex. This suggests that Mod5 not only functions in Tea1 anchoring to the cell tip, but may also perform additional roles at the cell tip that areTea1-independent.

6.2.6. Analysis of Tea3 localization in mod5-mutants in a tea1Δ background

Despite Tea1 interaction with the cell cortex in *mod5-231* to *mod5-251* these *mod5-mutants* form ectopic sites of growth. I decided to test if the morphological defects observed in *mod5-231* to *mod-251* were due to defects in Tea3 behavior. Because Tea1 binds Tea3 and Mod5, Tea1 could act as a bridge in Tea3-*mod5-mutant* defective interactions. Thus, Tea3 localization at the cell tip would not report a direct Tea3-Mod5 interaction.

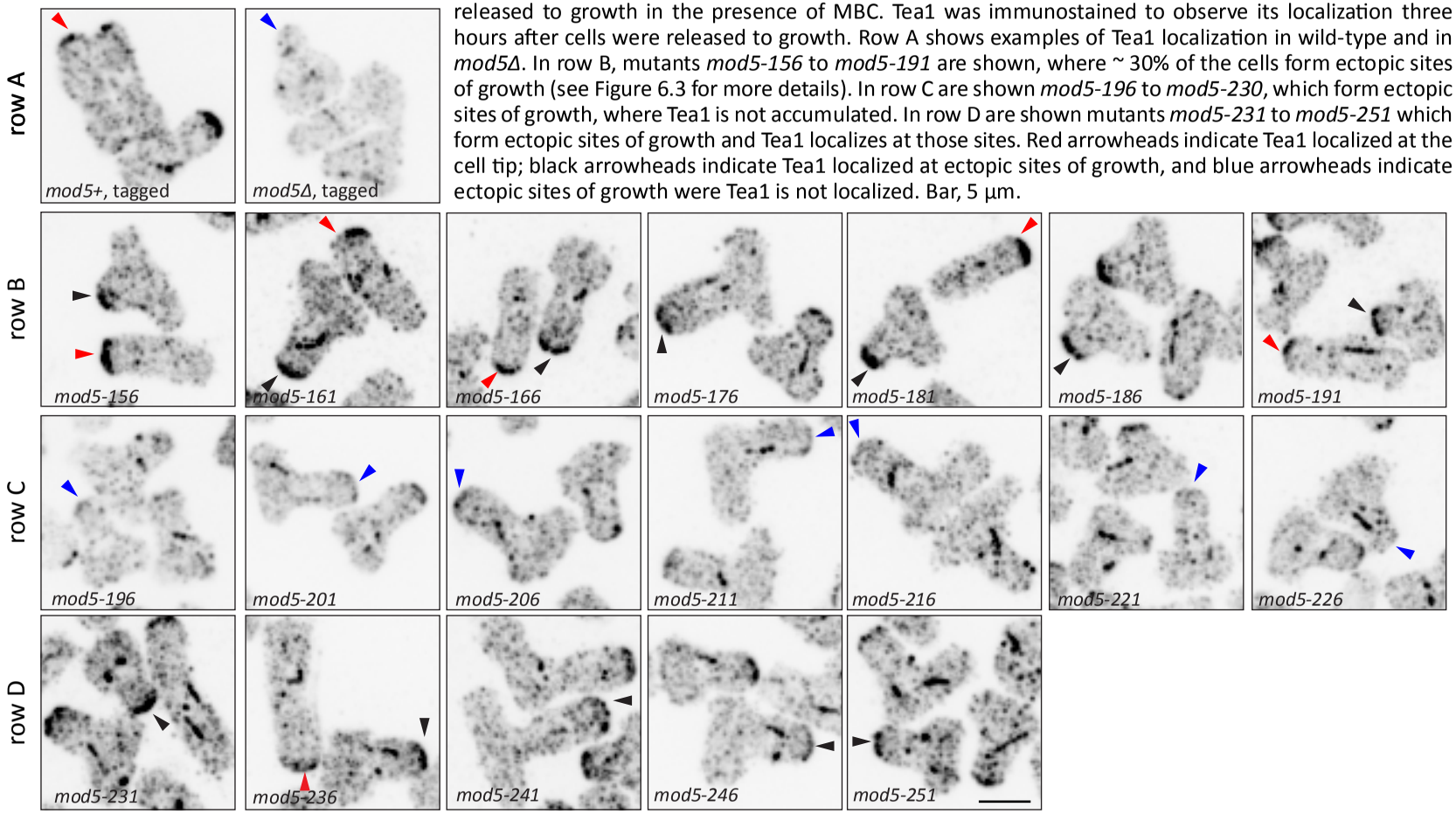

Figure 6.4- Morphology assay in the presence of MBC. Cells were grown until stationary phase and released to growth in the presence of MBC. Tea1 was immunostained to observe its localization three hours after cells were released to growth. Row A shows examples of Tea1 localization in wild-type and in *mod5Δ*. In row B, mutants *mod5-156* to *mod5-191* are shown, where ~ 30% of the cells form ectopic sites of growth (see Figure 6.3 for more details). In row C are shown *mod5-196* to *mod5-230*, which form ectopic sites of growth, where Tea1 is not accumulated. In row D are shown mutants *mod5-231* to *mod5-251* which form ectopic sites of growth and Tea1 localizes at those sites. Red arrowheads indicate Tea1 localized at the cell tip; black arrowheads indicate Tea1 localized at ectopic sites of growth, and blue arrowheads indicate ectopic sites of growth were Tea1 is not localized. Bar, 5 µm.

Therefore, Tea3 localization in the *mod5-mutants* was re-analyzed, but this time in a *tea1Δ* background. It was shown that in *tea1Δ* mutants, Tea3 and Mod5 physical interaction is Tea1-independent and Tea3 localizes around the entire cell membrane in foci that reflect the spread-out localization of Mod5 (Snaith et al., 2005). Moreover, in *tea1Δ mod5Δ* double mutant Tea3 localizes as cytoplasmic dots that show no apparent directionality in movement (Snaith et al., 2005). Tea3 localization in *tea1Δ* mutants was therefore analyzed to separate Tea1-dependent and Tea1-independent localizations.

Figure 6.5 shows Tea3-GFP localization in *mod5-mutants* in a *tea1Δ* background. In mutants *mod5-156* to *mod5-191* (Figure 6.5, row B), Tea3-GFP mostly localizes along the entire cell membrane, as in *tea1Δ* (Figure 6.5, row A). However, in the mutants *mod5-196* to *mod5-251* (Figure 6.5, rows C and D), Tea3-GFP localizes mostly as large dots in the cytoplasm and is not present at the cell membrane. This Tea3-GFP localization pattern is similar to what is observed in the *mod5Δ tea1Δ* double mutant (Figure 6.5, row A), and suggests that Tea3 does not interact with this set of Mod5-mutants. The Tea3-GFP localization pattern in *mod5-196* to *mod5-226* was predictable from the previous screens in *tea1+* cells (see Figure 6.2), because Tea3 did not accumulate at the cell tip. However, in *mod5-231* to *mod5-251* Tea3-GFP localizes like in the *mod5Δ tea1Δ* double mutant. This suggests that in these *mod5-mutants,* Tea3-GFP localization could be modulated by the presence of Tea1 (see Figure 6.2 for Tea3-GFP localization in $tea1^{+}$ background).

Contrary to what would be expected, the defects in the cell polarity establishment of the mutants *mod5-231* to *mod5-251* occur in spite of Tea1 association with the cell membrane. However, these mutants show defects in Tea3 localization, suggesting that Tea3 interaction with Mod5 may have consequences for establishment of the correct polarity axis.

Figure 6.6 shows a schematic diagram of the mapping of Mod5-interacting regions with Tea1 and Tea3. Using a direct mutagenic approach, the putative Tea1 and Tea3 interacting region of Mod5 was narrowed down from 100 aa to 35 aa. The overlap in the binding regions of Tea1 and Tea3 suggests that Tea1-Tea3-Mod5 do not form a three-way complex with single copies of each protein.

The screens performed separated the *mod5-mutants* into three classes, according to Tea1 and Tea3 localization patterns. In the class I of mutants, spanning amino acids 156 to 195, Tea1 and Tea3 localize as in wild-type. Mutants in class I demonstrate that amino

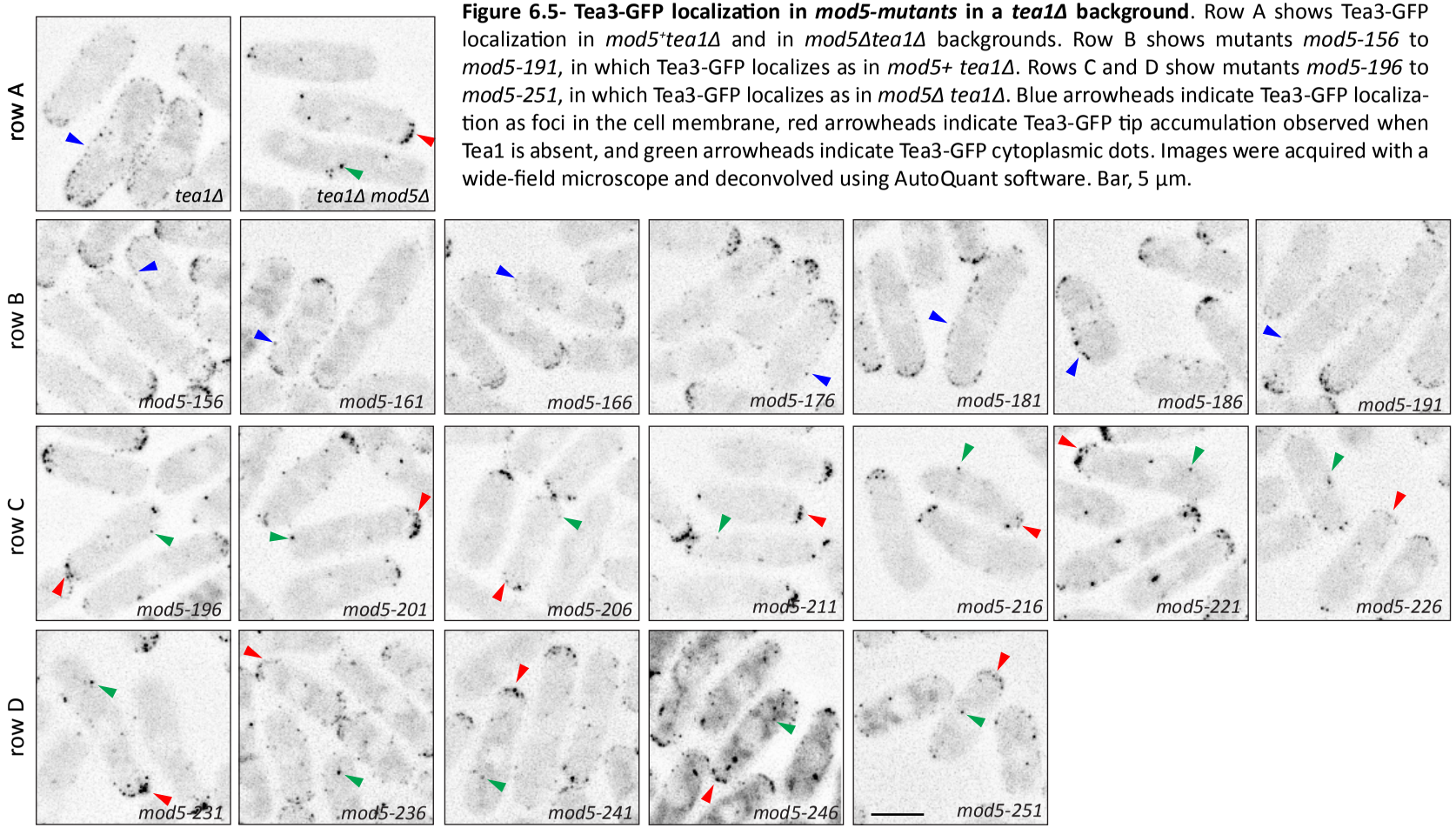

Figure 6.5- Tea3-GFP localization in *mod5-mutants* in a *tea1Δ* background. Row A shows Tea3-GFP localization in *mod5⁺tea1Δ* and in *mod5Δtea1Δ* backgrounds. Row B shows mutants *mod5-156* to *mod5-191*, in which Tea3-GFP localizes as in *mod5+ tea1Δ*. Rows C and D show mutants *mod5-196* to *mod5-251*, in which Tea3-GFP localizes as in *mod5Δ tea1Δ*. Blue arrowheads indicate Tea3-GFP localization as foci in the cell membrane, red arrowheads indicate Tea3-GFP tip accumulation observed when Tea1 is absent, and green arrowheads indicate Tea3-GFP cytoplasmic dots. Images were acquired with a wide-field microscope and deconvolved using AutoQuant software. Bar, 5 µm.

acids 156 to 195 are partially dispensable for Tea1 and Tea3 interacting to Mod5. The class II mutants are characterized by Tea1 and Tea3 localization as in *mod5Δ* mutants. Mutants belonging to class III, encompassing aa 231 to aa 256, presented the most interesting phenotype. In these mutants, although Tea1 localizes as in the wild-type cells, Tea3 localization is Tea1-dependent. Moreover, the mutants present defects in cell polarity establishment, despite Tea1 binding to the cell cortex.

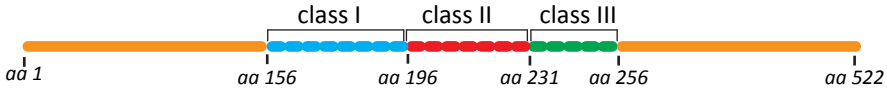

Figure 6.6- Schematic representation of the three classes of *mod5-mutants* classes. In class I (in blue) of *mod5-mutants* amino acids 156 to 195 are mutated. Class I is defined by Tea1 and Tea3 localization like in wild-type. Class II (in red) compromises amino acids 196 to 230 and in these mutants Tea1 and Tea3 localize as in *mod5Δ*. In class III, which includes amino acids 231 to 251, although Tea1 and Tea3 localize to the cell tip, the cells present morphological defects.

6.2.7. Localization of GFP-Mod5-mutants

Next, the localization of GFP-Mod5-mutants was examined. Due to the large number of *mod5-mutants* to be analyzed, I decided to use one *mod5-mutant* representative of each of the three defined classes. *mod5-156*, *mod5-226* and *mod5-231* were used to represent class I, class II and class III, respectively.

Figure 6.7 shows the localization of GFP-Mod5-156, GFP-Mod5-226, GFP-Mod5-231, as well as GFP-Mod5 localization in wild-type and *tea1Δ* backgrounds. Mod5-156 and Mod5-231 localization is restricted to the cell tip, as in wild-type cells. Mod5-226 spreads around the entire cell membrane, as in *tea1Δ* mutants. The localization patterns of the tested *mod5-mutants* show a correlation with the localization of Tea1 and Tea3 in such mutants. This means that, GFP-Mod5-156 and GFP-Mod5-231 are restricted to the cell tip and thus Tea1 and Tea3 accumulate at the same localization. Contrary, GFP-Mod5-226 spreads around the entire cell membrane and Tea1 and Tea3 do not accumulate at the cell tip. Therefore, the co-dependency of Tea1 and Mod5 tip-localizations is maintained in Mod5-156, Mod5-156 and Mod5-231. Moreover, it seems that although Tea3 localization in *mod5-231* is perturbed, it apparently does not influence Mod5-231 restriction to the cell tip.

Figure 6.7- GFP-*mod5-mutants* localization. Localization of wild-type GFP-Mod5 in wild-type (KS706) and in *tea1Δ* (KS714) background, and GFP-Mod5-156 (KS4524), Mod5-226 (KS4526) and Mod5-231 (KS4528) localization in wild-type background. Red arrowheads indicate Mod5 localization at the cell tip and black arrowheads indicate Mod5 localization around the cell membrane. Images are single z-sections and were acquired with a wide-field microscope. Bar, 5 µm.

6.2.8. Dynamics of Mod5-mutants at the cell tip

Next, I employed FRAP to examine the dynamics of Mod5-mutants at the cell tip, as an indicator of their interactions with Tea1. As described in Chapter III, in wild-type cells Mod5 does not turnover with the cell tip, but is dynamic within the cell tip and in *tea1Δ* cells.

Figure 6.8A and 8B show the recovery curve of GFP-Mod5-156 and GFP-Mod5-226, respectively, after photobleaching of the entire cell tip. The recovery curve of Mod5-156 is very much like wild-type GFP-Mod5 with tip-associated Mod5-156 exchanging very little with the non-tip-associated pool. By contrast, tip-associated Mod5-226 exchanges rapidly with the non-tip-associated pool. The fast dynamics observed for Mod5-226 are comparable with GFP-Mod5 in the *tea1Δ* background. Mod5-156 and Mod5-226 dynamics at the cell tip are predictable from Tea1 localization patterns described previously.

Figure 6.9A shows the recovery curve of GFP-Mod5-231 after photobleaching the entire cell tip. GFP-Mod5-231 turns over slowly, with the same dynamics as wild-type GFP-Mod5. Figure 6.9B shows the recovery curve of GFP-Mod5-231 after photobleaching half of the cell tip. The dynamics of Mod5-231 within the cell tip resembles Mod5 in wild-type. This indicates that despite the interacting and cell polarity defects observed in *mod5-231*, GFP-Mod5-231 is efficiently captured at the cell tip during exponential growth.

6.2.9. Analysis of Mod5-156, Mod5-226 and Mod5-231 physical interaction with Tea1 and Tea3

Next, I examined how the localization of Tea1 and Tea3 in the *mod5-mutants* was related to the formation of protein complexes among the three proteins. To address this problem I tested co-immunoprecipitation of Tea1 and Tea3 with the Mod5-mutants, in wild-type and in *tea1Δ* backgrounds. Due to the large number of *mod5-mutants* to be tested, only *mod5-156* (class I), *mod5-226* (class II) and *mod5-231* (class III) were analyzed, as representative members of each *mod5-mutants* class.

Figure 6.10 shows the western blot of the anti-GFP immunoprecipitation as well as the quantitation of the pull-down efficiency. The efficiency of Tea1 co-immunoprecipitation by GFP-Mod5-156 is similar to GFP-Mod5 (~ 116%). However, the efficiency of Tea1 co-immunoprecipitation by GFP-Mod5-226 is decreased to ~ 35% when compared with co-immunoprecipitation by GFP-Mod5. Tea1 is co-immunoprecipitated by GFP-Mod5-231 (~

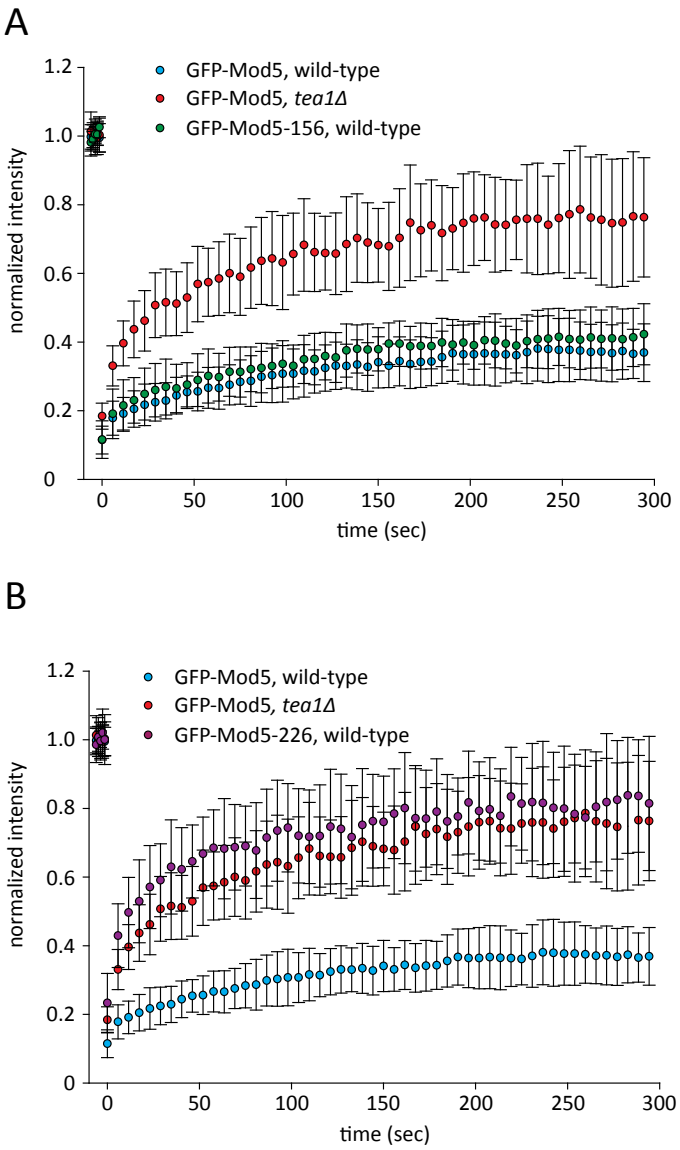

Figure 6.8- FRAP curves of *mod5-156* and *mod5-226*. The entire cell tips of *mod5-156* (KS4524) and *mod5-226* (KS4526) were photobleached and the fluorescence recovery was recorded. **A)** Mod5-156 (green curve) dynamics are similar to Mod5 dynamics in wild-type background (KS706) (blue curve). **B)** Mod5-226 (purple curve)dynamics are similar to Mod5 in a *tea1Δ* (KS714) background (red curve).

A

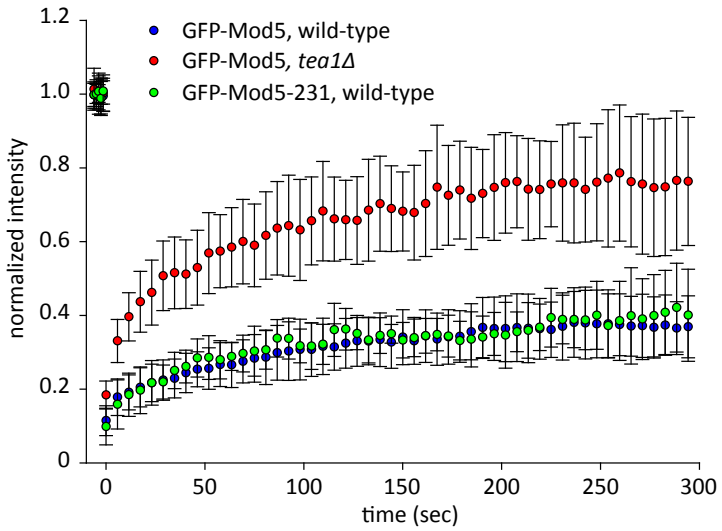

B

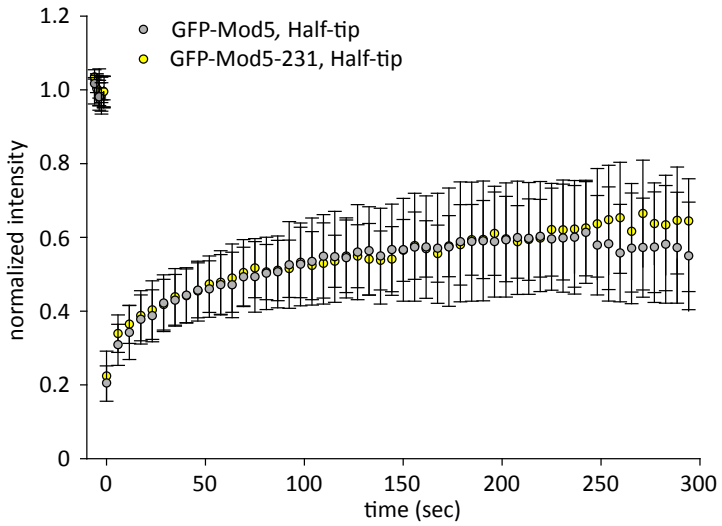

Figure 6.9- GFP-*Mod5-231* dynamics at the cell tip. A) GFP-Mod5-231 was photobleached from the entire cell tip and the fluorescence recovery was recorded every 5 sec for 5 min. The dynamics of GFP-Mod5-231 (KS4528) (green curve) is similar to wild-type GFP-Mod5 (KS706) (blue curve). **B)** GFP-Mod5-231 was photobleached from half the cell tip and the fluorescence recovery was recorded for 5 min every 5 sec. The dynamics of GFP-Mod5-231 within the cell tip is comparable to that of wild-type GFP-Mod5.

117%) to the same extent as with GFP-Mod5 and with GFP-Mod5-156 (~ 116%). These results demonstrate that the Tea1-tdTomato localization screen and Tea1 localization in the morphology assay were good approximations to indirectly infer the formation of Tea1-Mod5-mutants protein complexes. Moreover, the observation of Tea1 co-immunoprecipitation with GFP-Mod5-231 gives further evidence that the polarity defects observed in class III of *mod5-mutants* are not due to the disruption of an interaction with Tea1.

The efficiency of Tea3 immunoprecipitation by Mod5-156 is reduced to ~ 36% when compared with wild-type Mod5. In addition, in the absence of Tea1 the co-immunoprecipitation efficiency of Tea3 is further reduced to ~ 22% relative to wild-type Mod5. As expected from Tea3-GFP localization analysis, Tea3 co-immunoprecipitation by Mod5-226 is decreased to ~ 15%, when compared with wild-type Mod5. In addition, *tea1Δ* does not affect significantly Tea3 co-immunoprecipitation efficiency. This demonstrates that the reduction of the formation of protein complex containing Mod5-226 and Tea3 is independent of Tea1. Interestingly, Tea3 co-immunoprecipitation with Mod5-231 was found to be comparable to wild-type Mod5, both in the presence and in the absence of Tea1 (~ 71% and ~ 75% of wild-type, respectively). Tea3-GFP localization defects observed in *mod5-231* suggested that interaction of Tea3 with Mod5-231 was compromised and was Tea1-dependent. However, there is no direct correlation between cytological observations and biochemical results. Several reasons can be proposed to explain these results. First, GFP-Mod5 immunoprecipitations were performed under Mod5 over expression (~10 fold increase relative to wild-type, data not shown). When Mod5 is over expressed it localizes around the entire cell membrane (Snaith and Sawin, 2003). Therefore, the interaction of Mod5-231 with Tea3 identified here could be the result of an over expression artifact. This hypothesis can be tested by restoring Mod5 endogenous levels with the addition of 150 nM of thiamine. Second, co-immunoprecipitation assays do not distinguish between direct and indirect protein-protein interactions. Therefore, the observation of Tea3 co-immunoprecipitation with Mod5-231 could be due to the presence of the two proteins in the same complex, but not directly interacting. Finally, the results presented in Figure 6.10 could reflect an *in vivo* interaction between Tea3 and Mod5-231. The apparent contradiction between the biochemical and the cytological data could indicate that Tea3-Mod5 interaction is more complex then a simple protein-protein binding. Therefore, the

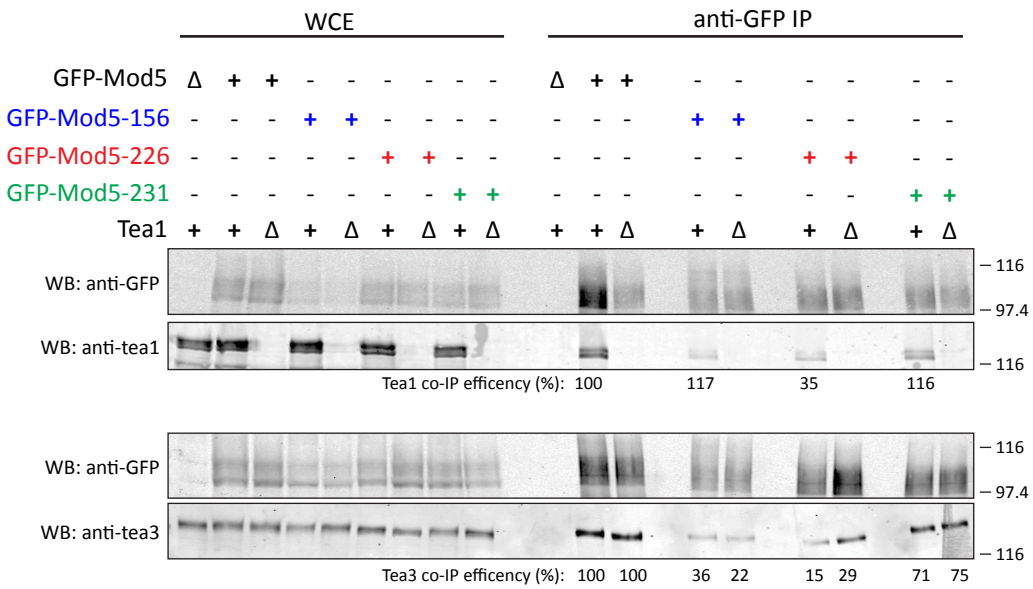

Figure 6.10- GFP-Mod5-mutants immunoprecipitation. GFP-Mod5 (KS706, KS714), GFP-Mod5-156 (KS4524, KS4995), GFP-Mod5-226 (KS4526, KS4997) and GFP-Mod5-231 (KS4528, KS4999) were immunoprecipitated from wild-type and *tea1Δ* backgrounds with anti-GFP antibody. Membranes were probed with anti-GFP and anti-Tea1 or with anti-GFP and anti-Tea3 antibodies. The efficiency of Tea1 and Tea3 co-immunoprecipitations was normalized to the amount of immunoprecipitated GFP-Mod5. Western blots and immunoprecipitation efficiencies are representative of two independent experiments.

mod5-231 mutation may not affect Tea3-Mod5 binding (Figure 6.10) but may perturb the subsequent function of Mod5 in Tea3 (Figures 6.4 and 6.5).

6.2.10. Tea3 is stably associated at the cell tip

The results obtained suggest that the severe cell polarity defects observed in *mod5-mutants* belonging to class III are related to Tea3 behavior and not with the disruption of their binding to Tea1. Therefore, Tea3 interaction with Mod5 may play a role in the establishment of the correct cell growth axis. To better understand how Tea3-Mod5 interaction can be involved in *de novo* establishment of cell polarity, the dynamics of Tea3 at cell tip were examined by FRAP.

Figure 6.11 shows the recovery curve of Tea3-GFP after photobleaching the entire cell tip or half of the cell tip. Tea3-GFP recovers equally slowly when it is photobleached from the entire cell tip and from half of the cell tip. This indicates that cell tip-associated Tea3-GFP turns over slowly both with the cytoplasm and within the cell tip. This suggests that Tea3 either binds a stable structure or forms a stable structure itself. Tea3 is not predicted to oligomerize beyond dimers (predicted with *MultiCoil*, (Wolf et al., 1997) (Arellano et al., 2002)) and therefore the formation of a self-stable structure, of the same type as is proposed for Tea1 (described in Chapter III), is unlikely. Because Tea3-GFP turnover within the cell tip is very similar to Tea1 turnover, I speculate that Tea3 is present at the cell tip as a component of the Tea1 cluster-network (described in Chapter III, the Tea1 cluster-network is proposed to be a stable structure of Tea1 polymers connected to each other due to protein-protein interactions).

6.2.11. Mod5 diffuses across the cluster-network, in tea3Δ

To better understand how Tea3 influences Mod5, I examined the dynamics of GFP-Mod5 in *tea3Δ* mutants. In *tea3Δ*, Mod5 localizes at the cell tip, but is not so tightly restricted as in wild-type and spreads around the cell tip (Snaith et al., 2005).

Figure 6.12A shows GFP-Mod5 recovery curve after photobleaching of the entire cell tip in wild-type and in *tea3Δ* and *tea1Δ* mutants. In *tea3Δ*, GFP-Mod5 fluorescence after photobleaching recovers to ~ 60% of this initial value within 300 sec, meaning that,

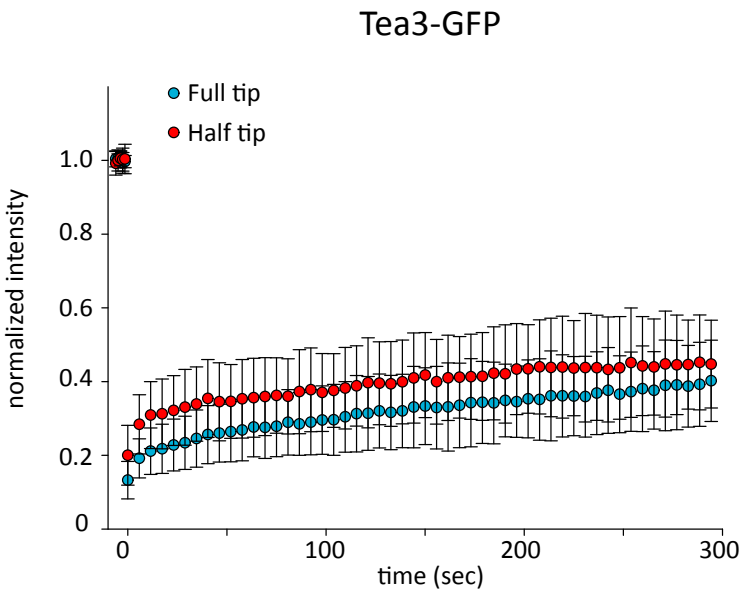

Figure 6.11- Tea3 is stably associated with the cell tip. Tea3-GFP (KS2331) was photobleached from the entire cell tip (blue curve) and from half the cell tip (red curve). The fluorescence recovery was recorded for 5 min every 5 sec. Tip-associated Tea3-GFP turns over slowly with the rest of the cell pool, and within the cell tip.

contrary to wild-type, in *tea3Δ* mutants tip-associated Mod5 can exchange with the rest of the cell membrane.

Figure 6.12B shows the recovery curve of GFP-Mod5 in *tea3Δ* in a half-tip FRAP experiment. The amount of GFP-Mod5 recovery after 300 sec (~ 65%) is only slightly increased when compared with the full-tip recovery (~ 60%). This means that GFP-Mod5 fluorescence recovery is due to its diffusion within the entire cell membrane and across the cluster-network (In Chapter III a diffusion-capture mechanism is proposed for the restriction of Mod5 at the cell tip). In a *tea3Δ* background, Mod5 capture within the cluster-network seems to be compromised and thus Mod5 diffuses faster.

6.3. Discussion

This chapter starts with the hypothesis that Tea1 and Tea3 binding sites to Mod5 could be separated and therefore used to dissect the molecular interactions among the three proteins. However, data shown here suggests that Tea1, Tea3 and Mod5 may bind in a three-way protein complex, in which the proteins are not present in a 1:1:1 stoichiometry. This observation makes it difficult that Tea1 and Tea3 binding sites to Mod5 could be separated using this experimental approach. In addition, the results obtained here suggest that defects in Tea3-Mod5 interaction may cause defects in cell polarity establishment. In this chapter is also shown that although Tea3 is non-essential for Mod5 restriction at the cell tip, Tea3 may reduce Mod5 diffusion across the cell tip.

In order to separate the interacting-regions of Tea1 and Tea3 to Mod5, I constructed nineteen Mod5 sequential substitution mutants within a region that was previously shown to be necessary for Tea1 and Tea3 binding to Mod5 (aa 156 to aa 256) (Snaith et al., 2005). Because it is known that Tea1 and Tea3 do not accumulate at the cell tip in *mod5Δ* cells, the localization of Tea1 and Tea3 in the *mod5-mutants* was used as readout of protein-protein interactions. In addition, defects in cell polarity establishment were also used to infer about Tea3 and Tea3 interactions with the *mod5-mutants*. Therefore, by using a combination of several indirect assays for protein-protein interactions it was possible to identify and dissect some of the complexity in the interactions of Tea1 and Tea3 with the *mod5-mutants*.

Thus, after several screening strategies, the *mod5-mutants* were divided into three classes (summarized in Figure 6.6). Class I shows that amino acids 156 to 195 are not

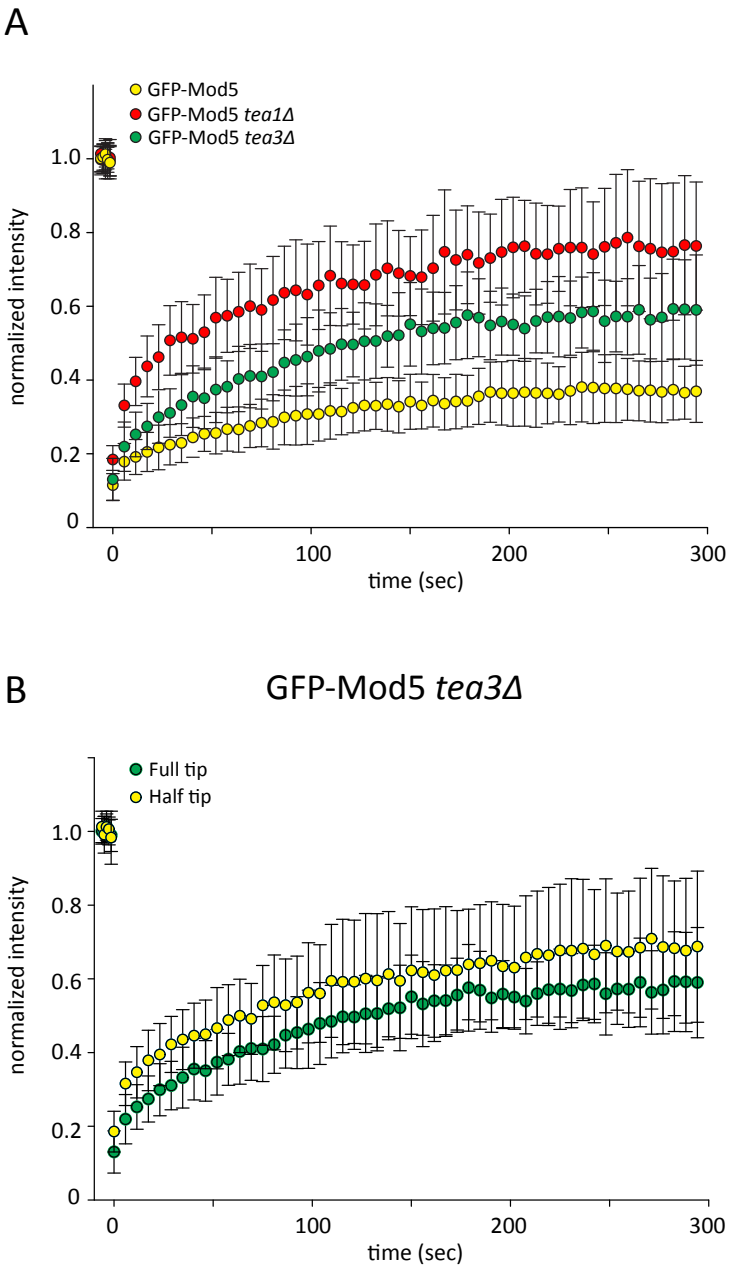

Figure 6.12- GFP-Mod5 dynamics in *tea3Δ* background. A) GFP-Mod5 was photobleached from the entire cell tip in wild-type (KS706) (blue), *tea1Δ* (KS714) (red) and *tea3Δ* (KS1171) (green) backgrounds. The recovery of fluorescence was followed for every 5 sec for 5 min. **B)** GFP-Mod5 recovery curves after photobleaching of the entire cell tip (green) and from half the cell tip (yellow) in *tea3Δ* mutants.

involved in the interaction of either Tea1 or Tea3 to Mod5. In class II of *mod5-mutants*, Tea1 and Tea3 do not accumulate at the cell tip and are co-transported on microtubule plus-ends towards the cell tip, as in *mod5Δ.* This class of *mod5-mutants* includes *mod5-196* to *mod5-226* and spans 35 amino acids. As expected, mutants in class II show defects in cell polarity establishment due to defective Tea1-Mod5 interactions and therefore lack of Tea1 productive binding to the cell tip. Mutants in class II could be useful to identify Mod5 binding partners independently of Tea1-Mod5 and Tea3-Mod5 interactions. Interestingly, in *mod5-mutants* belonging to class III, Tea1 localizes as in wild-type cells, but Tea3 localization is Tea1-dependent. Despite Tea1-dependent localization of Tea3 in class III of *mod5-mutants*, Mod5-231 (representative of class III) co-immunoprecipitates Tea3 (see discussion below), which indicates that Tea3 might interact with *mod5-mutants* belonging to class III (see discussion below). Overall, the mutagenic analysis of Mod5 showed that Tea1 and Tea3 interacting-region to Mod5 overlaps over 35 aa.

The *mod5-mutants* generated not only demonstrated that Tea1 and Tea3 interacting-region to Mod5 overlap, but also allowed to dissect how the organization of three proteins at the cell tip influences the establishment of the cell polarity axis. First, it was observed that Mod5-mutants in class III present defects in establishment of cell polarity independently of Tea1 binding to the cell cortex. In addition, in this class of *mod5-mutants* Tea3 localization was shown to be Tea1-dependent. This indicates that the defects in cell polarity establishment of class III of *mod5-mutants* could be due to defects in Tea3-Mod5 interaction. These observations suggest that Mod5 may have an additional role in cell polarity, independent of its role in the anchoring of Tea1 to the cell tip. However, because Mod5-231 was shown to co-immunoprecipitate Tea3 with similar efficiency as wild-type Mod5, the additional role of Mod5 in cell polarity cannot be simply of binding to Tea3. To reconcile the apparent contradiction between biochemical and cytological results I speculate that the role of Mod5-Tea3 interaction during cell polarity establishment requires that Mod5 not only binds to Tea3 but also incorporates Tea3 in the cluster-network (see discussion below).

Tea3 dynamics at the cell tip were analyzed by FRAP and showed that Tea3 is stably associated with the cell tip and its dynamics are similar to Tea1. However, and contrary to Tea1, Tea3 is not predicted to oligomerize beyond dimers (Arellano et al., 2002; Wolf et al., 1997). Therefore it is unlikely that Tea3 associates in a self-stable structure of the same

type as was proposed for Tea1 (for details see Chapter III). However, the similar dynamics of Tea3 and Tea1 suggest that Tea3 could be a component of the cluster-network. Therefore, I speculate that Tea1, Tea3 and Mod5 could simultaneously bind within the cluster-network and form a non-stoichiometric complex of high-molecular weight. Moreover, the overlapping in Tea1 and Tea3 interacting-region to Mod5 could be interpreted in the context of the non-stoichiometric binding of the three proteins. As proposed in Chapter III, Mod5 binds to the cluster-network in a diffusion-capture mechanism, and therefore it could, in principle, bind independently to Tea1 and Tea3 via the same amino acids region.

Although the Tea1 cluster-network is present in *tea3Δ* mutants, additional evidence suggests that its stability might be compromised (Snaith et al., 2005). First, Tea1 accumulation at the cell tip is reduced and upon MBC treatment Tea1 is lost from the non-growing tip at a faster rate than in wild-type (Snaith et al., 2005). Second, I showed here that Mod5 diffuses across the cluster-network at a faster rate and its cell tip accumulation is wider than in wild-type (Snaith et al., 2005). Based on these observations, I speculate that Tea3 might play a role in increasing the cluster-network compaction by bringing Tea1 polymers together (Figure 6.13). This would increase Mod5 restriction at the cell tip, by reducing the diffusion rate and increasing the capture frequency. The cell polarity establishment defects in the mutant *mod5-231* could be explained by a defect in Tea3-association to the cluster-network, which makes it a looser structure when compared with wild-type. Therefore, during cell polarity establishment in *mod5-231*, upon microtubule delivery Tea1 might 'slip' away from the cell tip and does not reinforce the cluster-network.

The Tea1-Tea3-Mod5 three-way interaction observed at the cell tip of *S. pombe* shares similarities with the CLASPs-LL5β-ELKS interaction observed in HeLa cells and fibroblasts (Lansbergen et al., 2006). Like Tea1, CLASPs are transported on microtubule plus-ends towards the cell periphery, and are anchored at the cell cortex. CLASPs bind to the membrane-associated protein LL5β, and become anchored at the cell cortex (Drabek et al., 2006). CLASPs are deposited close to focal adhesion or to the leading edge of lamellapodia and stabilize microtubule binding at the cell cortex (Drabek et al., 2006). Interestingly, the CLASPs-LL5β interaction at the cell cortex involves a third protein, EKLS, which is proposed to have a scaffold role in the complex formation. CLASP-LL5β-EKLS complex is present at the cell cortex in the form of immobile clusters. Although none of the proteins share

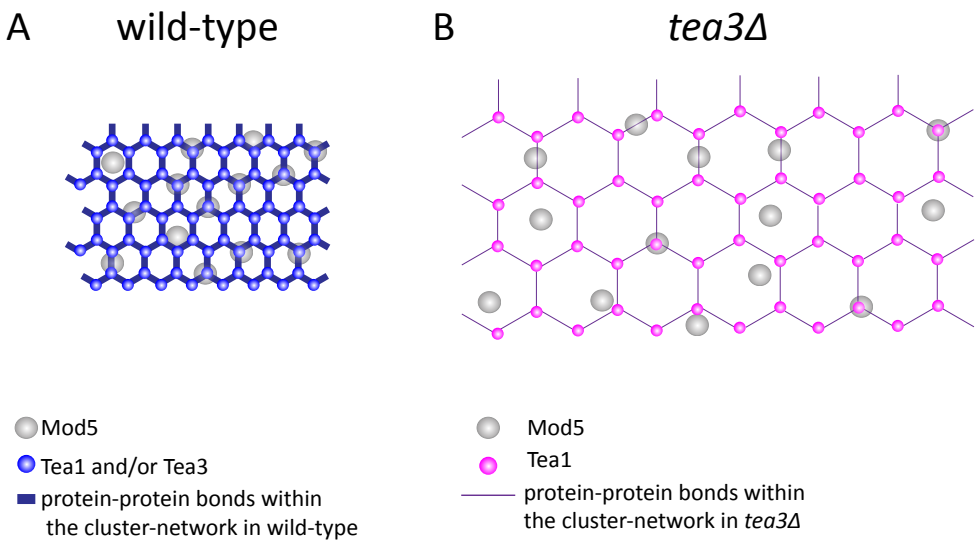

Figure 6.13- Schematic representation of the compaction of the Tea1 cluster-network in wild-type (A) and in *tea3Δ* (B)cells. Although Tea3 is not essential for Tea1 cluster-network formation, Tea3 could play a compaction role by bringing Tea1 polymers together. Tea3 incorporation into the cluster-network may require not only Tea3-Mod5 binding but Tea3 activation by Mod5. In *tea3Δ* cells, Mod5 diffuses faster within the cell tip because it encounters Tea1 cluster-network less frequently, and therefore is not as efficiently captured.

structural homology with Tea1, Tea3 or Mod5, the basic molecular mechanism underling microtubules anchoring to the cortex seems to share great similarities with the *S. pombe* mechanism proposed here. This indicates that microtubule-cortex interactions and consequent microtubule stabilization might not only be a conserved mechanism among species but also share functions in cell polarity establishment.

To summarize, I proposed that Tea1, Tea3 and Mod5 bind in a non-stoichiometric complex with high-molecular weight within the cluster network at the cell tip. Although Tea3 is non-essential for the formation of the cluster-network, Tea3 may increase compaction of the cluster-network. Thus, Tea3 reduces cluster-network diffusion and therefore influence cell polarity establishment.

Chapter VII: Concluding remarks and future work

The ability of cells to establish and maintain a polarized axis is essential in all eukaryotes. It has been shown that cells can polarize in response to both internal and external cues. Despite the wide range of cellular morphologies seen across eukaryotes it is known that cell polarization among different organisms shares same similar molecular mechanisms (Nelson, 2003). The roles of the cytoskeletal polymers are of special relevance for cell polarity due to their intrinsically polar properties and because they can act as track for vesicle transport (Li and Gundersen, 2008; Mullins, 2010).

S. pombe has been shown to be an important model organism to study cell polarity (Hayles and Nurse, 2001). In *S. pombe,* microtubules play a role during cell polarity establishment, and in addition microtubules transport on their plus-ends the key polarity regulator, Tea1 (Mata and Nurse, 1997; Sawin and Snaith, 2004). Upon microtubule contact with the cell tip Tea1 is deposited at the cell membrane. Over the last few years, several Tea1 binding partners have been identified, both at the cell membrane and at microtubule plus-ends (Martin, 2009). The identification of the membrane-associated protein Mod5 was a major breakthrough in the understanding of Tea1 anchoring to the cell membrane (Snaith and Sawin, 2003). Because of the localization co-dependency of Tea1 and Mod5, it has been proposed that the two proteins accumulate at the cell tip in a positive-feedback mechanism (Snaith and Sawin, 2003). That is, upon deposition at the cell tip, Tea1 would recruit Mod5 to the same location, and therefore more tip-localized Mod5 would be available to bind more newly-arrived Tea1.

The process of Tea1 anchoring and its subsequent role in cell polarity have been described in what resembles a linear succession of events (Martin, 2009; Siegrist and Doe, 2007). Firstly, Tea1 is transported to the cell tip on microtubule plus-ends. Secondly, Tea1 gets anchored due to an interaction with its membrane receptor, Mod5. Finally, Tea1 interacts with its downstream binding partners at the cell tip and plays a role in remodeling the actin cytoskeleton. Although Tea1 association on the microtubules and at the cell tips is described as a succession of linear events, it remains to be shown what molecular mechanisms lie behind Tea1 behavior. The molecular mechanisms by which Tea1 is transferred from the microtubule plus-ends and becomes anchored at the cell tip are particularly poorly understood.

In this thesis I described experiments that lead to the proposal of a model for Tea1 and Mod5 interaction at the cell tips. The proposed model suggests how Tea1 becomes anchored upon microtubule-based delivery and how Mod5 is restricted to the cell tip. Moreover, in this thesis I proposed that Tea1 dissociation from the cell tip is a phospho-regulated process. I also described the development of a robust SILAC method for *S. pombe*, based on re-engineering arginine catabolism. Finally, I proposed a mechanism by which an interaction between Tea3 and Mod5 might be involved in Tea1 anchoring at the cell tip and, by extension, in cell polarity.

In Chapter III I used a combination of FRAP, quantitative live cell-imaging and mathematical modeling to understand the molecular mechanism and dynamics of Tea1 anchoring to the cell tip. I demonstrated that Tea1 is stably associated with the cell tip, whereas Mod5 is mobile within the cell tip. We proposed that Tea1 is stable at the cell tip due to polymerization and formation of a cluster-network. We proposed that the role of Mod5 in Tea1 anchoring mechanism is to facilitate the formation of Tea1-Tea1 interactions within the cluster-network. In the model, Mod5 is restricted to the cell tip due to frequent binding and release to the cluster-network, in a diffusion-capture mechanism (Rudner et al., 2002).

In the formalization of the mathematical model, incorporation of Tea1 within the cluster-network is described as an autocatalytic reaction. Thus, Tea1 reinforces its own localization at the cell tip, in a process that requires directed Tea1 transport on microtubule plus-ends. Therefore, the model proposed here for Tea1 and Mod5 accumulation at the cell tip is significantly different from the hypothesis of a positive feedback loop between Tea1 and Mod5 (Snaith and Sawin, 2003). Whereas before it was proposed that Tea1 and Mod5 localizations were dependent on the accumulation of both proteins, in the new model, Tea1 and Mod5 accumulate at the cell tip as a consequence of Tea1 autocatalytic polymerization and its microtubule-based delivery.

In the model, Tea1 cluster-network has an emergent property of self-focusing, which suggests that the spatial stability of Tea1 is required for its roles in cell polarity establishment and as a polarity landmark. During *de novo* formation of the cluster-network, the self-focusing property can help the cell finding the center of the cell tip. In addition, during maintenance of polarized growth the cluster-network can filter out errors on microtubule-based deposition of Tea1 and promote robust directional cell growth.

Although I showed here evidence for Tea1 polymerization, further experimental evidence is still required to support the model. However, to demonstrate that not only a protein associates in an immobile cluster-network but also how the cluster-network is spatially and temporally organized can be experimentally challenging.

The formation of the high molecular weight structure of Tea1 should be examined *in vivo* by measuring the size of Tea1 complexes using sucrose gradients and gel filtration. These analyses can be performed in wild-type cells and in mutants where Tea1 cluster-network stability has been shown to be perturbed, such as *tea1Δ434-586* (more stable) or *tea1Δtrimer* and in *mod5Δ* (less stable or not formed).

It is important to understand the spatial organization of the Tea1 cluster-network at the cell tip, as it can be informative about its interaction with Tea1 binding partners. Others have used superresolution light microscopy to visualize protein clusters distribution at the cell membrane (Greenfield et al., 2009; Manley et al., 2008; Sieber et al., 2007). Supperresolution microscopy overcomes the light diffraction barrier and thus can resolve cellular structures at the nanoscale level (~ 10-20 nm resolution limit) (Patterson et al., 2010). Although in recent years several superresolution methods have been developed, the specific problem of Tea1 cluster-network spatial organization would benefit with the used of the superresolution method, PALM (Photoactivated Localization Microscopy) (Patterson et al., 2010). PALM allows the resolution of single-molecule localization, and therefore the distribution of Tea1 single-molecules in relation to each other within the cluster-network could be determined. Moreover, PALM allows the simultaneous spatial resolution of more that one protein. Thus, the relative distribution of Mod5 single-molecules within the cluster-network can also be determined. Therefore this approach could, in principle, spatially resolve Tea1 cluster-network organization *in vivo*.

In the mathematical model, it is predicted that Tea1 incorporation at the cluster-network would be higher at the center of the cell tip and lower at the periphery. To test this prediction, the efficiency of Tea1 incorporation at the cell tip could be spatially measured *in vivo*. To do this we can either use Tea1 tagged with a photoactivatable GFP version (H. Snaith, personal communication) or, instead, cell tip-associated Tea1 could be photobleached allowing the visualization of the incorporation of newly-arrived Tea1 packets.

The mathematical model of Tea1 cluster-network formation predicted an emergent property of self-focusing. This concept is of extreme importance because it may be similar

in other systems that require discrete focusing (Bement et al., 2005; Goryachev and Pokhilko, 2008; Yuce et al., 2005). It would be interesting to experimentally demonstrate the existence of such mechanism. The self-focusing is a direct consequence of the prediction of the cluster-network width narrowing during *de novo* formation until it reaches steady state. The cluster-network *de novo* formation could be reconstituted using artificially bent *S. pombe* cells, in which Tea1 and Mod5 accumulate at ectopic sites of the membrane (Minc et al., 2009; Terenna et al., 2008). This experimental approach could be used to follow the ectopic accumulation of Tea1 and Mod5 until steady state and measure the size of the cluster-network as it forms *de novo*.

Despite the large number of Tea1 binding partners identified so far, there is very little information of how Tea1 interactions with itself and with other proteins are regulated in time and space. In the beginning of the work presented in Chapter IV, I hypothesized that phosphorylation might regulate Tea1 interaction with its binding-partners. I used MS to identify Tea1 phosphorylation residues and determined that Tea1 phosphorylated residues are located within an unstructured region of the protein, between the N-terminal Kelch repeats and the C-terminal coiled-coil. Evidence showed that this region might be needed to promote Tea1 dissociation from the cell tip. I speculated that multisite phosphorylation of Tea1 regulates its dissociation from the cluster-network through electrostatic repulsion (Serber and Ferrell, 2007).

However, further support is needed to confirm that phosphorylation is indeed involved in Tea1 dissociation from the cluster-network. Therefore it is necessary to test how dissociation from cell tip of non-phosphorylated and phospho-mimetic versions of Tea1 behave, using live-cell imaging and FRAP. In addition, the formation of Tea1-Tea1 interactions in the non-phosphorylatable and phospho-mimetic mutants should also be examined and quantified both *in vivo* and *in vitro*. Once the roles of Tea1 phosphorylation have been experimentally confirmed it would be interesting to immunoprecipitate Tea1 phospho-mutants and quantify Tea1 differential interactions using SILAC.

Moreover, it would be informative to study the consequences for cluster-network formation when Tea1 turnover with the cell tip is reduced/increased due to perturbations in Tea1 phospho-regulation. It would also be necessary to examine the consequences for cell polarity establishment when Tea1 does not dissociate/associate with the cell tip.

I also showed preliminary evidence for Tea1 differential phosphorylation dependent on Tea1 localization. Therefore, it could be very informative to repeat the proteomic comparison described in section 4.2.5, but using the SILAC method described in Chapter V to make the comparison quantitative. The proteomic analysis of Tea1 using the SILAC method could be extended to identify differential Tea1 binding-partners.

It is still an unanswered question what are the kinases that have Tea1 as substrate. However, the data presented Chapter IV show that Tea1 is multisite phosphorylated. This suggests that Tea1 might be the substrate of more than one kinase. Therefore, it would necessary to identify the combination of multisite phosphorylation and kinase(s) necessary for Tea1 regulation.

During the experimental approach used to compare Tea1 phosphorylated residues used in Chapter IV it was clear that MS experiments present statistical variation among themselves. This made it difficult to reliably compare MS samples. In Chapter V I described the development of a method for robust SILAC, which allows quantitative MS, in *S. pombe.* We found that arginine is extensively converted to proline, glutamine, glutamate and lysine, which makes protein quantification extremely challenging. The conversion of arginine was prevented by genetically re-engineering the arginine catabolism pathway. Moreover, we manipulated the concentrations of the medium components in order to achieve robust cellular growth under the experimental conditions used to perform SILAC.

As a proof-of-principle of the method, we compared the proteome in late G2 phase of the cell cycle with the proteome at the G1/S transition. In this experiment we quantified ~ 70% of the *S. pombe* proteome and identified proteins that are either down-regulated or up-regulated during the cell cycle progression. However, this analysis was far from being comprehensive, as it compares only two phases of the cell cycle. Thus, to correctly quantify the variation of protein levels during cell cycle, all the cell cycle stages could be analyzed. Moreover, the MS analysis might be biased towards high abundance proteins. Therefore, in order to quantify the entire *S. pombe* proteome, the sample fractionation methods used in MS should be improved (de Godoy et al., 2008).

Although the motivation for developing a SILAC method for *S. pombe* was to compare Tea1 phosphorylated residues among several mutants, this method is robust enough to be used in any quantitative MS experiment. Therefore, the entire *S. pombe* community can

use it as a tool in the quantitation of protein-protein interactions, differential post-translational modifications or proteome-wide comparison studies.

In Chapter VI I used a directed mutagenic analysis aiming to separate Tea1 and Tea3 binding sites to Mod5. The data obtained in the mutagenic analysis interpreted in the context of the results presented in Chapters III and VI, suggests that rather than forming a 1:1:1 complex, Tea1, Tea3 and Mod5 might bind simultaneous in a high molecular-weight complex with multiple copies of each protein.

Results described in Chapter VI indicate that Mod5-Tea3 interaction plays a role in cell polarity establishment. I speculated that such a role depends on Mod5 not only binding to Tea3, but also promoting Tea3 incorporation into the cluster-network. Although Tea3 is dispensable for the formation of the cluster-network, evidence shown here supports the idea of Tea3 being a structural component of the Tea1 cluster-network. FRAP analysis showed that in a *tea3Δ* mutant, Mod5 diffuses not only within the cluster-network, like in wild-type cells, but also across the cluster-network. This suggested that Tea3 could have a non-essential compaction role in the cluster-network by bringing Tea1 clusters together. The compaction role of Tea3 would be of significance importance during *de novo* formation of the cluster network, because Tea3 could avoid Tea1 “slippage” from the cluster-network upon microtubule-based delivery and thus reinforce cluster-network formation.

To confirm the compaction role of Tea3 in the cluster-network the properties of the cluster should be re-analyzed in a *tea3Δ* mutant. Therefore, the amount and distribution of Tea1 at the cell tip in *tea3Δ* mutants should be measured using live-cell quantitative microscopy. Moreover, Tea1 dynamicity at the cell tip should also be determined by FRAP in a *tea3Δ* mutant. The proposed more sparse distribution of Tea1 and Mod5 single-molecules within the cluster-network in *tea3Δ* mutants could also be analyzed by PALM, as described above. In addition, the changes in the kinetic parameters measured in *tea3Δ* mutants could be incorporated in a refined mathematical model of the formation of the cluster-network. Thus, the compaction role of Tea3 in the cluster-network could be tested *in silico*.

Appendix I: Quantification of Tea1 and Mod5 copy number

A1.1. Quantification of total copy number of Tea1 and Mod5 per cell

The total copy number of Tea1 and Mod5 were determined using quantitative immunoblotting, as previously described (Wu and Pollard, 2005). In this method recombinant versions of Tea1 and Mod5 were used to calibrate the immunoblotting band intensity of the proteins at their endogenous levels.

Concentrations of recombinant Tea1-6xHis and 6xHisMBP-Mod5-(28-447aa) were determined with the BSA calibration curve shown in Figures A1.1 and A1.2, respectively. Tea1-6xHis concentration was determined to be 1 µg/µL and 6xHisMBP-Mod5-(28-447aa) was 300 ng/µL.

Next, Tea1 and Mod5 copy number per cell was determined. Total extracts of wild-type cells were loaded in the same SDS-PAGE gel with known amounts of Tea1-6xHis (Figure A1.1C) or of 6xHisMBP-Mod5-(28-447aa) (Figure A1.2C), mixed with 50 µg of total extract from *tea1Δ* or *mod5Δ* cells, to avoid differences during transfer to the nitrocellulose membrane. Figures A1.1D and A1.2D show the calibration curves of Tea1-6xHis and 6xHisMBP-Mod5(28-447aa), respectively, used to extrapolated the amount of endogenous protein per cell. There are $1.64x10^{-3}$ pg of Tea1 per cell, and $2x10^{-4}$ pg of Mod5. The mass of each protein was converted to number of copies per cell. I found that there are 8000 copies of Tea1 and 2000 copies of Mod5 per cell (Table A2.1).

A1.2. Quantification of Tea1 and Mod5 local concentration using fluorescence microscopy

Once the number of Tea1 and Mod5 molecules per cell was determined, fluorescence microscopy was used to quantify the local concentration of Tea1 and Mod5 at the cell tip. Fluorescence counts were converted to number of molecules using internal controls (Wu and Pollard, 2005). When a protein is GFP-tagged under its endogenous promoter, its fluorescence intensity is a direct readout of its copy number (Wu et al., 2008). This quantitative approached has been used in several studies, such as counting *S. pombe* proteins involved in cytokinesis (Wu and Pollard, 2005), or in the definition of the molecular architecture of proteins in *S. cerevisiae* kinetochore (Joglekar et al., 2006).

Figure A1.3A depicts the imaging acquisition protocol used for quantification. The entire cell volume (12 z-sections spaced with 0.6 µm intervals), of untagged cells and cells expressing Tea1-GFP and GFP-Mod5, was acquired with the same exposure time. The images were corrected for offset and uneven illumination as described (Wu and Pollard, 2005). Offset illumination results from camera electronic noise. It was corrected by subtracting from the image of interest an image acquired under the same conditions, but without illumination. Uneven illumination across the field of view was corrected by defining the illumination ratio across the field of view. Recombinant GFP was imaged under the same conditions as the samples and divided by the maximum pixel intensity of the entire image. The subtracted images were divided by the ratio of illumination across the field of view. After illumination correction, the images of the samples were sum projected and used for quantification.

The integrated fluorescence intensity of entire cells was determined and the cell background (cytoplasm auto-fluorescence) was corrected by subtracting integrated fluorescence intensity of untagged cells from integrated fluorescence intensity of cells expressing Tea1-GFP and GFP-Mod5. The corrected integrated fluorescence intensity of Tea1-GFP and GFP-Mod5 cells was converted to total number of molecules per cell, as determined by quantitative immunoblotting.

Total integrated fluorescence intensity was then used to determine copy number of Tea1 and Mod5 specifically localized at the cell tip. To quantify the cell tip-associated fluorescence intensity the cell geometry was taken into consideration. Figure A1.3A shows a cartoon of the cell geometry. If the cell tip is a perfect half-sphere with an infinitely thin surface, the fluorescence intensity of its surface corresponds to the protein associated with the cell tip (Figure A1.3B).

The corrected images of Tea1-GFP and GFP-Mod5 described above were used to measure the fluorescence intensity at the cell tip. Figure 3B shows the three regions of interest (ROI) measured; each of these has with the same area. ROI **A** contains fluorescence signal from the image background only. ROI **B** contains fluorescence signal from the cell tip, the cytoplasm and image background. The fluorescence intensity contribution from the cell is the projection of a half-sphere with radius *r*. ROI **C** contains fluorescence signal from the cytoplasm and from the image background. The contribution from cytoplasm is the projection of a cylinder with radius *r* and length *r*.

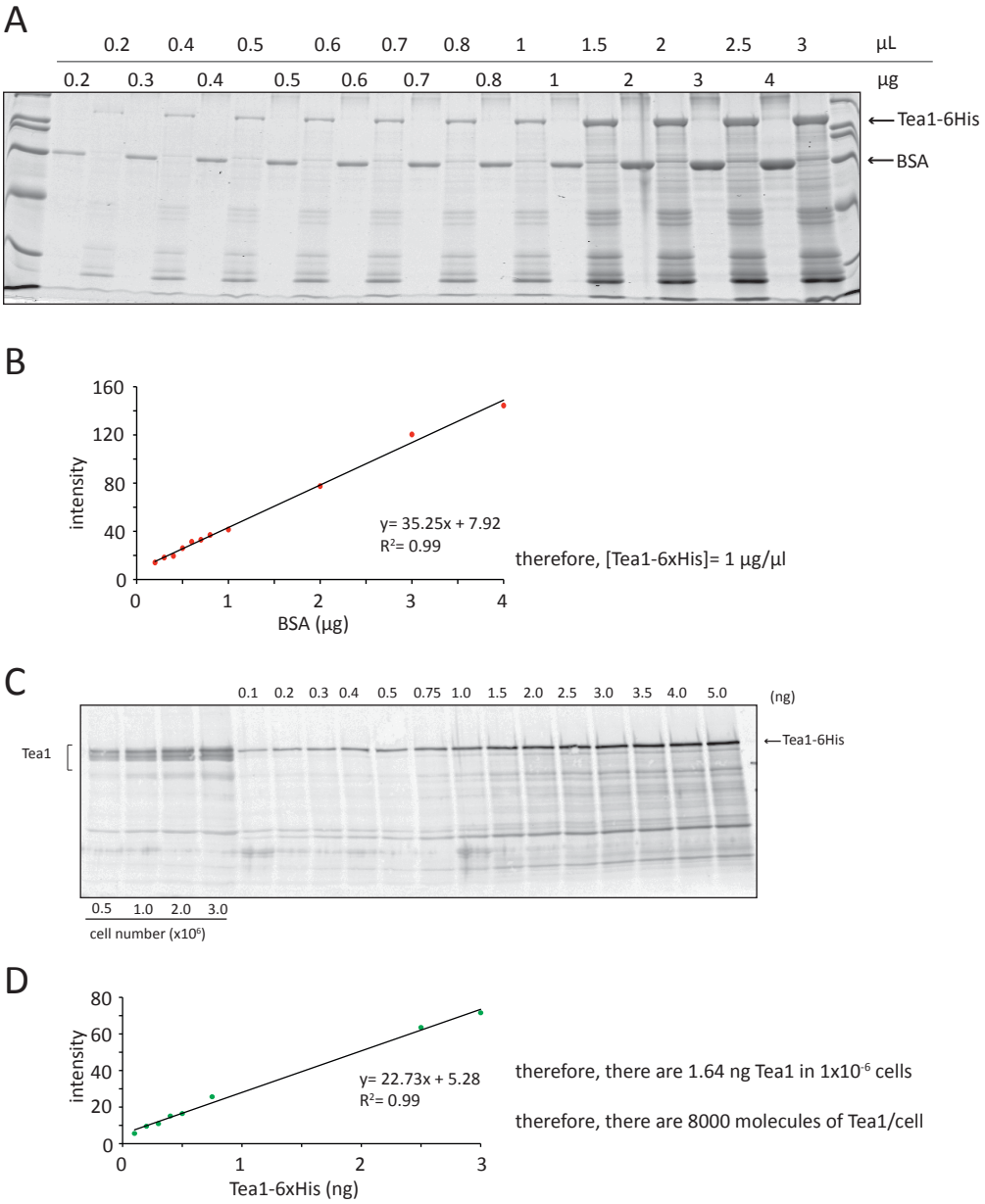

Figure A1.1- Measurement of total copy number of Tea1 molecules per cell. A) Coomassie-stained SDS-PAGE showing the loading of known amounts of BSA and known volumes of recombinant Tea1-6xHis. **B)** BSA calibration curve used to convert band intensity into protein amount. **C)** Known amounts of Tea1-6xHis mixed with 50 µg of *tea1Δ* cell extract, and total extracts of wild-type cells were analysed by Western blot. Samples were probed with affinity purified sheep anti-Tea1 antibody. Band intensity was determined using an Odyssey scanner. **D)** Tea1-6His calibration curve, used to convert intensity of Tea1 bands to amount of Tea1 per number of cells. Using the Avogadro constant, number of Tea1 molecules per cells was determined to be ~8000.

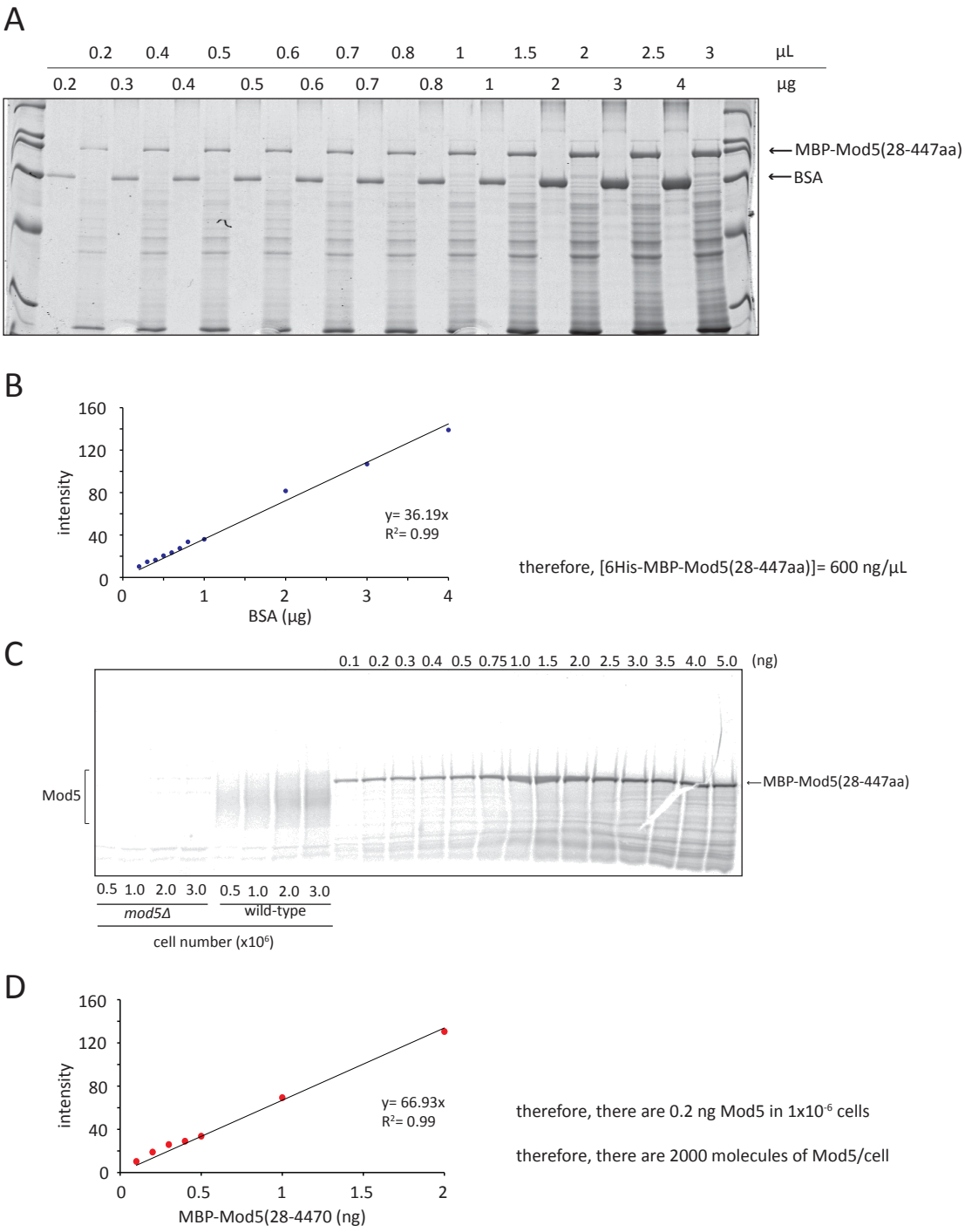

Figure A1.2-Measurement of total copy number of Mod5 molecules per cell. A) Coomassie-stained SDS-PAGE gel showing the loading of known amounts of BSA and known volumes of recombinant 6xHis-MBP-Mod5(28-447). **B)** BSA calibration curve used to convert band intensity into protein amount. **C)** Known amounts of 6xHis-MBP-Mod5(28-447) mixed with *mod5Δ* cell extract, and total extracts of *mod5Δ* and wild-type cells were analyzed by Western blot. Samples were probed with an affinity-purified sheep anti-Mod5 antibody. Band intensity was determined using an Odyssey scanner. **D)** 6His-MBP-Mod5(28-447) calibration curve, used to convert intensity of Mod5 bands to amount of Mod5 per number of cells. Using the Avogadro constant, number of Mod5 molecules per cells was determined to be ~2000.

The cell tip associated signal, named **S**, is measured in ROI **B** after subtracting the contribution of signal from the image background and from the cytoplasm. The fractional contributions of image background and cytoplasm to the total signal of ROI **B** can be determined from geometric considerations. The volume of a half-sphere is 2/3 πr^3 and the volume of a half-cube is $4r^3$.

(1) $$S = B - (\frac{4r^3 - \frac{2}{3}\pi r^3}{4r^3})A - (\frac{\frac{2}{3}\pi r^3}{4r^3})D$$

In (1), *D* is an imaginary half-cube containing only cytosolic signal. *D* was calculated by considering that when *C* is measured it is made up of contributions from *D* and from *A*:

(2) $$C = (\frac{\pi r^2}{4r^2})D + (\frac{4r^2 - \pi r^2}{4r^2})A$$

D can be substituted in (1) and the expression for *S* then simplifies to:

$$S = B - \frac{A}{3} - \frac{2C}{3}$$

The fluorescence intensity at the cell tip, determined in this manner was then converted to local number of molecules, using the ratio of cell-tip fluorescence to cell fluorescence. There are 1510 ± 500 (mean ± SD) molecules of Tea1 and 380 ± 200 (mean ± SD) molecules of Mod5 per cell tip.

A1.3. Measurement of number of Tea1 molecules per packets using fluorescence intensity

The number of Tea1 molecules per microtubule-associated packet was determined using single confocal z-sections of corrected images. Cell background was corrected by subtracting the fluorescence intensity of a region in the cytoplasm with the same area as the Tea1 packet. Fluorescence intensity of Tea1 per packet was converted to number of molecules using conversion factors from analysis above. There are 81 ± 25 (mean ± SD) Tea1 molecules per packet.

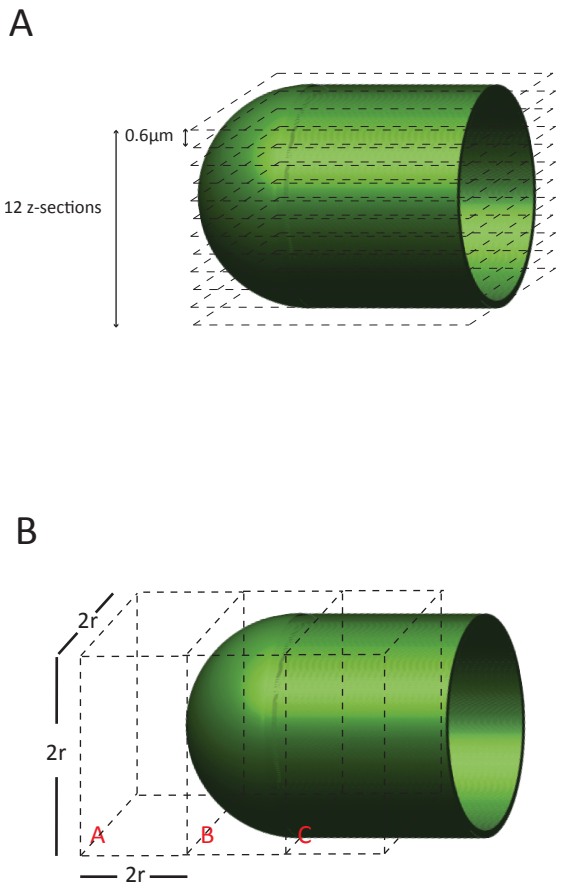

Figure A1.3-Measurement of number of Tea1 and Mod5 molecules per cell tip. A) Measurement of total cell intensity. Schematic diagram of imaging conditions used to acquire the entire cell volume. **B) Schemactic diagram of strategy to determine integrated fluorescence intensity at the cell tip.** The cell tip region was divided in three ROI with the same area: ROI **A** includes the image background, ROI **B** includes the cell tip associated signal, image background and cytoplasm signal, ROI **C** includes the cytoplasm signal and image background.

Appendix II: Formalization of the mathematical and computational implementation of the model described in Chapter III

The mathematical formalization described in this appendix is not of my responsibility and was performed by Dr Andrew Goryachev from the Center for Systems Biology at University of Edinburgh.

A2.1. Formalization of the model and computational implementation

Tea1-Mod5 interaction at the cell tip was modeled based on experimental evidence described in Chapter III. In the model, Tea1 is targeted by microtubulesto the cell tip and is present at the cell tip in cluster-networks. Mod5 promotes the formation of Tea1-Tea1 "bonds" and is restricted to the cell tip due to a diffusion-capture mechanism. It is known that Tea1 has several binding partners and can form complexes with a range of molecular weights (Glynn et al., 2001). However, such interactions are not critical for the model behavior and if they form "bridges" between Tea1 molecules in the cluster-network, these can also be counted as Tea1-Tea1 "bonds". In Chapter III, evidence for Tea1-Tea1 interaction was presented, as well as evidence for the absence of Mod5-Mod5 interactions. Evidence for Tea1-Mod5 interactions has already been shown elsewhere (Snaith et al., 2005). Figure 3.9A shows the kinetic model used to formalize Tea1-Mod5 interaction at the cell tip. Formation of a Tea1 cluster-network is dependent on Tea1 deposition at the cell membrane upon microtubule contact with the cell tip and consequent microtubule depolymerization. T_{MT} describes Tea1 delivered to the cell tip at a rate constant k_0. Once Tea1 is at the cell membrane (T_{mem}) it either remains there because it has a certain affinity to the cell membrane, or it is recycled back to the cytoplasm (T_{cyt}) with a rate constant k_2. T_{cyt} can become microtubule associated an unlimited number of times. T_{mem} can also bind reversibly (k_1/k_{-1}) membrane-associated Mod5 ($Mod5_{mem}$) (Figure 3.9B i). When present in the bimolecular complex Tea1·Mod5 (*TM*), Tea1 can form reversible bonds (k_3,k_{-3}) with other *TM* bimolecular complexes or with Tea1 in the polymeric form (*P*) (Figure 9B ii). The latter reaction is not restricted to be direct Tea1-Tea1 intractions and can, for example, represent bridges by other Tea1 interactors.

To ensure polymerization beyond linear polymers each Tea1 molecule was assumed to form at least three bonds. Mod5 binding to the polymer is designated M_{pol} and according to our hypothesis, Mod5 readily associates with and dissociates from the polymeric network. In the polymeric network each Mod5 molecule can only bind one molecule of Tea1, thus at

any given localization within the polymer $T_{pol} \geq M_{pol}$. Since lifting this restriction resulted in model behavior that contradicted experimental results (data not shown), we adopted the above inequality and the underlying stoichiometric assumption as the most consistent with the available data.

In considering dissociation of Tea1-Tea1 bonds, we recognized three distinct potential outcomes. First, Tea1 can dissociate from the polymer as a Tea1 monomer (outcome 1). Second, Tea1 can dissociate from the polymer in a bimolecular complex with Mod5, *TM* (outcome 2). And third Tea1 does not dissociate from the polymer but changes Tea1 network connectivity (outcome 3). In the simulations, Tea1 dissociation as a monomer (outcome 1) did not alter qualitatively the model behavior. There were no experimental evidences for monomeric Tea1 dissociation therefore, and to reduce modeling complexity, it was omitted from the mechanism. Outcome 2, *TM* dissociation, was considered as the main pathway for polymer remodeling and fluidity. The probability of *TM* dissociation is proportional to the local concentration of polymerized Mod5 ($Mod5_{pol}$). Outcome 3 describes the formation and the dissociation of Tea1-Tea1 "bonds" that alter the connectivity of the network, but not affect the existence of the network. These events were not registered in the model context. This approach is similar to what is commonly followed in modeling actin dynamics (Carlsson and Sept, 2008). It bypasses the necessity of considering an infinite number of molecular species representing all possible stoichiometric complexes. The decrease in detail to describe all the molecular species also averages all fluctuations in the spatial density of Tea1 within the cluster-networks. The concentrations profiles obtained from simulations and presented throughout the Chapter III therefore represent the average of all the microscopic events over many stochastic realizations. The averaging in simulation allows comparison with population-averaged experimental measurements.

Using the mass-action rate law formalism, the above reaction mechanism can be summarized as a system of five coupled reaction-diffusion equations:

$$\begin{aligned}
\dot{M}_m &= k_{-1}TM - k_1 T_m \cdot M_m + k_{-1}M_p - k_1 M_m \cdot (T_p - M_p) + D_m \Delta M_m \\
\dot{T}_m &= F(r, T_{cyt}) + k_{-1}TM - k_1 T_m \cdot M_m - k_2 T_m + D_m \Delta T_m \\
\dot{TM} &= k_1 T_m M_m - k_{-1}TM - 2k_3 TM^2 + k_{-3}M_p - k_3 TM \cdot T_p + D_m \Delta TM \\
\dot{M}_p &= 2k_3 TM^2 + k_3 TM \cdot T_p - k_{-3}M_p + k_1 M_m \cdot (T_p - M_p) - k_{-1}M_p + D_p \Delta M_p \\
\dot{T}_p &= 2k_3 TM^2 + k_3 TM \cdot T_p - k_{-3}M_p + D_p \Delta T_p
\end{aligned} \quad (1)$$

In the equations, subscripts *mem* and *pol* have been reduced respectively to *m* and *p* for brevity. To enforce the inequality $M_{pol} \leq T_{pol}$, the incorporation of monomeric Mod5 into the polymeric network is given by $k_1 M_m \cdot (T_p - M_p)$. Microtubule-based delivery of Tea1 to the membrane is represented by the term $F\ (r,\ T_{cyt})$, which is a function of the spatial location on the membrane and the amount of Tea1 in the cytoplasm.

The number of molecules of Tea1 and Mod5 were converted to concentration at the cell membrane. Calculations of concentrations were computed per membrane volume, V_{mem}. Following an approach previously developed (Goryachev and Pokhilko, 2008; Kholodenko et al., 2000), V_{mem} represents a thin ($h \approx$ 10 nm) layer of the cytoplasm immediately below the membrane. *S. pombe* cell geometry was considered to be represented by a spherocylinder. The average diameter and length of *S. pombe* cells, in a growing population, were measured and found to be 4 µm and 11 µm, respectively. This results in a geometric cell volume (V) of 121.5 μm^3 and a cell surface (S) of 138 μm^2. Therefore, $V_{mem} = S \cdot h$ = 1.38 μm^3 and 1000 molecules per V_{mem} result in a concentration of 1.2 µM.

In our simulations we considered *de novo* formation of the cluster-networks. Therefore at the beginning of the simulations the entire Tea1 pool (8000 molecules/cell) is present in the cytoplasm.

During our experiments we realized that a fraction of the cell pool of GFP-Mod5 is not membrane-bound and was detected in the cytoplasm and/or in the vacuoles. However, FRAP data shown that the non-membrane-bound pool of Mod5 does not dynamically exchange with the membrane-bound pool. Therefore, for modeling proposes the non-membrane-bound fraction of Mod5 was discarded. The unknown initial concentration of membrane-bound Mod5 ($Mod5_{mem}$) was varied in the simulations, to fit the experimental data.

The diffusion coefficient of monomeric Mod5 was estimated from the FRAP data of GFP-Mod5 in *tea1Δ* to be $D_{mem} \approx$ 0.05 μm^2/sec. For simplicity, diffusion coefficients of T_{mem} and *TM* were assumed to be equal to D_{mem}. Diffusion coefficient of Tea1-Mod5 polymer was taken to be much slower. In order to achieve the best fit with the experimental data D_{pol} was varied between 10^{-6} and 10^{-3} μm^2/sec.

Microtubule-based delivery of Tea1 was described with a Tea1 input function. Experimental observations indicated that when Tea1 does not accumulate at cell tips, more

Tea1 is delivered on microtubules per unit of time, suggesting that Tea1 accumulation at the cell tip limits the number of microtubule-delivered Tea1 molecules to the cell tip. Therefore, the number of Tea1 molecules delivered is proportional to Tea1 pool in the cytoplasm. The Tea1 input function can be formalized as:

(2) $$F(r, T_{cyt}) = k_0 \left(1 - \int_S T_{mem} dS / T_{tot}\right) f(r),$$

In (2) T_{tot} is the total cellular Tea1, the integral represents the overall amount of Tea1 on the membrane, k_0 is the maximal intensity of Tea1 input at the initiation of cluster-network formation, and *f(r)* is the non-dimensional spatial function with values in the interval (0,1) that represents the microtubule target zone.

Experimental measurements demonstrated that at steady state (*ss*), microtubules deliver Tea1 to the cell tip at a rate of ~ 80 molecules/min (see details in Appendix I). This delivery corresponds to k_{ss}~ 0.01 µM/sec for the chosen cell geometry. Therefore according to (2), the expected maximal intensity of Tea1 input is $k_0 = k_{ss}/T^{ss}_{cyt}$, where T^{ss}_{cyt} is the fraction of Tea1 in the cytoplasm at the steady state.

There are technical constraints to measuring the spatial probability density function of Tea1 delivery experimentally. Therefore, it was assumed that the probability of microtubules encountering the surface of the hemispherical cell tips is uniformly distributed everywhere, except in the sphere-to–cylinder transition zone. In that zone, the probability of delivery drops rapidly.

Tea1 input was simulated in two ways. First, Tea1 considered to be delivered as a continuous flux, described by (2). Second, Tea1 was taken as uniformly delivered in discrete packets, deposited at random locations. After fitting the model, it was chosen to begin the packets delivery with 116 molecules of Tea1. As Tea1 accumulates at the cell tips, the number of Tea1 molecules per packet was proportionally decreased, as specified in (2). The simulations with discrete packet delivery result in a stochastic steady state. The steady state changes perpetually with the continued arrival of microtubule-delivered packets to the cell tips. These steady states were average over a period of time or over several independent realizations (the equivalent to experimental population average). The results obtained show an evolution to steady state at a rate comparable to that obtained in the simulations with continuous Tea1 input (2). This shows that the two methods of simulating Tea1 delivery are equivalent. However, the continuous input (2) provides a population-

averaged steady state. This not only has the advantage of averaging Tea1 deposition over multiple stochastic realizations, but also of saving computational cost.

Model (1), with the Tea1 input function (2) was numerically integrated using a standard finite difference algorithm implemented as a custom C code. The used parameters are defined as described above and summarized in the Table A2.1.

In order to leverage cylindrical symmetry of the system with continuous Tea1 input, simulations were either performed in 1D or in 2D. In 1D simulations, the plasma membrane is represented as a cross section of a circumference. Simulations in 1D not only show a good agreement with 2D simulations, but also are significantly less computationally expensive. To reduce computational expenses even further, most of the simulations were performed using only one half of the cell. As described below, the half-cell approach was not used in the FRAP simulations.

Table A2.1- Parameters of the Tea1-Mod5 cluster-network model

Constant	Value/Range	Optimized value*
k_0	(0.009-0.02) $\mu M.s^{-1}$	0.016 $\mu M.s^{-1}$or 116 molecules/packet
k_1	(0.1-10) $\mu M^{-1}.s^{-1}$	2 $\mu M^{-1}.s^{-1}$
k_{-1}	(0.1-10) s^{-1}	3 s^{-1}
k_2	(0.007-0.7) s^{-1}	0.07 s^{-1}
k_3	(0.01-0.9) $\mu M^{-1}.s^{-1}$	0.21 $\mu M^{-1}.s^{-1}$
k_{-3}	(0.001-0.1) s^{-1}	0.03 s^{-1}
Tea1 *total*	8000 molecules/cell	-
Mod5 *total*	2000 molecules/cell	-
M^0_{mem}	(0.72-2.4) μM	1.7 µM
D_m	0.05 $\mu m^2.s^{-1}$	-
D_p	(10-3-10-6) $\mu m^2.s^{-1}$	10-4 $\mu m^2.s^{-1}$

* Model parameters were varied in the indicate ranges to obtain optimal fit with the experimental data

A2.2. Simulation of FRAP curves

FRAP curves were computationally simulated using the parameters described in Table A2.1. The modeling of FRAP curves was a useful tool to fine-tune the model parameters to the experimental data.

To model FRAP curves, additional variables representing bleached species were introduced to the model. The chemical properties of the bleached species are the same as for the unbleached species. For example, the concentration of the bleached Tea1 molecules incorporated into the cluster-network, T^B_{pol}, is given by:

$$\dot{T}_p^B = k_3 TM^B(2TM^B + TM) + k_3 TM^B(T_p + T_p^B) - k_{-3} M_p \frac{T_p^B}{T_p + T_p^B} + D_p \Delta T_p^B$$

The initial concentrations for the FRAP modeling were computed by applying a bleaching efficiency profile to the steady state solution of the equations in (1). The bleaching efficiency profile was derived from the profile of the intensity of the laser beam used in the FRAP experiments. The laser used had a Gaussian intensity profile characterized by the beam diameter at half maximum intensity (1.42 µm for the full-tip FRAP experiments and 0.774 µm for the half-tip FRAP). Two separate input functions for the bleached and unbleached Tea1 were introduced to take into the consideration their microtubule-mediated membrane-cytoplasmic shuttling. The whole-cell model was used to perform FRAP simulation, so the contribution of the unbleached cluster-network present in the opposite cell tip was included in the fluorescence recovery.

A2.3. Calculation of incorporation efficiency

To calculate the efficiency of Tea1 incorporation into cluster-networks all Tea1-containing species present at the membrane were photobleached *in silico*. At the time of *in silico* photobleaching the system was at steady state with Tea1-packet input. The cell tip was divided in sub areas, and only Tea1-packets incorporated in a given sub area were considered to contribute to 'unbleached' Tea1. The kinetics of accumulation of 'unbleached' Tea1 within the chosen sub-area was monitored and average over a number of simulations. After averaging over multiple stochastic realizations, the accumulation curves could be fitted to a single-exponential function of the type $A[1-\exp(-t/\tau)]$. The absolute rate of incorporation averaged per tested area (in molecules/min) is then given simply by A/τ. To obtain the incorporation efficiency of a tested sub-area, as a fraction of 1, the absolute rate of incorporation averaged per tested area was normalized by the computed total rate of Tea1 delivery at steady state and further by the ratio of the tested area to the total area of the microtubules target zone.

A2.4. Calculation of polymerization reaction flux

In order to determine the spatial distribution of the T_{pol} polymerization reaction flux within the cluster network, the reaction fluxes shown in Figure 14B were computed at steady state. From (1), the steady state reaction flux was computed as $2k_3TM^2 + k_3TM \cdot T_p - k_{-3}M_p$, where all the variables correspond to their local steady state concentrations. Because the cluster-network concentration profiles are associated with spatial gradients, T_{pol} steady state diffusive flux is different from zero, and thus $D_{pol}/\Delta T_{pol} \neq 0$. However at steady state dT_{pol}/dt is zero and therefore, from the equation in (1), the diffusive flux must be exactly compensated by the local reaction flux.

Appendix III-List of Tea1 phospho-residues identified by MS.

wt exp #1	wt exp #2	*mod5Δ+MBC*	*tip1Δ299 mod5Δ*	*tea1Δ200*	*tea3Δ tea4Δ bud6Δ*	*pom1Δ*	*orb2-34*	*win1Δ wis4Δ*
	S11			S11				
					S21			
	T25							
					T26		T26	
S38								
		T55		T55	T55			
		S59						
	T62	T62	T62					
	S64			S64	S64	S64		
			S67					
				S421				
	T70							
					S425			
S434				T452			T452	
							Y438	
S442								
					S444			
		T448				T448		
					T452			
S454								
		T455				T455	T455	T455
S458	S458		S458		S458			S458
S462	S462	S462	S462		S462	S462	S462	S462
S467	S467	S467	S467	S467	S467	S467	S467	S467
S474		S474	S474					
S476	S476	S476	S476	S476	S476	S476	S476	S476
S477								S477
S478					S478	S478	S478	
			S483		S483			
		Y484	Y484					Y484
						S488		
	S491		S491			S491	S491	
			T496		T496			T496
S502								
S503			S503	S503	S503	S503	S503	
S506							S506	
S510								
							S524	
S553				S553			S553	
S556			S556	S556				
S558							S558	
S561								
				S569				
							S570	
S579			S579	S579			S579	
S586	S586						S586	
							T585	
S663							S663	S663
T664							T664	T664
		S658	S658					
		T661	T661		T661	T661		
		S663			S663			
		T664	T664					
								S672
		S972						
S1000								
							S1053	
							S1058	
							T1061	
S1068							S1068	
		S1082		S1082				
		S1086						
		S1088						
					S1109		S1109	
			S1111				S1111	

Appendix IV: Description of column titles in Tables 5.1, 5.3 and 5.4

The MaxQuant Software defines the column titles. This list was adapted from (de Godoy et al., 2008)

- *Protein IDs:* The identifier of the *S. pombe* open reading frame (ORF)
- *Protein Description:* Short description of the protein
- *G1/S : G2 SILAC ratio:* SILAC Ratio of protein abundances in the G1/S and G2 as determined by the MaxQuant software.
- *Peptides (seq):* Number of peptides contained in the protein, where only peptides differing in sequence are counted as distinct peptides
- *Unique Peptides (seq):* Number of unique peptides contained in the protein, where only peptides differing in sequence are counted as distinct peptides
- *Sequence Coverage [%]:* The percentage of sequence positions covered by measured peptides
- *Mol. Weight [kDa]:* The molecular weight of the protein in kilodaltons
- *Sequence Length:* The amino acid length of the protein sequence
- *FPR:* False positive rate of the protein as calculated by the MaxQuant software
- *Ratio H/L Normalized:* Normalized SILAC ratio („heavy" divided by „light") of the protein
- *Ratio H/L Significance (B):* p-value indicating significance of up or down regulation of the protein
- *Ratio H/L Count:* Number of quantitation events used for quantifying this protein
- *Intensity:* Summed peptide XICs for all measured isotope patterns
- *Intensity L:* Summed peptide XICs only for the „light" versions of peptides
- *Intensity H:* Summed peptide XICs only for the „heavy" versions of peptides

References

Adams, J., R. Kelso, and L. Cooley. 2000. The kelch repeat superfamily of proteins: propellers of cell function. *Trends Cell Biol*. 10:17-24.

Akhmanova, A., and C.C. Hoogenraad. 2005. Microtubule plus-end-tracking proteins: mechanisms and functions. *Curr Opin Cell Biol*. 17:47-54.

Akhmanova, A., and M.O. Steinmetz. 2008. Tracking the ends: a dynamic protein network controls the fate of microtubule tips. *Nat Rev Mol Cell Biol*. 9:309-22.

Altschuler, S.J., S.B. Angenent, Y. Wang, and L.F. Wu. 2008. On the spontaneous emergence of cell polarity. *Nature*. 454:886-9.

Alvarez-Tabares, I., A. Grallert, J.M. Ortiz, and I.M. Hagan. 2007. Schizosaccharomyces pombe protein phosphatase 1 in mitosis, endocytosis and a partnership with Wsh3/Tea4 to control polarised growth. *J Cell Sci*. 120:3589-601.

Anderson, C. 2002. Self-organization in relation to several similar concepts: are the boundaries to self-organization indistinct? *Biol Bull*. 202:247-55.

Aratyn, Y.S., T.E. Schaus, E.W. Taylor, and G.G. Borisy. 2007. Intrinsic dynamic behavior of fascin in filopodia. *Mol Biol Cell*. 18:3928-40.

Arellano, M., T. Niccoli, and P. Nurse. 2002. Tea3p is a cell end marker activating polarized growth in Schizosaccharomyces pombe. *Curr Biol*. 12:751-6.

Bahler, J., and P. Nurse. 2001. Fission yeast Pom1p kinase activity is cell cycle regulated and essential for cellular symmetry during growth and division. *EMBO J*. 20:1064-73.

Bahler, J., and J.R. Pringle. 1998. Pom1p, a fission yeast protein kinase that provides positional information for both polarized growth and cytokinesis. *Genes Dev*. 12:1356-70.

Barth, A.I., H.Y. Caro-Gonzalez, and W.J. Nelson. 2008. Role of adenomatous polyposis coli (APC) and microtubules in directional cell migration and neuronal polarization. *Semin Cell Dev Biol*. 19:245-51.

Basu, R., and F. Chang. 2007. Shaping the actin cytoskeleton using microtubule tips. *Curr Opin Cell Biol*. 19:88-94.

Behrens, R., and P. Nurse. 2002. Roles of fission yeast tea1p in the localization of polarity factors and in organizing the microtubular cytoskeleton. *J Cell Biol*. 157:783-93.

Bement, W.M., H.A. Benink, and G. von Dassow. 2005. A microtubule-dependent zone of active RhoA during cleavage plane specification. *J Cell Biol*. 170:91-101.

Bendall, S.C., C. Hughes, M.H. Stewart, B. Doble, M. Bhatia, and G.A. Lajoie. 2008. Prevention of amino acid conversion in SILAC experiments with embryonic stem cells. *Mol Cell Proteomics*. 7:1587-97.

Bieling, P., L. Laan, H. Schek, E.L. Munteanu, L. Sandblad, M. Dogterom, D. Brunner, and T. Surrey. 2007. Reconstitution of a microtubule plus-end tracking system in vitro. *Nature*. 450:1100-5.

Birkenbihl, R.P., and S. Subramani. 1995. The rad21 gene product of Schizosaccharomyces pombe is a nuclear, cell cycle-regulated phosphoprotein. *J Biol Chem*. 270:7703-11.

Boddy, M.N., and P. Russell. 1999. DNA replication checkpoint control. *Front Biosci*. 4:D841-8.

Bonaldi, T., T. Straub, J. Cox, C. Kumar, P.B. Becker, and M. Mann. 2008. Combined use of RNAi and quantitative proteomics to study gene function in Drosophila. *Mol Cell*. 31:762-72.

Brouhard, G.J., J.H. Stear, T.L. Noetzel, J. Al-Bassam, K. Kinoshita, S.C. Harrison, J. Howard, and A.A. Hyman. 2008. XMAP215 is a processive microtubule polymerase. *Cell*. 132:79-88.

Browning, H., D.D. Hackney, and P. Nurse. 2003. Targeted movement of cell end factors in fission yeast. *Nat Cell Biol*. 5:812-8.

Brunner, D., and P. Nurse. 2000. CLIP170-like tip1p spatially organizes microtubular dynamics in fission yeast. *Cell*. 102:695-704.

Buck, V., S.S. Ng, A.B. Ruiz-Garcia, K. Papadopoulou, S. Bhatti, J.M. Samuel, M. Anderson, J.B. Millar, and C.J. McInerny. 2004. Fkh2p and Sep1p regulate mitotic gene transcription in fission yeast. *J Cell Sci*. 117:5623-32.

Busch, K.E., and D. Brunner. 2004. The microtubule plus end-tracking proteins mal3p and tip1p cooperate for cell-end targeting of interphase microtubules. *Curr Biol*. 14:548-59.

Busch, K.E., J. Hayles, P. Nurse, and D. Brunner. 2004. Tea2p kinesin is involved in spatial microtubule organization by transporting tip1p on microtubules. *Dev Cell*. 6:831-43.

Busso, D., B. Delagoutte-Busso, and D. Moras. 2005. Construction of a set Gateway-based destination vectors for high-throughput cloning and expression screening in Escherichia coli. *Anal Biochem*. 343:313-21.

Carazo-Salas, R.E., C. Antony, and P. Nurse. 2005. The kinesin Klp2 mediates polarization of interphase microtubules in fission yeast. *Science*. 309:297-300.

Carlsson, A.E., and D. Sept. 2008. Mathematical modeling of cell migration. *Methods Cell Biol*. 84:911-37.

Carvalho, P., J.S. Tirnauer, and D. Pellman. 2003. Surfing on microtubule ends. *Trends Cell Biol*. 13:229-37.

Celton-Morizur, S., V. Racine, J.B. Sibarita, and A. Paoletti. 2006. Pom1 kinase links division plane position to cell polarity by regulating Mid1p cortical distribution. *J Cell Sci*. 119:4710-8.

Chang, F., D. Drubin, and P. Nurse. 1997. cdc12p, a protein required for cytokinesis in fission yeast, is a component of the cell division ring and interacts with profilin. *J Cell Biol*. 137:169-82.

Cheeseman, I.M., C. Brew, M. Wolyniak, A. Desai, S. Anderson, N. Muster, J.R. Yates, T.C. Huffaker, D.G. Drubin, and G. Barnes. 2001. Implication of a novel multiprotein Dam1p complex in outer kinetochore function. *J Cell Biol*. 155:1137-45.

Chesarone, M.A., A.G. DuPage, and B.L. Goode. 2010. Unleashing formins to remodel the actin and microtubule cytoskeletons. *Nat Rev Mol Cell Biol*. 11:62-74.

Coffey, D.S. 1998. Self-organization, complexity and chaos: the new biology for medicine. *Nat Med*. 4:882-5.

Cox, J., and M. Mann. 2008. MaxQuant enables high peptide identification rates, individualized p.p.b.-range mass accuracies and proteome-wide protein quantification. *Nat Biotechnol*. 26:1367-72.

de Godoy, L.M., J.V. Olsen, J. Cox, M.L. Nielsen, N.C. Hubner, F. Frohlich, T.C. Walther, and M. Mann. 2008. Comprehensive mass-spectrometry-based proteome quantification of haploid versus diploid yeast. *Nature*. 455:1251-4.

Desai, A., and T.J. Mitchison. 1997. Microtubule polymerization dynamics. *Annu Rev Cell Dev Biol*. 13:83-117.

DeWard, A.D., and A.S. Alberts. 2008. Microtubule stabilization: formins assert their independence. *Curr Biol*. 18:R605-8.

Dixit, R., B. Barnett, J.E. Lazarus, M. Tokito, Y.E. Goldman, and E.L. Holzbaur. 2009. Microtubule plus-end tracking by CLIP-170 requires EB1. *Proc Natl Acad Sci U S A*. 106:492-7.

Drabek, K., M. van Ham, T. Stepanova, K. Draegestein, R. van Horssen, C.L. Sayas, A. Akhmanova, T. Ten Hagen, R. Smits, R. Fodde, F. Grosveld, and N. Galjart. 2006. Role of CLASP2 in microtubule stabilization and the regulation of persistent motility. *Curr Biol*. 16:2259-64.

Dragestein, K.A., W.A. van Cappellen, J. van Haren, G.D. Tsibidis, A. Akhmanova, T.A. Knoch, F. Grosveld, and N. Galjart. 2008. Dynamic behavior of GFP-CLIP-170 reveals fast protein turnover on microtubule plus ends. *J Cell Biol*. 180:729-37.

Drummond, D.R., and R.A. Cross. 2000. Dynamics of interphase microtubules in Schizosaccharomyces pombe. *Curr Biol*. 10:766-75.

Dyson, H.J., and P.E. Wright. 2005. Intrinsically unstructured proteins and their functions. *Nat Rev Mol Cell Biol*. 6:197-208.

Elion, E.A. 2000. Pheromone response, mating and cell biology. *Curr Opin Microbiol*. 3:573-81.

Fantes, P.A., and J. Creanor. 1984. Canavanine resistance and the mechanism of arginine uptake in the fission yeast Schizosaccharomyces pombe. *J Gen Microbiol*. 130:3265-73.

Feierbach, B., and F. Chang. 2001. Roles of the fission yeast formin for3p in cell polarity, actin cable formation and symmetric cell division. *Curr Biol*. 11:1656-65.

Feierbach, B., F. Verde, and F. Chang. 2004. Regulation of a formin complex by the microtubule plus end protein tea1p. *J Cell Biol*. 165:697-707.

Fischer, R., N. Zekert, and N. Takeshita. 2008. Polarized growth in fungi--interplay between the cytoskeleton, positional markers and membrane domains. *Mol Microbiol*. 68:813-26.

Flynn, N.E., C.J. Meininger, T.E. Haynes, and G. Wu. 2002. The metabolic basis of arginine nutrition and pharmacotherapy. *Biomed Pharmacother*. 56:427-38.

Fukata, M., T. Watanabe, J. Noritake, M. Nakagawa, M. Yamaga, S. Kuroda, Y. Matsuura, A. Iwamatsu, F. Perez, and K. Kaibuchi. 2002. Rac1 and Cdc42 capture microtubules through IQGAP1 and CLIP-170. *Cell*. 109:873-85.

Glynn, J.M., R.J. Lustig, A. Berlin, and F. Chang. 2001. Role of bud6p and tea1p in the interaction between actin and microtubules for the establishment of cell polarity in fission yeast. *Curr Biol*. 11:836-45.

Goryachev, A.B., and A.V. Pokhilko. 2008. Dynamics of Cdc42 network embodies a Turing-type mechanism of yeast cell polarity. *FEBS Lett*. 582:1437-43.

Gould, K.L., and V. Simanis. 1997. The control of septum formation in fission yeast. *Genes Dev*. 11:2939-51.

Greenfield, D., A.L. McEvoy, H. Shroff, G.E. Crooks, N.S. Wingreen, E. Betzig, and J. Liphardt. 2009. Self-organization of the Escherichia coli chemotaxis network imaged with super-resolution light microscopy. *PLoS Biol*. 7:e1000137.

Gruhler, A., J.V. Olsen, S. Mohammed, P. Mortensen, N.J. Faergeman, M. Mann, and O.N. Jensen. 2005. Quantitative phosphoproteomics applied to the yeast pheromone signaling pathway. *Mol Cell Proteomics*. 4:310-27.

Guimaraes, G.J., Y. Dong, B.F. McEwen, and J.G. Deluca. 2008. Kinetochore-microtubule attachment relies on the disordered N-terminal tail domain of Hec1. *Curr Biol*. 18:1778-84.

Gundersen, G.G. 2002. Evolutionary conservation of microtubule-capture mechanisms. *Nat Rev Mol Cell Biol*. 3:296-304.

Hayles, J., and P. Nurse. 2001. A journey into space. *Nat Rev Mol Cell Biol*. 2:647-56.

Hirokawa, N., R. Nitta, and Y. Okada. 2009. The mechanisms of kinesin motor motility: lessons from the monomeric motor KIF1A. *Nat Rev Mol Cell Biol*. 10:877-84.

Honnappa, S., S.M. Gouveia, A. Weisbrich, F.F. Damberger, N.S. Bhavesh, H. Jawhari, I. Grigoriev, F.J. van Rijssel, R.M. Buey, A. Lawera, I. Jelesarov, F.K. Winkler, K. Wuthrich, A. Akhmanova, and M.O. Steinmetz. 2009. An EB1-binding motif acts as a microtubule tip localization signal. *Cell*. 138:366-76.

Hoog, J.L., C. Schwartz, A.T. Noon, E.T. O'Toole, D.N. Mastronarde, J.R. McIntosh, and C. Antony. 2007. Organization of interphase microtubules in fission yeast analyzed by electron tomography. *Dev Cell*. 12:349-61.

Howell, A.S., N.S. Savage, S.A. Johnson, I. Bose, A.W. Wagner, T.R. Zyla, H.F. Nijhout, M.C. Reed, A.B. Goryachev, and D.J. Lew. 2009. Singularity in polarization: rewiring yeast cells to make two buds. *Cell*. 139:731-43.

http://old.genedb.org/genedb/pombe/.

http://www.geneontology.org/.

Huang, Y., T.G. Chew, W. Ge, and M.K. Balasubramanian. 2007. Polarity determinants Tea1p, Tea4p, and Pom1p inhibit division-septum assembly at cell ends in fission yeast. *Dev Cell*. 12:987-96.

Hutterer, A., M. Glotzer, and M. Mishima. 2009. Clustering of centralspindlin is essential for its accumulation to the central spindle and the midbody. *Curr Biol*. 19:2043-9.

Hwang, E., J. Kusch, Y. Barral, and T.C. Huffaker. 2003. Spindle orientation in Saccharomyces cerevisiae depends on the transport of microtubule ends along polarized actin cables. *J Cell Biol*. 161:483-8.

Iden, S., and J.G. Collard. 2008. Crosstalk between small GTPases and polarity proteins in cell polarization. *Nat Rev Mol Cell Biol*. 9:846-59.

Iglesias, P.A., and P.N. Devreotes. 2008. Navigating through models of chemotaxis. *Curr Opin Cell Biol*. 20:35-40.

Jaffe, A.B., and A. Hall. 2005. Rho GTPases: biochemistry and biology. *Annu Rev Cell Dev Biol*. 21:247-69.

Janson, M.E., R. Loughlin, I. Loiodice, C. Fu, D. Brunner, F.J. Nedelec, and P.T. Tran. 2007. Crosslinkers and motors organize dynamic microtubules to form stable bipolar arrays in fission yeast. *Cell*. 128:357-68.

Joglekar, A.P., D.C. Bouck, J.N. Molk, K.S. Bloom, and E.D. Salmon. 2006. Molecular architecture of a kinetochore-microtubule attachment site. *Nat Cell Biol*. 8:581-5.

Kamasaki, T., R. Arai, M. Osumi, and I. Mabuchi. 2005. Directionality of F-actin cables changes during the fission yeast cell cycle. *Nat Cell Biol*. 7:916-7.

Kang, P.J., A. Sanson, B. Lee, and H.O. Park. 2001. A GDP/GTP exchange factor involved in linking a spatial landmark to cell polarity. *Science*. 292:1376-8.

Kardon, J.R., and R.D. Vale. 2009. Regulators of the cytoplasmic dynein motor. *Nat Rev Mol Cell Biol*. 10:854-65.

Karsenti, E. 2008. Self-organization in cell biology: a brief history. *Nat Rev Mol Cell Biol*. 9:255-62.

Kholodenko, B.N., J.B. Hoek, and H.V. Westerhoff. 2000. Why cytoplasmic signalling proteins should be recruited to cell membranes. *Trends Cell Biol*. 10:173-8.

Kim, H., P. Yang, P. Catanuto, F. Verde, H. Lai, H. Du, F. Chang, and S. Marcus. 2003. The kelch repeat protein, Tea1, is a potential substrate target of the p21-activated kinase, Shk1, in the fission yeast, Schizosaccharomyces pombe. *J Biol Chem*. 278:30074-82.

Kim, J.S., and R.T. Raines. 1993. Ribonuclease S-peptide as a carrier in fusion proteins. *Protein Sci*. 2:348-56.

Kim, S.Y., and J.E. Ferrell, Jr. 2007. Substrate competition as a source of ultrasensitivity in the inactivation of Wee1. *Cell*. 128:1133-45.

King, J.S., and R.H. Insall. 2009. Chemotaxis: finding the way forward with Dictyostelium. *Trends Cell Biol*. 19:523-30.

Komarova, Y., C.O. De Groot, I. Grigoriev, S.M. Gouveia, E.L. Munteanu, J.M. Schober, S. Honnappa, R.M. Buey, C.C. Hoogenraad, M. Dogterom, G.G. Borisy, M.O. Steinmetz, and A. Akhmanova. 2009. Mammalian end binding proteins control persistent microtubule growth. *J Cell Biol*. 184:691-706.

Kozubowski, L., K. Saito, J.M. Johnson, A.S. Howell, T.R. Zyla, and D.J. Lew. 2008. Symmetry-breaking polarization driven by a Cdc42p GEF-PAK complex. *Curr Biol*. 18:1719-26.

Kumar, P., K.S. Lyle, S. Gierke, A. Matov, G. Danuser, and T. Wittmann. 2009. GSK3beta phosphorylation modulates CLASP-microtubule association and lamella microtubule attachment. *J Cell Biol*. 184:895-908.

La Carbona, S., C. Le Goff, and X. Le Goff. 2006. Fission yeast cytoskeletons and cell polarity factors: connecting at the cortex. *Biol Cell*. 98:619-31.

Lansbergen, G., and A. Akhmanova. 2006. Microtubule plus end: a hub of cellular activities. *Traffic*. 7:499-507.

Lansbergen, G., I. Grigoriev, Y. Mimori-Kiyosue, T. Ohtsuka, S. Higa, I. Kitajima, J. Demmers, N. Galjart, A.B. Houtsmuller, F. Grosveld, and A. Akhmanova. 2006. CLASPs attach microtubule plus ends to the cell cortex through a complex with LL5beta. *Dev Cell*. 11:21-32.

Lehninger, A.L., D.L. Nelson, and M.M. Cox. 2000. Lehninger principles of biochemistry. Worth Publishers, New York. 1 v. (various pagings) pp.

Li, R., and B. Bowerman. 2010. Symmetry breaking in biology. *Cold Spring Harb Perspect Biol*. 2:a003475.

Li, R., and G.G. Gundersen. 2008. Beyond polymer polarity: how the cytoskeleton builds a polarized cell. *Nat Rev Mol Cell Biol*. 9:860-73.

Lippincott-Schwartz, J., N. Altan-Bonnet, and G.H. Patterson. 2003. Photobleaching and photoactivation: following protein dynamics in living cells. *Nat Cell Biol*. Suppl:S7-14.

Lippincott-Schwartz, J., E. Snapp, and A. Kenworthy. 2001. Studying protein dynamics in living cells. *Nat Rev Mol Cell Biol*. 2:444-56.

Loiodice, I., J. Staub, T.G. Setty, N.P. Nguyen, A. Paoletti, and P.T. Tran. 2005. Ase1p organizes antiparallel microtubule arrays during interphase and mitosis in fission yeast. *Mol Biol Cell*. 16:1756-68.

Loo, T.H., and M. Balasubramanian. 2008. Schizosaccharomyces pombe Pak-related protein, Pak1p/Orb2p, phosphorylates myosin regulatory light chain to inhibit cytokinesis. *J Cell Biol*. 183:785-93.

Manley, S., J.M. Gillette, G.H. Patterson, H. Shroff, H.F. Hess, E. Betzig, and J. Lippincott-Schwartz. 2008. High-density mapping of single-molecule trajectories with photoactivated localization microscopy. *Nat Methods*. 5:155-7.

Mann, M., and O.N. Jensen. 2003. Proteomic analysis of post-translational modifications. *Nat Biotechnol*. 21:255-61.

Marco, E., R. Wedlich-Soldner, R. Li, S.J. Altschuler, and L.F. Wu. 2007. Endocytosis optimizes the dynamic localization of membrane proteins that regulate cortical polarity. *Cell*. 129:411-22.

Marks, J., I.M. Hagan, and J.S. Hyams. 1986. Growth polarity and cytokinesis in fission yeast: the role of the cytoskeleton. *J Cell Sci Suppl*. 5:229-41.

Martin, S.G. 2009. Microtubule-dependent cell morphogenesis in the fission yeast. *Trends Cell Biol*. 19:447-54.

Martin, S.G., and M. Berthelot-Grosjean. 2009. Polar gradients of the DYRK-family kinase Pom1 couple cell length with the cell cycle. *Nature*. 459:852-6.

Martin, S.G., and F. Chang. 2006. Dynamics of the formin for3p in actin cable assembly. *Curr Biol*. 16:1161-70.
Martin, S.G., W.H. McDonald, J.R. Yates, 3rd, and F. Chang. 2005. Tea4p links microtubule plus ends with the formin for3p in the establishment of cell polarity. *Dev Cell*. 8:479-91.
Martin, S.G., S.A. Rincon, R. Basu, P. Perez, and F. Chang. 2007. Regulation of the formin for3p by cdc42p and bud6p. *Mol Biol Cell*. 18:4155-67.
Martin-Cuadrado, A.B., E. Duenas, M. Sipiczki, C.R. Vazquez de Aldana, and F. del Rey. 2003. The endo-beta-1,3-glucanase eng1p is required for dissolution of the primary septum during cell separation in Schizosaccharomyces pombe. *J Cell Sci*. 116:1689-98.
Mason, J.M., and K.M. Arndt. 2004. Coiled coil domains: stability, specificity, and biological implications. *Chembiochem*. 5:170-6.
Mata, J., and P. Nurse. 1997. tea1 and the microtubular cytoskeleton are important for generating global spatial order within the fission yeast cell. *Cell*. 89:939-49.
Matsuyama, A., A. Shirai, Y. Yashiroda, A. Kamata, S. Horinouchi, and M. Yoshida. 2004. pDUAL, a multipurpose, multicopy vector capable of chromosomal integration in fission yeast. *Yeast*. 21:1289-305.
Mennella, V., G.C. Rogers, S.L. Rogers, D.W. Buster, R.D. Vale, and D.J. Sharp. 2005. Functionally distinct kinesin-13 family members cooperate to regulate microtubule dynamics during interphase. *Nat Cell Biol*. 7:235-45.
Minc, N., S.V. Bratman, R. Basu, and F. Chang. 2009. Establishing new sites of polarization by microtubules. *Curr Biol*. 19:83-94.
Misteli, T. 2001. The concept of self-organization in cellular architecture. *J Cell Biol*. 155:181-5.
Mitchison, J.M., and P. Nurse. 1985. Growth in cell length in the fission yeast Schizosaccharomyces pombe. *J Cell Sci*. 75:357-76.
Mitchison, T., and M. Kirschner. 1984. Dynamic instability of microtubule growth. *Nature*. 312:237-42.
Moseley, J.B., A. Mayeux, A. Paoletti, and P. Nurse. 2009. A spatial gradient coordinates cell size and mitotic entry in fission yeast. *Nature*. 459:857-60.
Motegi, F., R. Arai, and I. Mabuchi. 2001. Identification of two type V myosins in fission yeast, one of which functions in polarized cell growth and moves rapidly in the cell. *Mol Biol Cell*. 12:1367-80.
Mullins, R.D. 2010. Cytoskeletal mechanisms for breaking cellular symmetry. *Cold Spring Harb Perspect Biol*. 2:a003392.
Murray, A.W., and T. Hunt. 1993. The cell cycle : an introduction. Oxford University Press, New York. xii, 251 p. pp.
Nelson, W.J. 2003. Adaptation of core mechanisms to generate cell polarity. *Nature*. 422:766-74.
Nern, A., and R.A. Arkowitz. 2000. Nucleocytoplasmic shuttling of the Cdc42p exchange factor Cdc24p. *J Cell Biol*. 148:1115-22.
Ong, S.E., B. Blagoev, I. Kratchmarova, D.B. Kristensen, H. Steen, A. Pandey, and M. Mann. 2002. Stable isotope labeling by amino acids in cell culture, SILAC, as a simple and accurate approach to expression proteomics. *Mol Cell Proteomics*. 1:376-86.
Ong, S.E., I. Kratchmarova, and M. Mann. 2003. Properties of 13C-substituted arginine in stable isotope labeling by amino acids in cell culture (SILAC). *J Proteome Res*. 2:173-81.

Padte, N.N., S.G. Martin, M. Howard, and F. Chang. 2006. The cell-end factor pom1p inhibits mid1p in specification of the cell division plane in fission yeast. *Curr Biol*. 16:2480-7.

Park, H.O., and E. Bi. 2007. Central roles of small GTPases in the development of cell polarity in yeast and beyond. *Microbiol Mol Biol Rev*. 71:48-96.

Park, S.K., L. Liao, J.Y. Kim, and J.R. Yates, 3rd. 2009. A computational approach to correct arginine-to-proline conversion in quantitative proteomics. *Nat Methods*. 6:184-5.

Patterson, G., M. Davidson, S. Manley, and J. Lippincott-Schwartz. 2010. Superresolution imaging using single-molecule localization. *Annu Rev Phys Chem*. 61:345-67.

Pelham, R.J., Jr., and F. Chang. 2001. Role of actin polymerization and actin cables in actin-patch movement in Schizosaccharomyces pombe. *Nat Cell Biol*. 3:235-44.

Petersen, J., D. Weilguny, R. Egel, and O. Nielsen. 1995. Characterization of fus1 of Schizosaccharomyces pombe: a developmentally controlled function needed for conjugation. *Mol Cell Biol*. 15:3697-707.

Petrie, R.J., A.D. Doyle, and K.M. Yamada. 2009. Random versus directionally persistent cell migration. *Nat Rev Mol Cell Biol*. 10:538-49.

Philips, J., and I. Herskowitz. 1998. Identification of Kel1p, a kelch domain-containing protein involved in cell fusion and morphology in Saccharomyces cerevisiae. *J Cell Biol*. 143:375-89.

Piel, M., and P.T. Tran. 2009. Cell shape and cell division in fission yeast. *Curr Biol*. 19:R823-7.

Pinar, M., P.M. Coll, S.A. Rincon, and P. Perez. 2008. Schizosaccharomyces pombe Pxl1 is a paxillin homologue that modulates Rho1 activity and participates in cytokinesis. *Mol Biol Cell*. 19:1727-38.

Prilusky, J., C.E. Felder, T. Zeev-Ben-Mordehai, E.H. Rydberg, O. Man, J.S. Beckmann, I. Silman, and J.L. Sussman. 2005. FoldIndex: a simple tool to predict whether a given protein sequence is intrinsically unfolded. *Bioinformatics*. 21:3435-8.

Pruyne, D., A. Legesse-Miller, L. Gao, Y. Dong, and A. Bretscher. 2004. Mechanisms of polarized growth and organelle segregation in yeast. *Annu Rev Cell Dev Biol*. 20:559-91.

Qyang, Y., P. Yang, H. Du, H. Lai, H. Kim, and S. Marcus. 2002. The p21-activated kinase, Shk1, is required for proper regulation of microtubule dynamics in the fission yeast, Schizosaccharomyces pombe. *Mol Microbiol*. 44:325-34.

Rafelski, S.M., and W.F. Marshall. 2008. Building the cell: design principles of cellular architecture. *Nat Rev Mol Cell Biol*. 9:593-602.

Resh, M.D. 2006. Trafficking and signaling by fatty-acylated and prenylated proteins. *Nat Chem Biol*. 2:584-90.

Rudner, D.Z., Q. Pan, and R.M. Losick. 2002. Evidence that subcellular localization of a bacterial membrane protein is achieved by diffusion and capture. *Proc Natl Acad Sci U S A*. 99:8701-6.

Samejima, I., S. Mackie, E. Warbrick, R. Weisman, and P.A. Fantes. 1998. The fission yeast mitotic regulator win1+ encodes an MAP kinase kinase kinase that phosphorylates and activates Wis1 MAP kinase kinase in response to high osmolarity. *Mol Biol Cell*. 9:2325-35.

Sandblad, L., K.E. Busch, P. Tittmann, H. Gross, D. Brunner, and A. Hoenger. 2006. The Schizosaccharomyces pombe EB1 homolog Mal3p binds and stabilizes the microtubule lattice seam. *Cell*. 127:1415-24.

Sawin, K.E., C.C. Bicho, and H.A. Snaith. 2009. Inexpensive synthetic-based matrix for both conventional and rapid purification of protein A- and TAP-tagged proteins. *Anal Biochem*.

Sawin, K.E., M.A. Hajibagheri, and P. Nurse. 1999. Mis-specification of cortical identity in a fission yeast PAK mutant. *Curr Biol*. 9:1335-8.
Sawin, K.E., P.C. Lourenco, and H.A. Snaith. 2004. Microtubule nucleation at non-spindle pole body microtubule-organizing centers requires fission yeast centrosomin-related protein mod20p. *Curr Biol*. 14:763-75.
Sawin, K.E., and H.A. Snaith. 2004. Role of microtubules and tea1p in establishment and maintenance of fission yeast cell polarity. *J Cell Sci*. 117:689-700.
Sawin, K.E., and P.T. Tran. 2006. Cytoplasmic microtubule organization in fission yeast. *Yeast*. 23:1001-14.
Scott, F.L., B. Stec, C. Pop, M.K. Dobaczewska, J.J. Lee, E. Monosov, H. Robinson, G.S. Salvesen, R. Schwarzenbacher, and S.J. Riedl. 2009. The Fas-FADD death domain complex structure unravels signalling by receptor clustering. *Nature*. 457:1019-22.
Serber, Z., and J.E. Ferrell, Jr. 2007. Tuning bulk electrostatics to regulate protein function. *Cell*. 128:441-4.
Sheeman, B., P. Carvalho, I. Sagot, J. Geiser, D. Kho, M.A. Hoyt, and D. Pellman. 2003. Determinants of S. cerevisiae dynein localization and activation: implications for the mechanism of spindle positioning. *Curr Biol*. 13:364-72.
Shimada, Y., M.P. Gulli, and M. Peter. 2000. Nuclear sequestration of the exchange factor Cdc24 by Far1 regulates cell polarity during yeast mating. *Nat Cell Biol*. 2:117-24.
Sieber, J.J., K.I. Willig, C. Kutzner, C. Gerding-Reimers, B. Harke, G. Donnert, B. Rammner, C. Eggeling, S.W. Hell, H. Grubmuller, and T. Lang. 2007. Anatomy and dynamics of a supramolecular membrane protein cluster. *Science*. 317:1072-6.
Siegrist, S.E., and C.Q. Doe. 2007. Microtubule-induced cortical cell polarity. *Genes Dev*. 21:483-96.
Slaughter, B.D., S.E. Smith, and R. Li. 2009. Symmetry breaking in the life cycle of the budding yeast. *Cold Spring Harb Perspect Biol*. 1:a003384.
Snaith, H.A., I. Samejima, and K.E. Sawin. 2005. Multistep and multimode cortical anchoring of tea1p at cell tips in fission yeast. *EMBO J*. 24:3690-9.
Snaith, H.A., and K.E. Sawin. 2003. Fission yeast mod5p regulates polarized growth through anchoring of tea1p at cell tips. *Nature*. 423:647-51.
Snaith, H.A., and K.E. Sawin. 2005. Tea for three: control of fission yeast polarity. *Nat Cell Biol*. 7:450-1.
Snell, V., and P. Nurse. 1994. Genetic analysis of cell morphogenesis in fission yeast--a role for casein kinase II in the establishment of polarized growth. *EMBO J*. 13:2066-74.
Sprague, B.L., and J.G. McNally. 2005. FRAP analysis of binding: proper and fitting. *Trends Cell Biol*. 15:84-91.
Steen, H., and M. Mann. 2004. The ABC's (and XYZ's) of peptide sequencing. *Nat Rev Mol Cell Biol*. 5:699-711.
Strickfaden, S.C., M.J. Winters, G. Ben-Ari, R.E. Lamson, M. Tyers, and P.M. Pryciak. 2007. A mechanism for cell-cycle regulation of MAP kinase signaling in a yeast differentiation pathway. *Cell*. 128:519-31.
Takeshita, N., Y. Higashitsuji, S. Konzack, and R. Fischer. 2008. Apical sterol-rich membranes are essential for localizing cell end markers that determine growth directionality in the filamentous fungus Aspergillus nidulans. *Mol Biol Cell*. 19:339-51.
Tasto, J.J., J.L. Morrell, and K.L. Gould. 2003. An anillin homologue, Mid2p, acts during fission yeast cytokinesis to organize the septin ring and promote cell separation. *J Cell Biol*. 160:1093-103.
Tatebe, H., K. Shimada, S. Uzawa, S. Morigasaki, and K. Shiozaki. 2005. Wsh3/Tea4 is a novel cell-end factor essential for bipolar distribution of Tea1 and protects cell polarity under environmental stress in S. pombe. *Curr Biol*. 15:1006-15.

Terenna, C.R., T. Makushok, G. Velve-Casquillas, D. Baigl, Y. Chen, M. Bornens, A. Paoletti, M. Piel, and P.T. Tran. 2008. Physical mechanisms redirecting cell polarity and cell shape in fission yeast. *Curr Biol*. 18:1748-53.

Tyson, J.J., K.C. Chen, and B. Novak. 2003. Sniffers, buzzers, toggles and blinkers: dynamics of regulatory and signaling pathways in the cell. *Curr Opin Cell Biol*. 15:221-31.

Ubersax, J.A., and J.E. Ferrell, Jr. 2007. Mechanisms of specificity in protein phosphorylation. *Nat Rev Mol Cell Biol*. 8:530-41.

Van Hoof, D., M.W. Pinkse, D.W. Oostwaard, C.L. Mummery, A.J. Heck, and J. Krijgsveld. 2007. An experimental correction for arginine-to-proline conversion artifacts in SILAC-based quantitative proteomics. *Nat Methods*. 4:677-8.

Verde, F., D.J. Wiley, and P. Nurse. 1998. Fission yeast orb6, a ser/thr protein kinase related to mammalian rho kinase and myotonic dystrophy kinase, is required for maintenance of cell polarity and coordinates cell morphogenesis with the cell cycle. *Proc Natl Acad Sci U S A*. 95:7526-31.

Watanabe, T., S. Wang, J. Noritake, K. Sato, M. Fukata, M. Takefuji, M. Nakagawa, N. Izumi, T. Akiyama, and K. Kaibuchi. 2004. Interaction with IQGAP1 links APC to Rac1, Cdc42, and actin filaments during cell polarization and migration. *Dev Cell*. 7:871-83.

Waterman-Storer, C.M., R.A. Worthylake, B.P. Liu, K. Burridge, and E.D. Salmon. 1999. Microtubule growth activates Rac1 to promote lamellipodial protrusion in fibroblasts. *Nat Cell Biol*. 1:45-50.

Wedlich-Soldner, R., S. Altschuler, L. Wu, and R. Li. 2003. Spontaneous cell polarization through actomyosin-based delivery of the Cdc42 GTPase. *Science*. 299:1231-5.

Wedlich-Soldner, R., and R. Li. 2003. Spontaneous cell polarization: undermining determinism. *Nat Cell Biol*. 5:267-70.

Win, T.Z., Y. Gachet, D.P. Mulvihill, K.M. May, and J.S. Hyams. 2001. Two type V myosins with non-overlapping functions in the fission yeast Schizosaccharomyces pombe: Myo52 is concerned with growth polarity and cytokinesis, Myo51 is a component of the cytokinetic actin ring. *J Cell Sci*. 114:69-79.

Witte, H., and F. Bradke. 2008. The role of the cytoskeleton during neuronal polarization. *Curr Opin Neurobiol*. 18:479-87.

Wolf, E., P.S. Kim, and B. Berger. 1997. MultiCoil: a program for predicting two- and three-stranded coiled coils. *Protein Sci*. 6:1179-89.

Wu, J.Q., C.D. McCormick, and T.D. Pollard. 2008. Chapter 9: Counting proteins in living cells by quantitative fluorescence microscopy with internal standards. *Methods Cell Biol*. 89:253-73.

Wu, J.Q., and T.D. Pollard. 2005. Counting cytokinesis proteins globally and locally in fission yeast. *Science*. 310:310-4.

Wu, X., X. Xiang, and J.A. Hammer, 3rd. 2006. Motor proteins at the microtubule plus-end. *Trends Cell Biol*. 16:135-43.

Xu, H., B. Andi, J. Qian, A.H. West, and P.F. Cook. 2006. The alpha-aminoadipate pathway for lysine biosynthesis in fungi. *Cell Biochem Biophys*. 46:43-64.

Yamano, H., J. Gannon, and T. Hunt. 1996. The role of proteolysis in cell cycle progression in Schizosaccharomyces pombe. *EMBO J*. 15:5268-79.

Yin, C.C., and F.A. Lai. 2000. Intrinsic lattice formation by the ryanodine receptor calcium-release channel. *Nat Cell Biol*. 2:669-71.

Yuce, O., A. Piekny, and M. Glotzer. 2005. An ECT2-centralspindlin complex regulates the localization and function of RhoA. *J Cell Biol*. 170:571-82.

Zimniak, T., K. Stengl, K. Mechtler, and S. Westermann. 2009. Phosphoregulation of the budding yeast EB1 homologue Bim1p by Aurora/Ipl1p. *J Cell Biol*. 186:379-91.